



HAL
open science

Design of 2D and 3D antennas on flexible materials

Hong Phuong Phan

► **To cite this version:**

Hong Phuong Phan. Design of 2D and 3D antennas on flexible materials. Optics / Photonic. Université Grenoble Alpes, 2018. English. NNT : 2018GREAT106 . tel-02138893

HAL Id: tel-02138893

<https://theses.hal.science/tel-02138893>

Submitted on 24 May 2019

HAL is a multi-disciplinary open access archive for the deposit and dissemination of scientific research documents, whether they are published or not. The documents may come from teaching and research institutions in France or abroad, or from public or private research centers.

L'archive ouverte pluridisciplinaire **HAL**, est destinée au dépôt et à la diffusion de documents scientifiques de niveau recherche, publiés ou non, émanant des établissements d'enseignement et de recherche français ou étrangers, des laboratoires publics ou privés.

THÈSE

Pour obtenir le grade de

**DOCTEUR DE LA COMMUNAUTE UNIVERSITE
GRENOBLE ALPES**

Spécialité : **Optique et Radiofréquences**

Arrêté ministériel : 25 mai 2016

Présentée par

Hong Phuong PHAN

Thèse dirigée par **Tan Phu VUONG**, Professeur, Grenoble INP, et
codirigée par **Philippe BENECH**, Professeur, Université Grenoble
Alpes et **Pascal XAVIER**, Professeur, Université Grenoble Alpes

préparée au sein du **Laboratoire IMEP-LAHC**
dans l'**École Doctorale Electronique, Electrotechnique,
Automatique et Traitement du signal (EEATS)**

Conception d'antennes 2D et 3D sur des matériaux flexibles

Thèse soutenue publiquement **le 15 novembre 2018**
devant le jury composé de :

M. Christian PERSON

Professeur, IMT Atlantique, Président

M. Fabien FERRERO

Professeur, LEAT, Université Côte d'Azur, Rapporteur

Mme. Valérie VIGNERAS

Professeur, Institut Polytechnique de Bordeaux, Rapporteur

Mme. Delphine BECHEVET

Professeur, Ecoles supérieures de suisse occidentale, Membre

M. Dominique LO HINE TONG

Senior Scientist, Technicolor, Membre

M. Tan-Phu VUONG

Professeur, Grenoble INP, Membre

M. Philippe BENECH

Professeur, Université Grenoble-Alpes, Membre

M. Pascal XAVIER,

Professeur, Université Grenoble-Alpes, Membre

M. Pascal BOREL,

Senior Scientist, Centre technique du papier, Membre invité

M. Patrick CHAN,

Product director, Uwinloc, Membre invité

M. Alejandro NIEMBRO,

Wireless Connectivity Engineer, Schneider Electric, Membre invité



Acknowledgement

This work has been financed by the National Agency for the Research (l'Agence National pour la Recherche –ANR) in the frame of the Stick'It project with the other partners Technicolor (THCR), Centre Technique du Papier (CTP) et l'Institut Mines-Télécom (IMT) Atlantique. The thesis has been realized at IMEP-LAHC laboratory, INP Grenoble.

I would like to express my sincere gratitude to my supervisor, Prof. Tan-Phu VUONG, and my co-supervisors, Prof. Philippe BENECH and Prof. Pascal XAVIER for their help, guidelines and support that contributed to the research work presented in this manuscript.

I would like to thank Prof. Christian PERSON from IMT Atlantique, Dr. Dominique LO HINE TONG from Technicolor, Dr. Pascal BOREL, Ms. Anastasia DELATTRE and Mr. Damien IZOARD from CTP, the partners of the project who helped me clarify many problems related to the topic.

I also would like to express my thanks to the engineers and technicians, Mr. Nicolas CORRAO, Mrs. Martine GRI from IMEP-LAHC laboratory, and Mr. Antoine PISA from Phelma, who have supported me a lot during my experimental validations.

I would like to express my recognition to the administrative staff, including Isabelle, Valérie, Annaïck, Dahlila, Fabienne, Anais who have helped me a lot during all the period of working on my PhD on the administrative aspects.

I would like to thank my colleagues and friends, Ngan, Phong, Hamza, Thibaud and the others from IMEP-LAHC for their support.

I would like to express a deep love and gratitude to my family including my Father who always encouraged me in the process of life-long learning to obtain new knowledge and to be helpful for the society, the memory of my Mother who passed away during the first year of my PhD, my younger sister and her family for their love, their mental as well as material support. Finally, I would like to thank my beloved twins Alexandra-Sashunya and Lev-Levunya who are always there to support me by their love, their charm, for the dinners they made for me when I came back home late during all the time of my PhD.

Table of Content

Acknowledgement.....	ii
Table of Content.....	i
List of tables	iv
List of figures	iv
Introduction	13
1. Chapter 1 – State-of-the-art.....	15
1.1. Flexible substrate materials – Paper substrate and challenges	15
1.1.1. Traditional RF substrates for flexible electronics	15
1.1.2. Kapton polyimide	16
1.1.3. Polydimethylsiloxane (PDMS) substrates.....	16
1.1.4. Textile substrates.....	17
1.1.5. Plastic materials.....	19
1.1.6. Paper materials	20
1.1.7. Other substrate materials	24
1.2. Printing technologies for flexible electronics	24
1.2.1. Conductive inks used for printed flexible electronics	24
1.2.1.1. Metal-based inks	24
1.2.1.2. Organic polymer-based inks.....	25
1.2.2. Printing techniques on flexible substrates	25
1.2.2.1. Inkjet printing method	26
1.2.2.1. Screen printing method	26
1.2.2.2. Slot-die printing.....	27
1.2.2.3. Gravure printing	27
1.2.2.4. Gravure-offset printing.....	27
1.2.2.5. Flexographic printing	27
1.2.2.6. Micro-contact printing.....	27
1.2.2.7. Nano-imprinting lithography.....	28
1.2.2.8. Dry transfer printing.....	28

1.3.	Antennas on paper substrates: two-dimensional structures	30
1.3.1.	Paper-based antennas using adhesive metal tapes.....	30
1.3.2.	Inkjet-printed antennas	32
1.3.3.	Screen-printed antennas	34
1.4.	Three-dimensional antennas	35
1.5.	MIMO antennas	35
1.5.1.	MIMO technique	36
1.5.2.	MIMO antennas on rigid and flexible substrates	37
1.5.3.	Techniques for reduction of mutual coupling between antennas in MIMO systems	38
	Conclusions for Chapter 1	53
	Objectives of the thesis	54
	References for Chapter 1	55
2.	Chapter 2 – Design of Single-Band Antennas on Paper	66
2.1.	Characterization of electromagnetic properties of paper.....	66
2.2.	CPW-fed monopole antennas	69
2.3.	Inverted-F antennas on E4D paper	71
2.4.	Antennas with air-filled SIW technology on paper	77
	Conclusions for Chapter 2	83
	References for Chapter 2.....	84
3.	Chapter 3 – Design of Wide-Band and Multi-Band Antennas on Paper	86
3.1.	Microstrip-fed wideband antennas	86
3.1.1.	“Sapin” antenna	86
3.1.2.	“Modified Sapin” antenna	92
3.1.3.	“Robe” antenna.....	96
3.1.4.	“Mushroom-Shaped with Two Arms” antenna	99
3.1.5.	“Hello-Shaped” dual-band antennas	102
3.2.	Microstrip-fed multi-band antennas	108
	Conclusions for Chapter 3	111
	References for Chapter 3.....	113

4.	Chapter 4 – Three-Dimensional and MIMO Antenna Systems	114
4.1.	System of two flat antennas in an ABS plastic box.....	114
4.2.	Study of Antenna Bending Effects	125
4.2.1.	Basic theory for the study.....	126
4.2.2.	Study of bending effects of a wide-band monopole antenna	133
4.3.	System of antennas in a box with restricted dimensions	139
4.3.1.	Wide-band antenna bent under 90 degrees placed in ABS box with restricted dimensions.....	139
4.3.2.	Two wideband antennas placed in an ABS box - one flat and another bent under 90 degrees	142
4.3.3.	System of two 90-degree bent antennas placed in ABS box.....	152
	Conclusions for Chapter 4.....	154
	References for Chapter 4.....	155
	Conclusions and Perspectives	157
5.	Appendix 1 – Characterization of electromagnetic properties of substrate materials.....	163
5.1.	Non-resonance methods using waveguides or transmission lines.....	163
5.1.1.	The techniques using waveguides	163
5.1.2.	The techniques using planar transmission lines	167
5.2.	Resonance methods using resonators	170
5.2.1.	Waveguide resonance cavity	170
5.2.2.	Planar transmission line resonators	173
5.2.3.	Microstrip resonator	174
5.3.	Recommendations for choosing methods	178
	Conclusions for Appendix 1	186
	References for Appendix 1	187
6.	Appendix 2 – Antenna fabrication and measurement	190
	Abstract	192
	Résumé.....	194
	Liste des publications	196

List of tables

Table 1.1. Dielectric properties of some normal textile fabrics [18].	18
Table 1.2. Properties of some typical flexible substrate materials.	23
Table 1.3. Comparison of printing methods.	28
Table 1.4. Comparison of paper-based antennas.	39
Table 1.5. Examples for 3D antennas.	40
Table 1.6. Examples for MIMO antennas.	44
Table 1.7. Examples of decoupling structures in MIMO antenna systems.	46
Table 2.1. The measurement results at 2.5 GHz.	67
Table 2.2. The measurement results at 900 MHz.	68
Table 3.1. The proposed microstrip-fed building block monopole antennas designed on E4D paper.	112
Table 5.1. Comparison of methods.	178
Table 5.2. Recommendations of methods for characterization of different materials.	186

List of figures

Figure 1.1. (a) Fabricated prototypes of screen printed planar antennas on textile substrate; (b) Screen printed antenna integrated into firefighter suit [27].	19
Figure 1.2. A chipless RFID tag on paper substrate [43].	23
Figure 1.3. Moisture sensor tag for intelligent packaging [44].	23
Figure 1.4. Classification of printing techniques [52].	26
Figure 1.5. (a) Single monopole and (b) antenna array with copper tape [56].	31
Figure 1.6. Cavity-backed SIW antenna on paper substrate [57]: (a) Front side with microstrip feeding line; (b) Back side with radiating slot.	31
Figure 1.7. Geometry of CP origami antenna [58]: (a) Circularly polarized origami antenna structure; (b) Feeding network.	31
Figure 1.8. Simulated and measured performance of the CPW-fed monopole in [59].	32
Figure 1.9. Inkjet-printed dipole for UHF RFID tag [60].	32

Figure 1.10. Connection between an RFID dipole on paper substrate and a CMOS Si chip [60]: (a) Mechanical drawing of the PCB test-fixtured and zoom of its central zone with a highlight of the transformer structure; (b) Realization of the system.	33
Figure 1.11. Paper-based high gain antenna with AMC structure [62].	33
Figure 1.12. Antipodal Vivaldi antenna: (a) front; and (b) back sides [63].	33
Figure 1.13. Multiband antenna for curved wireless devices: (a) front and (b) back sides [65].	34
Figure 1.14. IFA proposed by D. E. Anagnostou et al., front and back [66].	34
Figure 1.15. Meandered-line dipole antenna structure [68]: (a) Antenna geometries; (b) Printed prototype.	35
Figure 1.16. Block diagram of a MIMO system [90 (Jensen, 2004)].	36
Figure 2.1. CPW-fed monopole antennas using the adhesive copper with their reflection coefficients: (a) On PRC, $h=65\mu\text{m}$; (b) On PET (Polyethylene Terephthalate), $h=100\mu\text{m}$; (c) On CnCanle paper, $h=786\mu\text{m}$	70
Figure 2.2. Simulated radiation patterns of CPW-fed monopole antennas using the adhesive copper on CnCanle paper, $h=786\mu\text{m}$: (a) In x-z plan (E-plan); (b) In x-y plan (H-plan).	71
Figure 2.3. Printed single-band PIFA on E4D 200 paper: (a) Front side; (b) Back side.	73
Figure 2.4. Geometrical study of the single-band IFA structure on E4D 200; (a) Effect of L_s with $h = 4 \text{ mm}$; (b) Effect of h with $L_s = 21.5 \text{ mm}$	74
Figure 2.5. Reflection coefficient of the single-band PIFA - Simulation compared with measurement for 3 prototypes: (a) With the initial simulation; (b) With the more proper simulation.	75
Figure 2.6. Simulated radiation patterns of the single-band IFA at the resonant frequency: (a) In x-z plane (E-plane); (b) In x-y plane (H-plane).	76
Figure 2.7. Printed dual-band IFA on E4D 200: (a) Front side; (c) Back side.	76
Figure 2.8. Reflection coefficient of the dual-band IFA - Simulation compared with Measurement for 2 prototypes.	77
Figure 2.9. Simulated radiation patterns of the dual-band IFA: (a) In x-z plane ($\varphi = 0^\circ$), at 2.45 GHz; (b) In x-y plane ($\theta = 90^\circ$), at 2.45 GHz; (c) In x-z plane ($\varphi = 0^\circ$), at 5.5 GHz; (d) In x-y plane ($\theta = 90^\circ$), at 5.5 GHz.	78

Figure 2.10. Configuration of an antenna based on Air-Filled SIW Technology: (a) Back side with the feed line; (b) Front side with the slot antenna; (c), (d) The cross sections of the air-filled cavity.	79
Figure 2.11. Radiation characteristics of the antenna with $N = 3$, $L_c = 34$ mm, $W_c = 36$ mm:(a) Return loss; (b) Realized gain of the antenna in 3D at 5 GHz.	80
Figure 2.12. Effect of the cavity height on the total efficiency of the antenna at its resonant frequency for $L_c = 34$ mm and $W_c = 36$ mm.	81
Figure 2.13. Effect of the cavity length on the total efficiency of the antenna at its resonant frequency for $N = 3$, $W_c = 36$ mm.	81
Figure 2.14. Effect of the cavity width on the total efficiency of the antenna at its resonant frequency for $N = 3$, $L_c = 34$ mm.	82
Figure 3.1. The design process of the antennas: (a) Initial trapezoidal structure; (b) Modification of the initial structure; (c) Final structure of “Sapin” antenna; (d) Spherical coordinate system.....	87
Figure 3.2. $ S_{11} $ parametric study of the initial designs.	88
Figure 3.3. Simulated reflection coefficient of the antenna with rectangular ground plane versus rounded ground plane.	89
Figure 3.4. $ S_{11} $ parametric study of the proposed antenna “Sapin” for $W_{02} = 28$ mm, $L = 59$ mm, $h_{01} = 22$ mm, $h_{02} = 3$ mm, $h_{03} = 21.3$ mm, $h_{04} = 30$ mm.	89
Figure 3.5. A prototype obtained by the screen printing technology; (a) Front side; (b) Back side; (c) The prototype with the connector.	90
Figure 3.6. Reflection coefficient of the antenna “Sapin”– Simulation compared to measurement.	90
Figure 3.7. Simulated and measured radiation patterns of “Sapin”: (a) x-z plane ($\varphi = 0^\circ$), at 2.45 GHz; (b) x-y plane ($\theta = 90^\circ$), at 2.45 GHz; (c) x-z plane ($\varphi = 0^\circ$), at 5.5 GHz; (d) x-y plane ($\theta = 90^\circ$), at 5.5 GHz.....	91
Figure 3.8. “Modified Sapin” antenna geometry; (a) Front side; (b) Back side.	93
Figure 3.9. Simulated reflection coefficients of the antennas with rectangular ground plane versus rounded ground plane.	93
Figure 3.10. A prototype obtained by the screen printing technology; (a) Front side; (b) Back side; (c) The prototype with the connector.	94

Figure 3.11. Reflection coefficient of the antenna antenna “Modified Sapin” – Simulation compared to measurement.....	94
Figure 3.12. Simulated and measured radiation patterns of “Modified Sapin”: (a) x-z plane ($\varphi = 0^\circ$), at 2.45 GHz; (b) x-y plane ($\theta = 90^\circ$), at 2.45 GHz; (c) x-z plane ($\varphi = 0^\circ$), at 5.5 GHz; (d) x-y plane ($\theta = 90^\circ$), at 5.5 GHz.	95
Figure 3.13. “Robe” antenna geometry: (a) Front side; (b) Back side; (c) Prototype obtained by the screen printing technology with the connector.	97
Figure 3.14. Reflection coefficient of “Robe” – Simulation compared to measurement.....	97
Figure 3.15. Simulated and measured radiation patterns of “Robe”: (a) x-z plane ($\varphi = 0^\circ$), at 2.45 GHz; (b) x-y plane ($\theta = 90^\circ$), at 2.45 GHz; (c) x-z plane ($\varphi = 0^\circ$), at 5.5 GHz; (d) x-y plane ($\theta = 90^\circ$), at 5.5 GHz.	98
Figure 3.16. Evolution of the antenna design process: (a) Circular; (b) Mushroom-shaped; (c) Mushroom-shaped with two arms and its geometries, front side; (d) Back side; (e) A fabricated prototype.....	99
Figure 3.17. Return loss of the antenna – Simulation compared to measurement.	100
Figure 3.18. Radiation patterns of the antenna - simulation compared to measurement: (a) x-z plane ($\varphi = 0^\circ$), at 2.45 GHz; (b) x-y plane ($\theta = 90^\circ$), at 2.45 GHz; (c) x-z plane ($\varphi = 0^\circ$), at 5.5 GHz; (d) x-y plane ($\theta = 90^\circ$), at 5.5 GHz.	101
Figure 3.19. Optimized geometries of the antennas: (a) "Hello 1", front and back sides; (b) "Hello 2", front and back sides.	102
Figure 3.20. $ S_{11} $ parametric study of “Hello 2”; (a) for various radii of the “head”; (b) for various lengths of the “arm”. The other geometrical parameters are shown in Figure 3.19.....	103
Figure 3.21. The simulated reflection coefficient $ S_{11} $ of the antennas with the geometrical parameters are shown in Figure 3.19.	104
Figure 3.22. The reflection coefficient $ S_{11} $ of the antennas - simulation compared to measurement of two prototypes: (a) "Hello 1"; (b) "Hello 2".....	105
Figure 3.23. Simulated and measured radiation patterns of “Hello 1”: (a) x-z plane ($\varphi = 0^\circ$), at 2.45 GHz; (b) x-y plane ($\theta = 90^\circ$), at 2.45 GHz; (c) x-z plane ($\varphi = 0^\circ$), at 5.5 GHz; (d) x-y plane ($\theta = 90^\circ$), at 5.5 GHz.	106

Figure 3.24. Simulated and measured radiation patterns of “Hello 2”: (a) x-z plane ($\varphi = 0^\circ$), at 2.45 GHz; (b) x-y plane ($\theta = 90^\circ$), at 2.45 GHz; (c) x-z plane ($\varphi = 0^\circ$), at 5.5 GHz; (d) x-y plane ($\theta = 90^\circ$), at 5.5 GHz.	107
Figure 3.25. The design procedure, the antenna without “wings”: (a) front and (b) back sides; The antenna with “wings”: (c) front and (d) back sides.	108
Figure 3.26. The reflection coefficient of the antenna 1 – simulation compared to measurement.	109
Figure 3.27. The reflection coefficient of the antenna 2 – simulation compared to measurement.	109
Figure 3.28. Radiation patterns of the antenna 1 - simulation vs. measurement: (a) x-z plane ($\varphi = 0^\circ$), at 2.45 GHz; (b) x-y plane ($\theta = 90^\circ$), at 2.45 GHz; (c) x-z plane ($\varphi = 0^\circ$), at 5.5 GHz; (d) x-y plane ($\theta = 90^\circ$), at 5.5 GHz.	110
Figure 4.1. The system of two flat antennas in a 85 mm × 85 mm × 85 mm ABS plastic box: (a) CST simulation structure; (b) CST simulation structure – rotated view corresponding to the experimental realization; (c) Experimental realization in the assembling process; (d) The distance d_1	115
Figure 4.2. Study of S-parameters of the system for various distances d_1 : (a) S11; (b) S22;	117
Figure 4.3. Study of S-parameters of the system for various materials of the box: (a) S11; (b) S22; (c) S21.	118
Figure 4.4. Study of S-parameters of the system for various wall thicknesses of the box: (a) S11; (b) S22; (c) S21.	120
Figure 4.5. S-parameters of the first system - simulation compared to measurement; (a) Return loss of the antennas simulation vs. measurement; (b) Isolation between the antennas in ABS box. .	121
Figure 4.6. The system of two flat antennas in a 85 mm × 85 mm × 85 mm ABS plastic box: (a) Antenna system in spherical coordinates; (b) The x-z plane ($\varphi = 0^\circ$); (c) The x-y plane ($\theta = 90^\circ$).	122
Figure 4.7. Simulated and measured realized gain radiation patterns of Antenna 1: (a) In x-z plane ($\varphi = 0^\circ$) at 2.45 GHz; (b) In x-y plane ($\theta = 90^\circ$) at 2.45 GHz; (c) In x-z plane ($\varphi = 0^\circ$) at 5.5 GHz; (d) In x-y plane ($\theta = 90^\circ$) at 5.5 GHz.	123

Figure 4.8. Simulated and measured realized gain radiation patterns of Antenna 2: (a) In x-z plane ($\varphi = 0^\circ$) at 2.45 GHz; (b) In x-y plane ($\theta = 90^\circ$) at 2.45 GHz; (c) In x-z plane ($\varphi = 0^\circ$) at 5.5 GHz; (d) In x-y plane ($\theta = 90^\circ$) at 5.5 GHz.	124
Figure 4.9. Basic theoretical study of a dipole: (a) The straight dipole; (b) The dipole consisting of two misaligned parts, the second one is tilted under an angle ε_θ	126
Figure 4.10. The normalized radiated power $g(\theta, \varepsilon_\theta)$ of the studied dipole: (a) for $\varepsilon_\theta = 0^\circ, 60^\circ, 90^\circ$ with the red, blue and black 2nd part of the dipole, respectively; (b) The case $\varepsilon_\theta = 90^\circ$ for various ratios L_1 / L	129
Figure 4.11. Planar dipole on 0.21 mm thick E4D paper substrate: (a) Straight; (b) Bent under 120 degrees; (c) Bent under 90 degrees.	130
Figure 4.12. Return loss of a simple dipole on 0.21 mm thick E4D paper.	130
Figure 4.13. Realized gain radiation patterns at 2.45 GHz of the simple dipoles on 210- μm thick E4D paper: (a) In x-z plane ($\varphi = 0^\circ$); (b) In x-y plane ($\theta = 90^\circ$).	131
Figure 4.14. Planar monopole on 210- μm thick E4D paper substrate: (a) Straight; (b) Bent with $\varepsilon_\theta = 60^\circ$; (c) Bent with $\varepsilon_\theta = 90^\circ$	131
Figure 4.15. Return loss of a simple monopole on 210- μm thick E4D paper.....	132
Figure 4.16. Realized gain radiation patterns at the resonant frequency of the simple monopoles on 210- μm thick E4D paper: (a) In x-z plane ($\varphi = 0^\circ$); (b) In x-y plane ($\theta = 90^\circ$).....	132
Figure 4.17. Study of bending effects of “Mushroom-shaped with two arms” antenna: (a) CST simulation structure with illustration of tilted angle ε_θ and the bending position h; (b) Experimental realization.	133
Figure 4.18. 2.45 GHz radiation patterns of 90-degree bent antenna at the various bending positions: (a) x-z plane (E-plane, $\varphi = 0^\circ$); (b) x-y plane (H-plane, $\theta = 90^\circ$).	134
Figure 4.19. 2.45 GHz radiation patterns of 90-degree bent antenna at 30 mm for various bending radii: (a) x-z plane (E-plane, $\varphi = 0^\circ$); (b) x-y plane (H-plane, $\theta = 0^\circ$).	134
Figure 4.20. Reflection coefficient of a flat antenna and under bending.	135
Figure 4.21. Radiation patterns of the antenna without bending and with bending: (a) x-z plane (E-plane), at 2.45 GHz; (b) x-y plane (H-plane), at 2.45 GHz; (c) x-z plane (E-plane), at 5.5 GHz; (d) x-y plane (H-plane), at 5.5 GHz.	136

Figure 4.22. Radiation patterns of 120-degree bent antenna at the position 30 mm: (a) x-z plane (E-plane), at 2.45 GHz, (b) x-y plane (H-plane), at 2.45 GHz, (c) x-z plane (E-plane), at 5.5 GHz, (d) x-y plane (H-plane), at 5.5 GHz.	137
Figure 4.23. Radiation patterns of 90-degree bent antenna at the position 30 mm: (a) x-z plane (E-plane), at 2.45 GHz; (b) x-y plane (H-plane), at 2.45 GHz; (c) x-z plane (E-plane), at 5.5 GHz; (d) x-y plane (H-plane), at 5.5 GHz.	138
Figure 4.24. A wide-band antenna bent under 90 degrees in a box: (a) CST Simulation structure; (b) Experimental realization.	139
Figure 4.25. Reflection coefficient of the flat antenna and under bending in air and in ABS box.	140
Figure 4.26. Simulated and measured realized gain radiation patterns of the bent antenna in a ABS plastic box: (a) Antenna in spherical coordinates; Realized gain radiation patterns of the antenna: (b) In x-z plane ($\varphi = 0^0$) at 2.45 GHz; (c) In x-y plane ($\theta = 90^0$) at 2.45 GHz; (d) In x-z plane ($\varphi = 0^0$) at 5.5 GHz; (e) In x-y plane ($\theta = 90^0$) at 5.5 GHz.	141
Figure 4.27. The system of two antennas in an ABS box with dimensions 150 mm \times 150 mm \times 30 mm: (a) CST simulation structure; (b) Experimental realization.	142
Figure 4.28. Return loss of the antenna system.	143
Figure 4.29. Isolation between the antennas in the system.	144
Figure 4.30. The antenna system in a 150 mm \times 150 mm \times 30 mm ABS plastic box: (a) Antenna system in spherical coordinates; (b) The x-z plane ($\varphi = 0^0$); (c) The x-y plane ($\theta = 90^0$).	144
Figure 4.31. Simulated and measured realized gain radiation patterns of Antenna 1: (a) In x-z plane ($\varphi = 0^0$) at 2.45 GHz; (b) In x-y plane ($\theta = 90^0$) at 2.45 GHz; (c) In x-z plane ($\varphi = 0^0$) at 5.5 GHz; (d) In x-y plane ($\theta = 90^0$) at 5.5 GHz.	145
Figure 4.32. Simulated and measured realized gain radiation patterns of Antenna 2: (a) In x-z plane ($\varphi = 0^0$) at 2.45 GHz; (b) In x-y plane ($\theta = 90^0$) at 2.45 GHz; (c) In x-z plane ($\varphi = 0^0$) at 5.5 GHz; (d) In x-y plane ($\theta = 90^0$) at 5.5 GHz.	146
Figure 4.33. CST simulation structure of the system in a 310 mm \times 207 mm \times 45 mm ABS box.	147
Figure 4.34. System of two antennas in a real ABS box with the dimensions of 310 mm \times 207 mm \times 45 mm: (a) The ABS box in the experiment; (b) The open ABS box with 2 antennas; (c) The location of the antennas in the box.	148
Figure 4.35. Return loss of the antenna system.	149

Figure 4.36. Isolation between the antennas.	149
Figure 4.37. Simulated and measured realized gain radiation patterns of Antenna 1: (a) In x-z plane ($\varphi = 0^0$) at 2.45 GHz; (b) In x-y plane ($\theta = 90^0$) at 2.45 GHz; (c) In x-z plane ($\varphi = 0^0$) at 5.5 GHz; (d) In x-y plane ($\theta = 90^0$) at 5.5 GHz.	150
Figure 4.38. Simulated and measured realized gain radiation patterns of Antenna 1: (a) In x-z plane ($\varphi = 0^0$) at 2.45 GHz; (b) In x-y plane ($\theta = 90^0$) at 2.45 GHz; (c) In x-z plane ($\varphi = 0^0$) at 5.5 GHz; (d) In x-y plane ($\theta = 90^0$) at 5.5 GHz.	151
Figure 4.39. CST simulation structure of the system of two antennas in the box.....	152
Figure 4.40. Simulated S- parameters of the system of two antennas, where both of them are bent under 90 degrees.....	152
Figure 4.41. Simulated realized gain radiation patterns of the antennas in the system of two bent antennas in a 150 mm \times 150 mm \times 30 mm ABS plastic box: (a) In x-z plane ($\varphi = 0^0$) at 2.45 GHz; (b) In x-y plane ($\theta = 90^0$) at 2.45 GHz; (c) In x-z plane ($\varphi = 0^0$) at 5.5 GHz; (d) In x-y plane ($\theta = 90^0$) at 5.5 GHz.....	153
Figure 5.1. (a) The sample in a waveguide, (b) The sample in a coaxial cable [1].	164
Figure 5.2. The method using a rectangular waveguide to characterize a thin sheet of a dielectric material.....	165
Figure 5.3. The reflection method to characterize thin materials.....	166
Figure 5.4. The method of two transmission lines.	168
Figure 5.5. Measurement of powder samples using the transmission line method.....	169
Figure 5.6. The transmission line method where the sample is a superstrate [6].....	170
Figure 5.7. A resonance cavity to characterized complex permittivity of a material [1]: (a) TE ₁₀₁ mode in rectangular resonant cavity; (b) TM ₀₁₀ mode in cylindrical resonant cavity.	171
Figure 5.8. (a) Split-cylinder cavity; (b) Shifting S ₂₁ between an empty and a loaded cavity [5].	172
Figure 5.9. (a) The sample is loaded in a cylindrical cavity; (b) The sample is loaded in a dielectric resonator then put in a cylindrical cavity [16].....	173
Figure 5.10. Open cavity at one side [1].	173
Figure 5.11. Planar transmission lines to characterize liquid materials [1]: (a) Longitudinal view; (b) Top view; (c) Current distribution.....	174

Figure 5.12. Microstrip ring resonator (a) Configuration diagram; (b) Fabricated prototype [17, 18].	176
Figure 5.13. Simulated and measured $ S_{21} $ by the ring resonator in (a) [17], (b) [18].	176
Figure 5.14. The method using a slot antenna [23]: (a) 3D view; (b) Section views.	177
Figure 5.15. The method using a microstrip antenna [24].	177
Figure 6.1. Measurement of reflection coefficient of the antenna.	191
Figure 6.2. Experimental setup for measurement of radiation patterns of the antenna, where the transmit antenna is at x-direction: (a) x-y plane ($\theta = 90^\circ$) measurement; (b) x-z plane ($\phi = 0^\circ$) measurement.	191

Introduction

Together with the possibility of printing technologies, printed flexible electronics was developed intensively and becomes a familiar term nowadays, that put a milestone in electronics technology.

This work has been done in the frame of the project “Stick’It” funded by the French National Research Agency.

It aims globally to promote printing and associated techniques to develop a completely new RF product line with specific research activities on new material engineering and RF characterization. More specifically, the targeted applications are primarily home-networking devices such as set-top boxes of various forms and sizes. Therefore, it is necessary to design antennas that can be industrially printed on flexible substrates such as paper or plastic materials.

Paper has the advantage of being a low cost and biosourced material. The ambition of the Stick’It project was also that the outstanding results can be exploited for other applications for which RF components integration and cost are key parameters. The IMEP-LaHC brings its strong experience of printed RF electronics on paper.

The other partners of the project are:

- Institut Mines-Télécom (IMT) Atlantique as the coordinator of the project, an academic higher education and research institute specialized in telecommunications technologies;
- Technicolor (THCR), a huge international telecommunications corporation;
- Technical Center of Paper (CTP), a big research center focusing on paper materials for various applications.

This work focuses on the antenna design on paper substrates in regards to the integrated electronics and the efficiency in a realistic environment. The antennas will be designed for the applications in Set-Top Boxes that are multi-standard, multi-frequency and with limited dimensions. Thus, the objectives of the thesis can be outlined as:

1. Characterization of electromagnetic properties of some flexible substrate materials such as PET, cardboard, various types of paper;
2. Simulation, optimization and design of antennas on a flexible substrate for the applications in Set-Top Boxes. For that, the antennas should be:
 - Low cost;

- Environmental friendly;
- Wide-band and/or multi-band to cover all frequencies of the Set-Top Boxes;
- Flexible, with the capability of bending to be placed in Set-Top Boxes with restricted dimensions;
- With possibility of mass production.

Besides, these antennas should have stable electromagnetic properties in our characterization process.

3. Prototyping and testing of radiation characteristics of the antennas;
4. Investigation of 3D/MIMO antenna systems with the proposed paper-based antennas that can be used in practice.

The manuscript is organized as follows:

Chapter 1 provides a bibliographic overview of antennas on flexible materials including paper substrates, overview of printing methods for flexible substrates, from that the choice of paper as well as the printing method is made. The overview of 3D and MIMO antennas is also introduced.

Chapter 2 shows the results of characterization of flexible substrate materials in its first section. Then the chapter dedicates to some designs of single band antennas on paper substrates, varied from simple CPW-fed antennas with adhesive paper to verify the results of electromagnetic property characterization of paper and PET, to screen-printed modified IFAs and SIW structures. Most of designs, except for the SIW cavity-back antennas, are tested by measurement.

Chapter 3 presents the design of the building block antenna components operating at multi- band as well as a wide band of frequency focusing on two WLAN bands in order to avoid using multiple single-band antennas that makes the systems too bulky. The proposed antennas are designed on 104- μm thickness E4D paper (E4D 100), apart from “Hello-shaped” presented in 3.2 and the multi-band in 3.3 that will be designed on the same paper E4D with 210- μm thickness (E4D 200) based on screen printing technique.

At last, Chapter 4 presents three-dimensional systems consisting of two orthogonal antennas in a rectangular acrylonitrile-butadiene-styrene (ABS) plastic box. The box in the first case is with sufficient dimensions where the antennas can be located in and their performance remains good. Further, the ABS box in the next sections has very restricted one of dimensions. The solution to bend an antenna under 90 degrees to place into this package is proposed and analyzed, then the systems with at least one bent antenna are studied.

1. Chapter 1 – State-of-the-art

1.1. Flexible substrate materials – Paper substrate and challenges

Together with the possibility of printing technologies, printed flexible electronics was developed intensively and becomes a familiar term nowadays, that put a milestone in electronics technology. Multiple applications benefits of printed electronics can be listed as follows [1]:

1. There are many examples of printed electronics including flexible displays for mobile devices and “electronic papers”. Printing is cost competitive comparing with the traditional vapor deposition as it can avoid much expenses for large vacuum chambers.
2. It is possible to integrate multiple components by printing them on the same press with much lower cost and less time consuming than traditional fabrication methods.
3. The capital investment cost for printing is much lower than other fabrication means [2].

In order to design flexible electronic circuits, it is critical to decide which substrate is suitable among numerous ones. It can be polyethylene terephthalate (PET), polyethylene-naphthalate (PEN), polyimide (PI), Polydimethylsiloxane (PDMS), foil, paper or some other substrates, each of them has advantages and disadvantages that affect performance of circuits and the applications.

The main requirements for flexible substrates are proper dielectric properties such as dielectric constant not too close to 1 and low loss tangent (for example, $\tan\delta = 0.017 - 0.025$ for FR4), good flexibility, dimensional and thermal stability, recycle ability, high quality planar surface, excellent solvent resistance and low cost. The choice of substrates is also affected by applications such as sensors, displays, RFID or antennas for other applications.

1.1.1. Traditional RF substrates for flexible electronics

Among the traditional substrates such as FR4, Teflon, Taconic or Rogers, some thin ones can be used for printed flexible electronics and antennas in particular. For instance, a wideband flexible CPW-fed bow-tie slot antenna with overall size of 60 mm × 80 mm for WLAN or WiMAX systems was designed on 0.2-mm-thick flexible Rogers RO4003C shown in [3]. Another CPW-fed antenna of quasi-Yagi type on 0.127-mm thick Rogers RT5880 was proposed by the authors from University of Arizona [4-5] that reached the gain of 5.76 dBi at the resonant frequency of 1.55 GHz. An example of 3D antenna on this type of substrate is an advanced four-arm conical spiral antenna by etching, cutting and wrapping the same substrate Rogers 0.127-mm thick RT/duroid® 5880 developed by

American Nucleonics [6]. Superior physical and electrical properties of Rogers materials enable us to design and fabricate antennas with stable characteristics. Its flexibility provided deforming without cracking, fracturing, loosening copper, or tendency to unwrap, assuring reliable, long-life performance of the antenna.

1.1.2. Kapton polyimide

This substrate material is popular for its high quality and low loss property. Many research groups have proposed antennas on this substrate such as the CPW-fed monopole antennas UWB with two resonant frequencies of 2.2 and 5.3 GHz [7] and dual-band of 2.45 GHz and 5.5 GHz [8], good candidates for wearable and flexible telemedicine systems and wireless body area networks (WBANs) applications. A WLAN dual-band antenna fully insulated with biocompatible 10- μm thick Parylene C film on 0.127-mm thick Kapton polyimide substrate, realized using microfabrication techniques [9] proposed by Y. H. Jung et al. can be used for implantable applications. IFA antennas on this type of substrate for biomedical [10] and laptop computer [11] applications are also good examples of this group of flexible antennas.

Antennas on standard flexible substrates or Kapton polyimide have stable characteristics and high efficiency, but they are not subject to printing techniques. Thus, the products on this substrate are expensive due to traditional fabrication (etching) methods.

1.1.3. Polydimethylsiloxane (PDMS) substrates

The Polydimethylsiloxane (PDMS) substrates, commonly referred as silicone, have also been mentioned in certain researches, as a flexible, stretchable, optical transparent and biocompatible material used mostly for medical applications or body-centric communications networks. PDMS substrates have permittivity in the range of 2.68 – 3 and the loss $\tan\delta = 0.02 - 0.04$ comparable to FR4 that are suitable for antenna and microwave circuit design. The authors in [12] developed processes for both the stable metallization of PDMS surface and the selective patterning of conductive elements. The surface treatment via the oxygen plasma ions significantly affects the adhesion of metal layers to the PDMS surface. A PDMS-based flexible and implantable micro electrode for the sub retinal prosthesis after gold electroplating is presented in [12].

A transparent flexible microstrip-fed UWB antenna was proposed by a research group from Rennes, France using transparent conductive fabric tissue on transparent PDMS substrate [13]. This antenna can be used for future wireless technology and 5G.

Another flexible structure example is a microstrip-fed monopole antenna, where the conductive fibers are embroidered on PDMS substrate [14]. The antenna is well matched in the frequency range 3.43 GHz – 11.1 GHz. Roy B. V. B. Simorangkir et al. introduced antenna structures on PDMS used for body-centric communications such as a simple dual-band microstrip antenna structure operating at 2.4 GHz and 5.8 GHz using NCS95R-CR conductive fabric from Marktek Inc. [15] or a frequency-reconfigurable antenna with two varactors with the same NCS95R-CR conductive fabric [16]. Zhi Hao Jiang et al. proposed a PDMS-based circularly polarized antenna with AgNWs ink for Wireless Body-Area Networks applications [17].

The electromagnetic properties of PDMS are suitable for antenna and microwave circuit design. Moreover, these substrates are flexible, optical transparent and biocompatible, compatible for many applications. However, these substrates do not allow using direct-writing method for metal deposition causing some difficulties for low cost mass production.

1.1.4. Textile substrates

Antennas or electronic circuits designed on textile substrates can be integrated in clothes to be used for wearable and biomedical applications. The properties of these substrates for flexible electronics and antennas have been given in [18, 19].

Table 1.1 provides dielectric properties of some normal textile fabrics [18], where it can be seen a very narrow range of their permittivity, from 1.22 to 2.12, and their loss tangent is rather low (0.01 – 0.05) caused by the fact, that the materials are porous and filled by air.

Some popular methods of metal deposition on these substrates are such as using liquid textile adhesive, conductive spray technique, method of sewing, layered sheets by ironing and copper tape method. Besides, screen printing and inkjet printing methods can also be applied.

Many publications have been made on this issue including various antennas and electronic components designed on textile fabrics, among them just some selected ones are presented in this sub-section [20-31].

Frequency selective surfaces (FSS) are widely used in antenna design for various purposes such as gain enhancement or bandwidth improvement. FSS with the periodic structure using copper etched on an electro-textile [20] operating as a filter with a band stop between 10 and 12 GHz, can be used in on-body communications applications. Another periodic structure operating at millimeter-wave frequencies is presented in [21].

Table 1.1. Dielectric properties of some normal textile fabrics [18].

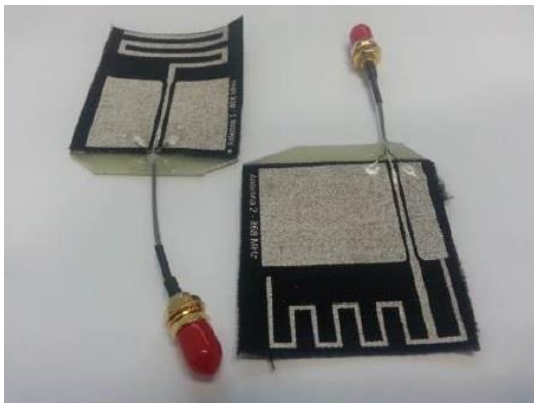
Non-conductive Fabric	ϵ_{r1}	tan δ
Felt	1.22	0.016
Cordura®	1.90	0.0098
Cotton	1.60	0.0400
100% Polyester	1.90	0.0045
Quartzel®Fabric	1.95	0.0004
Cordura/Lycra®	1.50	0.0093
Silk	1.75	0.012
Tween	1.69	0.0084
Panama	2.12	0.05
Jeans	1.7	0.025
Moleskin	1.45	0.05

Jingni Zhong et al. [22] proposed a spiral antenna with conductive textile threads on high-strength Kevlar fabric. This textile spiral exhibits a good bandwidth 0.3 GHz – 3 GHz with circularly polarized gain of 6.5 dBi across the 1 GHz – 3 GHz bandwidth. Another example of textile antennas is a patch antenna with transformer based on textile materials and operating in the frequency band 2.4–2.4835 GHz designed by the authors from University of Perugia, Italy [23-24]. In [25], the authors compared three Bluetooth microstrip-fed rectangular patch antennas designed on various textile materials, Goch, jean and leather for wearable applications and found, that in term of fabrication and performance, the leather textile material is the best choice.

A direct-write process such as inkjet printing can also be applied on this type of substrate [26] where the authors tested to print smart fabric electronic components including transistors, capacitors and antennas.

Screen printing method has been used to fabricate an UHF RFID antenna operating at 868 MHz for integration in a firefighter suit [27]. The meander line manufactured antennas and their application example on a suit are shown in Figure 1.1.

The substrate-integrated waveguide (SIW) technology has also been studied for the antenna structures with embroidered vias [28-31]. For example, a folded rectangular half-mode SIW cavity-backed antenna with a shielded stripline feed has been designed for 2.45 GHz ISM band [29]. A SIW-based two-element MIMO antenna system on textile has been proposed in [31] for WiFi 2.4/5.2/5.8 GHz.



(a)



(b)

Figure 1.1. (a) Fabricated prototypes of screen printed planar antennas on textile substrate; (b) Screen printed antenna integrated into firefighter suit [27].

Textile substrates are very convenient for wearable and biomedical applications. However, due to their porosity and compressibility, it is difficult to control their thickness under low pressure. Moreover, as most of antennas designed on these substrates are to be integrated in clothes, they can get wet because of human sweat so that the dielectric properties of the tissue change, that affects radiation characteristics of antennas.

1.1.5. Plastic materials

Flexible Plastic materials such as polyethylene terephthalate (PET), polyethylenenaphthalate (PEN), plastic insulating films are the potential candidates for various applications. Particularly, PET is popular for applications requiring high degree of bendability and transparency. The dielectric properties of plastic substrates PET and PEN are given in Table 1.2.

Antennas designed and printed on PET have been studied by various research groups. K. N. Paracha et al. from Malaysia, Saudi Arabia and Australia proposed a 2.45-GHz ISM band CPW-fed Z-shape antenna on PET realized by an office printer [32]. The antenna was found to have good performance, matched well at the resonant frequency, omni-directional with the maximum gain of 1.44 dBi and more than 60% radiation efficiency.

A wideband (7.7 GHz – 8.3 GHz) circularly polarized microstrip patch array antenna 4×4 designed and fabricated on PET by the authors from San Diego State University [33] reached over 15 dBi gain and over 75% radiation efficiency over all designed band. In [34-35], the authors studied

inkjet-printed 20-GHz CPW-fed monopole antennas on two types of flexible substrates, 140- μm thick PET with $\epsilon_r = 3.4$, $\tan\delta = 0.01$ and 700- μm thick Epson paper with $\epsilon_r = 4.2$, $\tan\delta = 0.01$ and found, that the spacing between silver nano-particle ink drops (drop spacing) had a strong effect on antenna performance. For a drop spacing of 30 μm the antenna performance was the best with 96% radiation efficiency for PET and 77% for Epson paper that is much thicker than PET.

The group of authors M. Barahona, D. Betancourt, and F. Ellinger designed UWB chipless tags on PET and bond paper and fabricated using screen printing with different inks: copper, aluminum and silver in order to compare them [36]. It was shown, that using these metallic inks is possible to obtain the desired RF characteristics and one can choose to reduce the cost of fabrication.

Certainly, flexible plastic substrates have low cost, lower loss ($\tan\delta \approx 0.005$) than some other flexible materials, a good choice for antenna flexible substrates. However, after printing, a heat treatment process is applied under high temperature that is needed to control strictly as polyester may start to shrink strongly. Thus, the authors of [36] used an inkjet printing process with a low cost printer and self-sintering conductive ink to fabricate an RFID antenna on PET. This substrate is biocompatible for wearable epidermal RFID application.

1.1.6. Paper materials

Recently, paper has been found as a solution for ultra-low cost flexible electronics substrate that enables direct write with better quality than polyester and facilitates mass fabrication process [37].

For communications system applications using paper as a material has many advantages listed as follows:

- First of all, paper as an organic-based substrate, is available world-wide. The increasing demand for mass production makes paper the best candidate for printed flexible electronics substrate.
- Paper usually has low surface profile and is suitable for direct write fabrication methods instead of the traditional metal etching techniques. A fast realization process, like inkjet printing or screen printing, which is discussed in more details in Section 1.3, can be used efficiently to print electronics on/in paper substrates.
- Paper is ecologically friendly materials and is suitable for “green” RF electronics and modules.

However, using paper substrates is also challenging for the following reasons:

- Paper substrates usually possess higher loss than many other flexible substrate materials;
- The knowledge of the dielectric properties such as dielectric constant (ϵ_r) and loss tangent ($\tan\delta$) is necessary for the design of any high frequency structures such as antennas on the paper substrate, and more importantly, if it is to be embedded inside the substrate. For paper, because of its small thickness and non-homogeneity, the process of RF characterization is difficult to be performed with high accuracy. The methods for high-frequency dielectric characterization of materials are described in Appendix 1.
- The cost for printing inks is still high due to its nano-particle fabrication technology;
- In order to benefit the advantage of their flexibilities, thin papers are usually used that leads to difficulties of designing CPW feed line with very narrow slots;
- Printing quality needs to be controlled properly;
- As paper substrates are very fragile, the interconnection remains a real issue.

Besides, some technological problems also exist and need to be solved. The fluid/ substrate interactions are also an issue including inertial spreading of ink droplets, absorption of a droplet on another one leading to non-smoothness of a metallic layer and evaporation of the ink liquids [38]. The registration of successive layers is another problem to be faced, particularly as substrates such as paper tend to swell, cockle and shrink during the printing and drying process. Finally, there is the issue of de-inking for paper recycling.

Types and properties of paper

Paper is fabricated by a process of dehydration, filtration, pressing and heating cellulose fibers. There are many types of paper that can be classified by various categories such as their applications (photocopy paper, paper for press as magazines or newspapers, printing and writing paper, wrapping paper, cardboard for different boxes, hygiene paper, etc.), their fabrication and treatment methods (paper with big proportion of wood, paper made of chemical pulp without wood, full paper that is very absorbent, coated paper consisting of multiple layers to improve its printing quality, etc.).

The properties of paper substrates can vary depending on their structure and composition. With the right set of additives and manufacturing processes, a paper substrate can reach a very wide range of properties. It can be hydrophilic or hydrophobic, porous or waterproof, opaque or translucent, rigid or

soft, fragile or solid, rough or smooth like glass. For example, by adding some paper textiles, we can easily solve any moisture absorption problems.

The choice of paper materials is made based on their sensitivity to humidity, their roughness, low barriers to gases and water vapor and transparency. The paper materials have great advantages, but in certain cases they can also be restrictive for printed electronics. However, they can be adapted if the nature of their fibers, fillers and other compounds is properly chosen and the surface is well globally or locally treated.

Note also that the paper substrates are conformable (folding memory), low cost (PET: about 6 €/ kg, Paper: 1 €/ kg) and that these materials have a better dimensional stability at high temperature than the PET or PEN generally used. In fact, at the thermal level, the dimensional stability of the substrate is important with respect to the temperature for conditions of use of the electronics (temperature resistance, the dissipation of a power element for example, etc.) but also during its manufacturing process. In certain cases it is necessary to carry out drying operations or even annealing at high temperature of one or more inks. In this case the substrate must not deform, at the risk of micro cracks appearance. Typically, a paper can withstand temperatures of about 140°C for a few seconds. It is also known that the dimensional stability of paper at temperature is higher than that of plastics.

Considering their electromagnetic properties, the dielectric constant of dry paper substrates is typically in the range of 2 – 5 (up to 20 GHz), which is lower than that of dry cellulose ($\approx 6 - 8$). These lower values ϵ_r of the paper are due to its porosity and the low dielectric constant of the air (≈ 1). The loss tangent of paper is in the range of 0.04 – 0.1 (up to 20 GHz). So the paper substrates have acceptable electrical performance up to 24 GHz [39].

Table 1.2 shows the electromagnetic, recycling ability and flexibility properties of some typical flexible substrate materials.

The typical requirement for very smooth and non-absorbent substrates for printed electronic components is a significant problem when considering the use of paper. Therefore, the raw paper surface was coated with different functional coatings by the Papiertechnische Stiftung (PTS) Munich at the pilot coating machine Vestra, then smoothness was adjusted by glazing before and/or after coating [39].

Finally, the studies of life cycle analysis of products in paper-based printed electronics show that their environmental impact is infinitely less than the same functionality in traditional electronics or in electronics printed on plastic substrates.

Table 1.2. Properties of some typical flexible substrate materials.

Substrate	ϵ_r (at up to 20 GHz)	$\tan\delta$ (at up to 20 GHz)	Recycling ability	Flexibility	Cost
Rogers RT5880 (thin)	2.2 ± 0.02	0.0009	No	Yes	High
Kapton polyimide	3.4	0.002	No	Yes	Medium
PDMS	2.68 – 3	0.02 – 0.04	No	Yes	Medium
Textile	1.22 – 2.12	0.0004 – 0.0098	Yes	Yes	Low
PET, PEN	3.2 – 3.5	0.015 – 0.02	Yes	Yes	Low
Paper	2 – 5	0.04 – 0.1	Yes	Yes	Very low

The most important parameters that characterize paper properties for printed electronics applications are the proper dielectric properties such as dielectric constant (ϵ_r) that must not be too close to 1 and loss tangent ($\tan\delta$) less than 0.1.

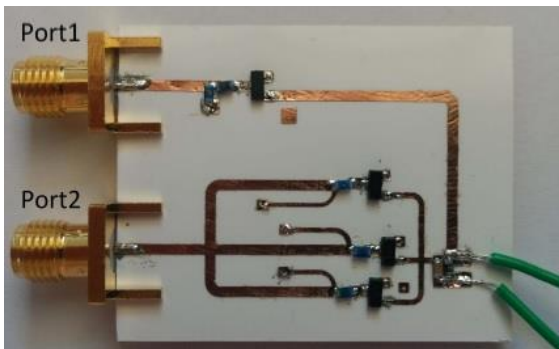


Figure 1.2. A chipless RFID tag on paper substrate [43].

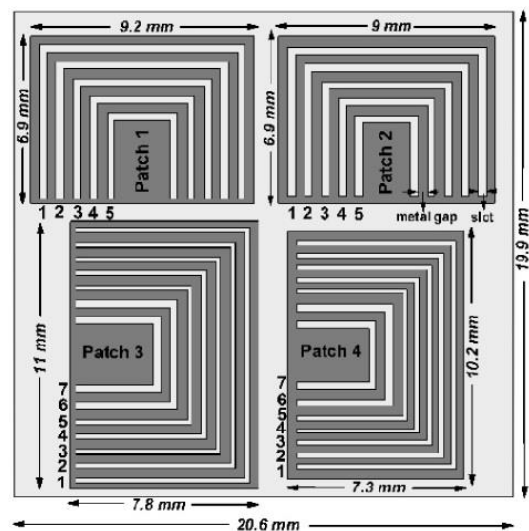


Figure 1.3. Moisture sensor tag for intelligent packaging [44].

Despite all challenges, research on paper substrates for flexible electronics is still an attractive tendency thanks to its wide availability and low cost. Some inkjet-printed RF components and systems on paper substrate can be listed as a high-Q inductor with ferromagnetic nanomaterial for printed flexible and wearable filters, resonators, and microwave matching networks [40], low-voltage In-Zn-O thin film transistor on paper substrate proposed by J. Jiang et al. that is a potential candidate for flexible paper electronics applications [41]. In order to shield GSM signals, the research group from Nadar College of Engineering, India introduced a frequency selective surface on 0.5-mm paper operating at two frequencies 930 MHz and 1720 MHz [42]. An RF harvesting rectifier [43] on 0.37-mm thick paper substrate designed to operate in all recently released LTE bands (range 0.79–0.96 GHz, 1.71–2.17 GHz and 2.5–2.69 GHz) or a paper-based tag (Figure 1.2) for near-field chipless-RFID systems presented by a Spanish research group [44] and another chipless RFID tag on 0.25-mm thick HP photo paper (Figure 1.3) used as a moisture sensor tag [45] for intelligent packaging are also good examples for paper-based flexible electronics.

1.1.7. Other substrate materials

Apart from the above mentioned substrates, there are also other ones that can be used in flexible electronics such as LCP (liquide crystalline polymer) [46], semiconductor [47-49], silicone elastomer [50], NinjaFlex 3-D printable material and natural rubber [51].

After considering various dielectric materials for flexible electronics, paper substrate was found to be the most suitable for our needs for a substrate material that is flexible, low cost, with acceptable RF properties (ϵ_r is not too close to 1 even though $\tan\delta$ is much more than that for FR4), recycling ability, and especially ability to make 3D structures.

The following section will present the printing technologies on flexible, including paper substrates.

1.2. Printing technologies for flexible electronics

1.2.1. Conductive inks used for printed flexible electronics

1.2.1.1. Metal-based inks

Silver (Ag) is the most widely used metal in conductive inks. Its main advantage is high conductivity in both non-oxide and oxide states. It is an interesting feature for applications requiring a long life

period. Nevertheless, its high cost may affect certain economic models (about 1000 € / kg, to reduce however to the small quantities printed by unit of surface).

Ink particles have several forms, spherical or non spherical. Their size goes from the nanometer sizes, mainly for the inkjet (cost 3 to 4 times higher), to microns for more robust processes. Recently, formulations based on Ag metal wires have emerged to create networks and replace transparent conductive planes.

For some applications, copper-based formulations have been and are still being developed. Their theoretical intrinsic conductivity is nearly equivalent to Ag. However, in practice, the main problem is the oxidation of copper that then becomes non-conductive, which makes this ink very sensitive to oxygen in general. Some formulations of Cu coated by Ag are being developed, and could be interesting alternatives in terms of performance/cost ratio.

Finally, other materials apparent to metals are also used, such as the family of oxides (ZnO in particular).

1.2.1.2. Organic polymer-based inks

These inks are used when the desired conductivity is not very important. Or in comparison, their resistivity is of the order of $1000\mu\Omega\cdot\text{cm}$, whereas the metal inks are of the order of a few $\mu\Omega\cdot\text{cm}$. The most commonly used organic polymers, doped or otherwise, are polythiophene (PTs), polyaniline (PANI) or polypyrrole (PPy). They may be used, in some cases, to replace transparent conductive deposits such as ITO or ZnO, or as a resistive ink.

These polymer inks are also found in a mixture with materials such as carbon nanotubes, which allows improving the conductivity. With an intrinsic conductivity about 12 times less, carbon is a material that is also used, but for "resistive" applications.

1.2.2. Printing techniques on flexible substrates

As mentioned in the first section of this chapter, printing is cost competitive comparing with the traditional vapor deposition. The comprehensive overview of printing technologies on various flexible electronics substrates is given in Figure 1.4 [52] where the non-contact printing techniques have become more popular thanks to their simplicity, affordability, high speed, adaptability to the fabrication process, high resolution and easy control. Besides, recently, other printing methods such as nano imprinting, micro-contact printing or dry transfer printing have also become attractive, especially for inorganic mono-crystalline semiconductor flexible substrates.

1.2.1.1. Inkjet printing method

Inkjet printing is a direct writing method with metallic solution deposition on a substrate. Based on ink delivery mechanism, an inkjet printer may operate in a continuous or drop-on-demand (DOD) mode [52-55], where droplets in the continuous mode are ejected through a nozzle head by a periodic perturbation. In DOD mode, drops are dispensed from an ink reservoir according to pulses controlled by a thermal or piezoelectric actuator. This DOD mode is more usable as it is more accurate and reduces the amount of ink in the printing process.

Another effective approach that is less time-consuming and low cost, therefore can be used in industry, is screen printing method.

1.2.1.1. Screen printing method

This technique is the most popular and mature technology that can be used for industrial mass production of flexible electronics [53].

A simple screen printer consists of screen, squeegee, press bed and substrate [52], where the ink is spread to the substrate through the screen by means of the squeegee. This printing technique gives good thickness of the metal (3 – 30 μm) with good conductivity of 1.7×10^6 S/m in our experiment without repetitive printing multiple layers so is less time-consuming than inkjet printing. Screen printing has demonstrated its feasibility through a number of printed electronic components such as sensors, multi-layer active devices and circuits.

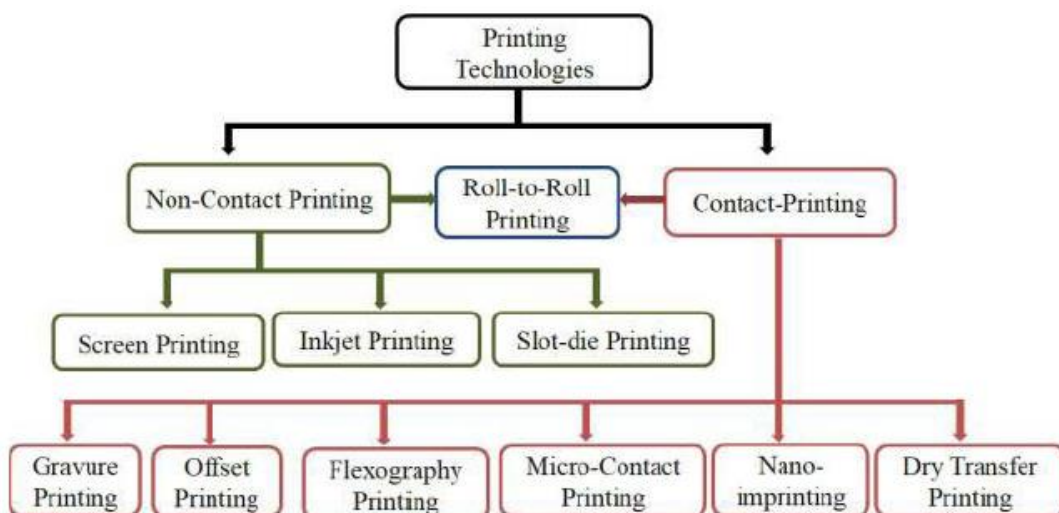


Figure 1.4. Classification of printing techniques [52].

1.2.1.2. Slot-die printing

In a slot die printing process, the solution is poured from top through a via-opening and a substrate mounted on a rotating cylinder [52]. This type of printing is favorable for large areas, but patterning of high resolution structures is difficult to obtain so that it is not suitable for antennas with small dimensions.

1.2.1.3. Gravure printing

Gravure printing is a contact printing technique that supplies inks through physical contact of the engraved structures with the substrate. The scheme of a gravure printer has been presented in [52], where ink is delivered from a nozzle dispenser, then transferred to a capillary to the substrate. The doctor blade removes extra ink from the gravure cylinder. It is capable to produce high quality patterns on a flexible substrate. However, this technique cannot produce uniform structures with sharp edge pattern lines, and it is needed to replace gravure cylinders after continuous use in roll-to-roll system that increases the maintenance cost of the printing technology.

1.2.1.4. Gravure-offset printing

Gravure-offset printing or offset printing is an advanced version of gravure printing. In this system, an extra elastic blanket is used to avoid damages to the cylinder due to direct contact with the substrate [52, 53]. However, this technique has the same problem of printing resolution as well as the previous gravure method.

1.2.1.5. Flexographic printing

Flexographic printing is used for high speed runs of printed electronics and is more attractive than gravure and offset for high resolution patterns [52]. A wide variety of ink (solvent-based, water-based, electron-beam curing inks, UV curing inks and two part chemically curing inks etc.) can be used for flexographic printing. The main weakness of flexography is high roughness of the printed layer surface causing errors in realization of electronic circuits.

1.2.1.6. Micro-contact printing

Micro-contact printing is a form of lithography based on relief patterns on a master PDMS stamp to form patterns of inks on the surface of a substrate [52, 53]. One of the challenges of this technique is that deformation of PDMS stamps due to their elasticity can lead to distorted printed patterns.

1.2.1.7. Nano-imprinting lithography

This printing technique creates patterns by mechanical deformation of an imprint resist, a monomer or polymer formulation cured by heat or UV light during the imprinting [52], and subsequent processes. During the process, the adhesion between the resist and the template is properly controlled. Using this technology for flexible electronics is still challenging and being studied today.

1.2.1.8. Dry transfer printing

This printing technique uses dry transfers, decals that can be applied without water or solvent. This technique is usually used on semiconductor substrates.

A brief summary of all printing method mentioned above is given in Table 1.3.

Table 1.3. Comparison of printing methods.

Printing method	Substrate	Thickness of printed metallic layer, μm	Resolution, μm	Comments
Gravure printing	Printing and writing paper, Polymer film, not for fragile substrates	0.1 – 12	15 – 75	- Unable to produce uniform structures with sharp edge pattern lines. - The gravure cylinders need to be replaced frequently.
Gravure-offset printing	Paper, Polymer film	0.5 – 2	20 – 50	- Fast rolling speed and non-uniform structure causes the wave-like edges of printed patterns and blank areas. - The blanket is absorbed continuously by the solvent that reduces ink viscosity and affects the printed patterns.
Flexography	Paper/cardboard,	0.5 – 8	40 – 80	- High roughness of the

printing	Polymer film, glass, metal, applicable for fragile substrates			printed layer surface, especially at line edges causing errors in realization of electronic circuits.
Slot-die printing	All substrates	0.15 – 60	200	- Bad resolution of printed patterns.
Screen printing	All substrates	3 – 30	50 – 100	- Good thickness of metal layer. - Limited resolution. - Suitable for mass production.
Inkjet printing	All substrates	0.01 – 1	15 – 100	- Very thin metallic ink layer. - Multiple printing layers need to be made. - Time consuming and high cost.
Microcontact/ nano-imprint	All substrates	0.18 – 0.7	1 – 20	- Deformation of PDMS stamps due to their elasticity can lead to distorted printed patterns.
Transfer printing	Semiconductor substrates	0.23 – 2.5	4 – 50	- Needs to process in a clean room. - Complexity, requires multiple steps.

The printing technology for paper substrates should give a thick enough conductive layer, at least 3 μm , with good conductivity. Besides, it must be subject to industrialization processes.

Among those listed methods, it is seen, that many of them can give good thickness of conductive layer, such as gravure printing, flexography, slot-die printing and screen printing. However, gravure printing cannot produce uniform structures with sharp edge pattern lines, slot-die printing has bad

resolution, flexography give too rough printed layer surface. In fact, the inkjet printing and screen printing are the most popular for paper substrates thanks to their low cost, acceptable precision. However, screen printing was chosen for our project as it gives good thickness of the metal (3 – 10 μm) with good conductivity of 1.7×10^6 S/m without repetitive printing multiple layers. Therefore, this technique is suitable for future mass production with big product series.

1.3. Antennas on paper substrates: two-dimensional structures

In the previous sections, some aspects of flexible, especially paper substrates and printing techniques were presented to validate the possibilities of using them as substrates for antenna design. It is known, that antennas on flexible substrates have high level of bendability that can facilitate packaging problems. Now we will overview some existing antennas from previous studies of different research groups.

1.3.1. Paper-based antennas using adhesive metal tapes

In this fabrication method, the shape of designed antennas is formed on a copper tape that is to be glued on paper substrate. The thickness of copper layer is usually about 0.35 mm. An example is the RF harvesting rectifier [43] on 0.37-mm thick paper substrate designed to operate in all recently released LTE bands (range 0.79 – 0.96 GHz, 1.71 – 2.17 GHz and 2.5 – 2.69 GHz).

A paper-based microstrip-fed monopole antenna and a 2×2 array based on it (Figure 1.5) and other circuits such as oscillator, mixer, matching network were made by gluing copper tape on 0.23-mm thick paper after etching [56]. The operating frequency of these circuits is 24 GHz.

Some years ago, a research group at University of Pavia, Italy proposed an antenna structure based on the Substrate-Integrated Waveguide (SIW), one of Substrate Integrated Circuits (SIC) topologies, designed on paper substrate (Figure 1.6) [57]. In order to fabricate this antenna, first of all, before making via holes, the authors glued aluminium foils on two faces of a sheet of paper with the thickness of 0.5 mm. However, due to high losses of the substrate, the antenna efficiency is very low, causing low realized gain.

H. Shah from M. Tentzeris' research group at Georgia Institute of Technology has worked on a version of a circular polarized origami antenna, that was realized by gluing adhesive copper tape on 0.25-mm thick paper before folding (Figure 1.7). This antenna operates over the bandwidth of 2.4 GHz – 5 GHz [58].

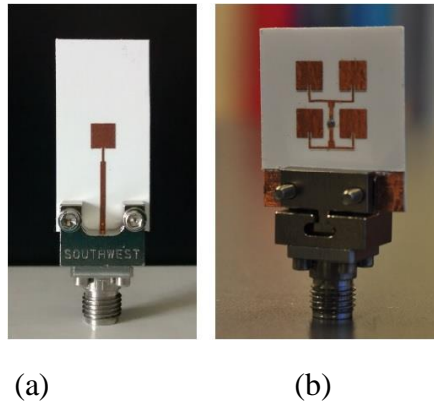


Figure 1.5. (a) Single monopole and (b) antenna array with copper tape [56].

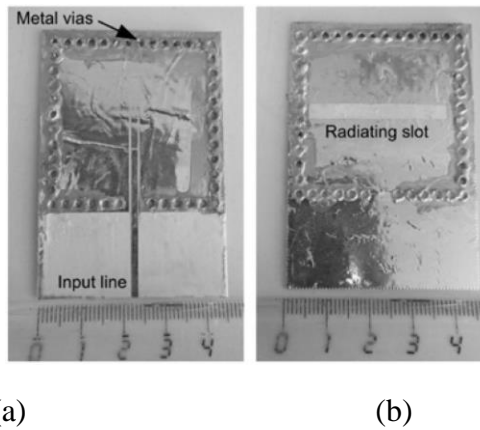


Figure 1.6. Cavity-backed SIW antenna on paper substrate [57]: (a) Front side with microstrip feeding line; (b) Back side with radiating slot.

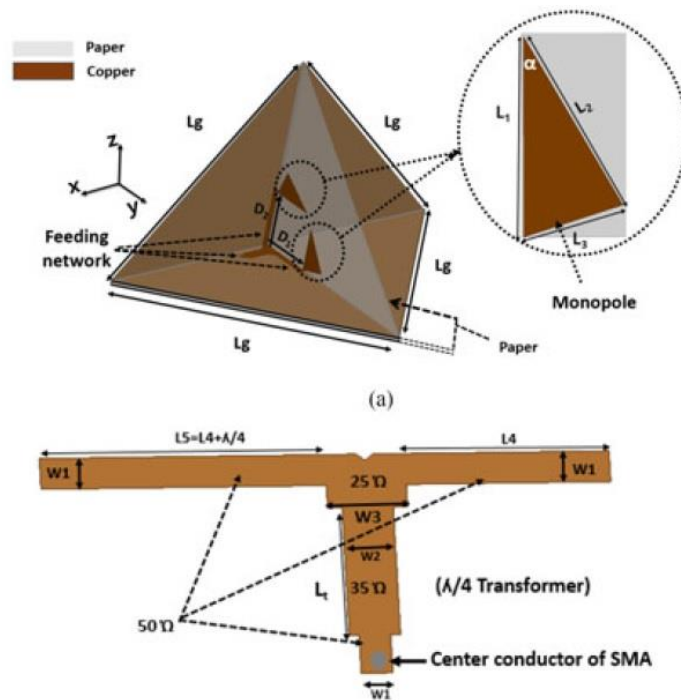


Figure 1.7. Geometry of CP origami antenna [58]: (a) Circularly polarized origami antenna structure; (b) Feeding network.

1.3.2. Inkjet-printed antennas

The inkjet printing on paper method is chosen by many antenna research groups.

M. Tentzeris' research group from Georgia Institute of Technology, Atlanta has been one of the most active in studying flexible antennas on paper substrates using inkjet-printing technology [59-61]. An inkjet-printed CPW-fed UWB antenna on 254- μm thick paper with permittivity ϵ_r in the range of 3 – 3.4 and rather low dielectric loss tangent of 0.06 – 0.07 with good matching characteristics (Figure 1.8) was depicted in [59]. An RFID tag presented in [59] designed on 0.2-mm thick paper (Figure 1.9) was also fabricated by inkjet printing method. A special connection between an RFID dipole on 0.26-mm thickness paper substrate and a CMOS Si chip was shown in Figure 1.10 based on a magnetic coupling transformer [61].

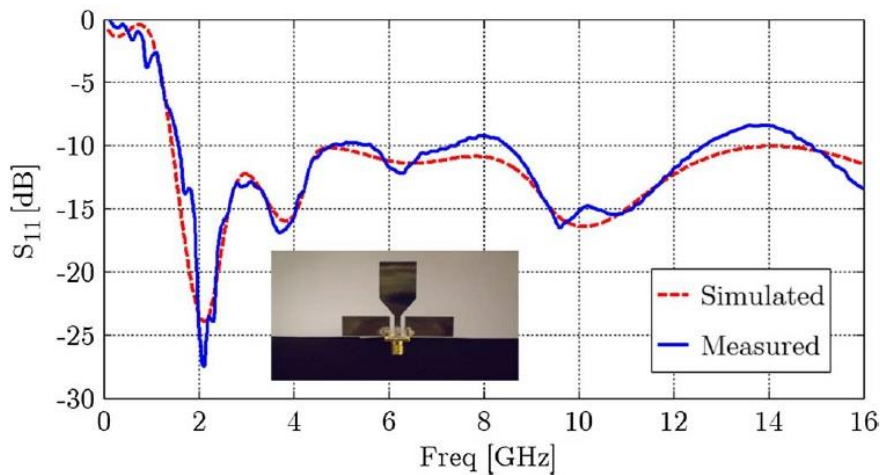


Figure 1.8. Simulated and measured performance of the CPW-fed monopole in [59].

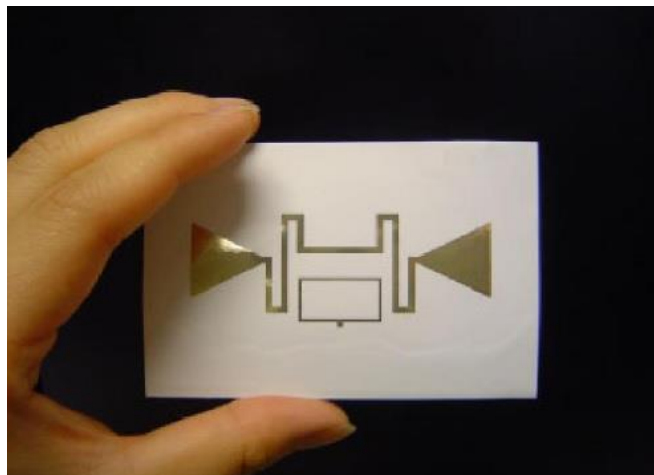


Figure 1.9. Inkjet-printed dipole for UHF RFID tag [60].

Atif Shamim's group of researchers from KAUST, Saudi Arabia also studies intensively this attractive subject [63-65], presenting a high gain antenna on a frequency selective surface (Figure 1.11) [63], high gain Vivaldi antenna (Figure 1.12) [63] on lossy paper substrate with $\tan\delta = 0.06$ and a multiband antenna for curved wireless devices (Figure 1.13) [64].

However, the thickness of a printed layer is small, about 0.01 0.5 μm , with a resistivity of about 23 $\mu\Omega\cdot\text{cm}$, so that it is necessary to print multiple layers to achieve a relatively thick pattern [52]. In addition, a sintering process after printing also takes a lot of time, and regardless the technique of using self-sintering conductive ink, the need for printing several layers makes this technique less practical. Because of these inconveniences, inkjet printing is popular for only prototyping.

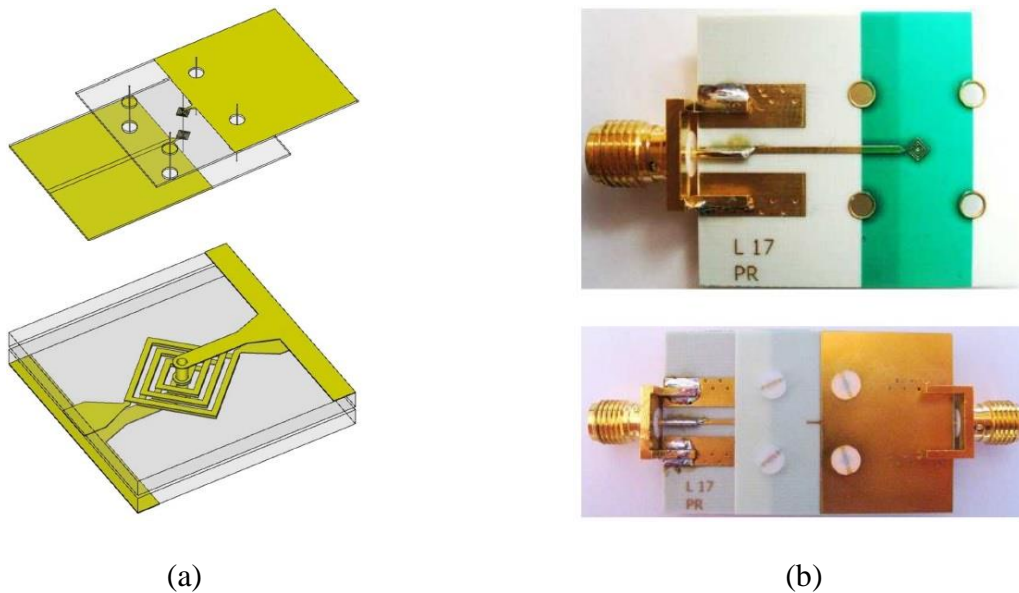


Figure 1.10. Connection between an RFID dipole on paper substrate and a CMOS Si chip [60]: (a) Mechanical drawing of the PCB test-fixture and zoom of its central zone with a highlight of the transformer structure; (b) Realization of the system.

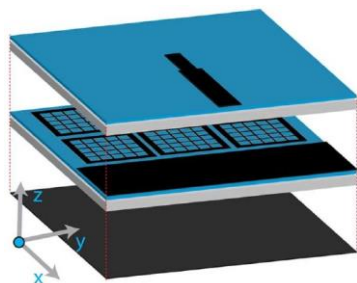


Figure 1.11. Paper-based high gain antenna with AMC structure [62].

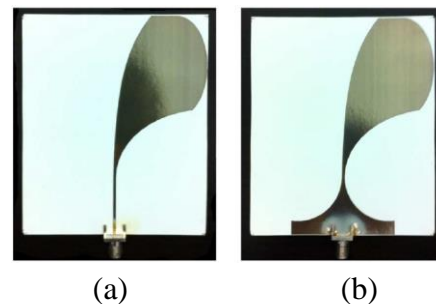


Figure 1.12. Antipodal Vivaldi antenna: (a) front; and (b) back sides [63].

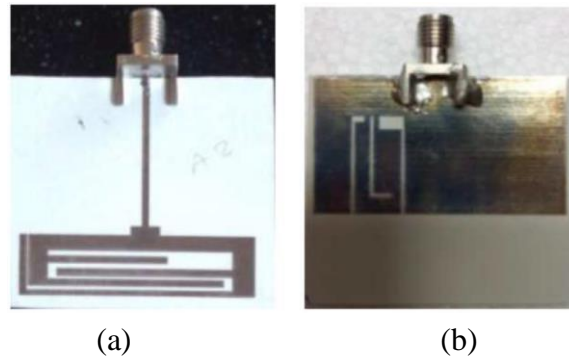


Figure 1.13. Multiband antenna for curved wireless devices: (a) front and (b) back sides [65].

D. E. Anagnostou et al. [66] used 250- μm thick paper with $\epsilon_r \approx 3.4$ and $\tan\delta \approx 0.065$ at 2.45 GHz to design and fabricate an inverted-F antenna at this frequency for WLAN application and flexible display (Figure 1.14).

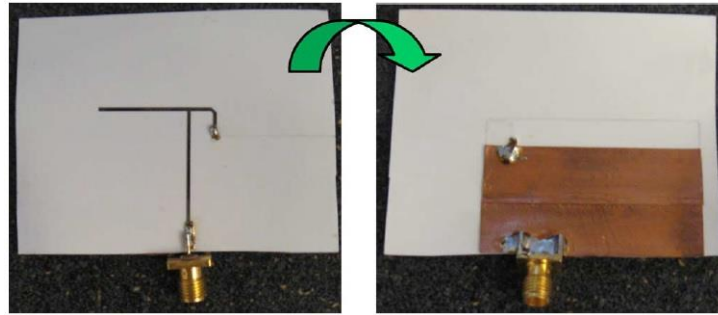


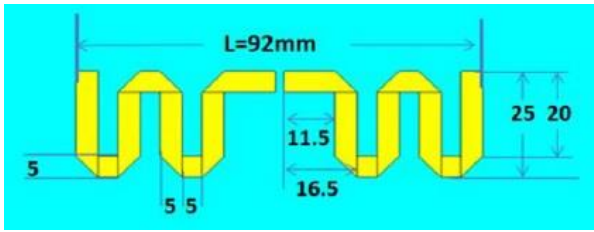
Figure 1.14. IFA proposed by D. E. Anagnostou et al., front and back [66].

1.3.3. Screen-printed antennas

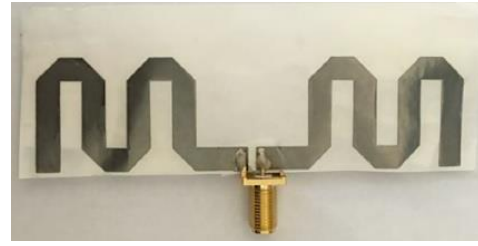
As mentioned above, screen printing technique can be used in mass production as it gives good thickness of the metal (3 – 30 μm) with good conductivity of 1.7×10^6 S/m without repetitive printing multiple layers so is less time-consuming than inkjet printing. The description in more details of this technique with some printed antennas is presented in [67].

Recently, an UHF RFID dipole antenna screen printed by high-conductivity graphene conductive ink on paper substrate has been proposed in [68] (Figure 1.15). The antenna is matched well in the bandwidth range from 968 MHz to 1042 MHz, has omni-directional radiation patterns, high bendability and can be used for low cost RFID tag applications.

The other authors have also proposed screen printed RFID tag dipoles on paper illustrated in [68, 69]. Especially, an antenna introduced in [70] has been designed and fabricated for RFID readers that can considerably reduce the cost of the RFID system.



(a)



(b)

Figure 1.15. Meandered-line dipole antenna structure [68]: (a) Antenna geometries; (b) Printed prototype.

In [71] the circuits were designed and realized using screen printing on plastic substrates, such as 125- μm thick ST506 PET, 100- μm thick Arron transparency, 50- μm thick Mylar A PET, and paper substrates such as 105- μm thick 4CC paper, 80 g/m^2 copy paper and 75- μm thick glossed paper to study the effects of the conductive material on the printed line bending reliability. Some examples of antennas on paper substrates classified by methods of deposition of metal stated above are given in Table 1.4.

Antennas on paper substrates have promising perspectives due to their amazing properties such as low cost, light weight, bendability. Even though the first researches paper-based antennas appeared in publications in 2000's, but this topic is still attractive nowadays.

1.4. Three-dimensional antennas

One of the important advantages of flexible antennas is the capability of making three-dimensional structures, where a good example is the origami antenna mentioned above [58]. Besides, many other 3D antenna structures have been presented in publications for the last decades. In Table 1.5, some examples for 3D antennas, from the bent structures to the systems created by installing antennas on 3D frames are provided, classified by the printing methods.

1.5. MIMO antennas

In this thesis, some MIMO structures consisting of our proposed paper-based antennas will be presented in Chapter 4. Therefore, in this sub-section, first of all, a brief introduction of MIMO systems will be given. Then, an overview of MIMO antennas on both rigid and flexible substrates will

be done and at last, we summarize decoupling techniques for reduction of mutual coupling between antennas in a MIMO system.

1.5.1. MIMO technique

Multiple-input–multiple-output (MIMO) wireless systems use multiple antenna elements at transmit and receive to improve capacity over single antenna topologies in multipath channels. Such systems operate by exploiting the spatial properties of the multipath channel, thereby offering a new dimension which can be used to enable enhanced communication performance [91 (Jensen, 2004)]. A block diagram of a MIMO system is illustrated in Figure 1.16.

While coding and signal processing are key elements to successful implementation of a MIMO system, the propagation channel and antenna design represent major parameters that ultimately impact system performance. As a result, considerable research has been devoted recently to these two areas. For example, assessing the potential of MIMO systems requires a new level of understanding concerning multipath channel characteristics. Furthermore, while we have extensive information concerning the behavior of antenna diversity in multipath channels, recent activity surrounding MIMO communications has exposed new issues related to the impact of antenna properties and array configuration on system performance.

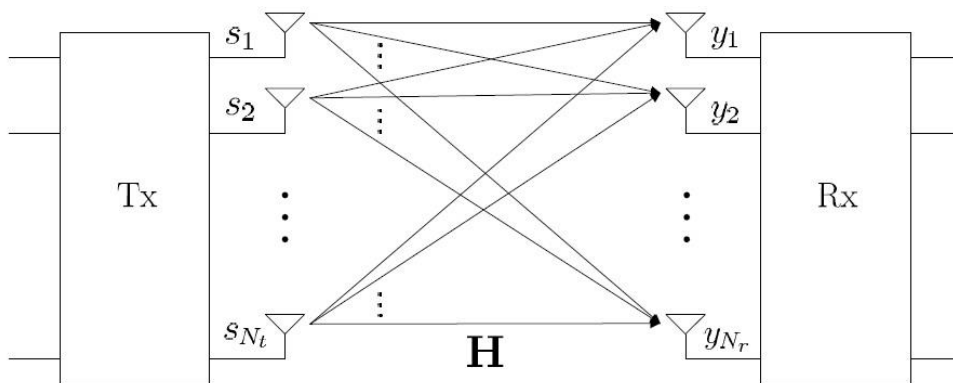


Figure 1.16. Block diagram of a MIMO system [90 (Jensen, 2004)].

For a multiple-input–multiple-output (MIMO) system, there are M number of transmit antennas and N number of receiving antennas, the wireless channel can be written as an $M \times N$ matrix with random independent elements, expressed as H . The capacity of a MIMO channel without any prior transmit information is

$$C = BW \cdot \log_2(1 + M \cdot N \cdot \text{SNR}) \quad (1.1)$$

where C is the channel capacity in bits/s, and SNR represent the received signal to noise power ratio. The noise mentioned here is additive white Gaussian noise (AWGN).

Thus, the capacity can be improved by making M and $N > 1$.

One of the important parameters of a MIMO antenna system is Envelope Correlation Coefficient (ECC) that is given by [91 (Jensen, 2004)]:

$$\rho_e = \frac{\left| \iint_{4\pi} [\bar{F}_1(\theta, \varphi) * \bar{F}_2(\theta, \varphi)] d\Omega \right|^2}{\iint_{4\pi} |\bar{F}_1(\theta, \varphi)|^2 d\Omega \cdot \iint_{4\pi} |\bar{F}_2(\theta, \varphi)|^2 d\Omega} \quad (1.2)$$

where $\bar{F}_i(\theta, \varphi)$ is three-dimensional radiation pattern when i -port is excited, Ω is the solid angle. In the case of lossless and single-mode antennas, the ECC can be calculated using S-parameters as follows:

$$\rho_{eij} = \frac{\left| S_{ij}^* S_{ii} - S_{ji}^* S_{jj} \right|^2}{\sqrt{\left(1 - |S_{ii}|^2 - |S_{ji}|^2\right) \cdot \left(1 - |S_{jj}|^2 - |S_{ij}|^2\right)} \cdot \eta_{radi} \cdot \eta_{radj}} \quad (1.3)$$

where ρ_{eij} is ECC between antenna elements i and j , S_{ij} is S-parameter between them, i. e. coupling, η_{radi} and η_{radj} are their radiation efficiencies. For 4G wireless systems, the value of 0.3 for ECC has been set as acceptable [91 (Jensen, 2004)]

A popular term for MIMO antennas is isolation that is usually found from the S-parameters:

$$\text{isolation} = -10 \log_{10}(|S_{ij}|) \quad (1.4)$$

It is seen from the equations (1.3) and (1.4), that the isolation and the correlation coefficient are different quantities as the isolation only presents the coupling level between two antennas and does not account for total radiation properties of each antenna.

Apart from the above mentioned parameters, there are some other ones listed in [92] that are not used in this thesis.

1.5.2. MIMO antennas on rigid and flexible substrates

As mentioned above, MIMO antenna systems are created to provide diversity to enhance capacity of wireless communications channel. There are five different types of diversity techniques that are commonly used for enhanced signal reception: 1) spatial; 2) temporal; 3) polarization; 4) frequency;

and 5) pattern. Among them, the spatial, polarization and pattern diversity schemes will be focused here as they are for practical implementation in WLAN and many other wireless communications systems. The Table 1.6 presents some examples of MIMO antenna systems covering different antenna types and for different applications, including the ones on rigid substrates [93-101].

1.5.3. Techniques for reduction of mutual coupling between antennas in MIMO systems

Reduction of mutual coupling is an important issue in building a MIMO antenna system. In this sub-section, various decoupling structures have also been presented for certain MIMO systems [102-122]. A summary of those structures is given in Table 1.7.

Table 1.4. Comparison of paper-based antennas.

Ref., Authors	Method of deposition of metal	Antenna type/Frequency/Application
[43], V. Palazzi et al., 2018	Adhesive metal/ Copper tape	RF harvesting rectifier at LTE 0.79 – 0.96 GHz, 1.71 – 2.17 GHz and 2.5 – 2.69 GHz
[56], Alimenti et al., 2012		2×2 Antenna array at 24 GHz
[58], M. Tentzeris' research group, 2017		Circular polarized origami antenna, 2.4 GHz – 5 GHz
[57], S. Moscato et al., 2016	Adhesive metal/ Aluminium foils	SIW-based, 4 GHz, 6.33 GHz, 9 GHz
[59-62], M. Tentzeris' research group, 2007-2013	Inkjet printing	CPW-fed UWB antenna, RFID dipole
[63-65], A. Shamim's research group, 2012-2016		High gain antennas
[66], D. E. Anagnostou et al., 2010		IFA, WLAN 2.45 GHz
[67], Noghalian et al., 2014	Screen printing	Patch monopole, bow-tie dipole antennas
[68], T. Leng et al., 2016		UHF RFID tags
[69], R. Valmiro, 2015		Dipole for RFID tags
[70], Y. Amin, 2012		Bow-tie RFID tag dipole antennas on PET and paper substrates
[71], Gary Elinoff, 2017		Antenna for RFID readers

Table 1.5. Examples for 3D antennas.

Ref., Authors	Substrate	Printing method	Frequency band	Application	Type of 3D/ Comments
[73 (Eom, 2016)]	3D printed Ecoflex elastomer and eutectic gallium- indium (EGaIn).	3D printing	Dual-band 2.03 GHz and 3.68 GHz.	RF stretchable sensor.	Flexible structure can be bent or stretched to create 3D. Under stretching, the frequencies are shifted 2.03 GHz to 1.89 GHz and 3.68 GHz to 3.40 GHz.
[74(Jun, 2015)]	Polylactic acid (PLA) plastic substrate.		3.1GHz – over 10.6GHz in free space.	On body (foot).	Flexible structure can be bent to create 3D.
[75], [76], M. Rizwan et al.	Flexible 3D printed Ninjaflex substrate.		UHF 915 MHz.	UHF RFID tag.	Stretchable structure.
[77 (Saintsing, 2015)]	3D printed materials: Tango Black, Shore 85.		Broadband 1 GHz – 4 GHz.	-	Flexible structure can be bent to create 3D even under the force of gravity.

[78 (Mirzaee, 2015)],	3D printed Polylactic acid (PLA) plastic substrate.	Additive manufacturing method, 3D printing PLA plastic substrate and conductive ABS material.	Centre frequency 7.81 GHz.	-	Flexible structure can be bent to create 3D.
[79 (Lin, 2017)]	3D printed NinjaFlex, $\epsilon_r = 1.55 - 2.07$, $\tan\delta = 0.02 - 0.04$,	3D printing, Embroidery.	UHF 915 MHz	UHF RFID.	The substrate has two printing layers, each having the thickness of 0.25mm and an infill of 100%. This makes the substrate height (thickness) 0.5 mm.
[80 (Traille, 2014)],	3D printed substrate.	3D printing, Inkjet printing.	-	Ambient energy harvesting for on-body autonomous wireless sensing network	-
[81 (Shah, 2017)],	Paper, 3D printed Polylactic acid (PLA) support.	3D printing, Inkjet printing	2.5–2.65 GHz and 2.48–2.62 GHz,	Wireless remote-sensing,	Origami.

[82 (George, 2013)]	Liquid crystal polymer substrate,	Inkjet printing	UHF RFID (902 MHz-928 MHz), centered at 915 MHz,	Wireless Sensor Network (WSN),	Cubic structure antenna.
[83 (Lopez, 2014)],	Pyralux AP 8525R material from Dupont, 0.0508-mm thick.		-	-	Circular polarization selective surface made of copper foil on 0.0508 mm thick Pyralux.
[84 (Tentzeris, 2014)],	Poly-methyl methacrylate (PMMA).		-	Wireless sensor, IoT node.	Cubic 3D wireless IoT node.
[85 (Eom S. H., 2016)	Paper substrate for the antennas, FR4 for the switching network.		1.66 GHz – 2.2 GHz.	Bi-directional sensor.	3D arrangement of 2 bow-tie antennas in the system.
[86 (Shamim, 2017)],	Teslin paper (synthetic) substrate or Kapton.		-	IoT Wearable applications.	Flexible structure can be bent and deformed to create 3D.-

[87 (Hamouda Z. , 2015)],	Kapton.	Screen printing	Dual-band 1.9 GHz and 5.7 GHz.	PCS, WLAN, and wireless network	Crumpled by using the 3D-printed support to create 3D structure.
[88 (Hawatmeh, 2016)],	150 μm thick ABS substrate.	Micro-dispensi ng	6 GHz	-	-
[89], M. Rizwan, 2017	Flexible 3D Printed Ninjaflex substrate.	Brush-painting	2.13 to 3.25 GHz.	On-body wearable applications.	Flexible structure can be bent to create 3D.
[90], A. S. M. Alqadami, 2018	2-mm thick PDMS.	Glued copper foil	1.63 GHz – 2.66GHz.	Wearable EM head imaging system.	An array of 12 bent antennas are embedded in a 3D PDMS elliptical structure to cover the human head and to be worn as a hat. Mutual coupling < -14 dB.

Table 1.6. Examples for MIMO antennas.

Ref., Authors	Substrate	Metal/ Printing method	Frequency band	Application	Comments
[93 (Zheng, 2014)],	FR4, 1mm thick.	Copper/Gravure	2.4-GHz (2400–2484-MHz)/5-GHz (5150–5850-MHz) WLAN.	Anti-interference MIMO WLAN applications.	Rigid substrate, Dual-band dual-polarized antenna array, which supports three data streams; Isolation above 20 dB.
[94 (Addaci, 2014)],	FR4, 0.8 mm thick.		2.4–2.48 GHz, 5.15–5.725 GHz.	Dual-Band WLAN	Isolation: 18.6 dB.
[95 (Soltani, 2015)]	FR4.		2.6 GHz.	-	20-port MIMO antenna structure was designed based on the canonical two-port antenna; 160 bps/Hz at SNR=30 dB for NLOS indoor environment.
[96 (Saeed, 2017)]	Rogers (RO3003), 1.52-mm thick.		2.4 GHz and 5.2 GHz.	WLAN.	Reconfigurable folded slot antenna with MIMO configuration ECC < 0.1.
[97 (Wen, 2018)]	Taconic TLY substrate		2.5–2.67 GHz.	-	4-port, low profile ($0.06\lambda_0$), probe-fed, bandwidth 6.5%, isolation 24.5%.

	$\epsilon_r = 2.2$				
[98 (Zhuo, 2018)]	FR4, 0.8-mm thick.		WLAN 2.4/5.2/5.8 GHz bands.	WLAN, smart watch	Overall dimensions 41×41×4.8 mm ³ , isolation >12 dB.
[99 (Zhai, 2016)]	Rogers for antennas and FR4 for decoupling structure.	Gluing and copper/gravure	2.4–2.485 GHz.	-	Four SIW cavity-backed antenna system; mushroom-type structure for decoupling; ECC < 0.005.
[100 (Timoshenko, 2015)]	0.635-mm thick polyimide.	Silver ink/ Inkjet	5.33 GHz.	-	Under bending conditions, return loss gets much worse and needs to compensate using an LC matching network.
[101 (Alqadami A., 2016)]	Multilayered PDMS substrate.	Copper foil	5.8 GHz.	WLAN.	Mutual coupling more than 30 dB, ECC in the order of 0.001, efficiency 72%.

Table 1.7. Examples of decoupling structures in MIMO antenna systems.

Ref., Authors	Substrate	Metal/ Printing method	Frequency band	Application	Decoupling technique		Comments
					Principle	Detailed	
[102 (Su, 2012)]	FR4, 1-mm thick.	Copper/ Gravure	2.4 GHz.	USB-dongle	Using neutralization line	Neutralization line connecting two antenna.	2-port MIMO antenna. Isolation below -20 dB at 2.4 GHz compared to -6 dB without this line; ECC under 0.006; TARC under -10dB.
[103 (Shi, 2017)]	FR4, 1-mm thick.	Copper/ Gravure	3.4–3.6 GHz and 4.55–4.75 GHz.	Mobile handsets			8-antenna MIMO system. Isolation improved from -4.6 dB to -28 dB at 3.5 GHz; from -7.9 dB to -17 dB at 4.6 GHz; ECC less than 0.05;
[104 (Diallo A., 2006)]							
[105 (Singh H. S., 2017)]	FR4, 0.8-mm thick.	Copper/ Gravure	GSM1800 (1740–1885 MHz), WiMAX	Mobile handsets		Using a defected ground structure	Two PIFA antennas, dimensions of radiating elements $13 \times 17 \times 0.8 \text{ mm}^3$. Isolation -10 dB and the ECC was below 0.002.

			(3250–3805 MHz).		Using parasitic elements	(DGS).	
[106 (Li Z., 2012)]	FR4, 0.8-mm thick.	Copper/Gravure	UMTS band (1920 MHz - 2170 MHz).	Mobile terminals		Two parasitic monopoles.	2-antenna system. Isolation improved from -8 dB to -20 dB.
[107 (Shoaib, 2015)]	FR4.	Copper/Gravure	GSM 1800 (1.71–1.88 GHz); GSM 1900 (1.85–1.99 GHz); WLAN (2.4–2.48 GHz); LTE band number 2–4, 9–10, 15–16, 23 (1.7–2.2 GHz); LTE band 7 (2.5–2.69 GHz)	Mobile handsets		Two slots on the ground layer.	Isolation less than -15 dB at all frequency bands.
[108 (Chiu,	FR4, 1.6-mm	Copper/Gravure	2 GHz – 2.7 GHz.			Using defected ground with	Two PIFA antennas located at the distance of $0.116\lambda_0$.

2007)]	thick.					slits as a bandstop filter	Isolation is more than 20dB.
[109 (Neyestan ak, 2008)]	FR4, 1.6-mm thick.	Copper/ Gravure	2.45 GHz.			Using PBG-Mushroom structure placed orthogonally to the antennas.	Two closely located parallel PIFA antennas. Isolation is improved from 7 dB to 38.8dB. Two closely located parallel microstrip patch antennas. Isolation is improved from 21 dB to 56dB.
[110 (Cheng, 2017)]	FR4, 1.6-mm thick.	Copper/ Gravure	5.8 GHz.			Using polarization-conversion isolator (PCI) placed on the same plane of the antennas.	A system of two patch antennas; The measured isolation is improved by 19.6 dB.
[111 (Li H. , 2009)]	FR4, 1.864-mm thick.	Copper/ Gravure	2.4 GHz.	2.4 GHz WLAN		Using slits as a bandstop filter.	Compact four-element planar MIMO antenna system. Isolation better than 20 dB.
[112 (Chen,	FR4, 0.8-mm	Copper/	2.45 GHz.			Using a circuit	2-antenna system.

2008)]	thick.	Gravure				with –two transmission lines. – a shunt reactive components.	Isolation improved from 2.5 dB to above 25 dB.
[113 (Lihao, 2010)]	FR4, 1.5-mm thick.	Copper/ Gravure	5 GHz – 10 GHz.	-		Using a split ring resonator (SRR).	Two PIFA antennas. Isolation improved by 6.43 dB.
[114 (Toktas, 2017)]	FR4, 1.6-mm thick.	Copper/ Gravure	2.5–13.3 GHz.	-		Using an additional monopole, V-shaped, neutralization line, plus-shaped and T-shaped forms.	2-antenna system. ECC lower than 0.2.
[115	FR4,	Copper/	3.2 – 10.6 GHz.	UWB.		Using stub	Two circular monopole antenna system.

(Najam, 2011)]	0.8-mm thick.	Gravure				decoupling structure.	Isolation was increased by 4 dB (from 11 dB to 15 dB).
[116 (Zhang, 2010)]	FR4, 0.8-mm thick.	Copper/ Gravure	2.4 GHz WLAN band.	Mobile handsets	Using parasitic elements.	Using a slot on the ground plane, the neighboring edges of the two PIFAs	Two PIFA antennas. Isolation is better than 40 dB with $0.0016\lambda_0$ spacing between the antennas.
[117 (Li, 2018)]	FR4, 0.8-mm thick.	Copper/ Gravure	2G/3G/4G, LTE bands 42/43 and LTE band 46.	Mobile handsets	Placement of antennas in system		12-antenna system. ECC lower than 0.15 in the LTE band 42/43 and lower than 0.1 in the LTE band 46;
[118 (Hussain, 2017)]	Rogers RO3003 0.76-mm thick for MIMO antennas on the top layer 0.13 mm thick for 28	Copper/ Gravure	1870 – 2530 MHz; 28 GHz with BW of 1.7 GHz.	Future mobile handsets		Multi-layer structure.	ECCs of MIMO system are 0.1343, 0.1815 and 0.0058 at 2.0, 2.25 and 2.35 GHz, respectively.

	GHz slot antennas.						
[119 (Jha, 2018)]	FR4, 1.56-mm thick.	Copper/Gravure	from sub-GHz to 5.5 GHz bands.	IoT applications			5-antenna system. ECC lower than 0.2 at 0.7 GHz, 0.8 GHz, 2.4 GHz, 2.7 GHz and 3.0 GHz.
[120 (Li G. , 2014)]	FR4, 0.9-mm thick	Copper/Gravure	LTE 2.57–2.92 GHz WiMAX 3.4–3.73 GHz	Hand-held terminals			Eight-element dual-band MIMO antenna array 140 mm × 70 mm × 9.55 mm; ECC less than 0.5.
[121 (Waldschmidt, 2004)]	Air.	-	1.5 GHz – 5 GHz.	Laptops or organizers	Using different modes	Antenna with different modes, independently fed.	Antenna with multimode diversity, a combination of pattern- and polarization diversity ECC below 0.1 in all frequency band from 1.5 GHz to 5 GHz
[122 (Kirsch, 2010)]	PET, 0.5-mm thick.	polymer conductive material	2.4 GHz.	MIMO ad-hoc network applications		Using polymer conductive antenna.	2-antenna system.

Thus, structures for reduction of mutual coupling in MIMO antennas are varied. Apart from the examples presented above, there are still many others. However, what we are interested in for this thesis is realization of MIMO antenna systems on flexible paper substrate.

One of the purposes of our project is to demonstrate, that 3D MIMO antennas can be built with our wideband antennas on paper substrates by 3D arrangement as well as bending or deforming antennas to place them in the system while the wideband property of the system is not much affected.

Conclusions for Chapter 1

1. After considering various dielectric materials for flexible electronics, paper substrate was chosen based on the requirements: flexible, low cost, with good RF properties, recycling ability, and especially ability to make 3D structures.

There are many types of paper with different thicknesses and properties. One of the important requirements for paper to be a good substrate is proper dielectric properties such as dielectric constant not too close to 1 and low loss tangent, that means at least the paper should be homogeneous and porous at the same time. Then, the paper substrate should be compatible with the available or chosen printing technology.

2. Among the techniques of metal deposition on substrates such as adhesive copper tapes or different printing methods, the inkjet and screen printing are the most popular for antennas on paper thanks to their low cost, acceptable precision. However, screen printing was chosen for our project as it gives good thickness of the metal (3 – 10 μm) with good conductivity of 1.7×10^6 S/m without repetitive printing multiple layers. Therefore, this technique is suitable for future mass production.
3. The overview of antennas on paper showed the promising perspectives of this substrate that have recently attracted many research groups. Nevertheless, most of the existing antennas are single or dual-band. Some wideband antennas have been proposed using CPW feeding method with narrow slots causing difficulties in fabrication with high precision.
4. Most of existing 3D or MIMO antennas are on rigid substrates such as Rogers or FR4, or based on 3D printing substrates, or on 3D arrangement of antennas in a system. One of the purposes of our project is to demonstrate, that 3D MIMO antennas can be built with our wideband antennas on paper substrates by 3D arrangement as well as bending or deforming antennas to place them in the system while the wideband property of the system is not much affected.

Objectives of the thesis

The goals and objectives of the thesis can be outlined as:

1. Characterization of electromagnetic properties of some flexible substrate materials such as PET, cardboard, various types of paper;
2. Simulation, optimization and design of antennas on E4D paper that has stable electromagnetic properties in our characterization process;
3. Prototyping and testing of radiation characteristics of the antennas;
4. Investigation of 3D/MIMO antenna systems that can be used in practice with the proposed paper-based antennas.

The manuscript is organized as follows. In Chapter 2, the results of characterization of flexible substrate materials are presented. Then the chapter dedicates to some designs of single band antennas on paper substrates, varied from simple CPW-fed antennas with adhesive paper to verify the results of electromagnetic property characterization of paper and PET, to screen-printed modified IFAs and SIW structures where most of designs, except for the SIW cavity-back antennas, is tested by measurement.

Further, Chapter 3 presents the design of the building block antenna components operating at multi-band as well as a wide band of frequency focusing on two WLAN bands in order to avoid using multiple single-band antennas that makes the systems too bulky. The proposed antennas are designed on 104- μm thick E4D paper (E4D 100), apart from “Hello-shaped” presented in 3.2 and the multi-band in 3.3 that will be designed on the same paper E4D with 210- μm thickness based on screen printing technique.

At last, Chapter 4 presents three-dimensional systems consisting of two orthogonal antennas in a rectangular acrylonitrile-butadiene-styrene (ABS) plastic box. The box in the first case is with sufficient dimensions where the antennas can be located in and their performance remains good. Further, the ABS box in the next sections has very restricted one of dimensions. The solution to bend an antenna under 90 degrees to place into this package is proposed and analyzed, then the systems with at least one bent antenna are studied.

References for Chapter 1

- [1] https://www.printedelectronicsnow.com/issues/2014-11-02/view_features/choosing-the-right-substrates-for-flexible-printed-electronics/46383
- [2] A. Hodgson, "The role of paper in the future of printed electronics", 2007, <http://citeseerx.ist.psu.edu/viewdoc/summary?doi=10.1.1.492.4568>
- [3] M. O. Sallam et al, "Wideband CPW-Fed Flexible Bow-Tie Slot Antenna for WLAN/WiMax Systems", IEEE Trans. On Antennas and Propagation, Vol. 65, pp. 4174-4277, N. 8, 2017.
- [4] M.-C. Tang, T. Shi, and R. W. Ziolkowski, "Flexible Efficient Quasi-Yagi Printed Uniplanar Antenna", IEEE Trans. On Antennas and Propagation, Vol. 63, pp. 5343-5350, N. 12, 2015.
- [5] M.-C. Tang, B. Zhou, and R. W. Ziolkowski, "Flexible Uniplanar Electrically Small Directive Antenna Empowered by a Modified CPW-Feed", IEEE Antennas and Wireless Propagation Letters, Vol. 15, pp. 914-917, 2016.
- [6] <https://www.rogerscorp.com/documents/647/acs/Rogers-RT-duroid-Material-Provides-Flexible-Substrates-in-New-Conical-Antenna.pdf>
- [7] Z. Hamouda et al. "Flexible UWB Organic Antenna for Wearable Technologies Applications", IET Microwaves, Antennas & Propagation, vol. 12, pp.150-166, Iss. 2, 2018.
- [8] O. E. Maleky et al. "Design of Simple Printed Dipole Antenna on Flexible Substrate for UHF Band", 11th Int. Conference Interdisciplinarity in Engineering, Romania, 2017.
- [9] Y. H. Jung; Y. Q.; S. Lee; T.-Y. Shih et al. "A Compact Parylene-Coated WLAN Flexible Antenna for Implantable Electronics", IEEE Antennas and Wireless Propagation Letters, Vol. 10, pp. 1382-1385, 2016.
- [10] A. H.-Omar, W. L. Thompson et al. "Adaptive Flexible Antennas for Wireless Biomedical Applications", 2016 IEEE 17th Annual Wireless and Microwave Technology Conference (WAMICON), Florida 2016.
- [11] S. Hong, Y. Kim et al. "A Flexible and Transparent Antenna on a Polyimide Substrate for Laptop Computers", IEEE AP-S, Vancouver 2015.
- [12] J. Y. Baek, G. H. Kwon et al. "Stable Deposition and Patterning of Metal Layers on the PDMS Substrate and Characterization for the development of the Flexible and

- Implantable Micro Electrode", *Advances in Nanomaterials and Processing*, Vols. 124-126, pp. 165-165, 2007.
- [13] A. Husameldin, E. Elobaid et al. "A Transparent and Flexible Polymer-Fabric Tissue UWB Antenna for Future Wireless Networks", *IEEE Antennas and Wireless Propagation Letters*, Vol. 16, pp. 1333-1336, 2017.
- [14] S. M. Abbas , S. C. Desai et al. "Design and Characterization of a Flexible Wideband Antenna Using Polydimethylsiloxane Composite Substrate", *Hindawi Int. Journal of Antennas and Propagation*", Volume 2018, Article ID 4095765.
- [15] B. V. Roy, B. Simorangkir et al. "Dual-Band Dual-Mode Textile Antenna on PDMS Substrate for Body-Centric Communications", *IEEE Antennas and Wireless Propagation Letters*, Vol. 16, pp. 677-680, 2017.
- [16] B. V. Roy, B. Simorangkir et al. "A method to Realize Robust Flexible Electronically Tunable Antennas Using Polymer-Embedded Conductive Fabric", *IEEE Trans. On Antennas and Propagation*, Vol. 66, pp. 50-58, N. 1, 2018.
- [17] Z. H. Jiang et al. "Compact, Highly Efficient, and Fully Flexible Circularly Polarized Antenna Enable by Silver Nanowires for Wireless Body-Area Networks", *IEEE Trans. on Biomedical Circuits and Systems*, vol. 11, pp. 920-932, N. 4, 2017.
- [18] R. Salvado, C. Loss et al. "Textile Materials for the Design of Wearable Antennas: A Survey", *Sensors*, 15841-15857, N. 12, 2012.
- [19] V. K. Singh, "A Review of Textile Materials for Wearable Antenna", *Journal of Microwave Engineering & Technologies*, Vol. 1, Iss. 3 (online), 2014.
- [20] S. Bashir, A. Chauraya et al. "A Flexible Fabric Metasurface for On Body Communication Applications", *Loughborough Antennas & Propagation Conference*, 2009.
- [21] M. Ghebrebrhan, F. Aranda et al. "Textile Frequency Selective Surface", *IEEE Microwave and Wireless Components Letters*, Vol. 27, pp. 989-991, N. 11, 2017.
- [22] J. Zhong, A. Kiourti et al. "Conformal Load-Bearing Spiral Antenna on Conductive Textile Threads", *IEEE Antennas and Wireless Propagation Letters*, Vol. 16, pp. 230-233, 2017.
- [23] M. Virili, H. Rogier et al. "Wearable Textile Antenna Magnetically Coupled to Flexible Active Electronic Circuits", *IEEE Antennas and Wireless Propagation Letters*, Vol. 13, pp. 209-212, 2014.

- [24] M. Virili, P. Mezzanotte et al. "Design of an UHF RFID Antenna on Flexible Substrate Magnetically Coupled to the Tag", Report of the short-term mission, 2012.
- [25] M. I. Ahmed, M. F. Ahmed, A. A. Shaalan, "Investigation and Comparison of 2.4 GHz Wearable Antennas on Three Textile Substrates and Its Performance Characteristics", *Journal of Antennas and Propagation*, pp. 110-120, N. 5, 2017.
- [26] Y. Li, "Direct Write Printed Flexible Electronic Devices on Fabrics", Ph. D. Thesis, University of Southampton, 2014.
- [27] T. Blecha, R. Linhart, J. Reboun, "Screen Printed Antennas on Textile Substrate", *Proceedings of the 5th Electronics System-integration Technology Conference (ESTC)*, 2014.
- [28] T. Kaufmann, and C. Fumeaux, "Wearable Textile Half-Mode Substrate-Integrated Cavity Antenna Using Embroidered Vias", *IEEE Antennas and Wireless Propagation Letters*, Vol. 12, pp. 805-808, 2013.
- [29] F.-X. Liu, Z. Xu et al. "Textile Folded Half-Mode Substrate-Integrated Cavity Antenna", *IEEE Antennas and Wireless Propagation Letters*, Vol. 15, pp. 1693-1697, 2016.
- [30] S. Yan, P. J. Soh, and G. A. E. Vandenbosch, "Dual-Band Textile MIMO Antenna Based on Substrate-Integrated Waveguide (SIW) Technology", *IEEE Trans. On Antennas and Propagation*, Vol. 63, pp. 4640-4647, N. 11, 2015.
- [31] A. Shafqat, F. A. Tahir, and M. U. Khan, "Textile Based Dual Band MIMO Quad-mode Substrate Integrated Waveguide Antenna for WiFi Application", *2017 Progress In Electromagnetics Research Symposium*, Singapore, 19–22 November 2017.
- [32] K. N. Paracha et al. "Low-cost Printed Flexible Antenna by Using an Office Printer for Conformal Applications", *Hindawi Int. Journal of Antennas and Propagation*", vol. 2018, Article ID 3241581.
- [33] A. T. Castro and S. K. Sharma, "Inkjet-Printed Wideband Circularly Polarized Microstrip Patch Array Antenna on a PET Film Flexible Substrate Material", *IEEE Antennas and Wireless Propagation Letters*, Vol. 77, pp. 176-179, N. 1, 2018.
- [34] A. A. Mohassieb et al. "Effect of Silver Nanoparticle Ink Drop Spacing on the Characteristics of Coplanar Waveguide Monopole Antennas Printed on Flexible Substrates", *IET Microwaves, Antennas & Propagation*, Vol. 11, pp. 1572-1577, Iss. 11, 2017.

- [35] S. Amendola, A. Palombi, G. Marrocco, "Inkjet-Printing of Epidermal RFID Antennas by Self-Sintering Conductive Ink", *IEEE Trans. on Microwave Theory and Techniques*, vol. 66, pp. 1561-1569, N. 3, 2018.
- [36] M. Barahona, D. Betancourt, and F. Ellinger, "Comparison of UWB Chipless Tags on Flexible Substrates Fabricated Using either Aluminum, Copper or Silver", *IEEE-APS Topical Conference on Antennas and Propagation in Wireless Communications (APWC)*, 2016.
- [37] R. Bollström, "Paper for printed electronics and functionality", Doctoral Thesis, Laboratory of Paper Coating and Converting, Department of Chemical Engineering, Center for Functional Materials, Finland 2013, ISBN 978-952-12-2934-3.
- [38] F. Alimenti, C. Mariotti et al. "Communication and Sensing Circuits on Cellulose", *Journal of Low Power Electronics and Applications*, pp. 154-164, N. 5, 2015.
- [39] B. Trnovec, M. Stanel et al. "Coated Paper for Printed Electronics", *Printed Electronics, Professional papermaking*, 2009.
- [40] H. Lee et al. "Inkjet Printed High-Q RF Inductors on Paper Substrate With Ferromagnetic Nanomaterial", *IEEE Microwave and Wireless Components Letters*, Vol. 26, pp. 419-421, N. 6, 2016.
- [41] S. Jiang et al. "Flexible Low-Voltage In-Zn-O Homojunction TFTs With Beeswax Gate Dielectric on Paper Substrates", *IEEE Electron Device Letters*, Vol. 37, pp. 287-290, N. 3, 2016.
- [42] R. Sivasamy et al. "A Low-Profile Paper Substrate-Based Dual-Band FSS for GSM Shielding", *IEEE Trans. On Electromagnetic Compatibility*, vol. 58, pp. 611-614, N. 2, 2016.
- [43] V. Palazzi, J. Hester et al. "A Novel Ultra-Lightweight Multiband Rectenna on Paper for RF Energy Harvesting in the Next Generation LTE Bands", *IEEE Trans. on Microwave Theory and Techniques*, vol. 66, pp. 366-379, N. 1, 2018.
- [44] C. Herrojo et al. "Near-Filed Chipless-RFID System With Erasable/Programmable 40-bit Tags Inkjet Printed on Paper Substrates", *IEEE Microwave and Wireless Components Letters*, Vol. 28, pp. 272-274, N. 3, 2018.
- [45] N. Javed, A. Habib et al. "Directly Printable Moisture Sensor Tag for Intelligent Packaging", *IEEE Sensors Journal*, Vol. 16, pp. 6147-6148, No. 16, Aug 2016.

- [46] B. K. Tehrani, B. S. Cook, and M. M. Tentzeris, "Inkjet Printing of Multilayer Millimeter-Wave Yagi-Uda Antennas on Flexible Substrates", *IEEE Antennas and Wireless Propagation Letters*, 2016
- [47] S. Derouin, "Flexible, Organic and Biodegradable: Stanford Researchers Developed New Wave of Electronics", *Stanford News*, 2017.
- [48] K. J. Yu, Z. Yan et al. "Inorganic semiconducting materials for flexible and stretchable electronics", *Review Article, Nature Partner Journal*, Singapore, 2017.
- [49] P. Gurrala, S. Oren et al. "Fully Conformal Square-Patch Frequency-Selective Surface Toward Wearable Electromagnetic Shielding", *IEEE Antennas and Wireless Propagation Letters*, Vol. 16, pp. 2602-2605, 2017.
- [50] M. Rizwan, M. W. A. Khan et al. "Flexible and Stretchable Brush-Painted Wearable Antenna on a Three-Dimensional (3-D) Printed Substrate", *IEEE Antennas and Wireless Propagation Letters*, Vol. 16, pp. 3108-3112, 2017.
- [51] R. Lakshmanan, S. K. Sukumaran, "Flexible Ultra Wide Band Antenna for WBAN Applications", *International Conference on Emerging Trends in Engineering, Science and Technology (ICETEST 2016)*.
- [52] S. Khan, L. Lorenzelli, R. S. Dahiya, "Technologies for Printing Sensors and Electronics Over Large Flexible Substrates: A Review", *IEEE Sensors Journal*, Vol. 15, pp. 3164-3186, No. 6, Jun 2015.
- [53] R. Colella, A. Rivadeneyra, et al. "Comparison of Fabrication Techniques for Flexible UHF RFID Tag Antennas", *IEEE Antennas and Propagation Magazine*, Vol. 59, pp. 159-168, Issue 5, Oct. 2017.
- [54] R. D. Bringans and Janos Veres, "Challenges and Opportunities in Flexible Electronics", 2016 *Int. Electron Devices Meeting*, San Francisco 2016.
- [55] J. Chang and T. Ge, "Challenges of Printed Electronics on Flexible Substrates", *IEEE 55th International Midwest Symposium on Circuits and Systems (MWSCAS)*, 2012.
- [56] F. Alimenti, P. Mezzanotte et al. "Microwave Circuits in Paper Substrates Exploiting Conductive Adhesive Tapes", *IEEE Microwave and Wireless Components Letters*, Vol. 22, pp. 660-662, N. 12, 2012.
- [57] S. Moscato, R. Moro, M. Pasian, M. Bozzi, L. Perregrini, "Innovative manufacturing approach for paper-based substrate integrated waveguide components and antennas", *IET Microwaves, Antennas & Propagation*, Vol. 10, pp. 256–263, Iss. 3, 2016.

- [58] S. I. H. Shah, M. M. Tentzeris, and S. Lim “Low-Cost Circularly Polarized Origami Antenna”, IEEE Antennas and Wireless Propagation Letters, Vol. pp. 2026-2029, 2017.
- [59] G. Shaker, S.S.-Naeini, N. Sangary, M. M. Tentzeris, "Inkjet Printing of Ultrawideband (UWB) Antennas on Paper-Based Substrates", IEEE Antennas and Wireless Propagation Letters, Vol. 10, pp. 111-113, 2011.
- [60] H. F. Abutarboush, M. M. Tentzeris et al. "Flexible LCP and Paper-based Substrates with Embedded Actives, Passives, and RFIDs", IEEE Polytronic Conference, 2007.
- [61] F. Alimenti, M. Virili, G. Orecchini, P. Mezzanotte, V. Palazzari, M.M. Tentzeris, L. Roselli, "A New Contactless Assembly Method for Paper Substrate Antennas and UHF RFID Chips", IEEE Trans. on Microwave Theory and Techniques, Vol. 59, pp. 627-637, No. 3, 2011.
- [62] S. Kim, B. Cook, T. Le, J. Cooper, H. Lee, V. Lakafosis, R. Vyas, R. Moro, M. Bozzi, A. Georgiadis, A. Collado, M. M. Tentzeris, “Inkjet-printed antennas, sensors and circuits on paper substrate”, IET Microwaves, Antennas & Propagation, Vol. 7, pp. 858-868, Iss. 10, 2013.
- [63] B. S. Cook, A. Shamim, “Utilizing Wideband AMC Structures for High-Gain Inkjet-Printed Antennas on Lossy Paper Substrate”, IEEE Antennas and Wireless Propagation Letters, Vol. 12, pp. 76-79, 2013.
- [64] B. S. Cook, A. Shamim, “Inkjet Printing of Novel Wideband and High Gain Antennas on Low-Cost Paper Substrate”, IEEE Trans. On Antennas and Propagation, Vol. 60, pp. 4148-4155, N. 9, 2012.
- [65] H. F. Abutarboush, M. F. Farooqui, and A. Shamim, “Inkjet-Printed Wideband Antenna on Resin-Coated Paper Substrate for Curved Wireless Devices”, IEEE Antennas and Wireless Propagation Letters, Vol. 15, pp. 20-23, 2016.
- [66] D.E. Anagnostou, A.A. Gheethan, A.K. Amert, K. W. Whites, "A Direct-Write Printed Antenna on Paper-Based Organic Substrate for Flexible Displays and WLAN Applications", Journal of Display Technology, Vol. 6, pp. 558-564, No.11, 2010.
- [67] S. Noghianian, B. Sayers et al. "Printing Antenna on Paper: A Cost-Effective Method", AP-S 2014.
- [68] T. Leng, X. Huang et al. “Graphen Nanoflakes Printed Flexible Meander-Line Dipole Antenna on Paper Substrate for Low-Cost RFID and Sensing Applications”, IEEE Antennas and Wireless Propagation Letters, Vol. 15, pp. 1565-1568, 2016.

- [69] R. Valmiro, K. Kitaguti, S. E. Barbine, "A Silk-Screen Printed RFID Antenna", 2015 Asia-Pacific Microwave Conference (APMC).
- [70] Y. Amin, Q. Chen et al. "Development and Analysis of Flexible UHF RFID Antennas for "Green" Electronics", Progress In Electromagnetics Research, Vol. 130, 1-15, 2012.
- [71] G. Elinoff (contributing writer), "Introducing a screen-printed, flexible antenna for RFID devices", Electronics Products, 2017.
- [72] T. Happonen, " Reliability Studies on Printed Conductors on Flexible Substrates under Cyclic Bending", Academic dissertation to be presented with the assent of the Doctoral Training Committee of Technology and Natural Sciences, University of Oulu, 2016.
- [73] S.-H. Eom, S. Lim, "RF Stretchable Sensor Using Flexible Substrate and Eutectic Gallium-Indium and Eutectic Gallium-Indium", Proceedings of ISAP2016, Okinawa, Japan.
- [74] S. Jun, B. Sanz-Izquierdo and M. Summerfield, "UWB Antenna on 3D Printed Flexible Substrate and Foot Phantom", 2015 Loughborough Antennas & Propagation Conference (LAPC).
- [75] M. Rizwan, M.W.A. Khan et al. "Flexible and stretchable 3D printed passive UHF RFID tag", Electronics Letters, Vol. 53, pp. 1054–1056, N. 15, 20th July 2017.
- [76] M. Rizwan, M. Guibert et al. "Embroidered Passive UHF RFID Tag on Flexible 3D Printed Substrate", 2017 Progress in Electromagnetics Research Symposium - Fall (PIERS - FALL).
- [77] C. D. Saintsing, K. Yu et al. "Planar Monopole Antennas on Substrates Fabricated Through an Additive Manufacturing Process", 2015 IEEE Radio and Wireless Symposium.
- [78] M. Mirzaee, S. Noghianian et al. "Developing Flexible 3D Printed Antenna Using Conductive ABS Materials", 2015 IEEE International Symposium on Antennas and Propagation & USNC/URSI National Radio Science Meeting.
- [79] T.-H. Lin, J. Bito et al. "Ambient Energy Harvesting from Two- Way Talk Radio for On-body Autonomous Wireless Sensing Network Using Inkjet and 3D Printing", 2017 IEEE MTT-S International Microwave Symposium (IMS).
- [80] A. Traille, A. Coustou et al. "Novel Inkjet Printed Modules for Sensing, Radar and Energy Harvesting Applications", 44th European Microwave Conference, 2014.
- [81] S. I. H. Shah and S. Lim, "Transformation from a Single Antenna to a Series Array Using Push/Pull Origami", Sensors 2017, 17, 1968; doi:10.3390/s17091968.

- [82] B. B. George, M. Nesasudha and Dr. Valarnathi, "A Compact 3-D Cubic Antenna for Wireless Sensor Networks", 2013 International Conference on Signal Processing, Image Processing and Pattern Recognition (ICSIPRI).
- [83] I. Lopez and J.-J. Laurin, " A Circular Polarization Selective Surface Implemented on a Flexible Substrate", IEEE Trans. On Antennas and Propagation, Vol. 62, pp. 3847-3852, N. 7, 2014.
- [84] M.Tentzeris, S. Kim et al. "Inkjet-printed “Zero-Power” Wireless Sensor and Power Management Nodes for IoT and “Smart Skin” Applications", 2014 XXXIth URSI General Assembly and Scientific Symposium (URSI GASS).
- [85] S.-H. Eom, Y. Seo and S. Lim, "Pattern Switchable Antenna System Using Inkjet-Printed Directional Bow-Tie for Bi-Direction Sensing Applications", Sensors (Basel). 2015 Dec; 15(12): 31171–31179.
- [86] A. Shamim, "3D Inkjet Printed Flexible and Wearable Antenna Systems", 2017 International Symposium on Antennas and Propagation (ISAP).
- [87] Z. Hamouda, J.-L.Wojkiewicz et al. "Dual-Band Elliptical Planar Conductive Polymer Antenna Printed on a Flexible Substrate", IEEE Trans. On Antennas and Propagation, Vol. 63, pp. 5864-5867, N.12, 2015.
- [88] D. Hawatmeh, E. Rojas-Nastrucci, and T. Weller, "A Multi-Material 3D Printing Approach for Conformal Microwave Antennas", 2016 International Workshop on Antenna Technology (iWAT).
- [89] M. Rizwan, M. Waqas Ahmad Khan et al. "Flexible and Stretchable Brush-Painted Wearable Antenna on a Three-Dimensional (3-D) Printed Substrate", IEEE Antennas and Wireless Propagation Letters, Vol. 16, pp. 3108-3112, 2017.
- [90] A. Alqadami, K. Bialkowski, A. Abbosh, " Flexible Quasi-Yagi Antenna Arrays For Wearable Electromagnetic Head Imaging Based on Polymer Technology", 2018 Australian Microwave Symposium (AMS).
- [91] M. A. Jensen and J. W. Wallace, "A Review of Antennas and Propagation for MIMO Wireless Communications", IEEE Trans. On Antennas and Propagation, Vol. 52, pp. 2810-2824, N. 11, 2004.
- [92] M. S. Sharawi, "Printed multi-band MIMO antenna systems and their performance metrics [wireless corner]", IEEE Antennas Propag. Mag., vol. 55, no. 5, pp. 218_232, Oct. 2013.

- [93] W. C. Zheng, L. Zhang et al. "Dual-Band Dual-Polarized Compact Bowtie Antenna Array for Anti-Interference MIMO WLAN", *IEEE Trans. On Antennas and Propagation*, Vol. 62, pp. 237-246, N.1, 2014.
- [94] R. Addaci, K. Haneda et al. "Dual-Band WLAN Multiantenna System and Diversity/MIMO Performance Evaluation", *IEEE Trans. On Antennas and Propagation*, Vol. 62, pp. 1409-1415, N.3, 2014.
- [95] S. Soltani, and R. D. Murch, "A Compact Planar Printed MIMO Antenna Design", *IEEE Trans. On Antennas and Propagation*, Vol. 63, pp. 1140-1149, N.3, 2015.
- [96] S. M. Saeed, C. A. Balanis et al. "Flexible Reconfigurable Antenna With MIMO Configuration", *AP-S 2017*.
- [97] Y. Wen , D. Yang, H. Zeng et al. "Bandwidth Enhancement of Low-Profile Microstrip Antenna for MIMO Applications", *IEEE Trans. On Antennas and Propagation*, Vol. 66, pp. 1064-1075, N.3, 2018.
- [98] T.-Y. Zhuo, W.-S. Chen, and C.-Y.-D. Sim, "WLAN MIMO Antennas for Smart Watch Applications", 2018 IEEE International Symposium on Electromagnetic Compatibility and 2018 IEEE Asia-Pacific Symposium on Electromagnetic Compatibility (EMC/APEMC).
- [99] G. Zhai, Z. N. Chen, and X. Qing, "Mutual Coupling Reduction of a Closely Spaced Four-Element MIMO Antenna System Using Discrete Mushrooms", *Trans. on Microwave Theory and Techniques*, vol. 64, pp. 3060-3067, N. 10, 2016.
- [100] A. Timoshenko, K. Lomovskaya et al. "Design of a Flexible MIMO Antenna with Return Loss Compensation", 2015 7th International Congress on Ultra Modern Telecommunications and Control Systems and Workshops (ICUMT).
- [101] A. Alqadami, M. F. Jamlos et al. "Assessment of PDMS Technology in a MIMO Antenna Array", *IEEE Antennas and Wireless Propagation Letters*, Vol. 15, pp. 1939-1942, 2016.
- [102] S.-W. Su, C.-T. Lee and F.-S. Chang, "Printed MIMO-Antenna System Using Neutralization-Line Technique for Wireless USB-Dongle Applications", *IEEE Trans. On Antennas and Propagation*, Vol. 60, pp. 456-463, N. 2, 2012.
- [103] X. Shi, M. Zhang et al. "Dual-Band 8-Element MIMO Antenna with Short Neutral Line for 5G Mobile Handset", 2017 11th European Conference on Antennas and Propagation (EUCAP).

- [104] A. Diallo, C. Luxey, P. Le Thuc, R. Staraj & G. Kossiavas, "Study and Reduction of the Mutual Coupling between Two Mobile Phone PIFAs Operating in the DCS1800 and UMTS Bands", IEEE Transactions on Antennas & Propagation, part. 1, vol. 54, n°11, pp. 3063-3074, November 2006.
- [105] H. S. Singh, K. Singh et al. "A Compact Mobile Handsets MIMO/Diversity Antenna for GSM1800 and WiMAX Applications", 2017 International Conference on Electrical and Computing Technologies and Applications (ICECTA).
- [106] Z. Li, Z. Du et al. "Reducing Mutual Coupling of MIMO Antennas With Parasitic Elements for Mobile Terminals", IEEE Trans. On Antennas and Propagation, Vol. 60, pp. 473-481, N. 2, 2012.
- [107] S. Shoaib, I. Shoaib et al. "MIMO Antennas for Mobile Handsets", IEEE Antennas and Wireless Propagation Letters, Vol. 14, pp. 799-802, 2015.
- [108] C.-Y. Chiu, C.-H. Cheng et al. "Reduction of Mutual Coupling Between Closely-Packed Antenna Elements", IEEE Trans. On Antennas and Propagation, Vol. 55, pp. 1732-1738, N. 6, 2007.
- [109] A. A. L. Neyestanak, F. Jolani, and M. Dadgarpour, "Mutual Coupling Reduction Between Two Microstrip Patch Antennas", 2008 Canadian Conference on Electrical and Computer Engineering.
- [110] Y. F. Cheng et al., "Reduction of Mutual Coupling Between Patch Antennas Using a Polarization-Conversion Isolator", IEEE Antennas and Wireless Propagation Letters, Vol. 16, pp. 1257-1260, 2017.
- [111] H. Li, J. Xiong and S. He, "A Compact Planar MIMO Antenna System of Four Elements With Similar Radiation Characteristics and Isolation Structure", IEEE Antennas and Wireless Propagation Letters, Vol. 8, pp. 1107-1110, 2009.
- [112] S.-C. Chen, Y.-S. Wang, and S.-J. Chung, "A Decoupling Technique for Increasing the Port Isolation Between Two Strongly Coupled Antennas", IEEE Trans. On Antennas and Propagation, Vol. 56, pp. 3650-3658, N. 12, 2008.
- [113] H. Lihao, Z. Huiling, H. Zhang, and C. Quanming, "Reduction of Mutual Coupling between Closely-Packed Antenna Elements with Split Ring Resonator (SRR)", 2010 International Conference on Microwave and Millimeter Wave Technology.
- [114] A. Toktas, M. Yerlikaya et al. "Reducing Mutual Coupling For a Square UWB MIMO Antenna Using Various Parasitic Structures", 2017 10th International Conference on Electrical and Electronics Engineering (ELECO).

- [115] A. Najam, Y. Duroc, and S. Tedjni, "UWB-MIMO Antenna With Novel Stub Structure", *Progress In Electromagnetics Research C*, Vol. 19, 245-257, 2011.
- [116] S. Zhang et al., "Reducing Mutual Coupling for an Extremely Closely-Packed Tunable Dual-Element PIFA Array Through a Resonant Slot Antenna Formed In-Between », *IEEE Trans. On Antennas and Propagation*, Vol. 58, pp. 2771-2776, N. 8, 2010.
- [117] Y. Li, C.-Y.-D. Sim et al. "12-Port 5G Massive MIMO Antenna Array in Sub-6GHz Mobile Handset for LTE Bands 42/43/46 Applications", *IEEE Access*, Vol. 6, 2018.
- [118] R. Hussain, A. T. Alreshaid et al. "Compact 4G MIMO antenna integrated with a 5G array for current and future mobile handsets", *IET Microwaves, Antennas & Propagation*, 2017, Vol. 11, Iss. 2, pp. 271-279.
- [119] K. R. Jha, B. Bukhari et al. "Compact Planar Multi-Standard MIMO Antenna for IoT Applications", *IEEE Trans. On Antennas and Propagation*, 2018 (accepted for publication).
- [120] G. Li, H. Zhai et al. "Isolation-Improved Dual-Band MIMO Antenna Array for LTE/WiMAX Mobile Terminals", *IEEE Antennas and Wireless Propagation Letters*, Vol. 13, pp. 1128-1131, 2014.
- [121] C. Waldschmidt, W. Wiesbeck, "Compact Wide-Band Multimode Antennas for MIMO and Diversity", *IEEE Trans. On Antennas and Propagation*, Vol. 52, pp. 1963-1969, N. 8, 2004.
- [122] N. J. Kirsch, N. A. Vacirca et al. "Performance of Transparent Conductive Polymer Antennas in a MIMO Ad-hoc Network", 2010 IEEE 6th International Conference on Wireless and Mobile Computing, Networking and Communications.

2. Chapter 2 – Design of Single-Band Antennas on Paper

In the previous chapter an overview of antennas on paper substrate and state-of-the-art of this issue were done. It is clear, that in order to design an antenna or a microwave electronic integrated circuit on a new substrate, it is necessary to measure its electromagnetic properties.

This chapter presents the results of characterization of electromagnetic properties of some flexible materials. Then the chapter dedicates to some designs of single band antennas on paper substrates, varied from simple CPW-fed antennas to verify the results of electromagnetic property characterization of paper and PET, to modified IFAs and SIW structures. Most of designs, except for the SIW cavity-backed antennas in the Section 2.4, are tested by measurement.

2.1. Characterization of electromagnetic properties of paper

In design processes of microwave circuits and antennas, knowledge of electromagnetic properties of substrate is very important. A linear and isotropic dielectric material is characterized by its permittivity as a function of frequency in harmonic operational regime. In practice, a quantity called relative dielectric permittivity is defined as follows:

$$\varepsilon(f) = \varepsilon_r(f) \cdot \varepsilon_0 \quad (2.1)$$

For a lossless dielectric material where there is no electric current, this value is real. In harmonic regime, the Maxwell equation "curl" (Maxwell-Ampère) has the following form:

$$\nabla \times \vec{H} = j\omega\varepsilon\vec{E}$$

For a lossy dielectric material with conductivity σ the Maxwell equation "curl" (Maxwell-Ampère) has the following form:

$$\nabla \times \vec{H} = j\omega\varepsilon\vec{E} + \sigma\vec{E} = j\omega\left(\varepsilon - j\frac{\sigma}{\omega}\right) \cdot \vec{E} \quad (2.2)$$

Thus, permittivity of a lossy dielectric material is a complex number $\varepsilon = \varepsilon - j\frac{\sigma}{\omega} = \varepsilon' - j\varepsilon''$.

The loss tangent is defined as $\tan \delta = \frac{\varepsilon''}{\varepsilon'}$ that varies with frequency.

A synthesis of measurement techniques used to characterize the complex permittivity of thin sheets of dielectrics such as plastic or different types of paper is given in the Appendix 1. This

section shows the measurement results for several flexible thin materials including E4D paper that will be used to design the antennas presented later.

The measurement results obtained by the method of perturbation reported in Table 2.1 and Table 2.2 are fairly stable so we can take average permittivity and loss tangent values for each 2.5 GHz and 925 MHz sample.

Table 2.1. The measurement results at 2.5 GHz.

Material	Thickness, μm	Width, mm	Permittivity ϵ_r	Loss tangent $\tan\delta$
Teslin	254	5	2.41	0.038
		6	2.27	0.036
Silver Image Laser	241 – 249	5	2.71	0.162
	245 (average)	6	2.72	0.156
PWC Paper for El	230	5	3.25	0.123
		6	3.19	0.121
CnCanlePaper	786	5	2.24	0.078
		5.8	2.191	0.078
PET-100-LD	100	5	3.34	0.012
		6	3.28	0.017
PRC printing paper	65	5	3.21	0.108
		6	3.58	0.064
PRP-60 pharmacist's paper	78	5	2.84	0.077
		6	2.87	0.070
BL200 glue paper	232 – 248	5	3.27	0.138
	240 (average)	6	2.99	0.144
E4D paper	104, 210, 387	5	3.18	0.091

Table 2.2. The measurement results at 900 MHz.

Material	Thickness, μm	Width	ϵ_r	$\tan\delta$
PST Teslin	254	9	2.83	0.033
Silver Image Laser	241 – 249 245 (average)	9	2.58	0.123
PWC Paper for El	230	9	2.69	0.107
CnCanlePaper	786	9	2.43	0.080
PET-100-LD	100	9	3.71	0.011
PRC printing paper	65	9	3.17	0.059
PRP-60 pharmacist's paper	78	9	2.48	0.077
BL200 glue paper	232 – 248 240 (average)	9	3.74	0.148
E4D paper	104, 210, 387	9	3.4	0.070

As the E4D paper is selected by our partner CTP (Technical Center of Paper), the measurement of E4D paper substrate was performed by the method of perturbation more properly than for the other substrates. It was done with 50 samples cut from various E4D paper sheets of three different thicknesses, 104 μm , 210 μm and 387 μm . The results were analyzed statistically and gave $\epsilon_r = 3.184$, $\tan\delta = 0.092$. The dispersions of the results measured at 2.5 GHz are 0.25% for ϵ_r and 0.26% for $\tan\delta$.

Some first CPW-fed antennas designed with adhesive copper glued on 786- μm thick CnCanle paper, 100- μm thick PET-100-LD and 65- μm thick PRC paper using the results shown in Table 2.1 and Table 2.2 are presented in the next section 2.2 in order to verify qualitatively these results of characterization [1].

The antennas designed based on screen printing technology on E4D paper and with via holes are presented in the other next sections 2.3 and 2.4 to show the possibility of this technique and

once again confirm the accuracy of characterization of electromagnetic properties of this thin paper material.

2.2. CPW-fed monopole antennas

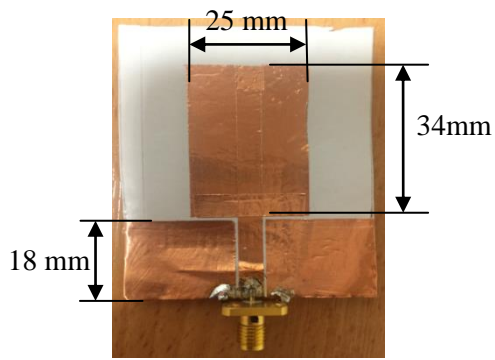
In the previous section the measurement results of electromagnetic properties for several materials were presented. Based on this, the first antennas using adhesive copper are designed to verify qualitatively the above mentioned results.

Here the monopole structures with a coplanar feed line (CPW) have been chosen because monopole antennas are well suited for connections and metallization on flexible substrates like paper. The main advantages of the CPW line are the faster manufacturing on one side of the substrate and the possibility of miniaturization of circuits at high frequencies.

The designed antennas are shown in Figure 2.1. The traditional rectangular patches in Figure 2.1(a) and (b) of dimensions $60 \text{ mm} \times 50 \text{ mm}$ with CPW feeding have initially half-wavelength dimensions, design on different thin flexible substrates such as $100 \mu\text{m}$ thickness PET, $65 \mu\text{m}$ thickness PRC paper, then optimized in CST Microwave Studio. The metallization of antennas were performed by using adhesive copper.

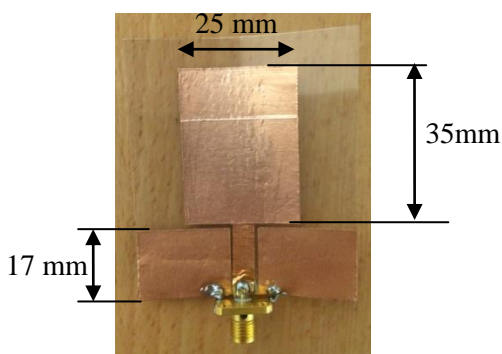
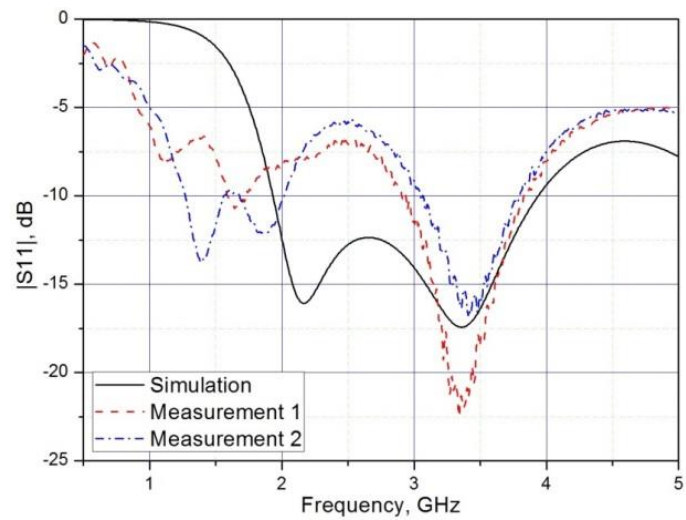
The last shape of the patch has the trapezium form (Figure 2.1(c)) of dimensions $60 \text{ mm} \times 50 \text{ mm}$ as an example of the possibility of saving an amount of metal of the patch while keeping the wide bandwidth of the antenna [1]. The simulated and measured curves S11 have good agreement in their shape, but the resonant frequency shift can be observed for all antennas. This can be explained by the small ground plan, so that the cable can easily be coupled with the antennas that shift the resonant frequency. Besides, the quality, the roughness of the adhesive copper, and the inaccuracy of the realization which involves manual cutting of the copper sheet, especially when there are too narrow slots in the structures, 0.2 mm and less in our case, also can affect the results of validation of the antennas.

All three antennas have omni-directional radiation patterns, where an example of that at the resonant frequency 2.5 GHz of the trapezium antenna on CnCanle paper with $h=786\mu\text{m}$ thickness is depicted in Figure 2.2. The simulated realized gain of these antennas is high as the metal used for the simulation was copper that is more ideal than in the practice. This value of the CPW-fed rectangular antenna on $100 \mu\text{m}$ thickness PET, $65 \mu\text{m}$ thickness PRC paper and $786 \mu\text{m}$ thickness CnCanle paper is 2.5 dBi , 2.6 dBi and 2.15 dBi , respectively.



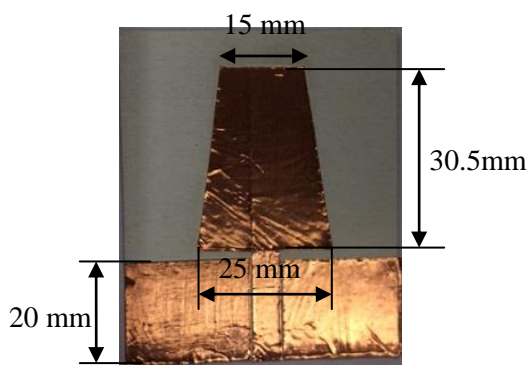
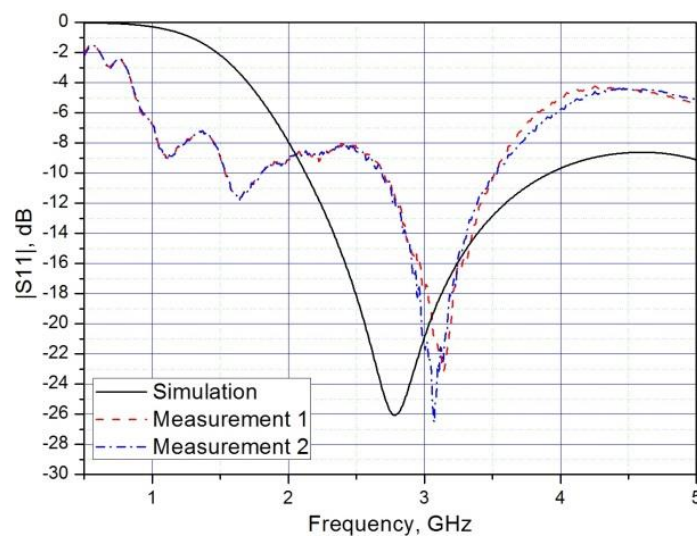
Overall dimensions : 50 mm
× 60 mm × 0.065 mm

(a)



Overall dimensions : 50mm ×
60mm × 0.1mm

(b)



Overall dimensions : 50mm ×
60mm × 0.768mm

(c)

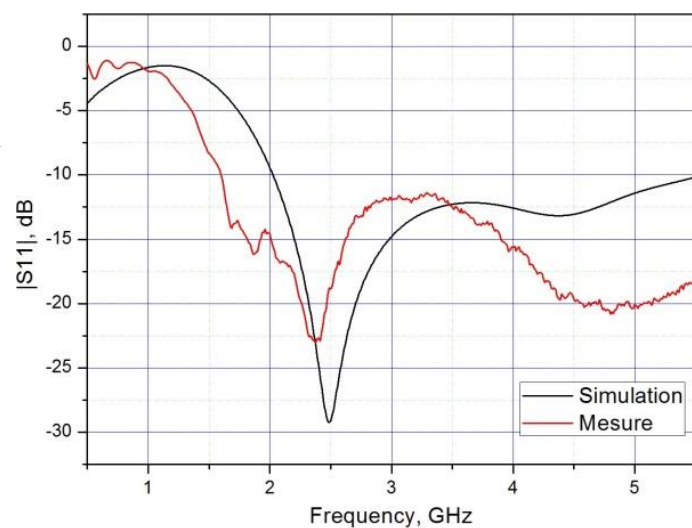


Figure 2.1. CPW-fed monopole antennas using the adhesive copper with their reflection coefficients: (a) On PRC, $h=65\mu\text{m}$; (b) On PET (Polyethylene Terephthalate), $h=100\mu\text{m}$; (c) On CnCanle paper, $h=786\mu\text{m}$.

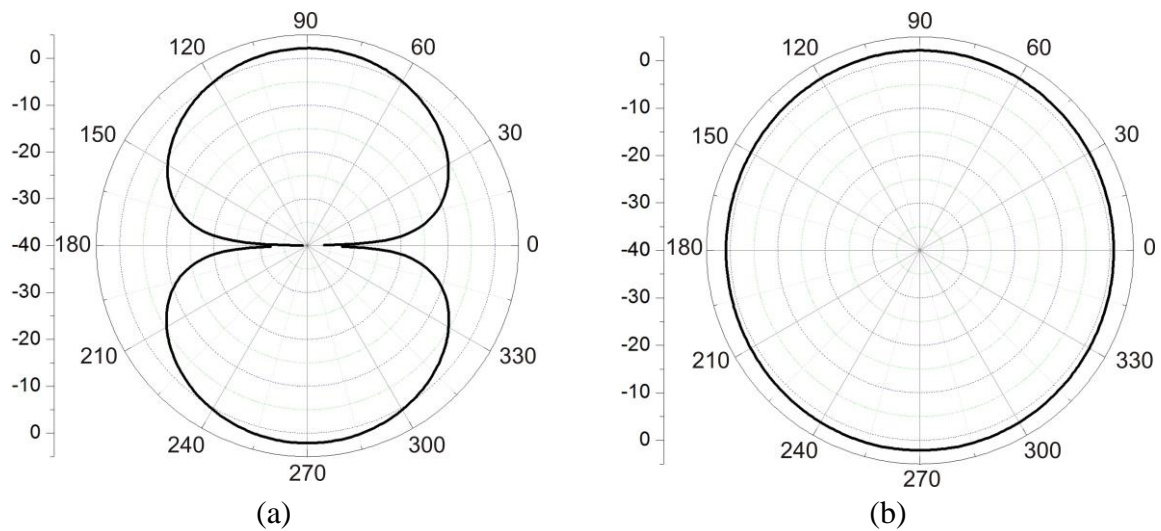


Figure 2.2. Simulated radiation patterns of CPW-fed monopole antennas using the adhesive copper on CnCanle paper, $h=786\mu\text{m}$: (a) In x-z plan (E-plan); (b) In x-y plan (H-plan).

The main disadvantage of CPW-fed antennas on paper is for very thin substrates, too narrow slots in 50-ohm CPW feed lines can cause difficulties in fabrication with high accuracy. To avoid this problem, with the double-side screen printing possibility, we chose the conventional microstrip feeding method for our further designs.

2.3. Inverted-F antennas on E4D paper

Inverted-F antennas (IFAs) have become popular for decades to be installed in cellular devices thanks to a number of advantages such as good electrical characteristics, small dimensions, cost-effective with the same losses as other antennas. Basically, the length of radiation part of an IFA is a quarter wavelength leading to its smaller dimension compared to other basic antennas. The theory of IFA has been revised in [2], and multiple attempts have been done to improve its dimensions by using metamaterial [3] or frequency band of this antenna such as modification of ground plane [4] or create multiple resonant frequencies by multiple short pins [5]. An IFA on paper substrate has also been designed and studied in [6].

In an IFA structure there is a feeding and at least one shorting pin, therefore there is at least one via hole to connect the antenna face to the face of ground plane. For an antenna on paper substrate, this via hole can cause some difficulties in fabrication process. In [6], the via hole was realized manually.

Figure 2.3 shows the IFA structure on 210- μm thick E4D paper designed at 2.45 GHz and fabricated prototype. This configuration is modified from the structure in [6], its advantage is that it is easy to add resonance frequencies by adding other stubs as shown later in this section. In order to fix the antenna with the connector, the holes at two sides of the feed line on the prototype have been made. The thickness of the printed metallic layer is 6 μm with the measured conductivity of 1.7×10^6 S/m. The length of the stub L_s on the top side (Figure 2.3(a)) was initially set as quarter wavelength according to the theory,

$$\frac{\lambda_g}{4} = \frac{1}{4} \cdot \frac{c}{f \cdot \sqrt{\epsilon_r}} = \frac{1}{4} \cdot \frac{3 \cdot 10^8}{2.45 \cdot 10^9 \cdot \sqrt{3.18}} = 0.0172\text{m} = 17.2\text{mm} \quad (2.3)$$

then the antenna was optimized to resonate at 2.45 GHz. Apart from this geometrical parameter L_s , the distance h between the stub and the ground plane also strongly affect the resonant frequency of the antenna and also needs to be optimized (Figure 2.4). A large stub with 2-mm width and 12-mm length was added to the ground plane in order to connect it to the antenna through the via hole of 0.5-mm diameter filled manually with a conductive glue (Figure 2.4(b)). After the S_{11} parametric studies the length of the stub was chosen to be 21.5 mm, the distance $h = 4$ mm. The overall dimensions of the antenna are 42 mm \times 43 mm \times 0.21 mm. The antenna matching characteristics - simulation vs. measurement of three different samples are presented in Figure 2.5(a) where we can see a huge disagreement between the simulated and measured resonant frequencies. However, the reflection coefficient of all three prototypes fit well to each other. Supposing, that this is caused by some improper effects of via hole metallization, the simulation was done again with defect models such as improper dimensions of the via hole with an abundant part of metal on both faces. As a result, the much better results were achieved shown in Figure 2.5(c).

The radiation patterns of this antenna shown in Figure 2.6 are very similar to omni-directional that makes this kind of antennas attractive.

As mentioned above, one of the advantages of this IFA structure is that it is easy to add resonant frequencies by adding stubs on the front side without changing the ground plane and the overall dimensions of the antenna. An example of a dual-band PIFA is shown in Figure 2.7, its matching characteristics in Figure 2.8, and its radiation patterns for realized gain at 2.45 GHz and 5.5 GHz in Figure 2.9.

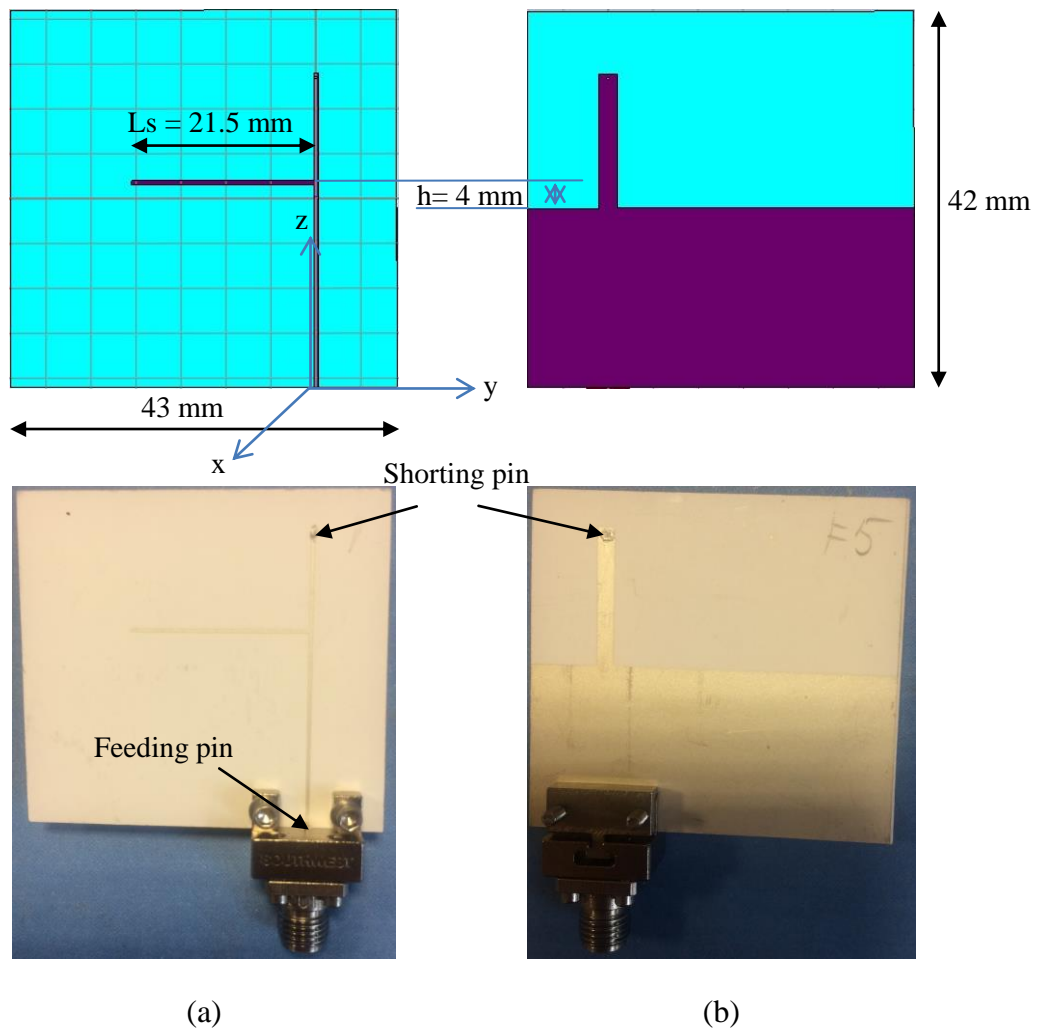
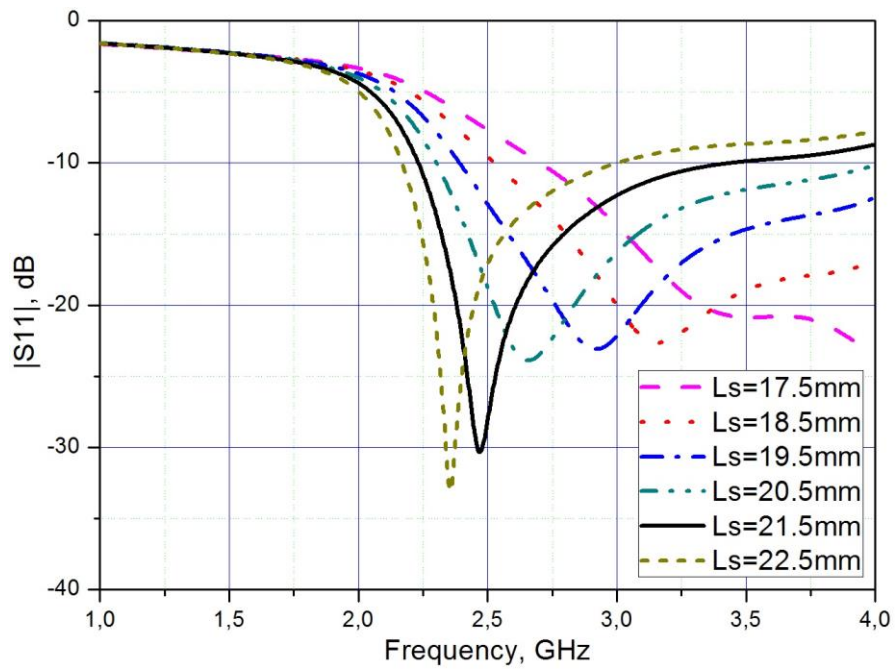
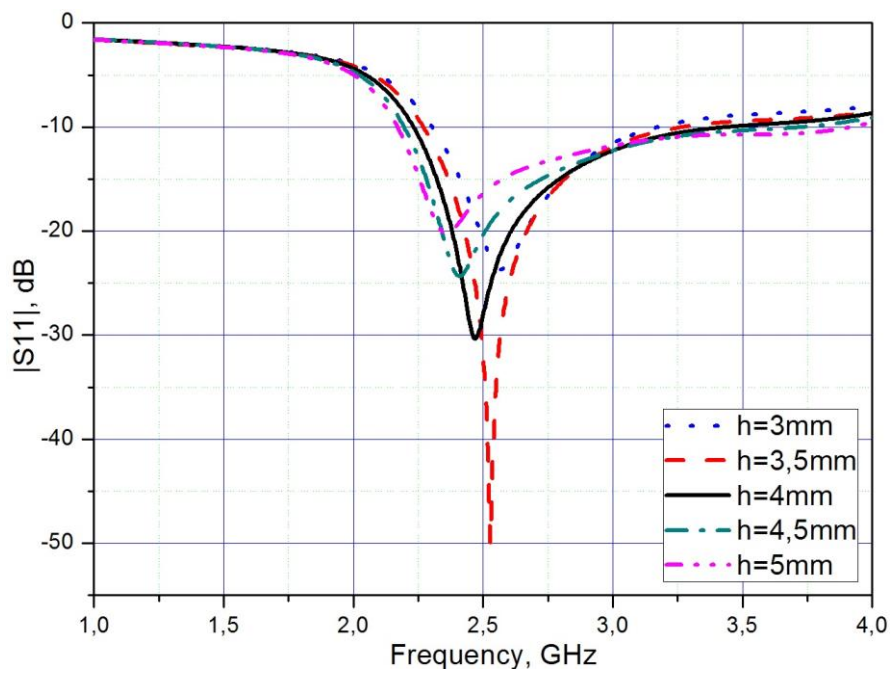


Figure 2.3. Printed single-band PIFA on E4D 200 paper: (a) Front side; (b) Back side.

This type of antenna has stable electrical properties. However, it causes some technological difficulties because of the existence of via holes. Furthermore, it can be designed to have only multi-band, but not wide-band characteristics as required by many set-top boxes (STB).

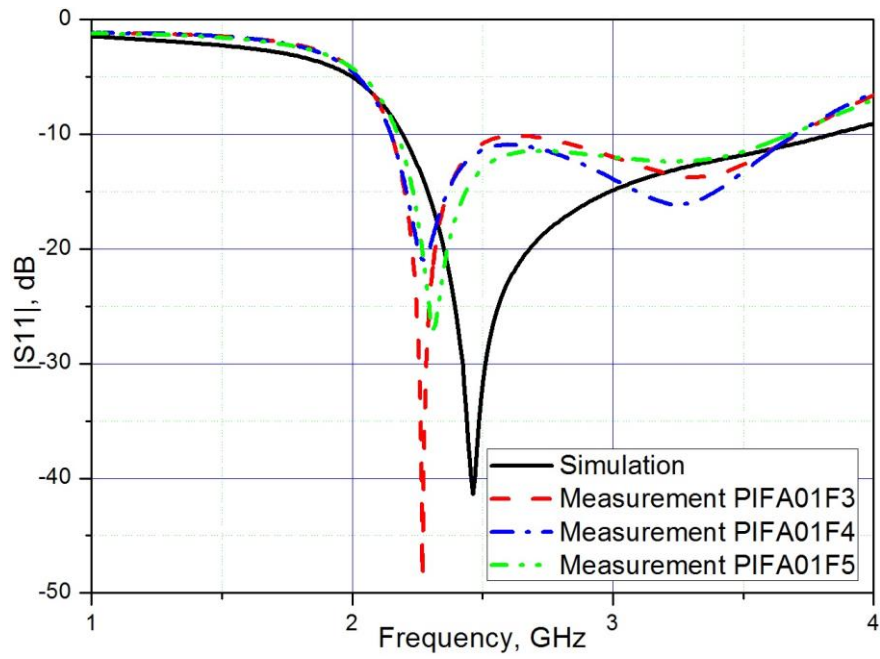


(a)

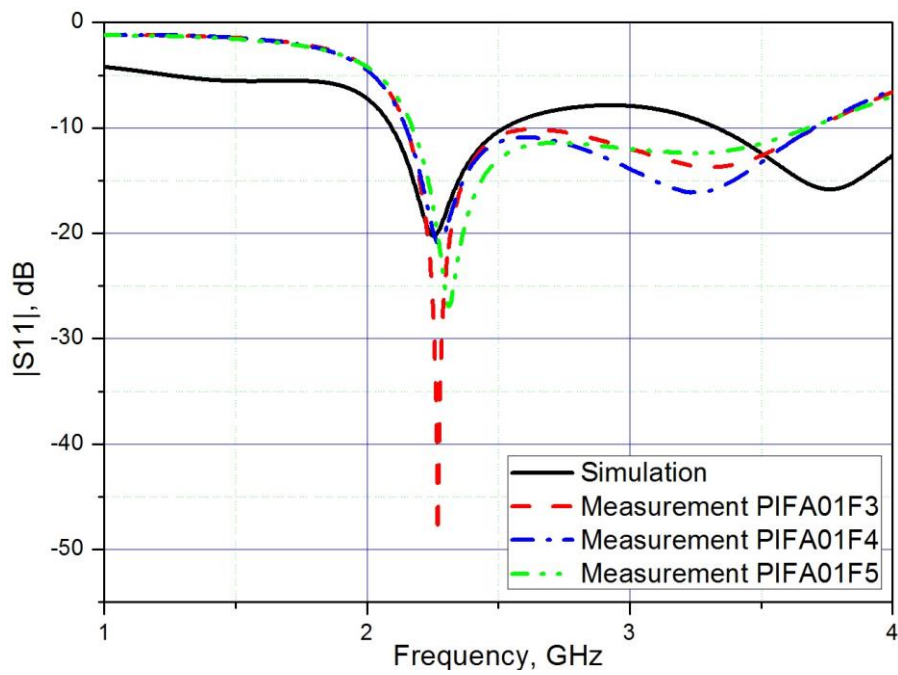


(b)

Figure 2.4. Geometrical study of the single-band IFA structure on E4D 200; (a) Effect of L_s with $h = 4$ mm; (b) Effect of h with $L_s = 21.5$ mm.



(a)



(b)

Figure 2.5. Reflection coefficient of the single-band PIFA - Simulation compared with measurement for 3 prototypes: (a) With the initial simulation; (b) With the more proper simulation.

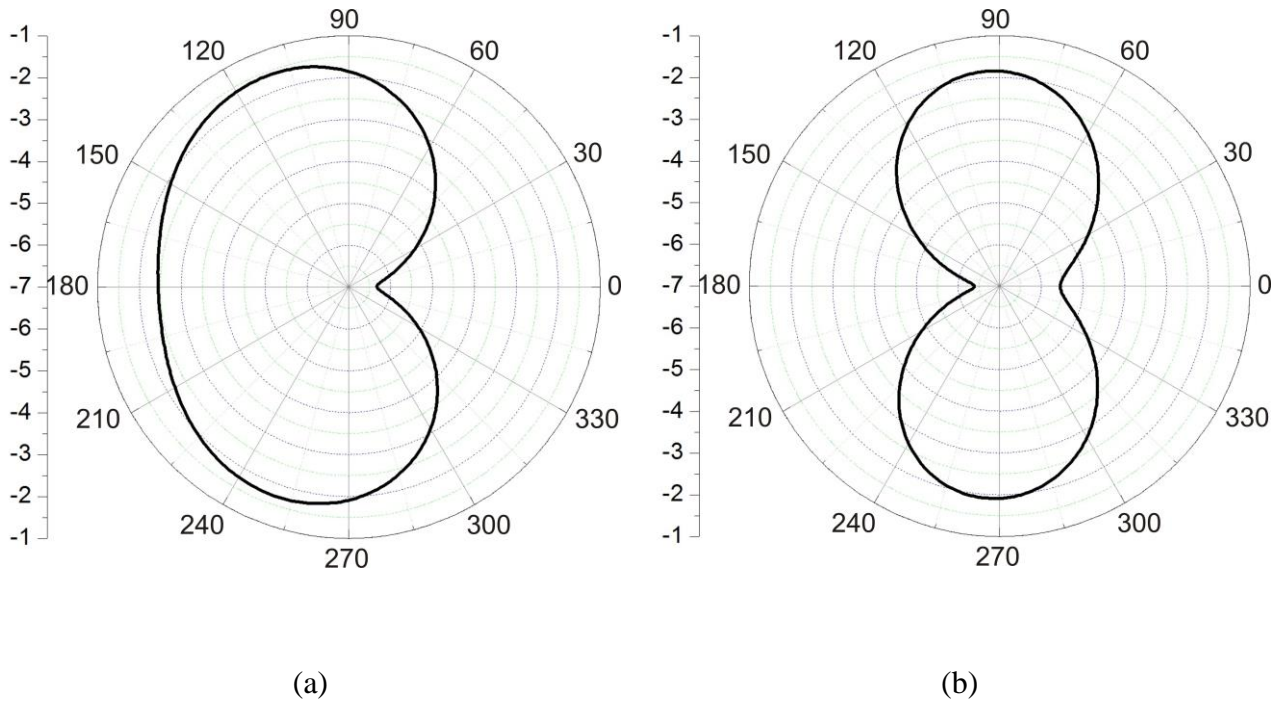


Figure 2.6. Simulated radiation patterns of the single-band IFA at the resonant frequency: (a) In x-z plane (E-plane); (b) In x-y plane (H-plane).

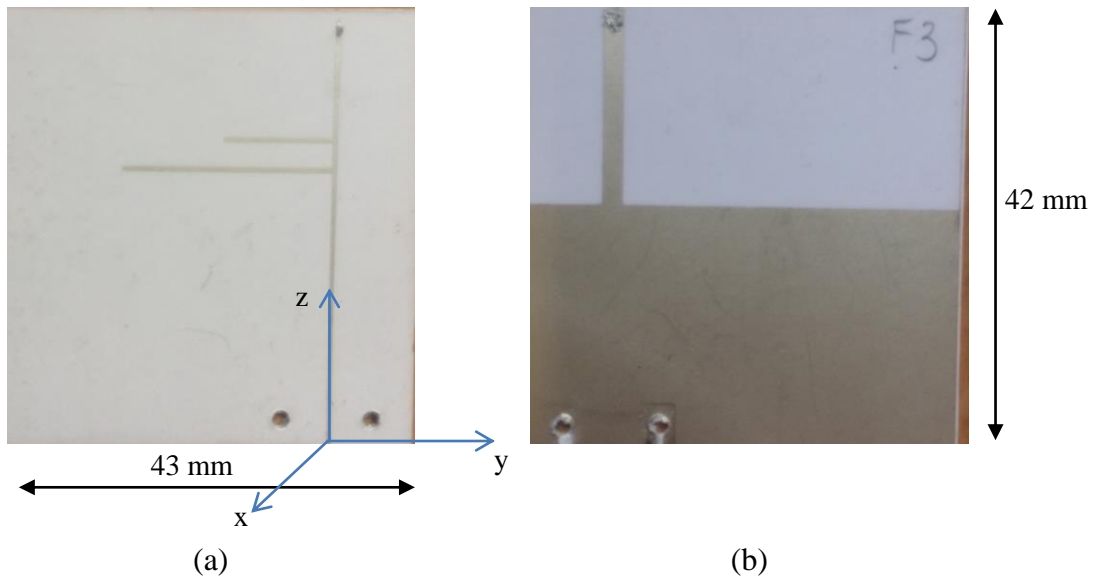


Figure 2.7. Printed dual-band IFA on E4D 200: (a) Front side; (c) Back side.

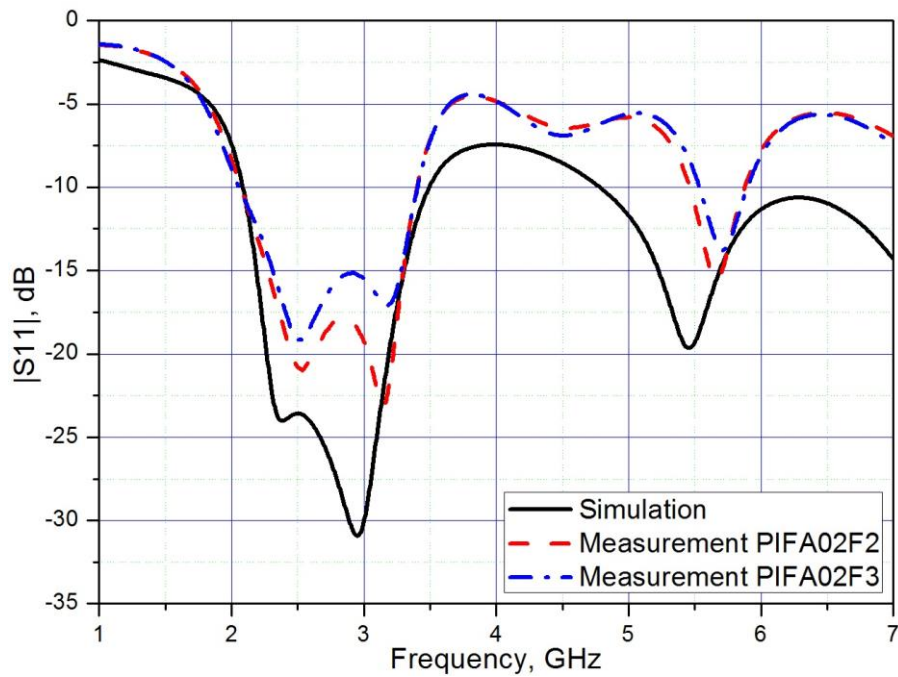


Figure 2.8. Reflection coefficient of the dual-band IFA - Simulation compared with Measurement for 2 prototypes.

2.4. Antennas with air-filled SIW technology on paper

The Substrate-Integrated Waveguide (SIW) is one of Substrate Integrated Circuits (SIC) topologies that have been introduced since the beginning of 2000's and have attracted researchers' attention thanks to their advantages such as compactness, light weight and are easily integrated in planar circuits [7]. The design of antennas using Substrate-Integrated Waveguide technique has been stated in some publications, usually to create cavity-backed structure in order to improve antenna gain [8, 9] or polarization properties at high frequencies [10]. Especially, in [11], the research group at University of Pavia, Italy proposed an antenna structure based on SIW designed on paper substrate. However, due to high losses of the substrate, the antenna efficiency is very low, causing low realized gain. The modified SIW technology proposed in [12] can solve this problem by filling an air layer in the SIW cavity to reduce losses of the total structure. This section analyzes a cavity-backed slot antenna based on air-filled SIW technology designed on multi-layer E4D paper.

Let us consider an antenna structure based on SIW technology, taken from [10], consisting of the E4D paper substrate, a microstrip feed line, the metallic layers on two faces of the substrate with via holes rows to create SIW structure. A slot is formed on a face plays role of an antenna (Figure 2.10).

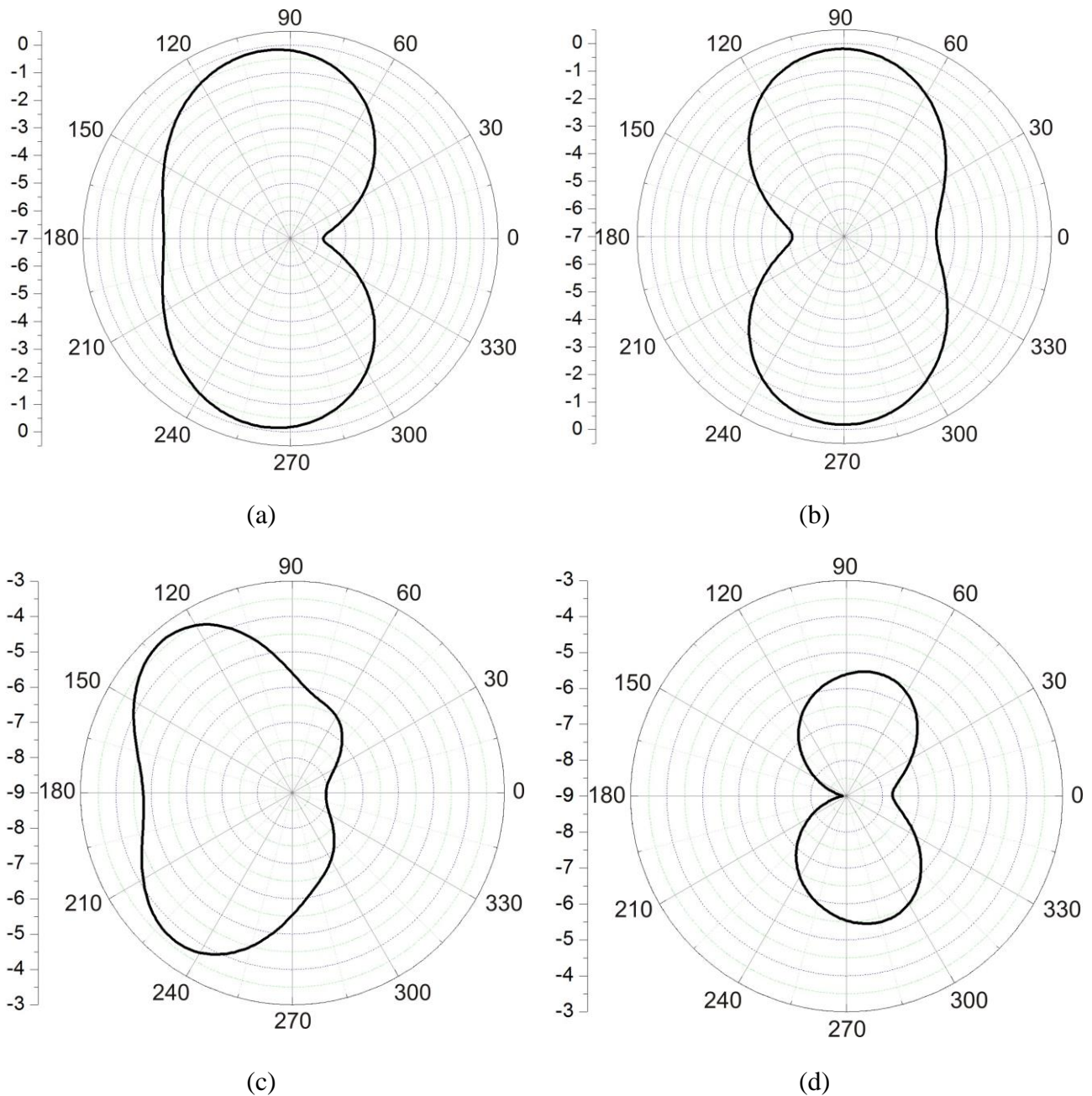


Figure 2.9. Simulated radiation patterns of the dual-band IFA: (a) In x-z plane ($\varphi = 0^\circ$), at 2.45 GHz; (b) In x-y plane ($\theta = 90^\circ$), at 2.45 GHz; (c) In x-z plane ($\varphi = 0^\circ$), at 5.5 GHz; (d) In x-y plane ($\theta = 90^\circ$), at 5.5 GHz.

Thus, the SIW structure acts as a back cavity to improve the gain of this antenna. The difference from the paper [10] is in an air-filled layer of dimensions $W_c \times L_c \times t_{subCav}$ in the substrate in order to reduce its dielectric losses (Figure 2.10(c) and (d)). The cavity height is chosen as $t_{subCav} = N \cdot 0.387 \text{ mm}$ as the biggest thickness of our E4D sheets is 0.387 mm, and several

E4D paper layers are glued together to create a thicker cavity. The matching characteristics and radiation patterns of the antenna are shown in Figure 2.11 with $N = 3$. The resonant frequency of the antenna is 5.2 GHz. The total efficiency is about 65%, much higher than 25% in the case without air cavity, so that the realized gain reached 5.17 dB despite high paper dielectric losses. Let us analyze the effect of the air cavity on the antenna total efficiency and realized gain.

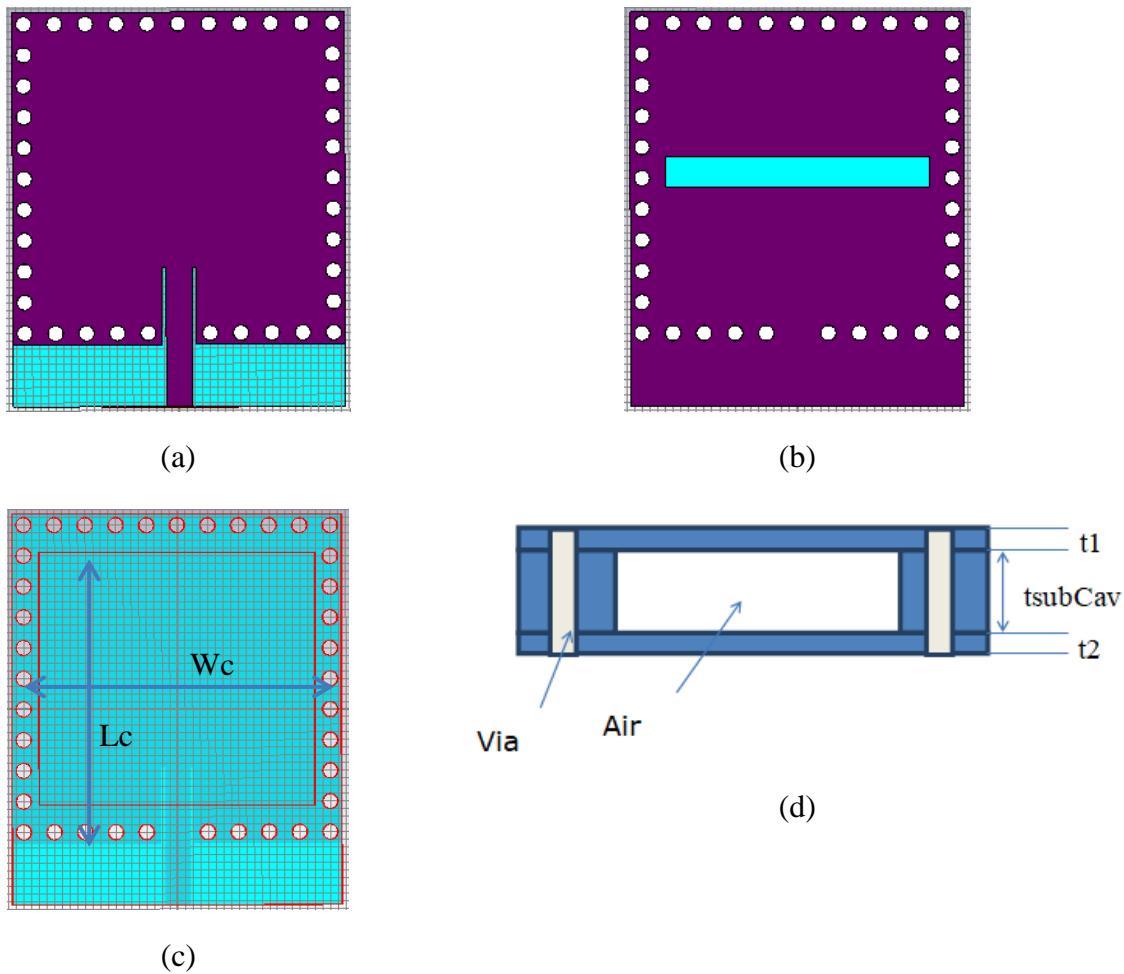
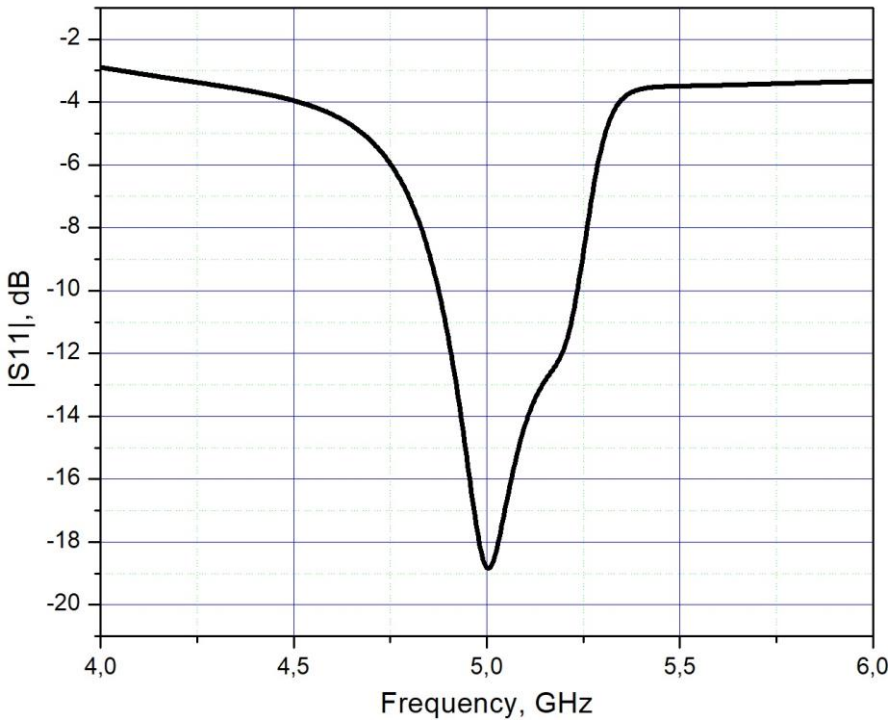


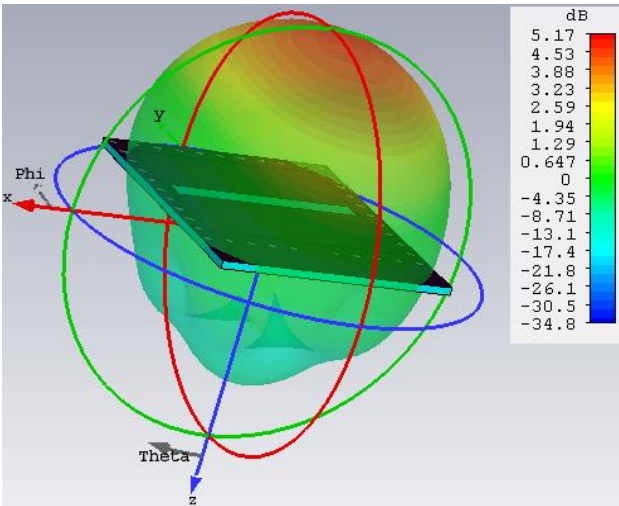
Figure 2.10. Configuration of an antenna based on Air-Filled SIW Technology: (a) Back side with the feed line; (b) Front side with the slot antenna; (c), (d) The cross sections of the air-filled cavity.

Fixing $L_c = 34$ mm and $W_c = 36$ mm, for $N = 1 - 6$, the resonant frequencies of the antenna are shifted, but not much, the first one $f_1 = 4.5 - 5.3$ GHz. For this type of antenna, when N increases, there is a trade-off between an increase of losses and the potential gain of the antenna. However, thanks to the air cavity, the losses increase not much. The total efficiency in

all cases is the best at the first resonant frequency, and reaches the highest value when $N = 3$, that means $t_{subCav} = 1.161$ mm (Figure 2.12).



(a)



(b)

Figure 2.11. Radiation characteristics of the antenna with $N = 3$, $L_c = 34$ mm, $W_c = 36$ mm:(a) Return loss; (b) Realized gain of the antenna in 3D at 5 GHz.

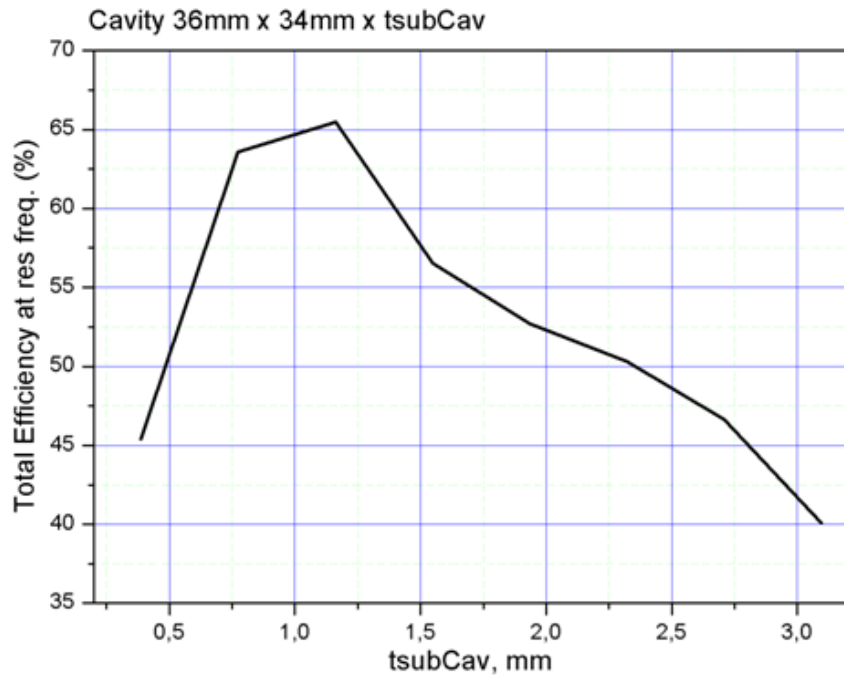


Figure 2.12. Effect of the cavity height on the total efficiency of the antenna at its resonant frequency for $L_c = 34$ mm and $W_c = 36$ mm.

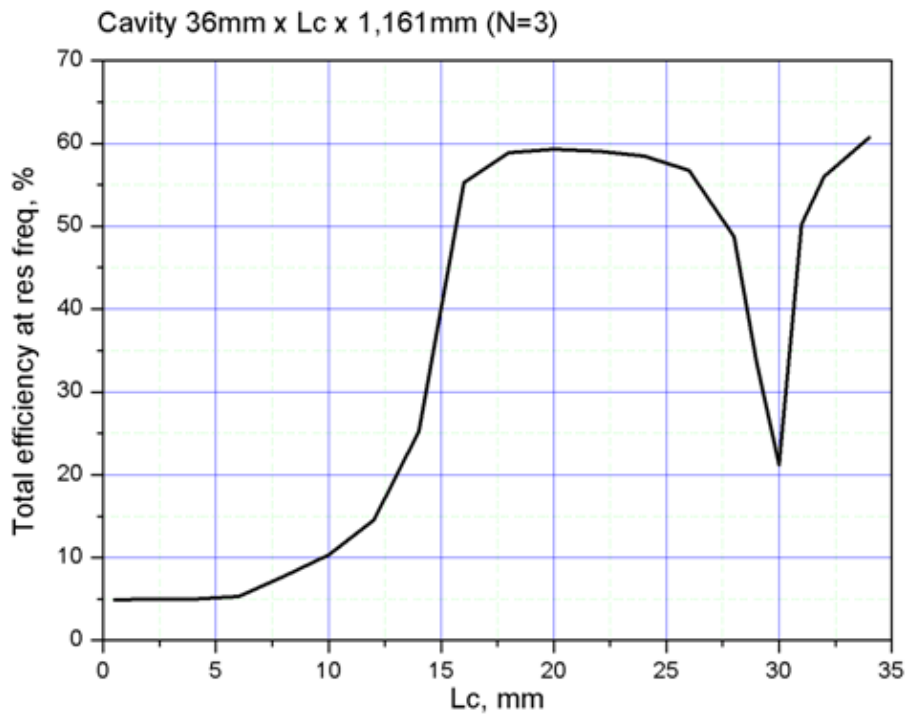


Figure 2.13. Effect of the cavity length on the total efficiency of the antenna at its resonant frequency for $N = 3$, $W_c = 36$ mm.

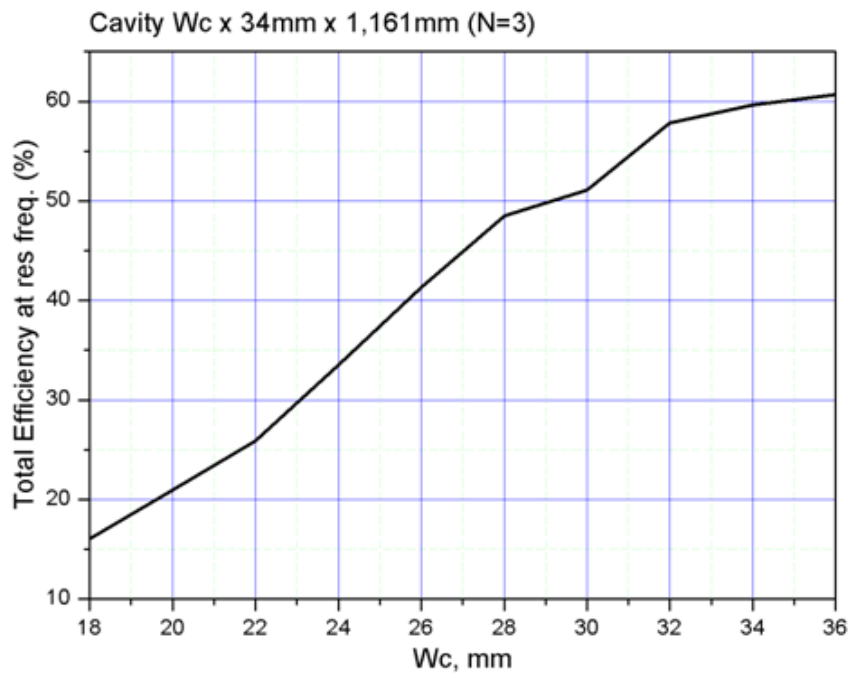


Figure 2.14. Effect of the cavity width on the total efficiency of the antenna at its resonant frequency for $N = 3$, $L_c = 34$ mm.

Now, let us consider the case, when $N = 3$, $W_c = 36$ mm, and L_c varies from 0.5 to 34 mm. A minimum of the total efficiency is observed at the value $L_c = 30$ mm, then this value grows sharply (Figure 2.13). L_c can still be increased but we limit it up to 34 mm in order to limit the antenna dimensions. Finally, $L_c = 34$ mm is chosen as for its considered values the total efficiency is the best.

When $N = 3$, $L_c = 34$ mm, and W_c is adjusted from 18 to 36 mm. The first resonant frequency is changed from 4.31 GHz to 5.1 GHz, and the total efficiency of the antenna is affected a lot and is the best for $W_c = 34$ mm (Figure 2.14). However, we do not increase L_c and W_c further in order not to increase the dimensions of the antenna.

The simulation results in this section are not compared to the measurement due to the current difficulties in realization of via holes on paper in the screen printing process. This kind of antennas gives high gain, acceptable total efficiency, so this section can be a good reference for design of a paper-based high gain antenna. However, in our case, its performance changes a lot under bending or deformation because the back cavity changes completely its form. Moreover, it operates at a single frequency, and its dimensions cannot be compact at lower frequency such as WLAN 2.45 GHz.

Conclusions for Chapter 2

1. Among different types of paper substrates, we chose E4D as it is compatible to the fabrication process with screen printing technology and the future mass production. This paper was characterized by the method of perturbation on 50 samples with the results: $\epsilon_r = 3.184$, $\tan\delta = 0.092$ at 2.5 GHz with the dispersions of 0.25% for ϵ_r and 0.26% for $\tan\delta$.
2. An inverted-F antenna (IFA) was designed on 0.21-mm thick E4D paper with the resonant frequency of 2.3 GHz. The total efficiency of the antenna is about 70%, the radiation patterns of this antenna at the resonant are very similar to omni-directional that makes this kind of antennas attractive. Another IFA was designed on the same paper with two WLAN resonant frequencies of 2.45 GHz and 5.5 GHz, that showed one of the advantages of the modified IFA – the easiness of adding resonant frequencies. This type of antenna has stable electrical properties. However, it causes some technological difficulties because of the existence of via holes.
3. The Substrate-Integrated Waveguide (SIW) cavity-backed antenna was designed at 5.2 GHz on three layers of 0.387-mm thick E4D paper glued together and a slot radiation element. The difference from the other authors' previous works is the existence of an air cavity inside the antenna, which could easily be realized in the process of gluing the paper layers. The total efficiency of the antenna is about 65%, much higher than 25% in the case without air cavity, so that the realized gain reached 5.17 dB despite high paper dielectric losses. However, this kind of antennas does not meet our need for transforming into three-dimensional structure(s), its performance changes a lot under bending or deformation because the back cavity changes completely its form.
4. The antennas designed in this chapter are single-band. However, a set-top box to be built nowadays is usually multi-standard, multi-frequency. Thus, in order to avoid using multiple single-band antennas that makes the system too bulky, the following chapter presents the design of the building block antenna components operating at multi- band as well as a wide band of frequency focusing on two WLAN bands.

References for Chapter 2

- [1] H. P. Phan, T.-P. Vuong, P. Benech, P. Xavier, J.-M. Duchamp, "Caractérisation de propriétés diélectriques des matériaux souples", GDR Ondes, Lyon, 19-21 Oct. 2015.
- [2] J. A. Ray, S. R. B. Chaudhuri "A review of PIFA technology", Antenna Week (IAW), 2011 India.
- [3] S. Manjula, B. Choudhury" Miniaturized Planar Inverted-F Antenna", Chapter 3 in the book "Metamaterial Inspired Electromagnetic Applications", Springer 2017.
- [4] S. E. Hosseini, A. R. Attari, and A. Pourzadi, "A Multiband PIFA with a Slot on the Ground Plane for Wireless Applications", International journal of Information and Electronics Engineering, Vol. 3, N4, 2013.
- [5] M. S. Ahmad, C. Y. Kim, and J. G. Park, "Multi shorting Pins PIFA Design for Multiband Communications", Hindawi International Journal of Antennas and Propagation, 2014.
- [6] D. E. Anagnostou, A.A.Gheethan et al., "A Direct-Write Printed Antenna on Paper-Based Organic Substrate for Flexible Displays and WLAN Applications", Journal of Display Technology, Vol. 6, pp. 558-564, No.11, 2010.
- [7] K. Wu, D. Deslandes, Y Cassivi, "The substrate integrated circuits - a new concept for high-frequency electronics and optoelectronics", Telecommunications in Modern Satellite, Cable and Broadcasting Services, 2003, TELSIS 2003, 6th International Conference on, pp. P-III-P-X, vol. 1, 2003.
- [8] W. Hong ; B. Liu ; G. Q. Luo ; Q. H. Lai ; J. F. Xu ; Z. C. Hao ; F. F. He ; X. X. Yin, " Integrated Microwave and Millimeter Wave Antennas Based on SIW and HMSIW Technology", International Workshop on Antenna Technology: Small and Smart Antennas Metamaterials and Applications, 2007. IWAT '07.
- [9] K. Kumar, S.Dwari, "Substrate Integrated Waveguide Cavity-Backed Self-Triplexing Slot Antenna", IEEE Antennas and Wireless Propagation Letters, vol. 16, pp. 3249-3252, 2017.
- [10] T. Zhang, W. Hong, Y. Zhang, and K.Wu, "Design and Analysis of SIW Cavity Backed Dual-Band Antennas With a Dual-Mode Triangular-Ring Slot", IEEE Trans. On Antennas and Propagation, Vol. 62, N. 10, 2014.

- [11] S.Moscato, R. Moro, M. Pasian, M.Bozzi, L.Perregrini, "Innovative manufacturing approach for paper-based substrate integrated waveguide components and antennas", *IET Microwaves, Antennas & Propagation*, 2016, Vol. 10, Iss. 3, pp. 256–263.
- [12] F.Parment, A.Ghiotto, T.-P.Vuong, J.-M. Duchamp, and K. Wu, "Air-Filled Substrate Integrated Waveguide for Low-Loss and High Power-Handling Millimeter-Wave Substrate Integrated Circuits", *IEEE Trans. on Microwave Theory and Techniques*, vol. 63, pp. 1228-1238, N. 4, 2015.

3. Chapter 3 – Design of Wide-Band and Multi-Band Antennas on Paper

In the previous chapter the single-band antennas such as CPW-fed monopoles, inverted-F, SIW cavity-backed antennas have been designed on paper substrates and tested. However, a set-top box to be built nowadays is usually multi-standard, multi-frequency. Thus, in order to avoid using multiple single-band antennas that makes the system too bulky, this chapter presents the design of the building block antenna components operating at multi-band as well as a wide band of frequency focusing on two WLAN bands. The proposed antennas are designed on 104- μm thick E4D paper (E4D 100), apart from “Hello-shaped” presented in the Section 3.2 and the multi-band in the Section 3.3 that will be designed on the same paper E4D with 210- μm thickness.

It is clear, that CPW feeding is the best candidate for wideband antenna structure, such as presented in [1-5]. Furthermore, they can easily be realized on one side of a substrate and also contribute to miniaturize antenna structures. However, for very thin substrates, too narrow slots in 50-ohm CPW feed lines can cause difficulties in fabrication with high accuracy or become impossible because of technological restrictions.

To avoid this problem, with the double-side printing possibility, we chose the conventional microstrip feeding method.

3.1. Microstrip-fed wideband antennas

3.1.1. “Sapin” antenna

The antenna structure called, by its shape (Figure 3.1(a)), “Sapin” (in French) [6], that means “Fir-tree”, was initially designed from a simple rectangular patch. Then, it was transformed into trapezoidal (Figure 3.1(a)) and modified into a triangular patch monopole (Figure 3.1(b)). Next, the edges of the patch were modified, rounded and the shape was optimized to get matching at two WLAN frequency bands. The ground planes of all designs are cleared under the antenna areas to provide their omni-directional radiation patterns. In order not to be confused further, Figure 3.1(d) reminds the spherical coordinate system with θ and φ , that clarifies that $\varphi = 0^\circ$ means x-z plane and $\theta = 90^\circ$ means x-y plane. The matching characteristics of the antennas in

this design process with geometric studies are shown in Figure 3.2. It can be noticed, that trapezoidal or simple triangular patches matched at only one frequency while a little modification of the triangle lower base gave another resonance at higher frequency.

In order to produce higher return loss over a wide frequency band, the ground planes of both antennas were rounded at the edges as shown in the double-face prototype pictures (Figure 3.2(c)), and their better performance can be seen in Figure 3.3, Figure 3.4 presents the final $|S_{11}|$ parametric optimization to choose the height h_{04} that had the strongest effect on the antenna matching characteristics. Finally, the obtained geometrical parameters are: $W = 28$ mm, $L = 57$ mm, $W_{02} = 24$ mm, $h_{01} = 22$ mm, $h_{02} = 3$ mm, $h_{03} = 21.3$ mm, $h_{04} = 30$ mm.

Due to high dielectric losses of the E4D paper ($\tan\delta = 0.092$), the monopole antenna proposed in this Section does not have high efficiency resulting in their low gain. At 2.45 GHz, The total efficiency of "Sapin" is 74.4% with the gain of 1.27 dBi, at 5.5 GHz these values are reduced to 56.8% with the gain of 0.94 dB.

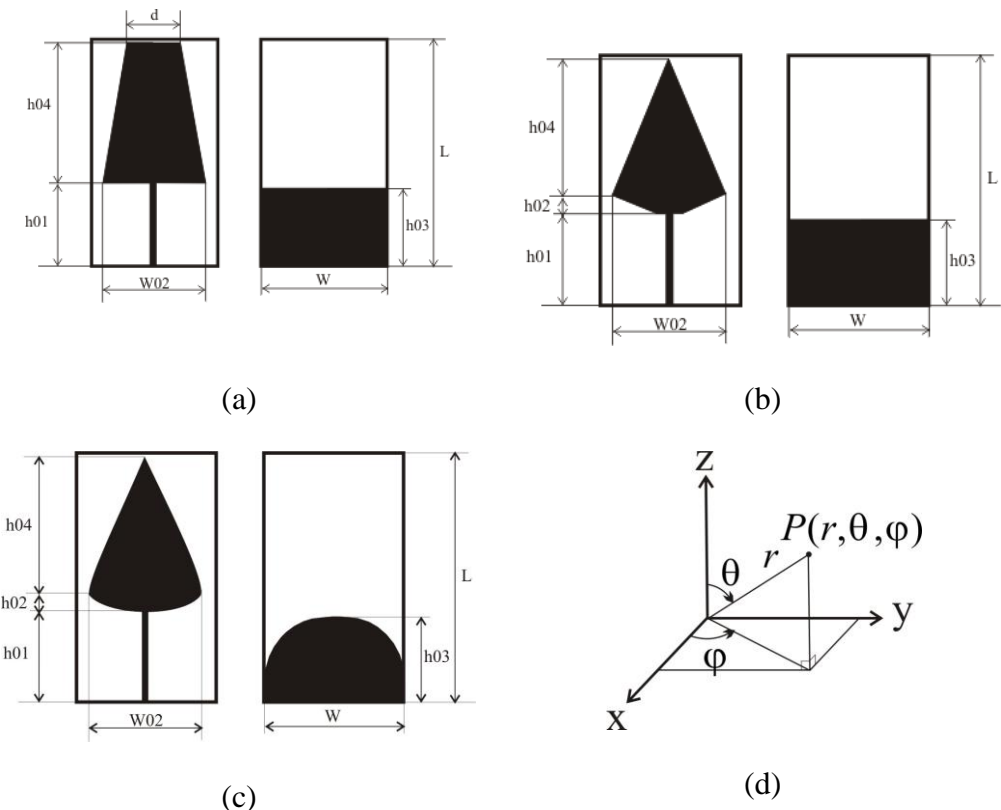


Figure 3.1. The design process of the antennas: (a) Initial trapezoidal structure; (b) Modification of the initial structure; (c) Final structure of "Sapin" antenna; (d) Spherical coordinate system.

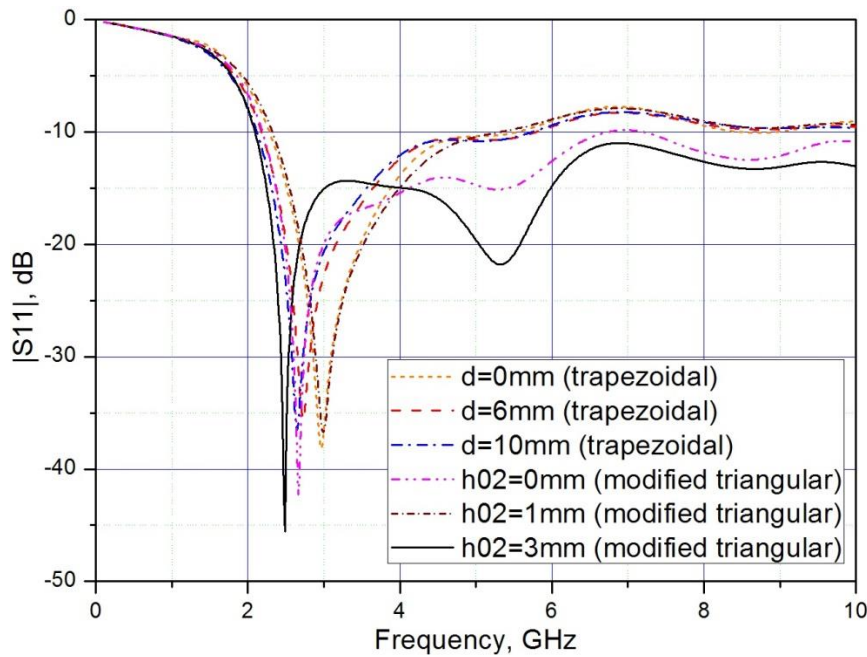


Figure 3.2. $|S_{11}|$ parametric study of the initial designs.

Six prototypes of the proposed design were fabricated at CTP (Technical Center of Paper) by screen printing technology on both faces shown in Figure 3.5. In order to test the antenna, its reflection coefficient and radiation patterns were characterized by using a Vector Network Analyzer (VNA) in IMEP-LAHC anechoic chamber as presented in Appendix 2. The simulation compared to measurement reflection coefficients were nearly identical for all six of them, and that of one prototype is presented in Figure 3.6.

It can be seen, that the measured resonant frequencies are very close to the simulated ones, the error was about 150 MHz at 2.45 GHz and 25 MHz at 5.5 GHz, which means around 7% and 0.5%, respectively. It can be explained by more significant tolerance of the measurement at lower frequency due to the cable not isolated enough by absorbers or the imprecision of dielectric properties of the E4D paper or the printing process still exists. Besides, the measured return loss of the antenna showed the very large bandwidth, from 2 GHz to over 10 GHz, a little larger than predicted by the simulation.

In Figure 3.7, a slight disagreement between the measurement and simulation radiation patterns is observed, that can be explained by the small ground plane of the antenna causing stronger coupling between the antenna and the cable, as well as the effect of the metallic motor and stretching of the cable of the measurement system.

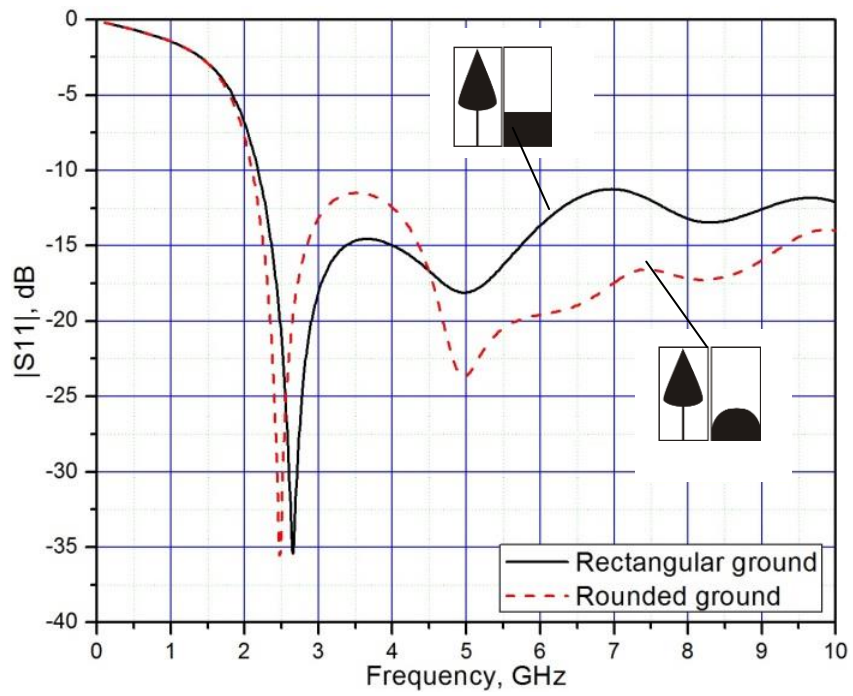


Figure 3.3. Simulated reflection coefficient of the antenna with rectangular ground plane versus rounded ground plane.

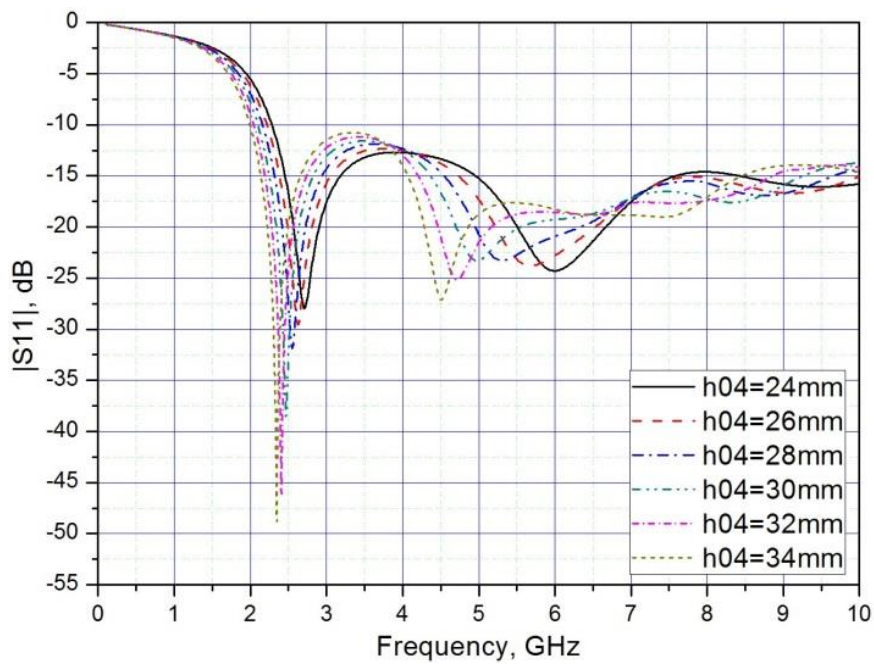


Figure 3.4. $|S_{11}|$ parametric study of the proposed antenna "Sapin" for $W_{02} = 28$ mm, $L = 59$ mm, $h_{01} = 22$ mm, $h_{02} = 3$ mm, $h_{03} = 21.3$ mm, $h_{04} = 30$ mm.

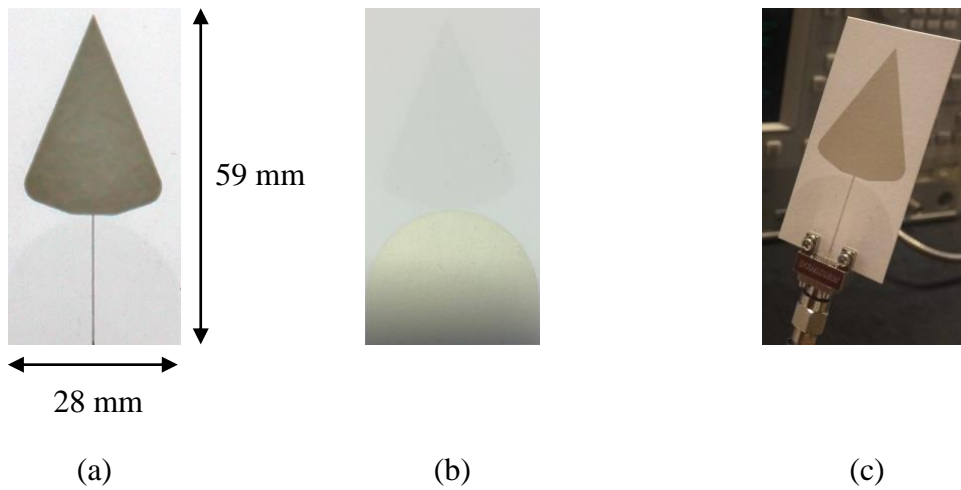


Figure 3.5. A prototype obtained by the screen printing technology; (a) Front side; (b) Back side; (c) The prototype with the connector.

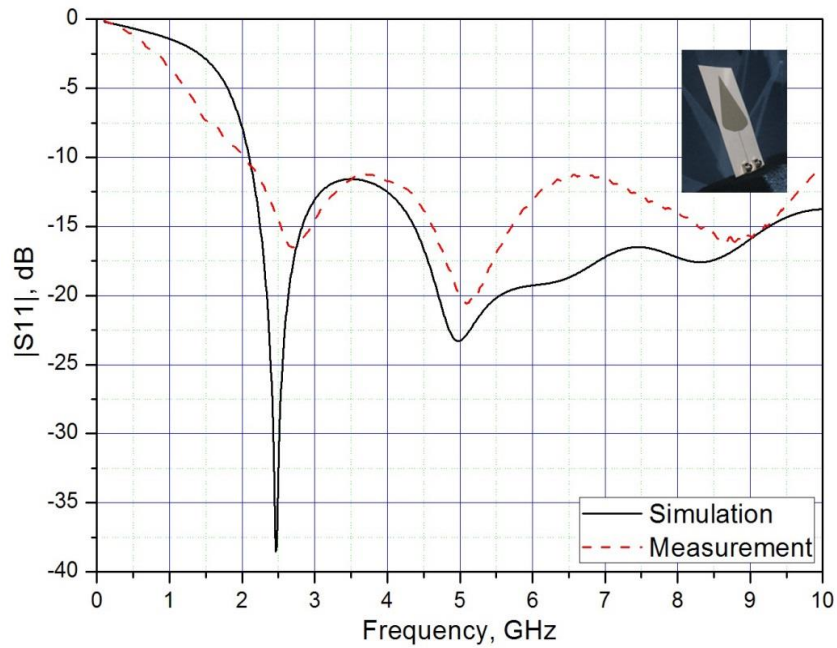


Figure 3.6. Reflection coefficient of the antenna “Sapin”– Simulation compared to measurement.

Another “Sapin” antenna has been designed based on the same principle but on E4D paper with the thickness of 210 μm , with the dimensions of 28 mm \times 57 mm. The performance of this antenna is also good as the first one over a very wide frequency band from 2 GHz to over 10 GHz that will be used further to create an antenna system placed in a plastic ABS box.

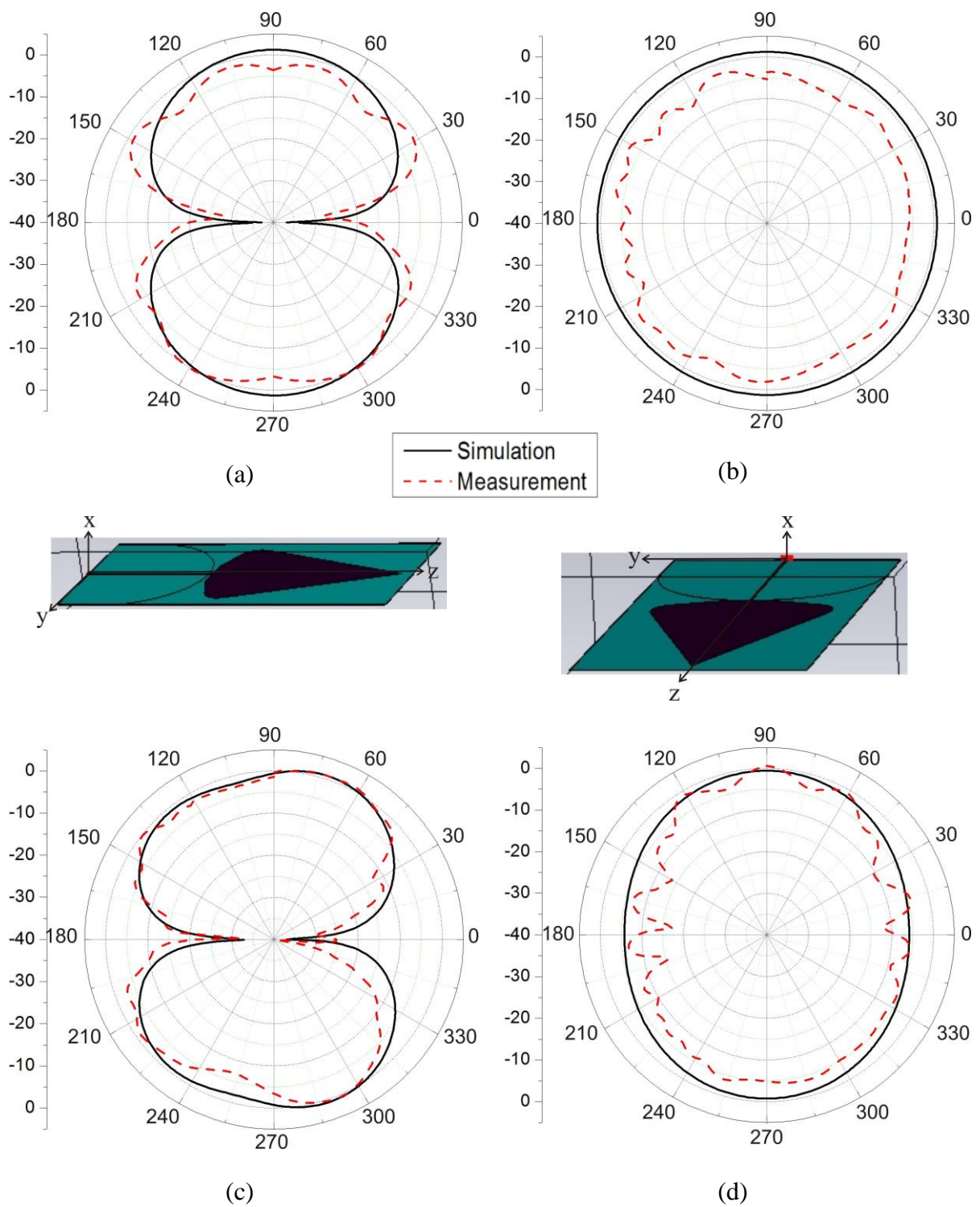


Figure 3.7. Simulated and measured radiation patterns of “Sapin”: (a) x-z plane ($\varphi = 0^\circ$), at 2.45 GHz; (b) x-y plane ($\theta = 90^\circ$), at 2.45 GHz; (c) x-z plane ($\varphi = 0^\circ$), at 5.5 GHz; (d) x-y plane ($\theta = 90^\circ$), at 5.5 GHz.

3.1.2. “Modified Sapin” antenna

Observing, that the current is distributed mainly on the borders of the antenna “Sapin” presented in the previous section, the antenna structure proposed in this section is its modification (Figure 3.8(a)) [7, 8], inspired by the “Symbol of the Death Hollows” in J. K. Rowling’s famous book Harry Potter (Figure 3.8(b)) in order to be more flexible in geometrical parameters’ optimization and reduce the sensitivity of the antennas’ geometries to their resonant frequencies. The ground plane of the design is cleared under the patch areas as well as in “Sapin” to provide its omni-directional radiation patterns and rounded at the edges to improve the matching characteristics.

This “Modified Sapin” structure reduces a huge amount of ink for mass production in the future. Besides, after a S11 parametric optimization, the length of the modified antenna was 50 mm, reduced by 7 mm compared to the original “Sapin”.

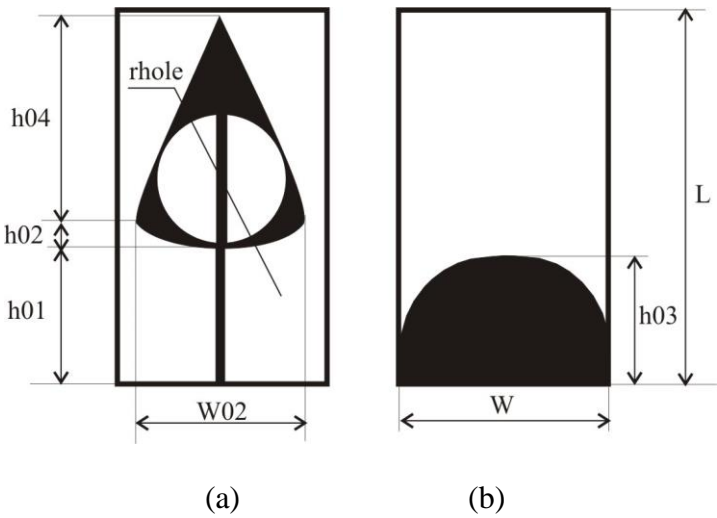
Figure 3.9 shows the reflection coefficient of both “Sapin” and “Modified Sapin” antennas with rectangular and rounded grounds over a wide range of frequency 0.1-10 GHz. It can be seen, that the matching properties of “Modified Sapin” is well provided even though its dimensions are less than “Sapin”. The bandwidth of the proposed antenna is very large at high frequency range, from 2.2 GHz up to over 10 GHz.

The efficiency of "Modified Sapin" antenna is also not high as well as in the case of “Sapin”. At 2.45 GHz, the total efficiency is 77% with the gain of 1.1 dBi, and at 5.5 GHz this value is reduced to 68% with the gain of 1.63 dBi, respectively.

The prototype with 2.92 mm Jack End Launch Connector is shown in Figure 3.10(c). The simulated and measured return loss of the antenna is shown in Figure 3.11. It can be noted, that the measured reflection coefficient fits well with the simulated one, especially for the resonant frequencies. At lower WLAN frequency 2.45 GHz, the error was about 40 MHz and 50 MHz at higher WLAN frequency 5.5 GHz, that means around 1.6% and 0.9%, respectively. It can be explained by more significant tolerance of the measurement at WLAN lower frequency due to the cable not isolated enough by absorbers or the imprecision of dielectric properties of the E4D paper. Besides, the measured return loss of the antennas showed the very large bandwidth, from 2.15 GHz to over 10 GHz for “Modified Sapin”, a little larger than predicted by the simulation.

In Figure 3.12, a slight disagreement between the measurement and simulation is observed, that can be explained by the small ground plane of the antenna causing stronger coupling between

the antenna and the cable, as well as the effect of the metallic motor and stretching of the cable of the measurement system.



$W = 28 \text{ mm}$, $L = 50 \text{ mm}$, $W02 = 24 \text{ mm}$, $h01 = 22 \text{ mm}$, $h02 = 3 \text{ mm}$, $h03 = 21.3 \text{ mm}$, $h04 = 23 \text{ mm}$, $rhole = 7.8 \text{ mm}$

Figure 3.8. “Modified Sapin” antenna geometry; (a) Front side; (b) Back side.

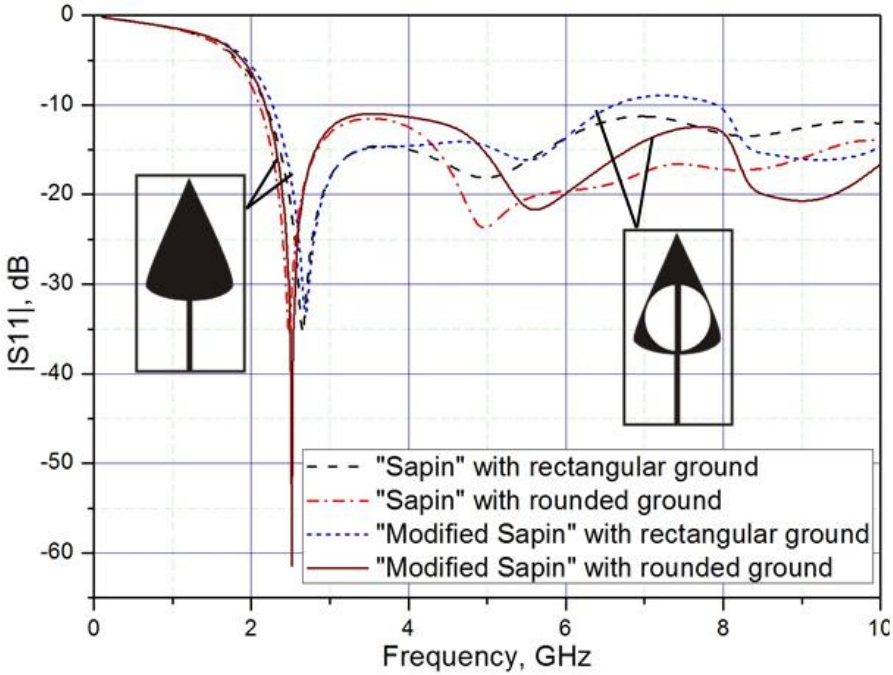


Figure 3.9. Simulated reflection coefficients of the antennas with rectangular ground plane versus rounded ground plane.

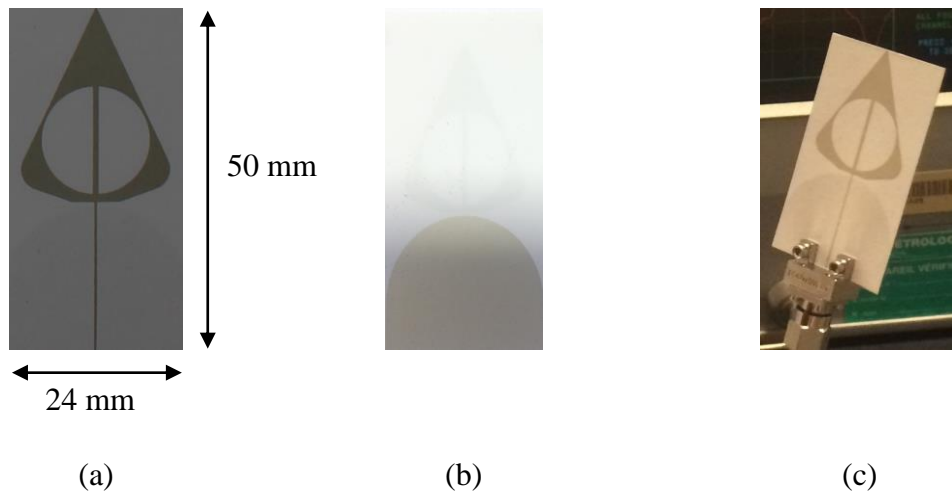


Figure 3.10. A prototype obtained by the screen printing technology; (a) Front side; (b) Back side; (c) The prototype with the connector.

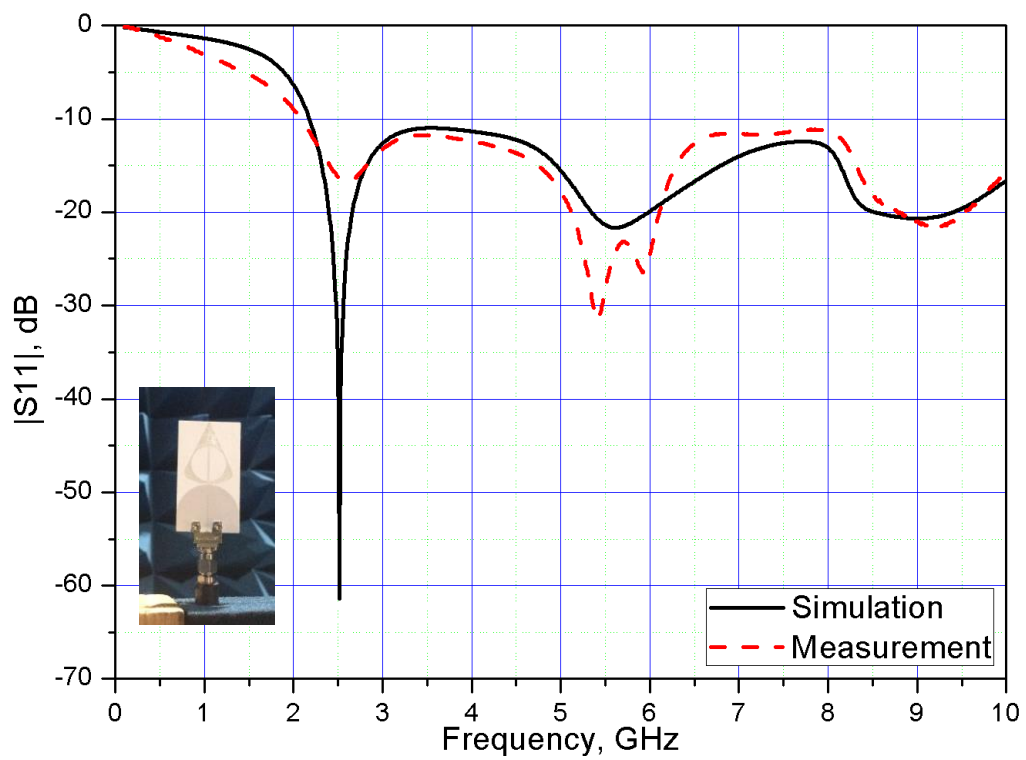


Figure 3.11. Reflection coefficient of the antenna antenna “Modified Sapin” – Simulation compared to measurement.

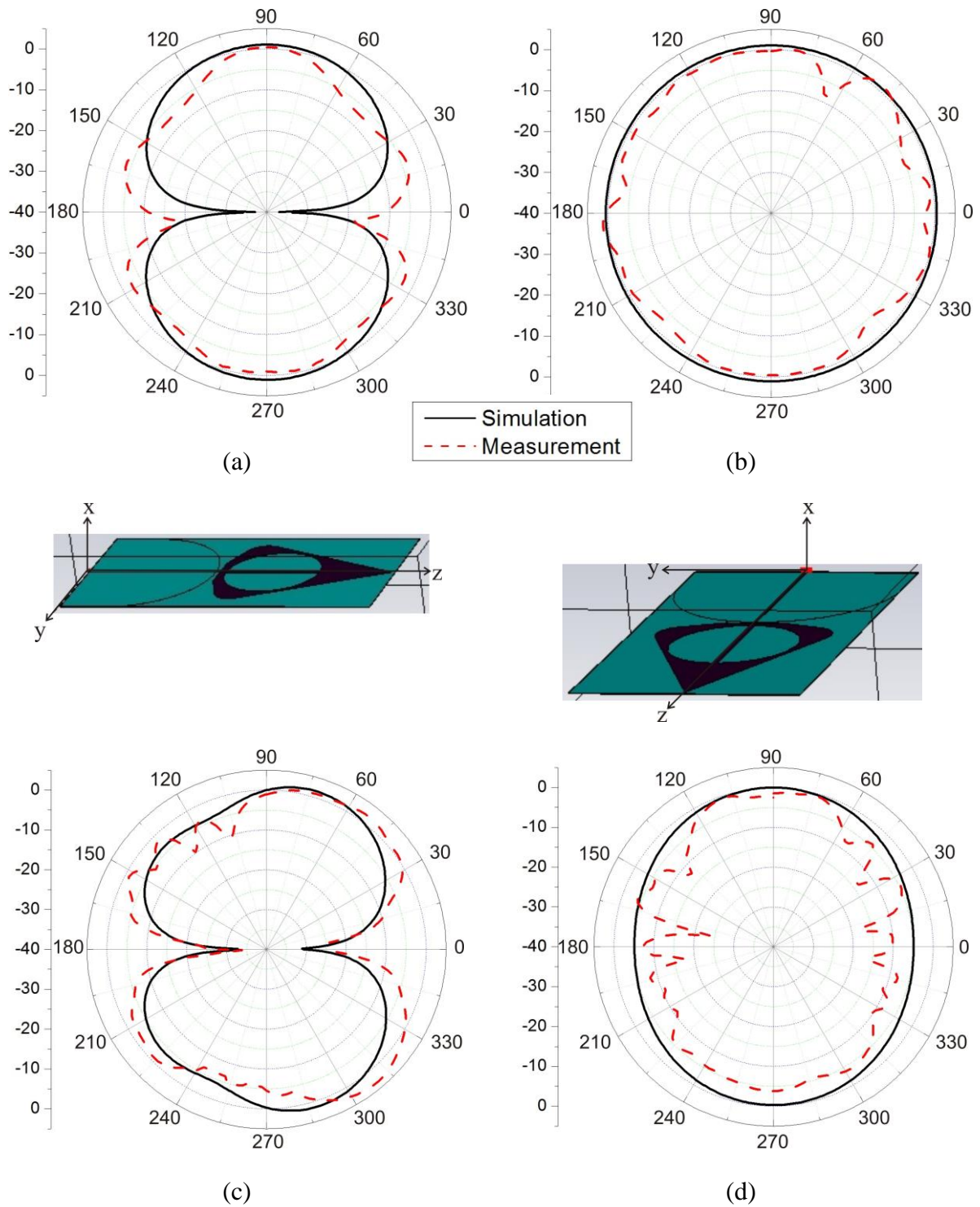
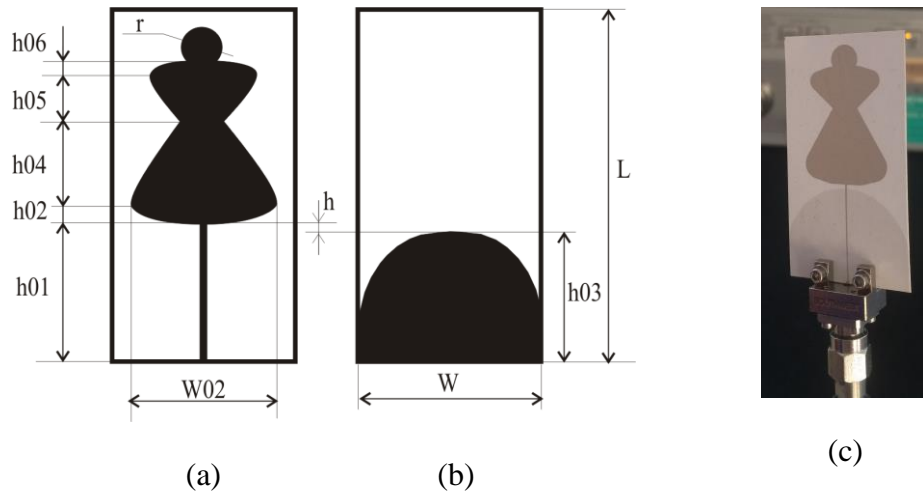


Figure 3.12. Simulated and measured radiation patterns of “Modified Sabin”: (a) x-z plane ($\varphi = 0^\circ$), at 2.45 GHz; (b) x-y plane ($\theta = 90^\circ$), at 2.45 GHz; (c) x-z plane ($\varphi = 0^\circ$), at 5.5 GHz; (d) x-y plane ($\theta = 90^\circ$), at 5.5 GHz.

3.1.3. “Robe” antenna

One of methods to reduce the cost of an antenna is to change its shape so that the amount of silver ink is reduced. In the previous “Modified Sapin”, the shape was changed by introducing a hole. The antenna structure on E4D paper of 104- μm thickness proposed in this section is also a modification of our previous design “Sapin” with reduction of metal at the edge of the shape (Figure 3.13(a)). As for the previous designs, the microstrip feeding method was also chosen to avoid the problem of narrow slots in CPW structures. The ground plane of the design is cleared under the patch areas to provide its omni-directional radiation patterns and rounded at the edges to improve the matching characteristics (Figure 3.13) [9]. After the S11 parametric optimization, the length of the modified antenna, named by its shape as “Robe” (that means “Dress” in English), was 49 mm, reduced by 10 mm compared to the original “Sapin”. The simulation shows, that the reflection coefficient of both “Sapin” and “Robe” antennas with rectangular and rounded grounds over a wide range of frequency 0.1 – 10 GHz. It is clearly seen, despite its dimensions less than “Sapin”, the matching properties of “Robe” is also well provided over a large bandwidth from 2.2 GHz to 3.3 GHz and from 4.4 GHz up to over 10 GHz. At two WLAN frequencies 2.45 GHz and 5.5 GHz it reaches very good matching with the return loss of 47 dB and 65 dB, respectively. The simulated realized gain is 1.21 dBi at 2.45 GHz and 1.66 dBi at 5.5 GHz, the total efficiency is 75.5% at 2.45 GHz and 60% at 5.5 GHz, that are acceptable for antennas on high loss paper substrate.

At the same run with the previous antennas, six prototypes of the design have been printed at CTP by using double-side screen printing technology (Figure 3.13(c)). The simulated and measured return loss results show a good fit for all prototypes, one of them is illustrated in Figure 3.14. Despite the big frequency shift of about 200 MHz at 2.45 GHz (8.1%) and 90 MHz at 5.5 GHz (1.6%), the measured matching bandwidth is well provided at wider frequency band compared to the simulated, from 1.65 GHz up to over 10 GHz. The results of simulation compared to measurement in the x-y plane ($\theta = 90^\circ$) and the x-z plane ($\varphi = 0^\circ$) are presented in Figure 3.15, where x-axis is in the normal direction and z-axis is parallel to the feed line of the antenna under test. The error between the measurement and simulation can be explained by the small ground plane of the antenna causing stronger coupling between the antenna and the cable, as well as the effect of the cable, the roughness of the metallic antenna layer and the tolerance of dielectric properties of the E4D paper.



$W = 28 \text{ mm}$, $L = 49 \text{ mm}$, $W02 = 24 \text{ mm}$, $h01 = 20 \text{ mm}$, $h02 = 1 \text{ mm}$, $h03 = 21.3 \text{ mm}$, $h04 = 15 \text{ mm}$, $h05 = 6 \text{ mm}$, $r = 3 \text{ mm}$

Figure 3.13. “Robe” antenna geometry: (a) Front side; (b) Back side; (c) Prototype obtained by the screen printing technology with the connector.

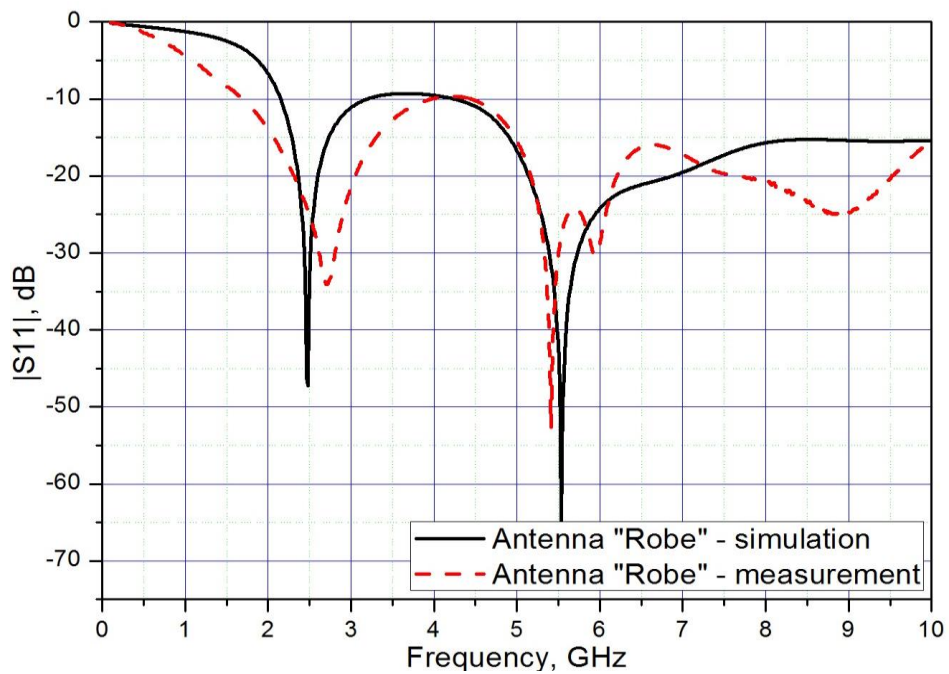


Figure 3.14. Reflection coefficient of “Robe” – Simulation compared to measurement.

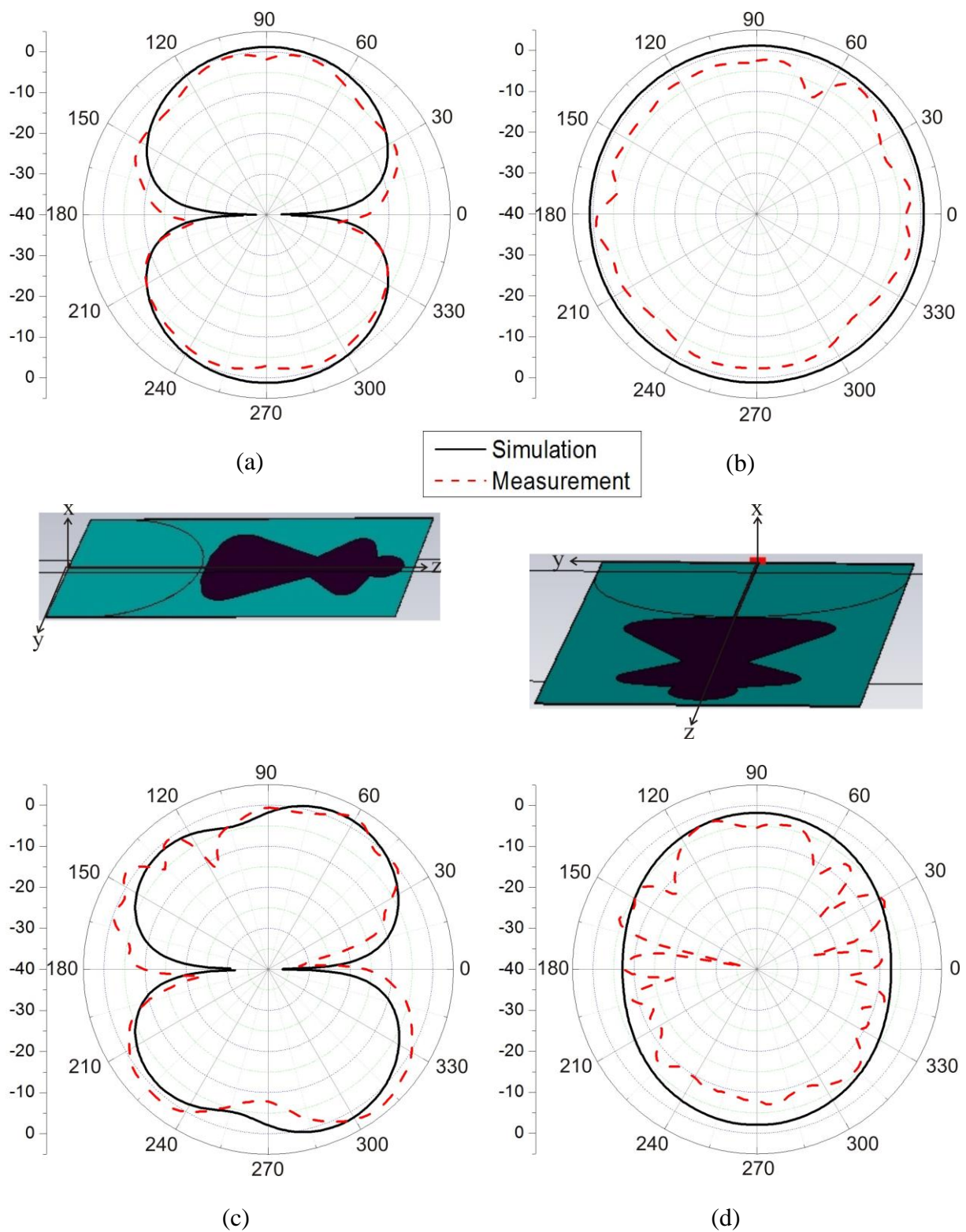


Figure 3.15. Simulated and measured radiation patterns of “Robe”: (a) x-z plane ($\varphi = 0^\circ$), at 2.45 GHz; (b) x-y plane ($\theta = 90^\circ$), at 2.45 GHz; (c) x-z plane ($\varphi = 0^\circ$), at 5.5 GHz; (d) x-y plane ($\theta = 90^\circ$), at 5.5 GHz.

3.1.4. "Mushroom-Shaped with Two Arms" antenna

The initial design of the antenna is a simple monopole with a circular patch (Figure 3.16(a)), then cut from two sides to be transformed into a mushroom-shaped patch monopole to get the resonant frequency at 5.5 GHz, the second WLAN frequency band (Figure 3.16(b)). In fact, a circular patch itself can be designed to cover a rather wide frequency band, but it is hard to control its size to resonate over a wide band with the best matching at two frequencies of interest. To facilitate the design process while keeping the symmetry and the dimensions of the structure, two symmetrical thin "arms" are added to aim at the lower frequency band around 2.45 GHz (Figure 3.16(c) and (d)).

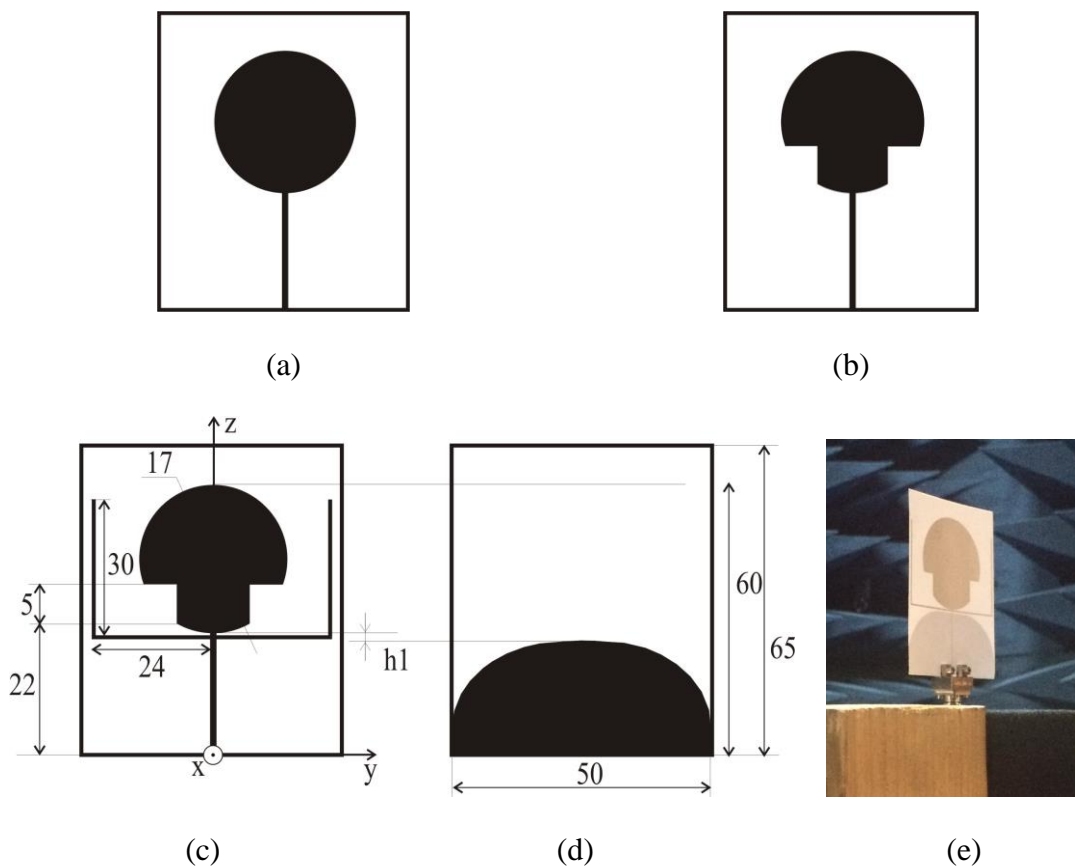


Figure 3.16. Evolution of the antenna design process: (a) Circular; (b) Mushroom-shaped; (c) Mushroom-shaped with two arms and its geometries, front side; (d) Back side; (e) A fabricated prototype.

Due to coupling effect, the radius of the "mushroom" as well as the length of the "arms" were to be adjusted to match well at two those WLAN frequency bands. In order to provide their omni-directional radiation patterns, the ground planes of all structures are cleared under the

antenna areas and then rounded at the upper corners to improve matching properties. Among its geometrical parameters, the distance h_1 from the bottom of the “mushroom” and the top of the ground plane (Figure 3.16(c) and (d)) has the strongest effect on the antenna matching property, as it affects the coupling interaction between the patch and the ground. The optimization process shows, that the optimum value is $h_1 = 1.5$ mm.

The measured return loss made on two different prototypes using 2.92-mm Jack End Launch Connectors versus simulation is shown in Figure 3.17. The simulated realized gain is 1.67 dBi at 2.45 GHz and 1.1 dBi at 5.5 GHz, the total efficiency is 69% at 2.45 GHz and 51% at 5.5 GHz.

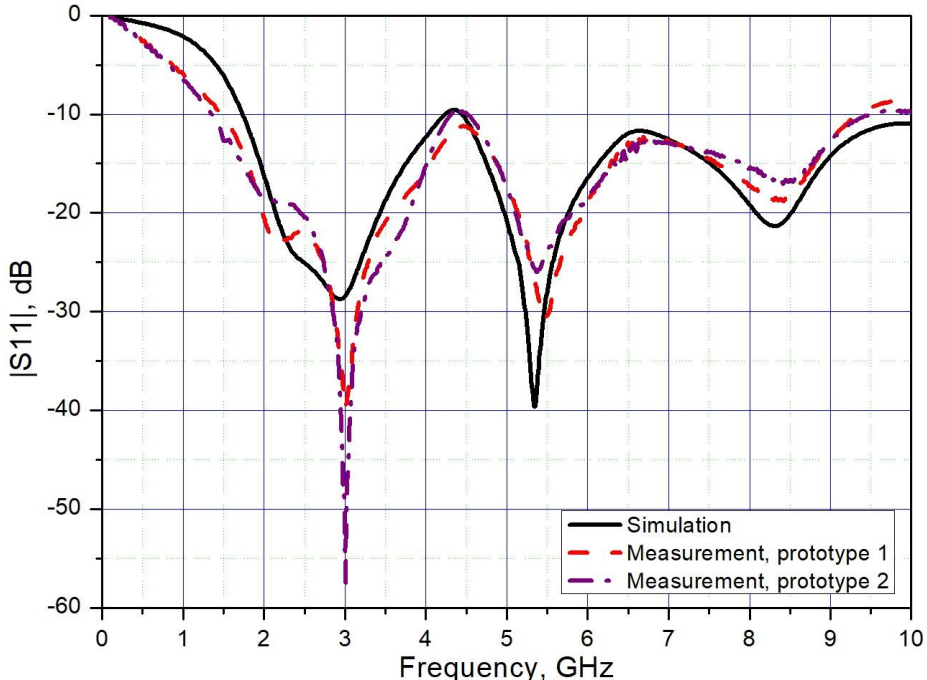


Figure 3.17. Return loss of the antenna – Simulation compared to measurement.

Figure 3.18 illustrates the simulation results of radiation patterns of the antenna, where one can notice, that the radiation patterns of the antenna are nearly omni-directional at 2.45 GHz while a little more directive at 5.5 GHz. A slight mismatch between the measurement and simulation is observed, that can be explained by the small ground plane of the antenna causing stronger coupling between the antenna and the cable, as well as the effect of the metallic motor and stretching/ twisting of the cable in the measurement system, as well as the imperfection of printed antenna edges.

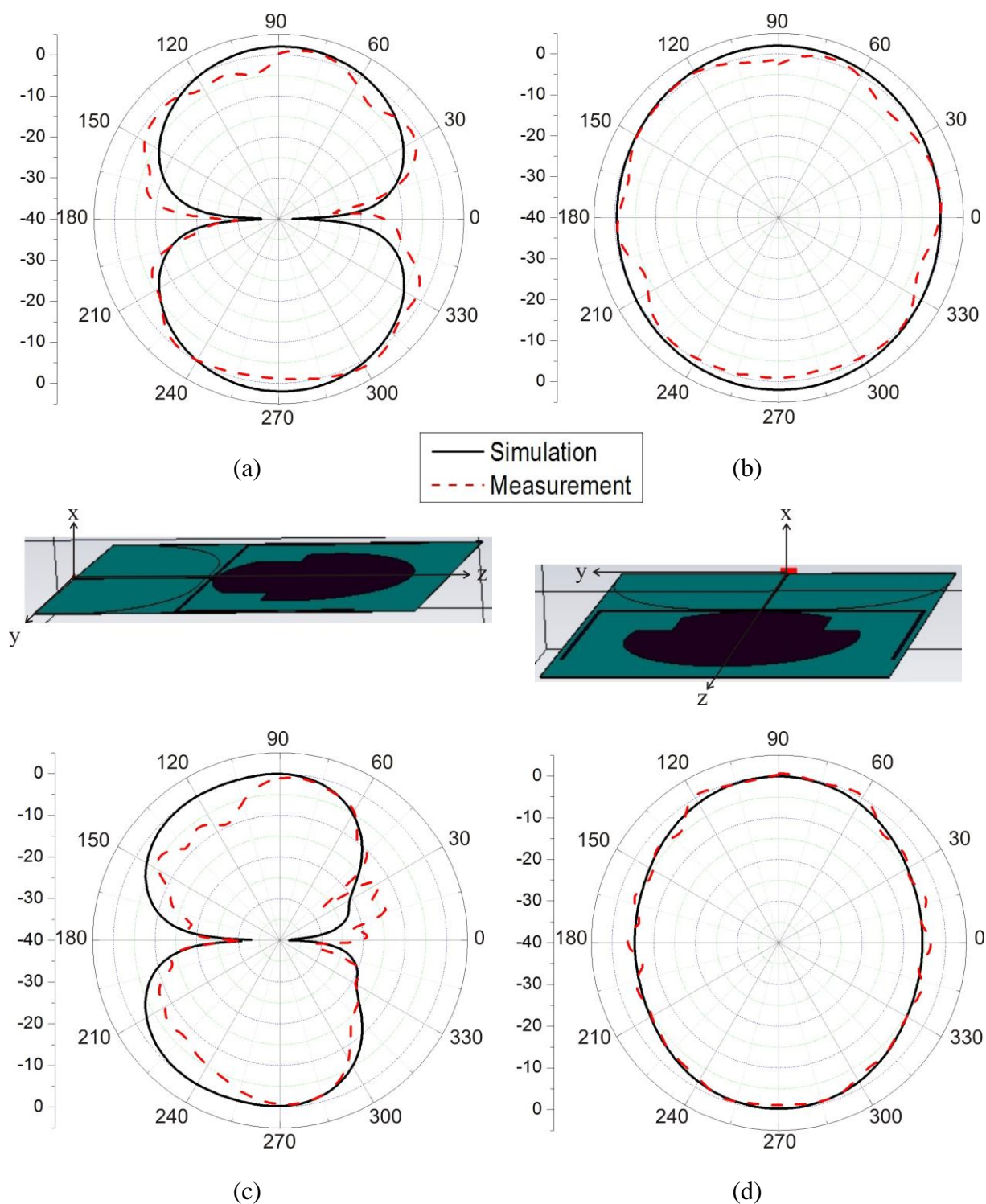


Figure 3.18. Radiation patterns of the antenna - simulation compared to measurement:(a) x-z plane ($\varphi = 0^\circ$), at 2.45 GHz; (b) x-y plane ($\theta = 90^\circ$), at 2.45 GHz; (c) x-z plane ($\varphi = 0^\circ$), at 5.5 GHz; (d) x-y plane ($\theta = 90^\circ$), at 5.5 GHz.

This antenna design is much larger than the others proposed in this chapter with nearly the same radiation characteristics. Therefore, it will be used only to study the bending effects in the air in the next chapter but cannot be well located in an ABS box to create MIMO antenna systems.

3.1.5. "Hello-Shaped" dual-band antennas

The initial design of the proposed antennas is a simple microstrip-fed monopole with a small circular patch calculated for 5.5 GHz. To facilitate the design process while keeping the compactness of the structure, a thin "arm" on the left added to aim at the lower frequency band around 2.45 GHz. The name "Hello" is inspired by the final shape of the antenna [10]. The ground plane of the structure is cleared under the antenna area to provide its omni-directional radiation patterns, where "Hello 2" is different from "Hello 1" by two rounded upper angles of this ground plane (Figure 3.19(a), (b)) to improve the matching properties. Moreover, the "Hello 2" structure saves an amount of ink that might be interesting for mass production in the future. Due to coupling effect, the radius of the "head" as well as the length of the "arm" of the antennas are to be adjusted to match well at two WLAN frequency bands. The parametric studies of "Hello 2" is illustrated in Figure 3.20 as an example, where it can be seen, that the radius of the "head" controls the higher frequency band while the length of the "arm" controls both lower and higher ones.

The geometry of the proposed antennas after optimization is shown in Figure 3.19(a) and (b) and their return loss is depicted in Figure 3.21. Their total dimensions are 42 mm × 28 mm × 0.21 mm. It can be noted through the simulation results, that the antennas are matched well at two WLAN frequency bands, especially the high frequency range of "Hello 2" is from 4.6 GHz up to over 10 GHz.

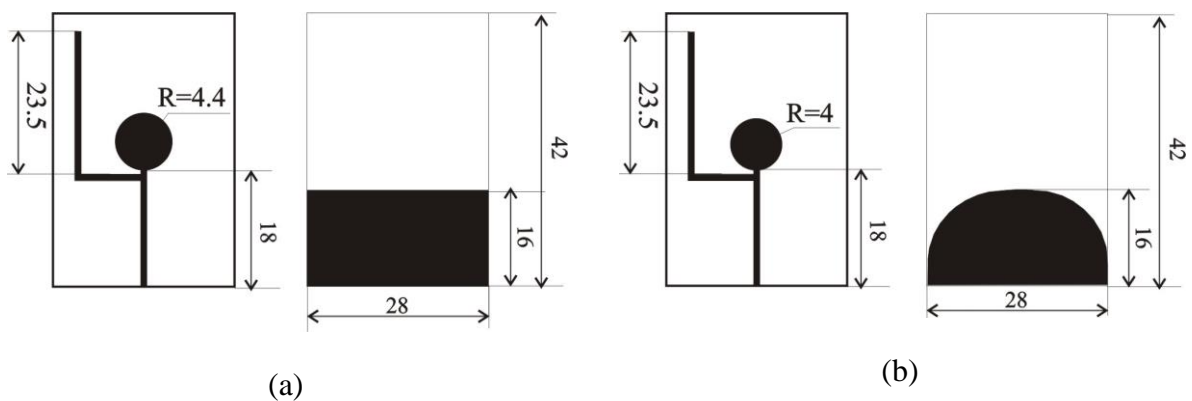
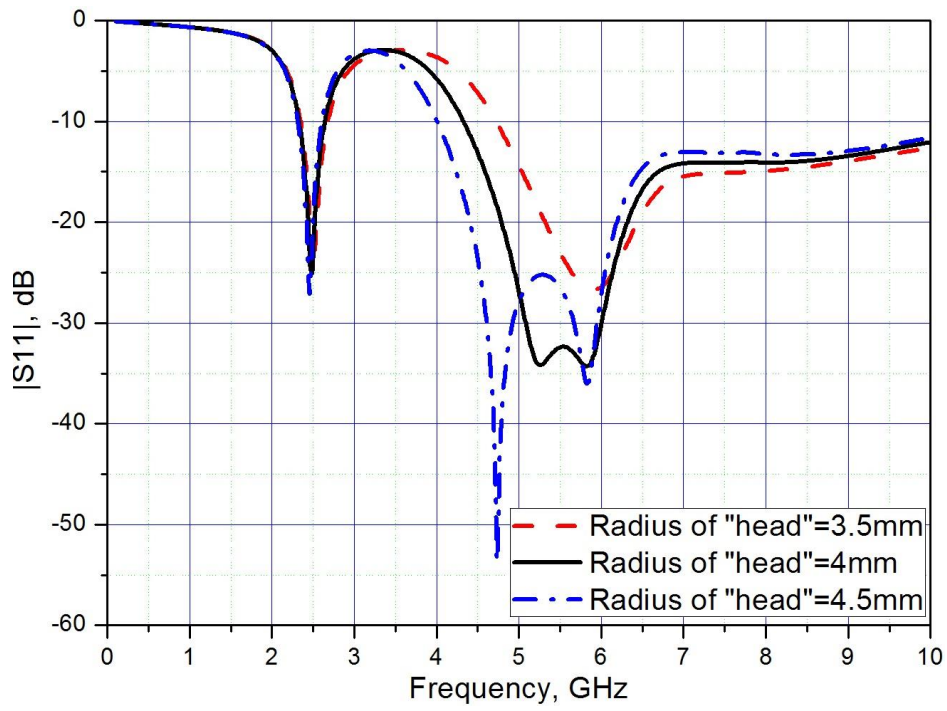
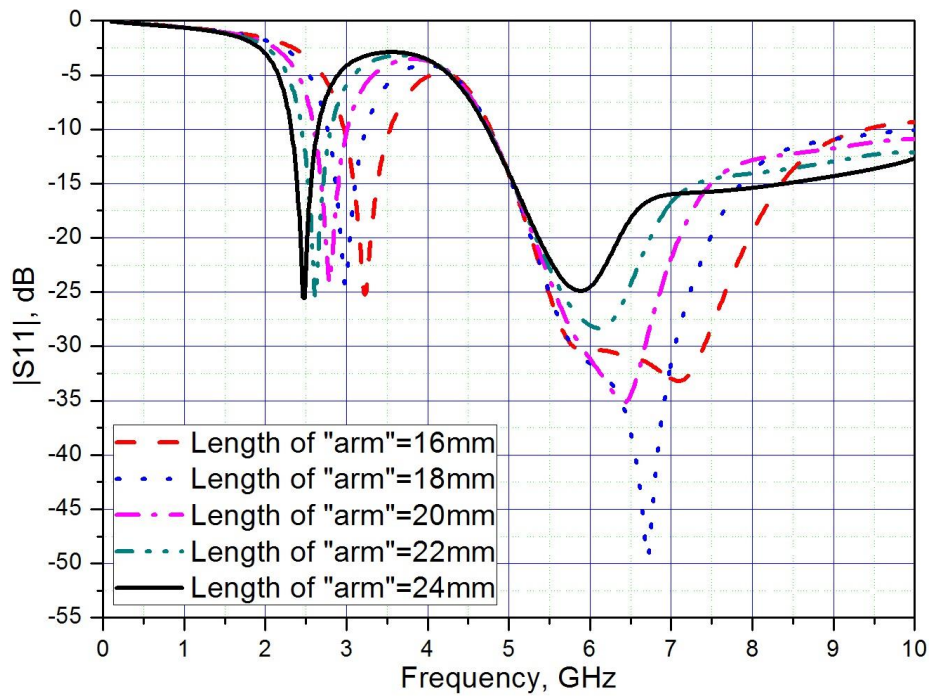


Figure 3.19. Optimized geometries of the antennas: (a) "Hello 1", front and back sides; (b) "Hello 2", front and back sides.



(a)



(b)

Figure 3.20. $|S_{11}|$ parametric study of "Hello 2"; (a) for various radii of the "head"; (b) for various lengths of the "arm". The other geometrical parameters are shown in Figure 3.19.

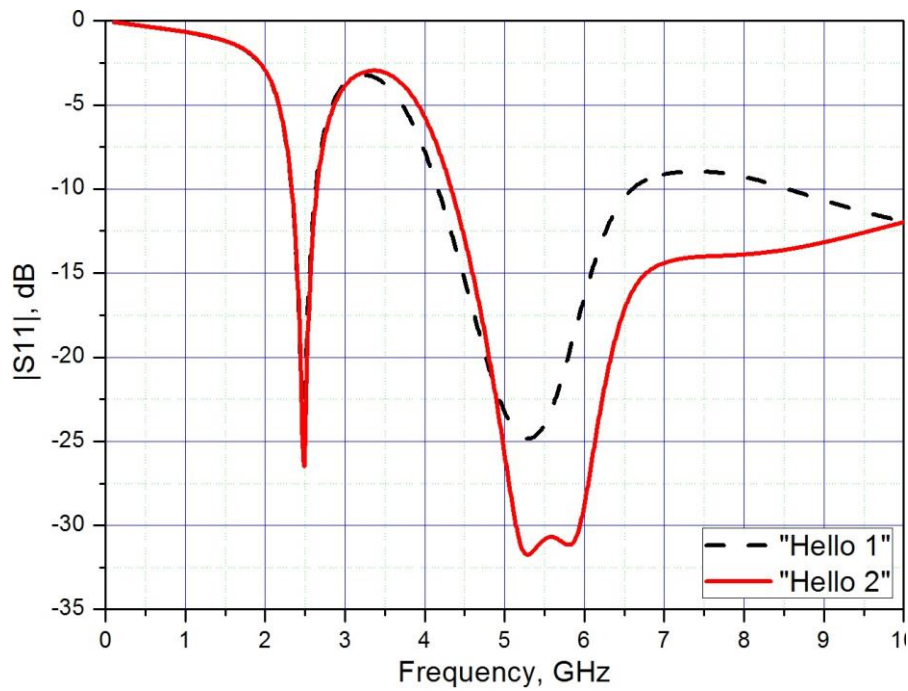


Figure 3.21. The simulated reflection coefficient $|S_{11}|$ of the antennas with the geometrical parameters are shown in Figure 3.19.

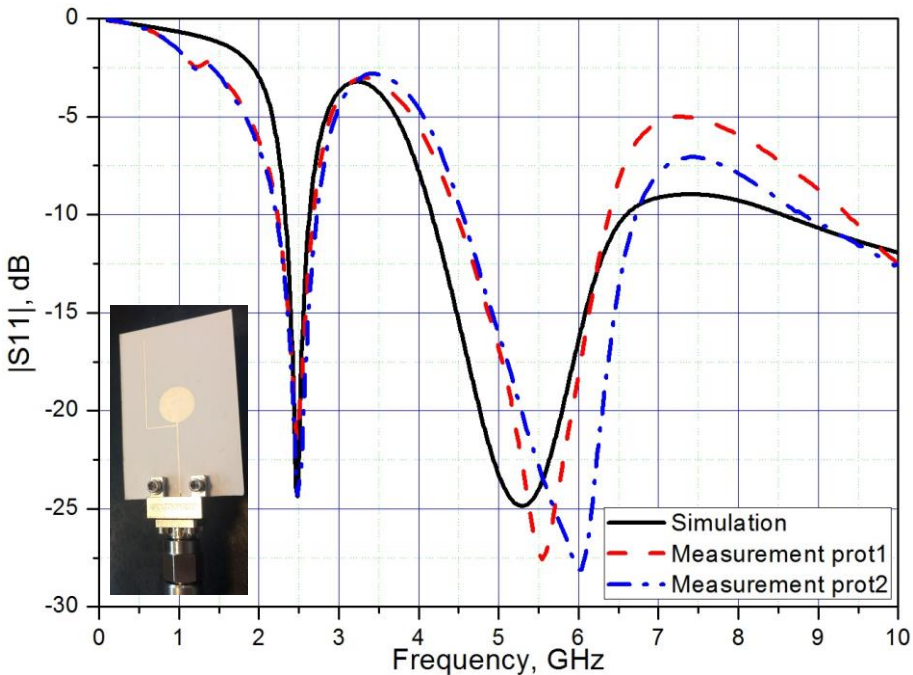
Due to high loss of the paper used for the design ($\tan\delta = 0.092$), the monopole antennas have low total efficiency, the simulated values are 67% at 2.45 GHz and 65% at 5.5 GHz for "Hello 1", 69% at 2.45 GHz and 67% at 5.5 GHz for "Hello 2". Their realized gain is 0.62 dBi and 1.53 dBi at 2.45 GHz and 5.5 GHz for "Hello 1", respectively. These values are 0.71 dBi and 1.51 dBi for "Hello 2".

As well as the previous designs, these antennas have been realized at CTP (Technical Center of Paper) with double-face screen printing technology, but in another run on 210- μm thick E4D paper. The 2.92-mm Jack End Launch Connector has been used for the measurement.

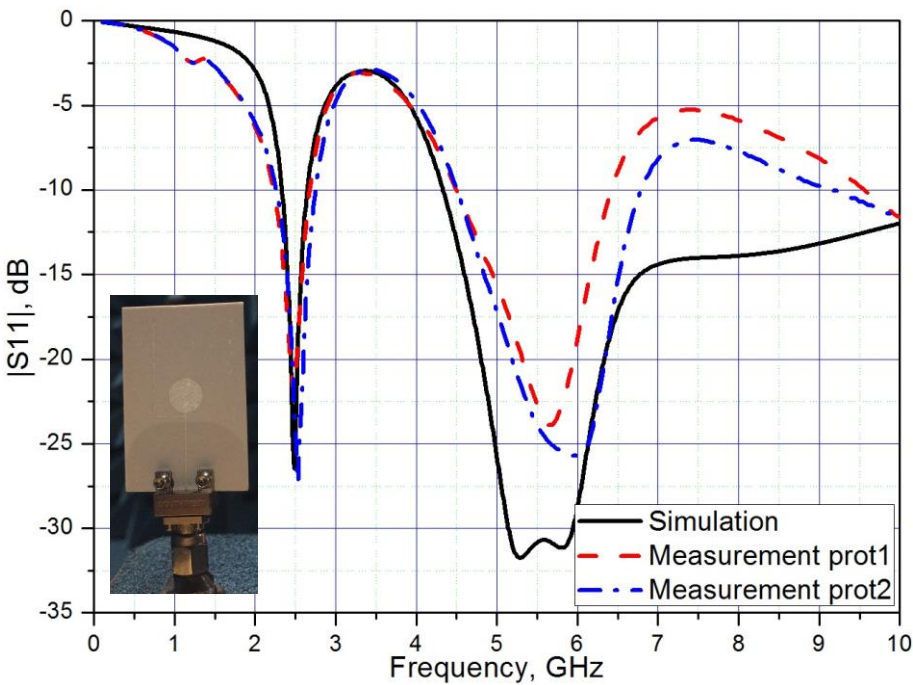
The measurement of both return loss and radiation patterns of the antennas has been performed in the anechoic chamber at IMEP-LAHC with a Vector Network Analyzer (VNA) Agilent 8720ES for all prototypes of each design.

It can be seen in Figure 3.22(a) and (b), that the form of measured reflection coefficient of all prototypes fits well with the simulated one, especially at the lower resonant frequency of 2.45 GHz. For "Hello 1", the measured resonant frequency is much shifted from the simulated by about 300-400 MHz at higher WLAN frequency 5.5 GHz, probably due to insufficient absorber covering the cable or the imprecision of dielectric properties of the paper. In spite of this error,

the matching bandwidth still covers all frequency bands of interest. The measured reflection coefficient at 5.5 GHz is better for “Hello 2” despite some difference in $|S_{11}|$ values.



(a)



(b)

Figure 3.22. The reflection coefficient $|S_{11}|$ of the antennas - simulation compared to measurement of two prototypes: (a) "Hello 1"; (b) "Hello 2".

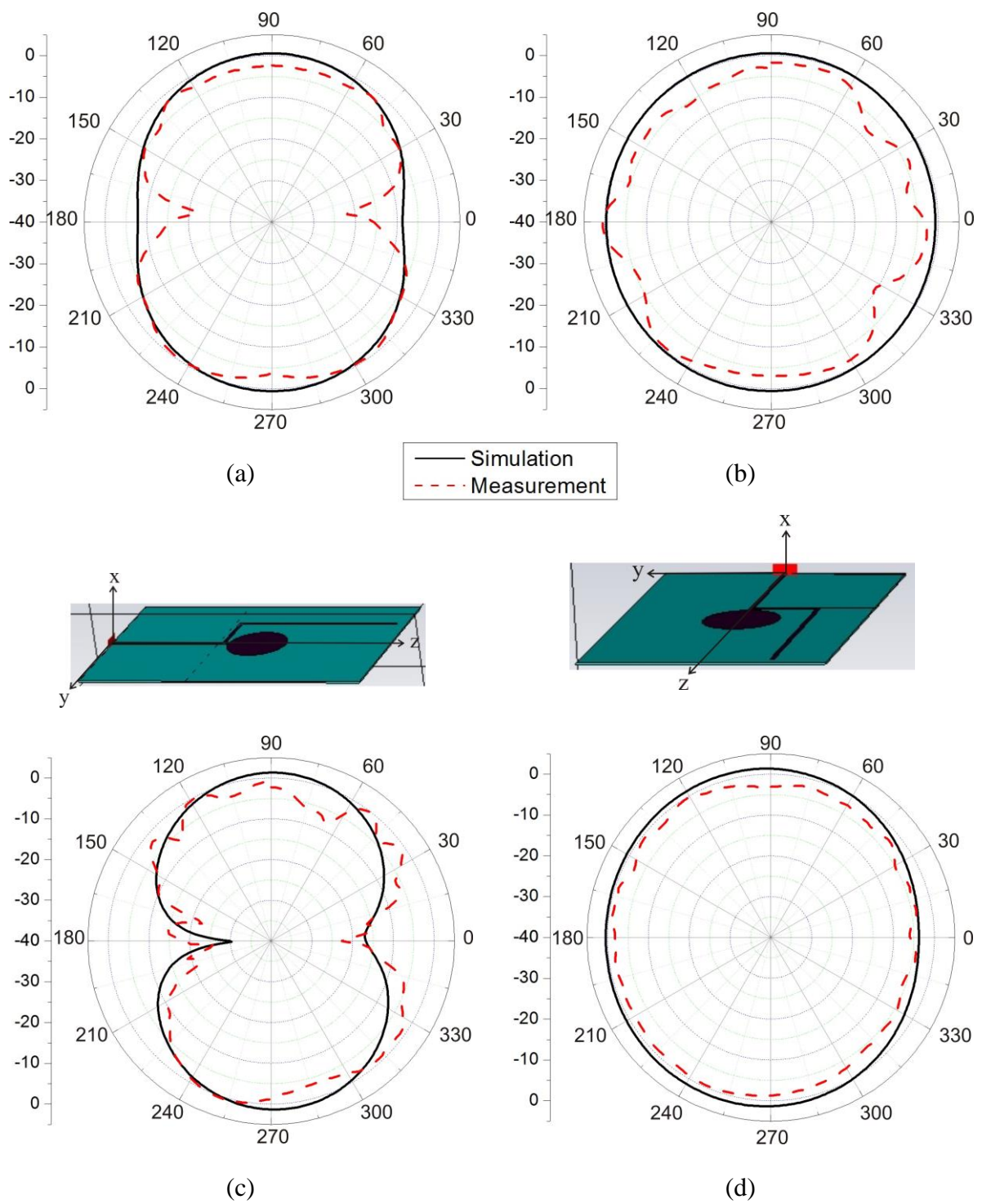


Figure 3.23. Simulated and measured radiation patterns of “Hello 1”: (a) x-z plane ($\varphi = 0^\circ$), at 2.45 GHz; (b) x-y plane ($\theta = 90^\circ$), at 2.45 GHz; (c) x-z plane ($\varphi = 0^\circ$), at 5.5 GHz; (d) x-y plane ($\theta = 90^\circ$), at 5.5 GHz.

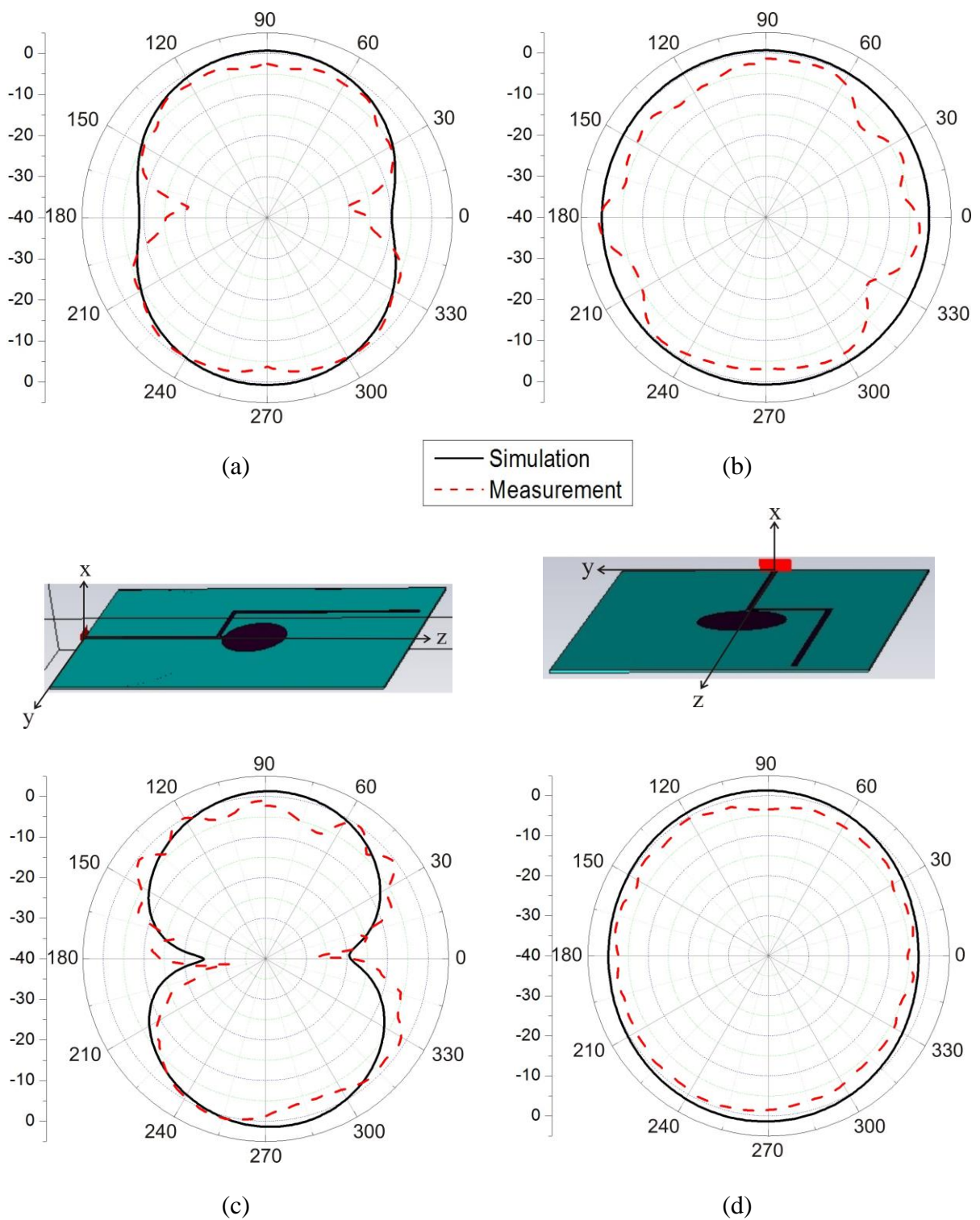


Figure 3.24. Simulated and measured radiation patterns of “Hello 2”: (a) x-z plane ($\varphi = 0^\circ$), at 2.45 GHz; (b) x-y plane ($\theta = 90^\circ$), at 2.45 GHz; (c) x-z plane ($\varphi = 0^\circ$), at 5.5 GHz; (d) x-y plane ($\theta = 90^\circ$), at 5.5 GHz.

The radiation patterns have been measured in the x-z plane ($\varphi = 0^\circ$) and the x-y plane ($\theta = 90^\circ$) where z-axis is normal to the antenna under test and directed to the transmit antenna as shown in Appendix 2. Figure 3.23 and Figure 3.24 show the nearly omni-directional radiation of both antennas at 2.45 GHz and 5.5 GHz. The difference between the simulation and measurement might be caused by the roughness of the metallic layer of the antennas.

3.2. Microstrip-fed multi-band antennas

The purpose of this section is to design compact multiple band antennas on 210- μm thick E4D paper (E4D 200). Based on the same principle used in the previous section, a multi-band antenna at higher frequencies is created by a patch with microstrip feed line, then the wings are added to create resonance at lower frequencies (Figure 3.25). Both patch and ground plane are rounded at the edges to get better matching over a wider frequency band. It is needed to note, that as these antennas are compact with very limited height (30 mm including the feed line according to the height of our package), the feed line is designed much shorter than that of the previous wide-band antennas. This antenna is rather compact with the overall dimensions of 24 mm \times 30 mm \times 0.21 mm.

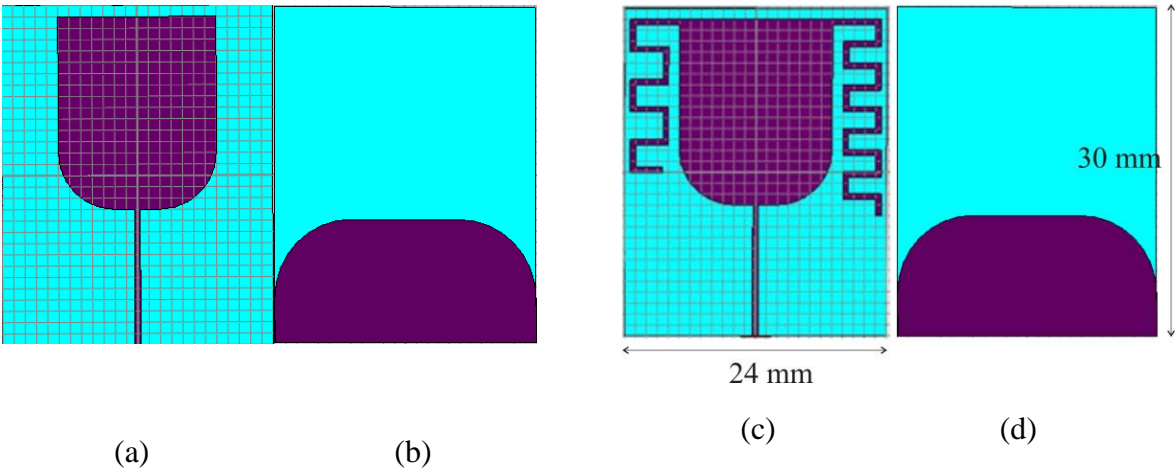


Figure 3.25. The design procedure, the antenna without “wings”: (a) front and (b) back sides; The antenna with “wings”: (c) front and (d) back sides.

In the same run of "Hello-shaped" antennas, the prototypes have been realized at CTP by screen printing technology with silver solution deposition of 6- μm thickness and 1.7×10^6 S/m conductivity.

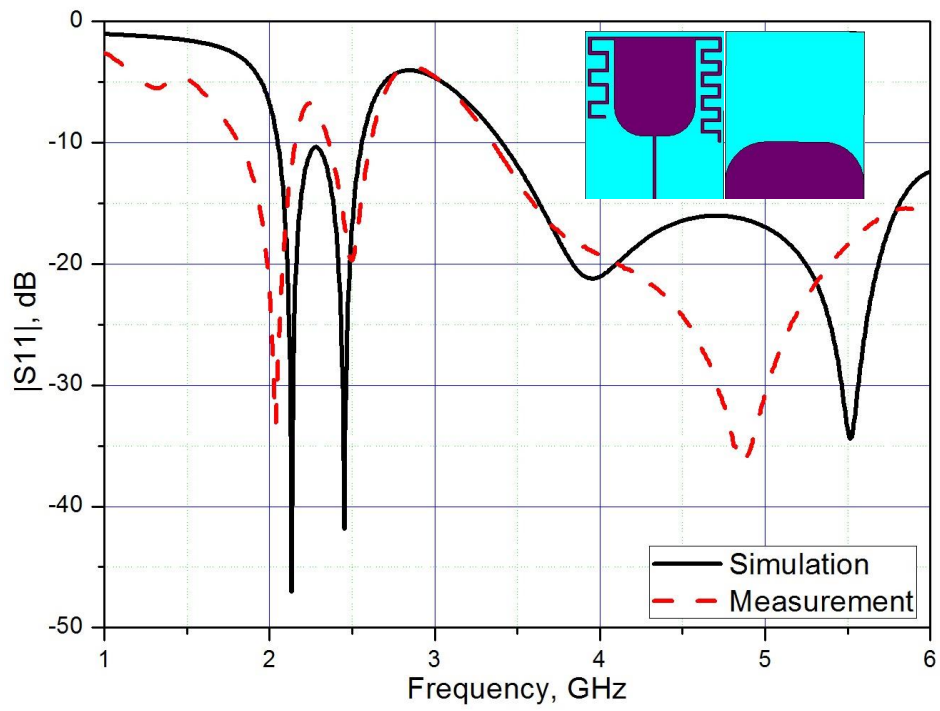


Figure 3.26. The reflection coefficient of the antenna 1 – simulation compared to measurement.

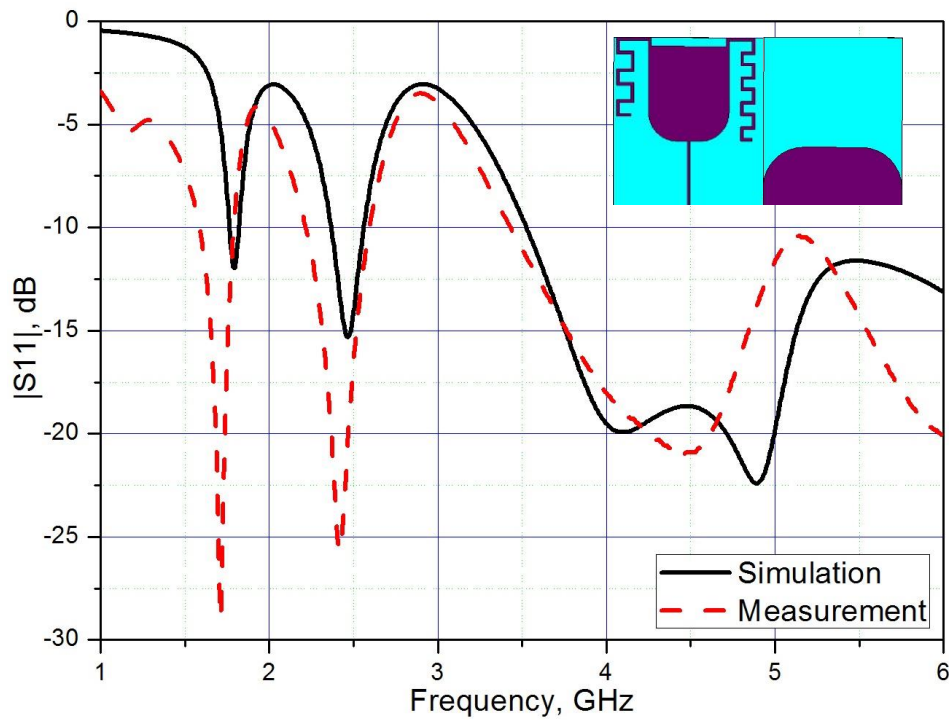


Figure 3.27. The reflection coefficient of the antenna 2 – simulation compared to measurement.

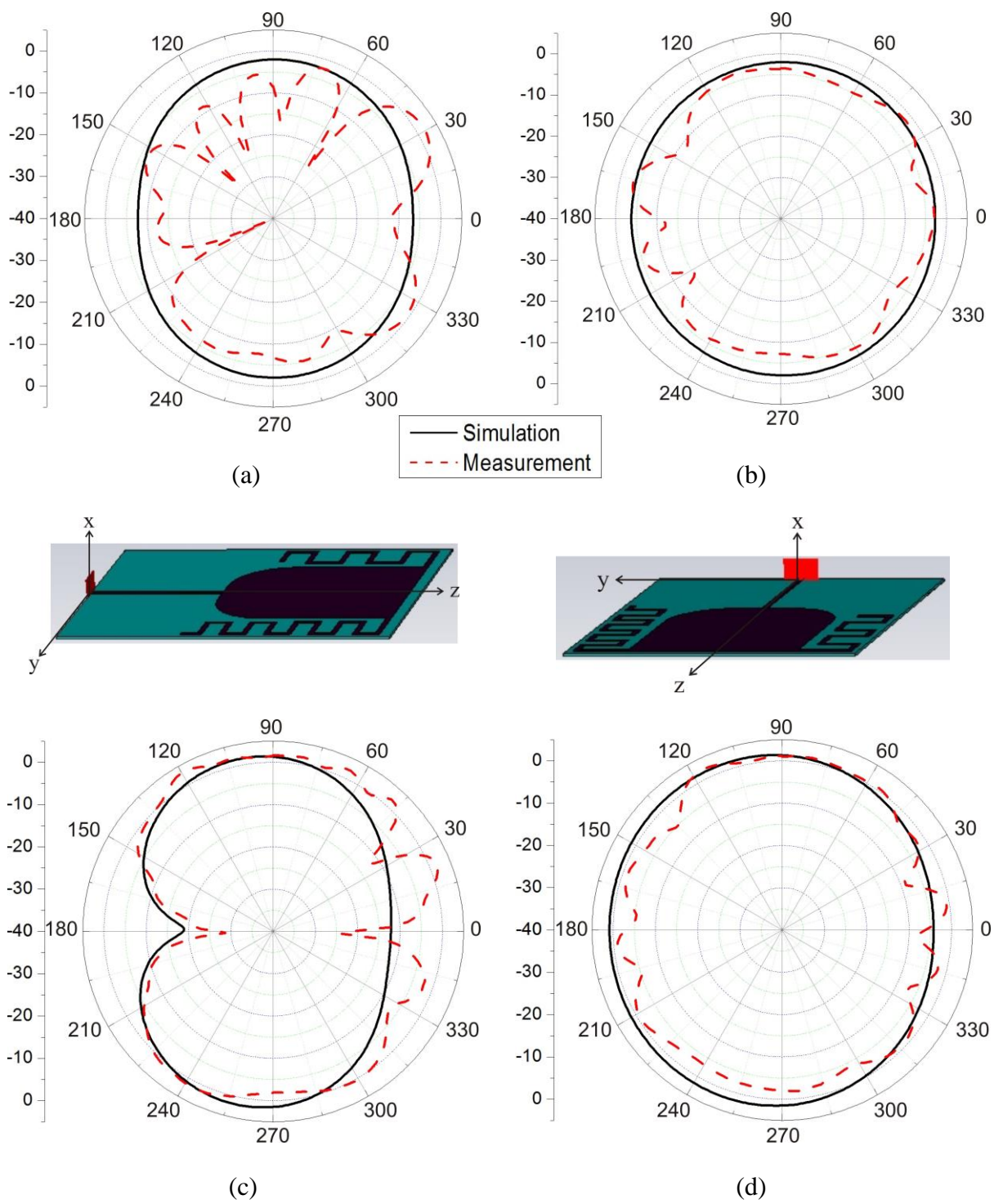


Figure 3.28. Radiation patterns of the antenna 1 - simulation vs. measurement: (a) x-z plane ($\varphi = 0^\circ$), at 2.45 GHz; (b) x-y plane ($\theta = 90^\circ$), at 2.45 GHz; (c) x-z plane ($\varphi = 0^\circ$), at 5.5 GHz; (d) x-y plane ($\theta = 90^\circ$), at 5.5 GHz.

Figure 3.26 and Figure 3.27 show the reflection coefficient of two antennas with the same design, the same dimensions of 24 mm × 30 mm × 0.21 mm and a little different wings, where it can be seen, that the agreement between them is much better at lower WLAN frequency (2.45 GHz) than that at higher frequency (5.5 GHz). However, the realized gain of the antenna is much lower at 2.45 GHz than that at 5.5 GHz as seen in Figure 3.28 for the first antenna.

Conclusions for Chapter 3

The overview in Chapter 1 showed that CPW-feeding method was usually used in wideband antennas. However, in order to avoid the problem of too narrow slots in 50-ohm CPW feed lines causing difficulties in fabrication with high accuracy due to technological restrictions, with the double-side printing possibility, the conventional microstrip feeding method was chosen for the designs in this work.

This chapter presented the microstrip-fed building-block monopole antennas designed on E4D paper summarized in Table 3.1. It can be seen, that the compact multiband antennas are suitable for using at higher frequencies over 4 GHz rather than at lower frequencies.

The main advantage of these antennas compared to the existing paper-based wideband antennas is the simplicity of the designs without too small details such as too narrow slots in CPW-feed lines. These antennas were designed and fabricated based on double-side screen printing technology and can be developed to future mass production.

Thanks to the flexibility, in the next chapter, some of the antennas proposed in this chapter are further used to create antenna systems in boxes where they can be bent when it is necessary.

Table 3.1. The proposed microstrip-fed building block monopole antennas designed on E4D paper.

	Dimensions	Matching bandwidth	Total efficiency	Realized gain	Applications
"Sapin"	28 mm × 59 mm × 0.104 mm	2 GHz – over 10 GHz	78% at 2.45 GHz, 56.8% at 5.5 GHz	1.27 dBi at 2.45 GHz, 0.94 dB at 5.5 GHz	Wideband, multi-standard set-top boxes
"Sapin"	28 mm × 57 mm × 0.21 mm	2 GHz – over 10 GHz	80% at 2.45 GHz, 64% at 5.5 GHz	1.97 dBi at 2.45 GHz, 1.3 dB at 5.5 GHz	
"Modified Sapin"	24 mm × 50 mm × 0.104 mm	2.2 GHz – over 10 GHz	78% at 2.45 GHz, 68% at 5.5 GHz	1.1dBi at 2.45 GHz, 1.63 dB at 5.5 GHz	
"Robe"	28 mm × 49 mm × 0.104 mm	2.2 GHz – 3.2 GHz, 4.3 GHz – over 10 GHz	78% at 2.45 GHz, 60% at 5.5 GHz	1.21dBi at 2.45 GHz, 1.66 dB at 5.5 GHz	
"Mushroom-shaped with two arms"	50 mm × 65 mm × 0.104 mm	1.7 GHz – over 10 GHz	69% at 2.45 GHz, 51% at 5.5 GHz	1.67 dBi at 2.45 GHz, 1.1 dB at 5.5 GHz	
"Hello 1"	28 mm × 42 mm × 0.21 mm	2.3 GHz – 2.7 GHz; 4.2 GHz – 6.6 GHz	67% at 2.45 GHz, 65% at 5.5 GHz	0.62dBi at 2.45 GHz, 1.53 dB at 5.5 GHz	Dual-band WLAN
"Hello 2"	28 mm × 42 mm × 0.21 mm	2.3 GHz – 2.7 GHz; 4.3 GHz – over 10 GHz	69% at 2.45 GHz, 67% at 5.5 GHz	0.71dBi at 2.45 GHz, 1.51 dB at 5.5 GHz	
Multi-band antenna 1	24 mm × 30 mm × 0.21 mm	Resonant frequencies: 2.2 GHz; 2.45 GHz; 4 GHz; 5.5 GHz	22%; 40%; 75% ; 65%, respectively	-3.9dBi; -1.82 dBi; 1.38 dBi; 2.14 dBi, respectively	Multi-band, multi-standard set-top boxes
Multi-band antenna 2	24 mm × 30 mm × 0.21 mm	Resonant frequencies: 1.8 GHz; 2.45 GHz; 4 GHz; 5 GHz	17%; 58%; 73%; 60%, respectively	-5.55dBi; -0.365 dBi; 1.42 dBi; 1.96 dBi, respectively	

References for Chapter 3

- [1] G. Shaker, Sa. S.-Naeini, N. Sangary, M. M. Tentzeris, "Inkjet Printing of Ultrawideband (UWB) Antennas on Paper-Based Substrates", *IEEE Antennas and Wireless Propagation Letters*, Vol. 10, pp. 111-113, 2011.
- [2] A. Tsitoa, P. Lemaitre-Auger et al. "Bending and Crumpling Effects on a Wearable Planar Monopole Antenna", *15th International Symposium on Antenna Technology and Applied Electromagnetics (ANTEM)*, 2012.
- [3] S. Jun, B. Sanz-Izquierdo and M. Summerfield "UWB Antenna on 3D Printed Flexible Substrate and Foot Phantom", *Loughborough Antennas & Propagation Conference (LAPC)*, 2015.
- [4] H. F. Abutarboush, M. F. Farooqui, A. Shamim « Inkjet-Printed Wideband Antenna on Resin-Coated Paper Substrate for Curved Wireless Devices », *IEEE Antennas and Wireless Propagation Letters*, Vol. 15, pp. 20-23, 2016.
- [5] M. C. Tang, T. Shi, and R. W. Ziolkowski «Flexible Efficient Quasi-Yagi Printed Uniplanar Antenna», *IEEE Trans. on Antennas and Propagation*, Vol. 63, pp. 5343-5350, No. 12, 2015.
- [6] H. P. Phan, T. P. Vuong, P. Benech, P. Xavier, P. Borel and A. Delattre, "Printed Flexible Wideband Microstrip Antenna for Wireless Applications", *2016 International Conference on Advanced Technologies for Communications (ATC'16)*, October 12-14, 2016, Hanoi, Vietnam
- [7] H. P. Phan, T. P. Vuong, P. Benech, P. Xavier, P. Borel and A. Delattre, "Low cost Wideband Antenna on Paper Substrate", *EuCAP 2017*, pp. 2177-2180, March 19-24, 2017, Paris, France.
- [8] H. P. Phan, T. P. Vuong, P. Benech, P. Xavier, P. Borel and A. Delattre, "Antenne à large bande sur papier", *JNM 2017*, 16-19 mai 2017, Saint-Malo, France.
- [9] H. P. Phan, T. P. Vuong, P. Benech, P. Xavier, P. Borel and A. Delattre, "Novel Ultra-Wideband "Robe" Antenna on High-Loss Paper Substrate", *AP-S 2017*, pp.319-320, July 9-14, 2017, San Diego, USA.
- [10] H. P. Phan, T. P. Vuong, P. Benech, P. Xavier, P. Borel, "'Hello-Shaped" Wideband Monopole Antennas on Paper Substrate", *International Conference on Advanced Technologies for Communications (ATC'17)*, October 18-20, 2017, Quy Nhon, Vietnam.

4. Chapter 4 – Three-Dimensional and MIMO Antenna Systems

In the previous chapters the 2D and 2.5D antennas including single-band (CPW-fed, IFAs, SIW cavity-backed structures), multi-band and wide-band ("Sapin", "Modified Sapin", "Robe", "Mushroom-Shaped with Two Arms", "Hello-Shaped" structures) have been designed and analyzed.

In order to create a space diversity of a system consisting of at least two antennas, antennas are set orthogonally to make three-dimensional and MIMO structures.

Besides, packaging issues always cause many discussions as packages are made of other materials such as plastic or rubber that can affect the antenna characteristics, as shift resonant frequencies or reduce antenna efficiency. Moreover, if the dimensions of the box are restricted, the antenna must be deformed to be installed inside.

This chapter presents three-dimensional MIMO systems consisting of two orthogonal antennas placed in a rectangular acrylonitrile-butadiene-styrene (ABS) plastic box. The box in the first case is with sufficient dimensions where the antennas can be located in and their performance remains good. Further, the ABS box in the next sections has one of dimensions that are very restricted. The solution to bend an antenna under 90 degrees to place into this package is proposed and analyzed, then the systems with at least one bent antenna are studied.

4.1. System of two flat antennas in an ABS plastic box

In this study, a system of wideband antennas such as "Sapin" on 0.21 mm thick E4D paper is considered to be installed into an ABS plastic box with the dimensions of 85 mm × 85 mm × 85 mm. The thickness of the box walls is 2.48 mm. The dimensions of the antenna are 28 mm × 57 mm so that it can easily be placed in the box (Figure 4.1). The electromagnetic properties of ABS plastic are determined by measurement using cavity perturbation method, and the obtained results are $\epsilon_r = 2.7$, $\tan \delta = 0.005$.

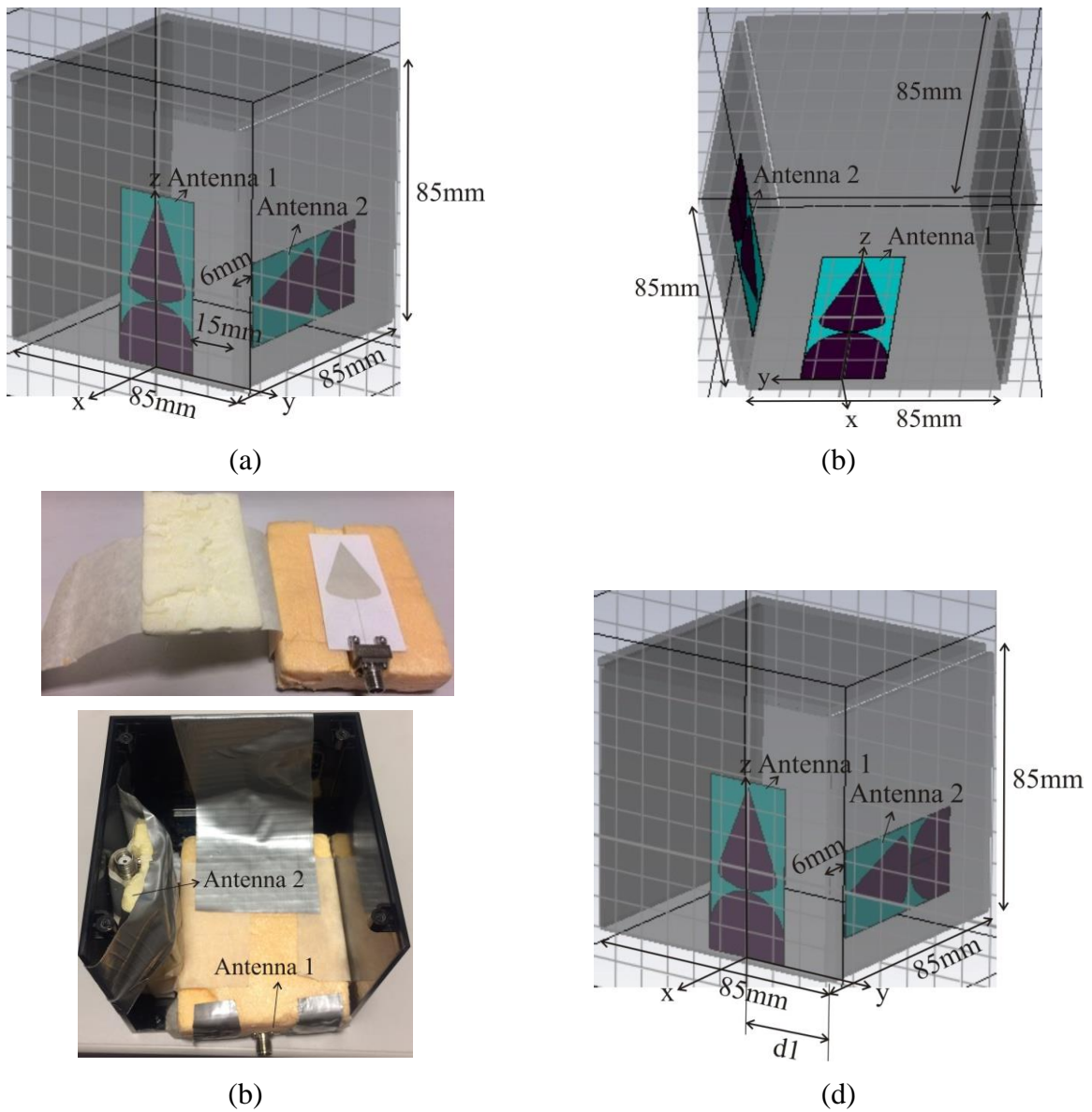
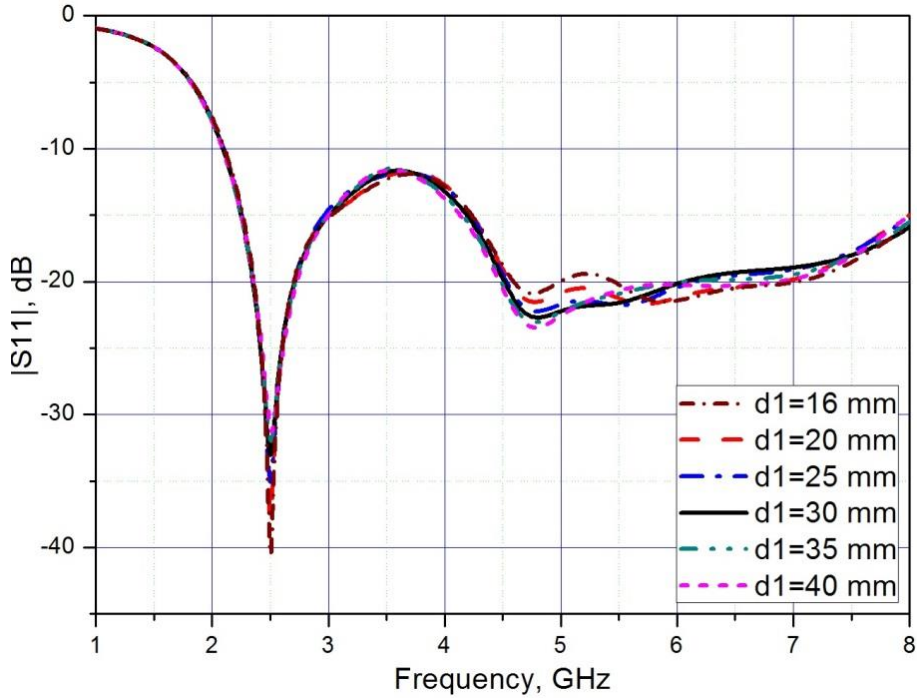


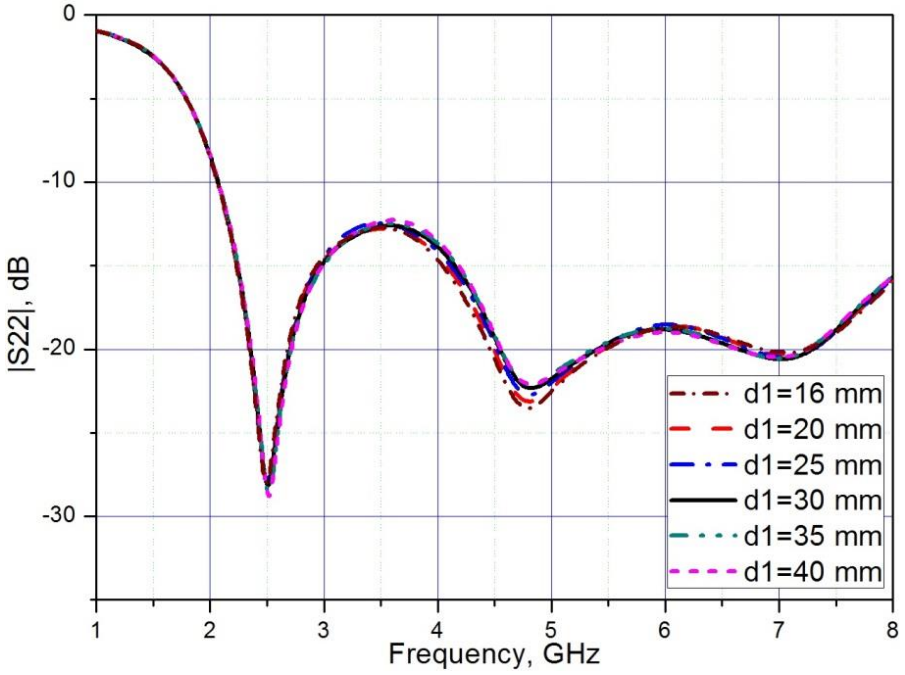
Figure 4.1. The system of two flat antennas in a 85 mm \times 85 mm \times 85 mm ABS plastic box: (a) CST simulation structure; (b) CST simulation structure – rotated view corresponding to the experimental realization; (c) Experimental realization in the assembling process; (d) The distance d_1 .

The simulation has been done for various distances d_1 between the Antenna 1 and the edge of the box (Figure 4.1(d)) as well as for various permittivity of the material and various wall thicknesses of the box. The results illustrated in Figure 4.2, Figure 4.2 and Figure 4.4 show, that the matching properties are nearly not affected by d_1 and those changes of the box. The transmission coefficients $|S_{21}|$ and $|S_{12}|$ become worse when the Antenna 1 approaches to the Antenna 2 (and it

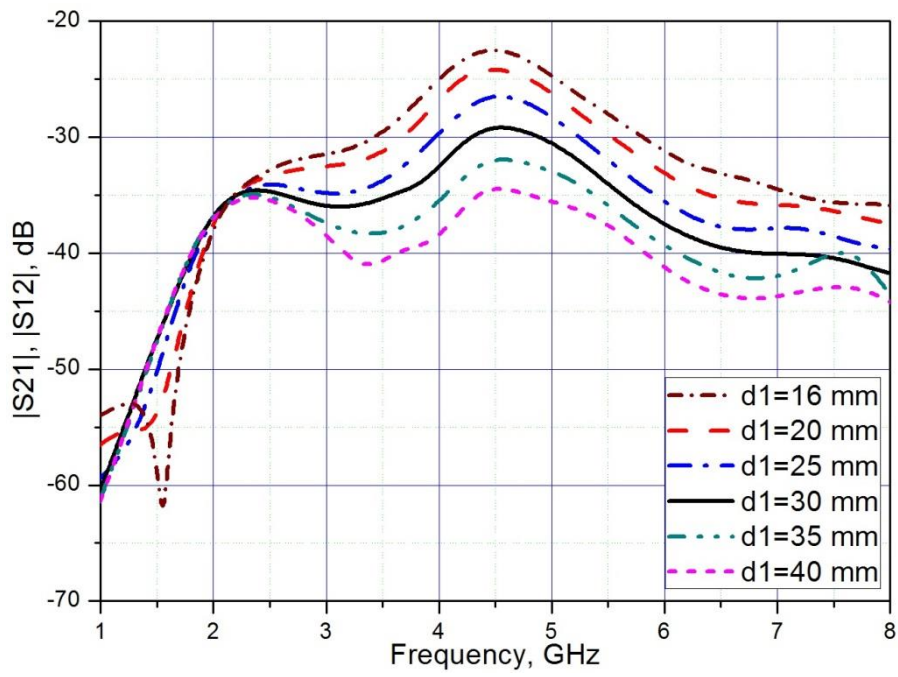
is obvious), and also varied for different parameters of the box. However, the isolation is always above 20 dB. Finally, the distance $d_1 = 15$ mm was chosen to facilitate the assembling process.



(a)

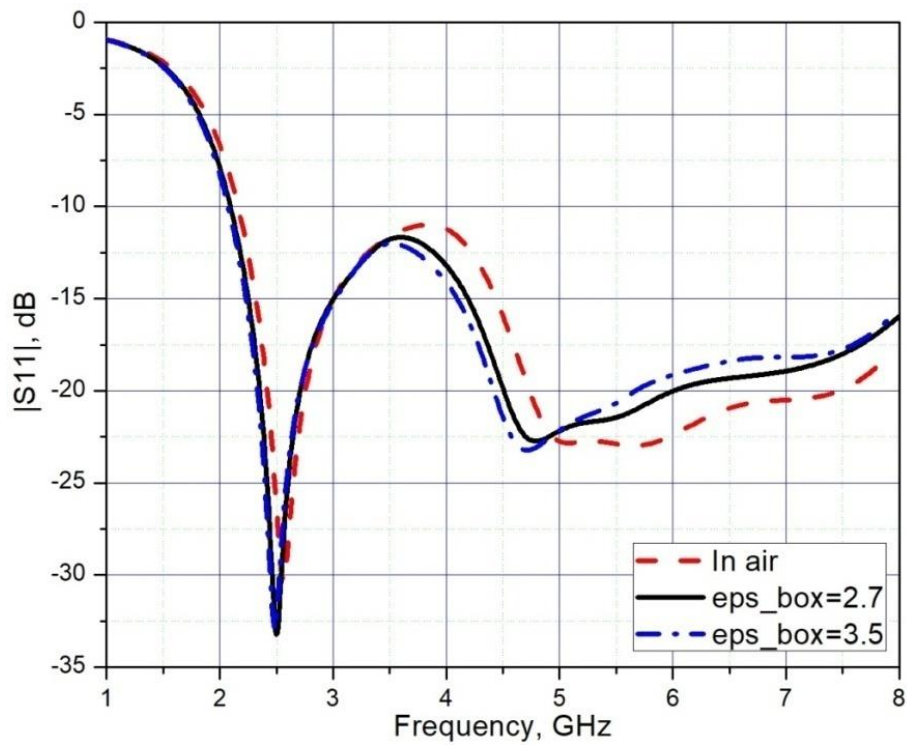


(b)

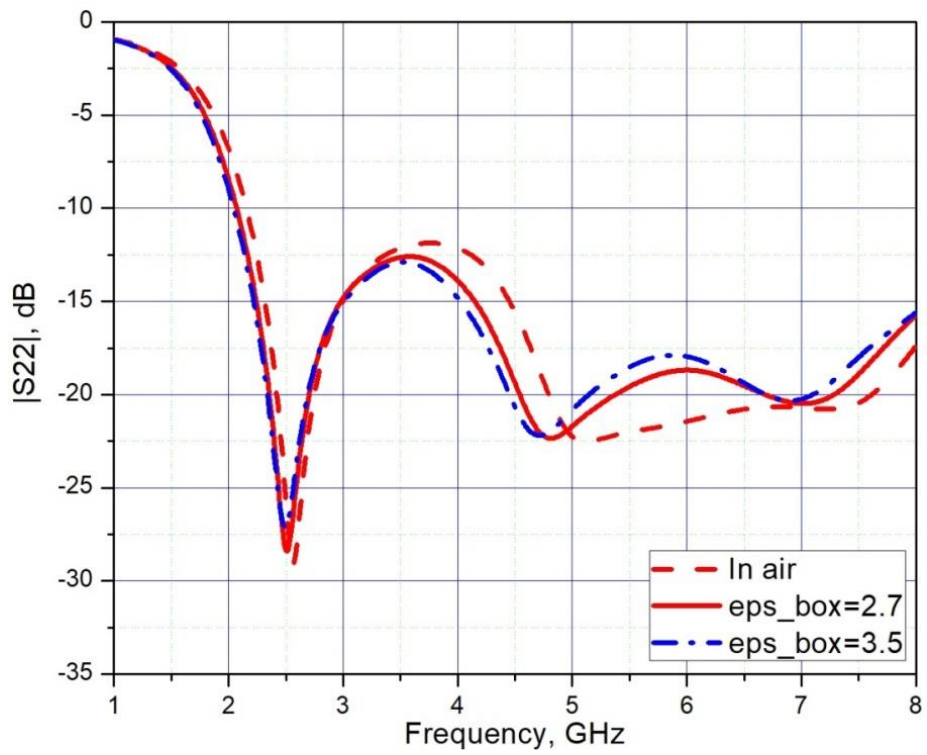


(c)

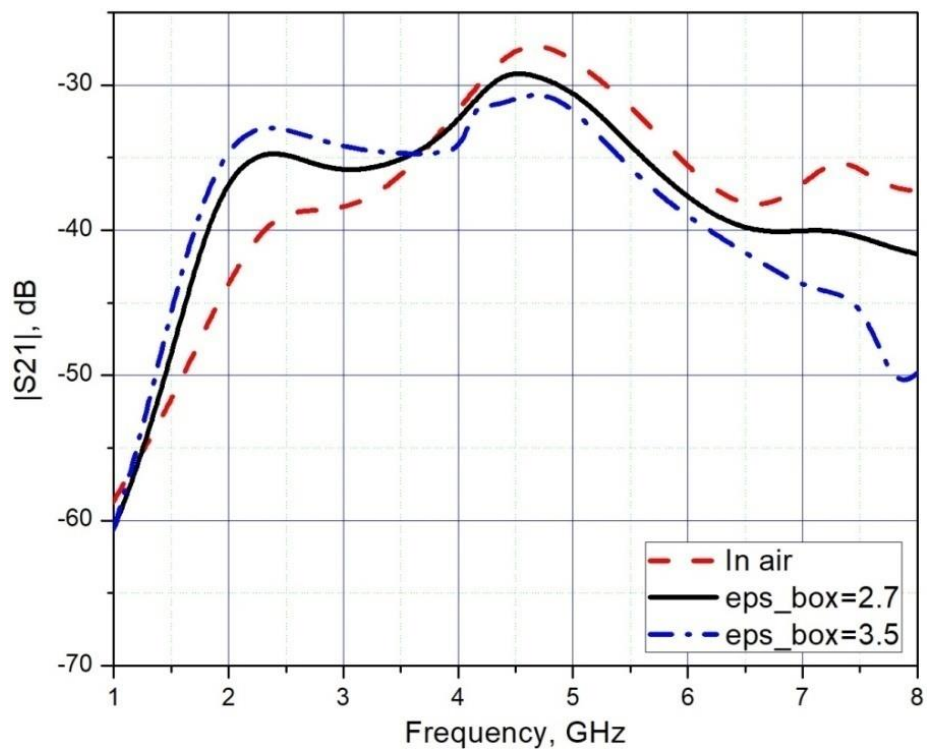
Figure 4.2. Study of S-parameters of the system for various distances d_1 : (a) S_{11} ; (b) S_{22} ; (c) S_{21} .



(a)

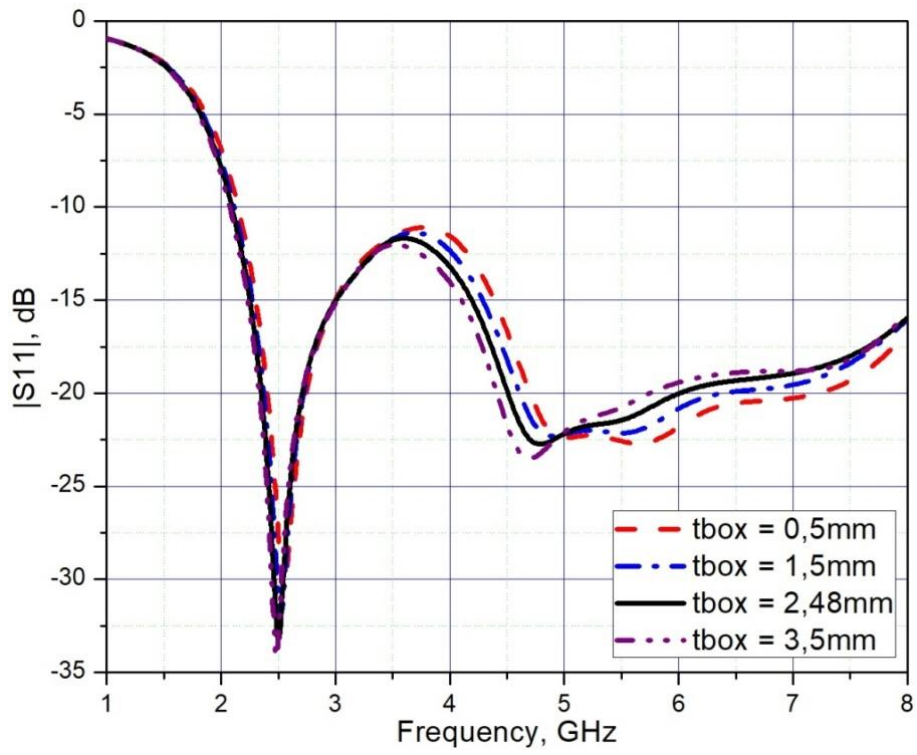


(b)

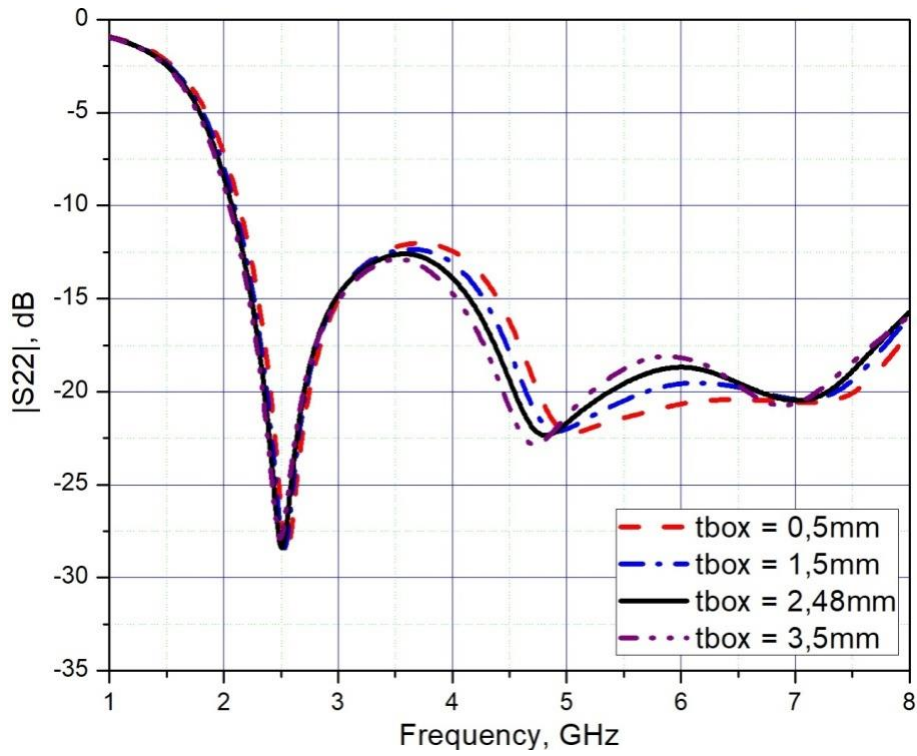


(c)

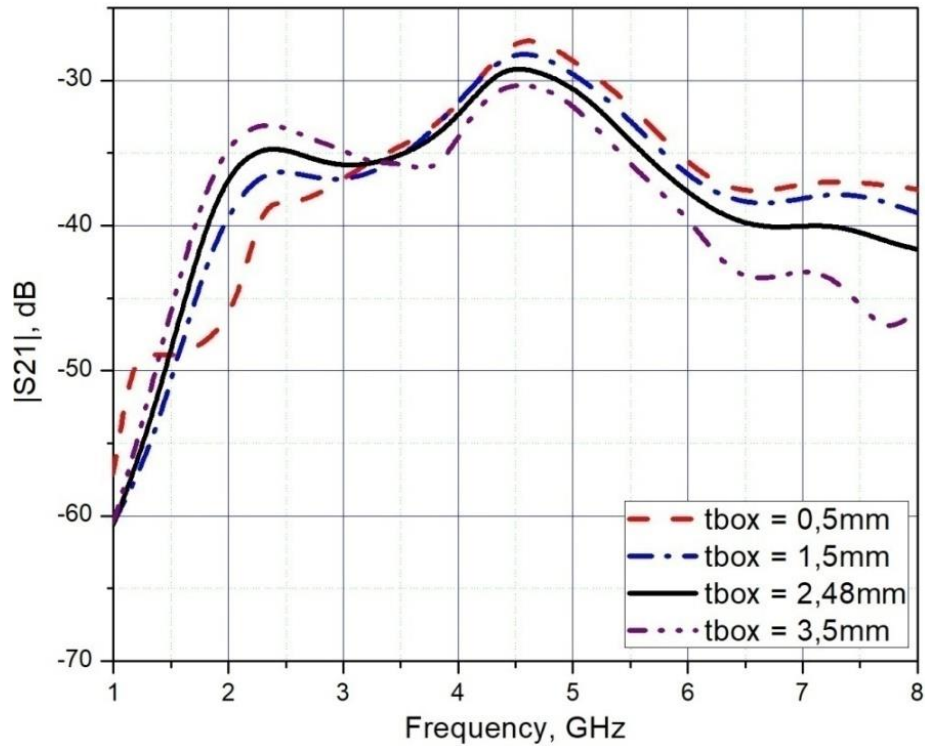
Figure 4.3. Study of S-parameters of the system for various materials of the box: (a) S11; (b) S22; (c) S21.



(a)



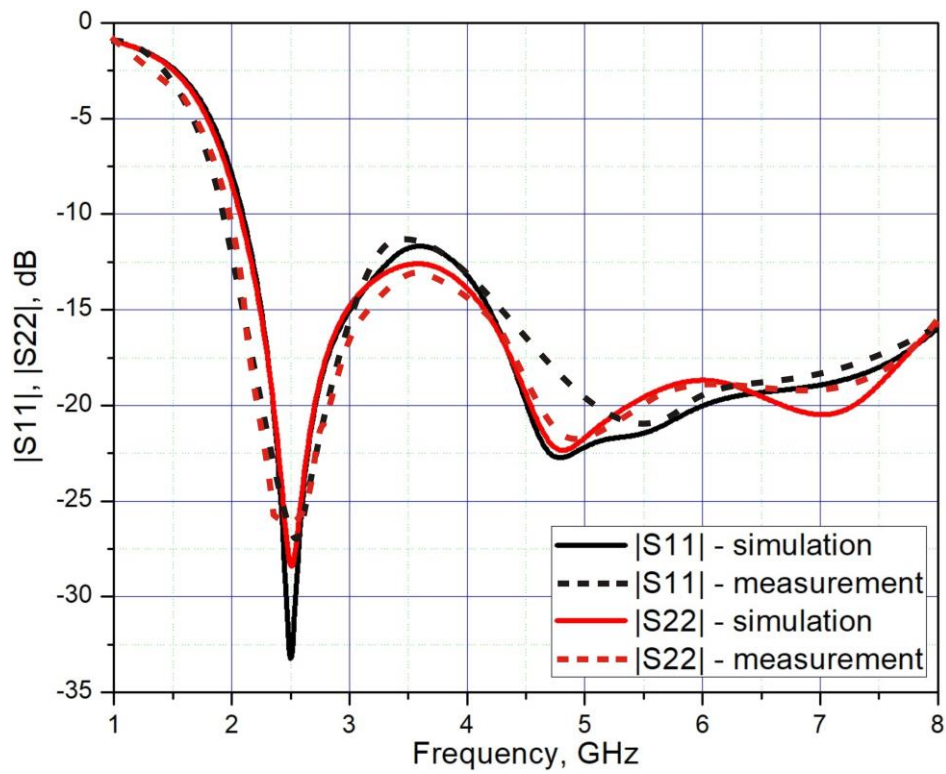
(b)



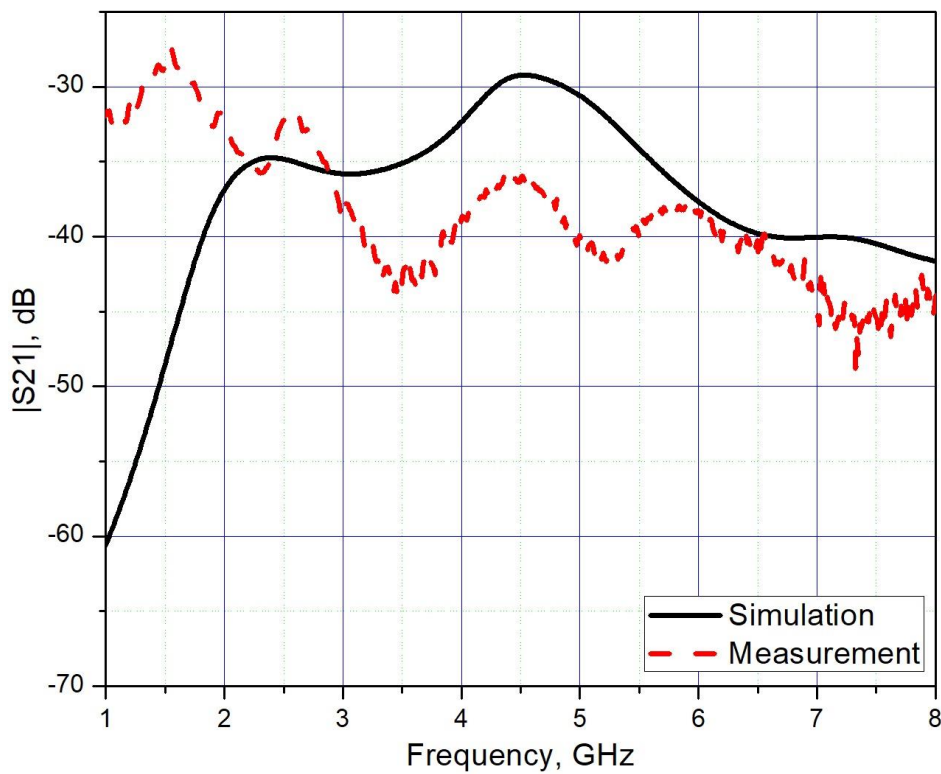
(c)

Figure 4.4. Study of S-parameters of the system for various wall thicknesses of the box: (a) S11; (b) S22; (c) S21.

S-parameters of the antennas are shown in Figure 4.5. It can be seen that the measured results of the reflection coefficient of two antennas fit well with the simulation. However, the measured transmission coefficient that shows isolation between the antennas in this case is lower than the simulated one in the band from 3 GHz to 5.5 GHz and higher than the simulated one in the bands from 1 GHz to 3 GHz and from 5.5 GHz to over 8 GHz since these values are very low, below -30 dB over all these frequency bands and very sensitive to any change of the system position, especially when the contacts between the antennas and the connectors are fragile. There is also probably a capacitive coupling between two antennas at lower frequencies (up to 3 GHz) that is not taken into account in the simulation causing the disagreement between the simulation and measurement at those frequencies. However, despite shifting of the resonant frequencies by 50 MHz for the resonance of 2.45 GHz and 100 MHz for the resonance of 5.5 GHz, the antennas still have large matching bandwidth from 2 GHz to over 8 GHz.



(a)



(b)

Figure 4.5. S-parameters of the first system - simulation compared to measurement; (a) Return loss of the antennas simulation vs. measurement; (b) Isolation between the antennas in ABS box.

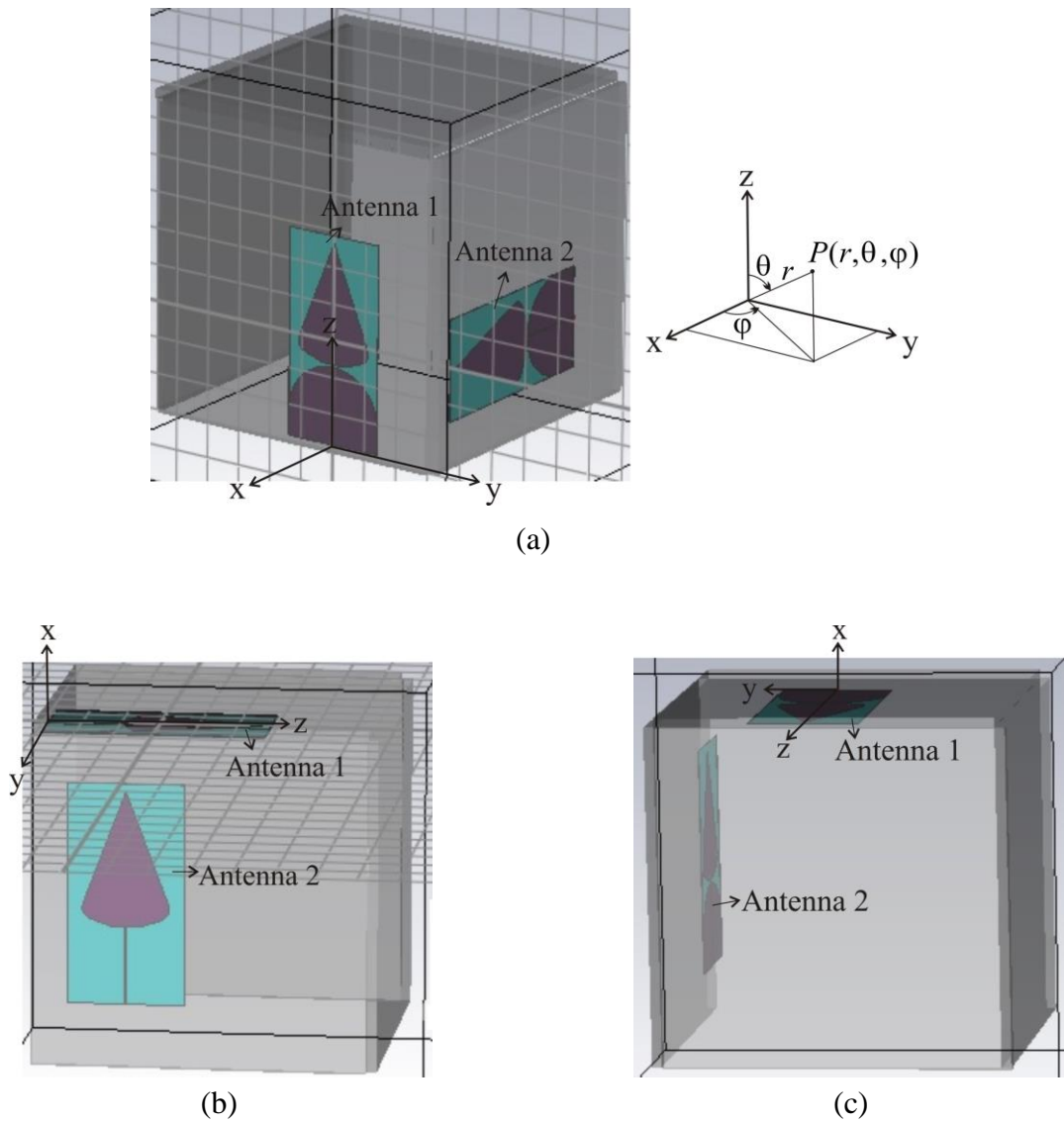


Figure 4.6. The system of two flat antennas in a 85 mm × 85 mm × 85 mm ABS plastic box: (a) Antenna system in spherical coordinates; (b) The x-z plane ($\phi = 0^\circ$); (c) The x-y plane ($\theta = 90^\circ$).

The simulation and measurement of radiation patterns of two antennas in the system have been carried out in two planes, the x-z plane ($\phi = 0^\circ$) and the x-y plane ($\theta = 90^\circ$) at two frequencies 2.45 GHz and 5.5 GHz.

Figure 4.6 illustrates the antenna system in spherical coordinates and those planes.

Figure 4.7 and Figure 4.8 depict the simulation and measurement realized gain radiation patterns for two antennas at two frequencies mentioned above.

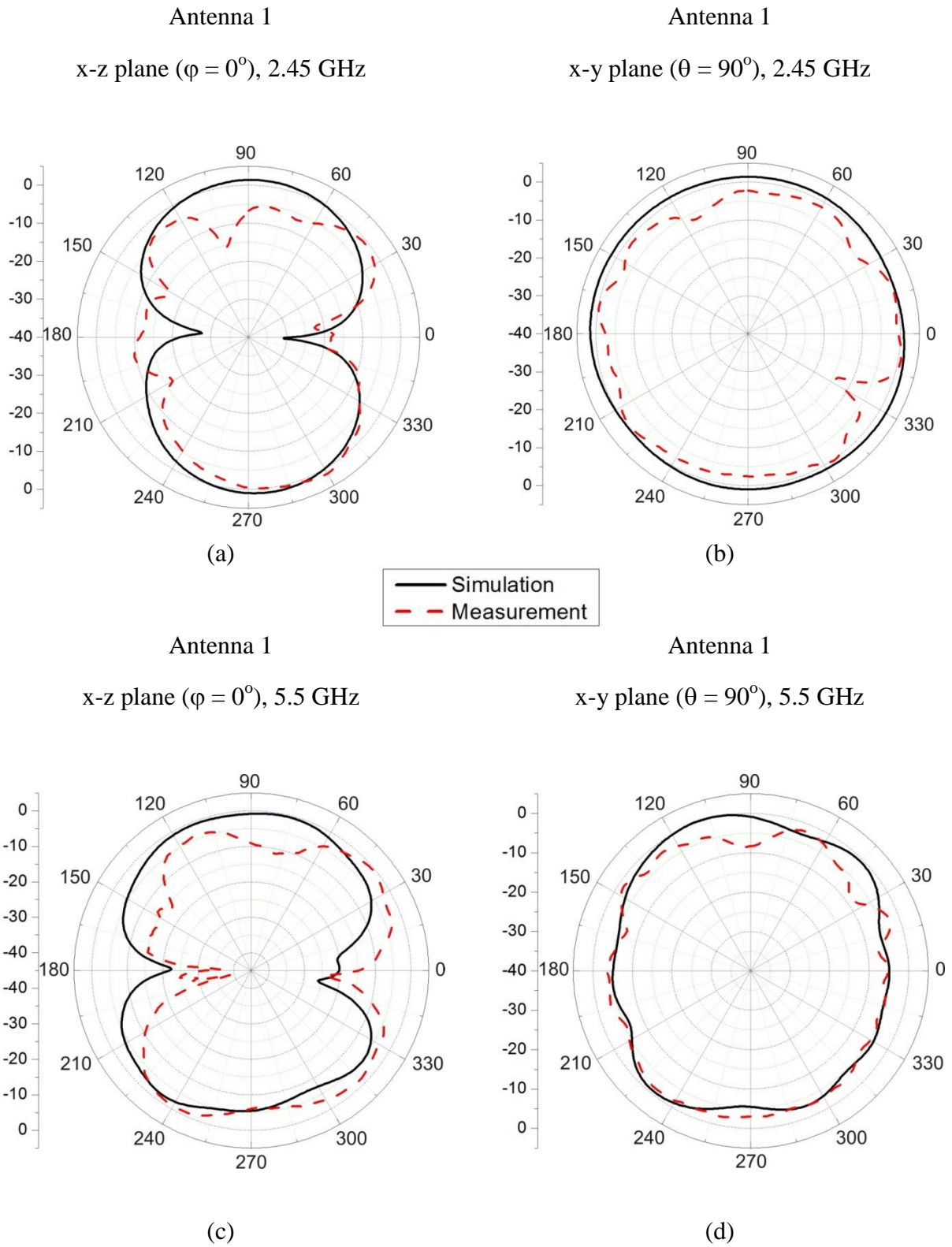


Figure 4.7. Simulated and measured realized gain radiation patterns of Antenna 1: (a) In x-z plane ($\varphi = 0^\circ$) at 2.45 GHz; (b) In x-y plane ($\theta = 90^\circ$) at 2.45 GHz; (c) In x-z plane ($\varphi = 0^\circ$) at 5.5 GHz; (d) In x-y plane ($\theta = 90^\circ$) at 5.5 GHz.

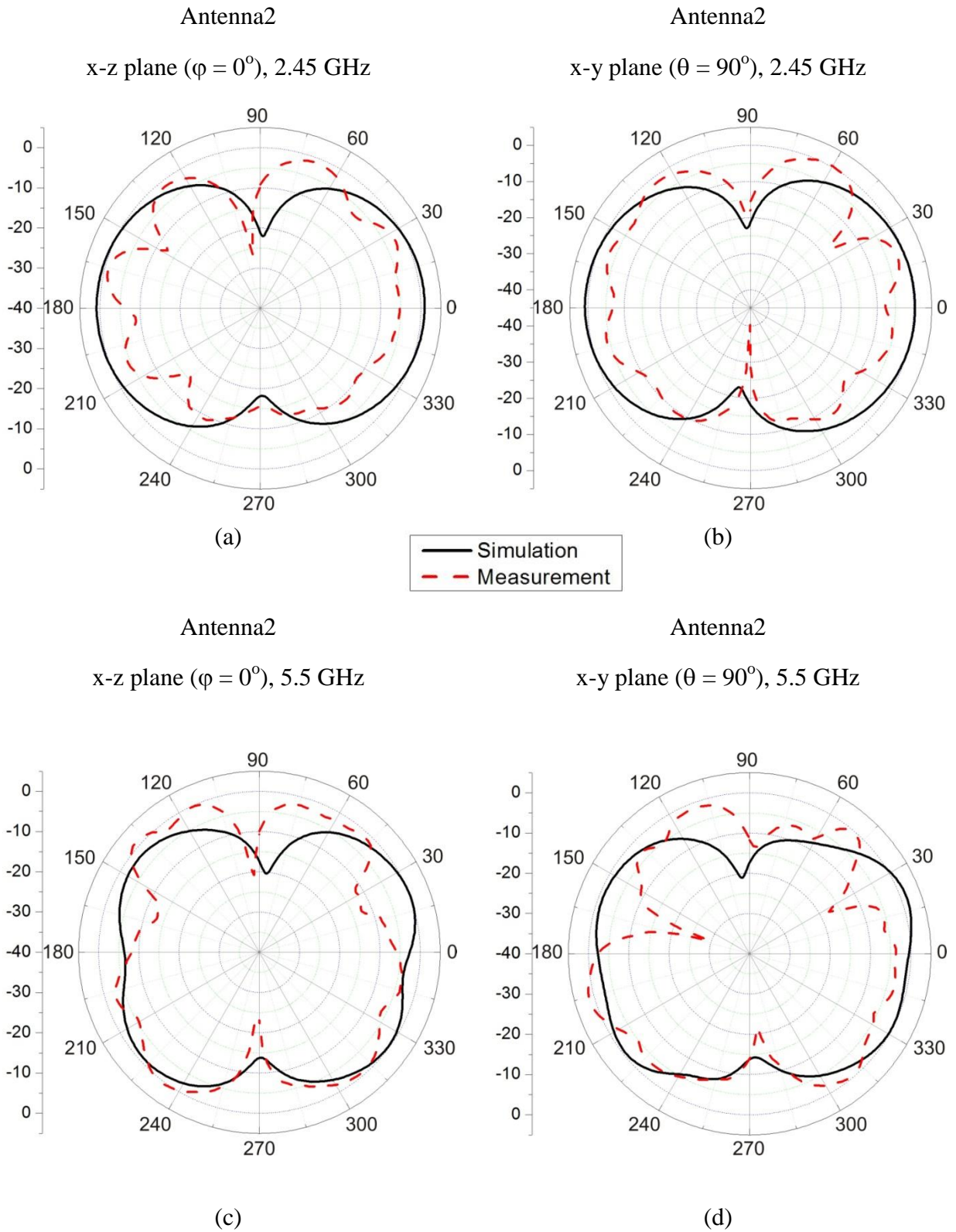


Figure 4.8. Simulated and measured realized gain radiation patterns of Antenna 2: (a) In x-z plane ($\varphi = 0^\circ$) at 2.45 GHz; (b) In x-y plane ($\theta = 90^\circ$) at 2.45 GHz; (c) In x-z plane ($\varphi = 0^\circ$) at 5.5 GHz; (d) In x-y plane ($\theta = 90^\circ$) at 5.5 GHz.

The errors between simulation and measurement, sometimes significant up to 10 dB, are caused by the coupling between two antennas in the system, the influence of their ground planes to each other that is not considered in the simulation. Besides, the arrangement errors of the measurement setup such as off-centering or cable twisting can also be reasons for this disagreement. However, in spite of all that, the radiation patterns of the antennas are still omni-directional, and the space diversity of the system can clearly be seen.

The simulated total efficiency of both antennas in the system is about 80% at 2.45 GHz and 64% at 5.5 GHz. The Envelope Correlation Coefficient (ECC) calculated by the formula (1.3) is much less than 0.05 at both those frequencies.

This system of two wide-band antennas in an ABS box described above has very good performance, but cannot always be realized because of a restricted size of packages. Today, consumer electronics market usually has very strict requirements, one of them is the compactness and low cost that makes big challenge for designers and manufacturers.

When the height of the box is less than that of the antenna, one of the solutions is bending the first antenna to place it into the box. The following section will study the effects of bending on the antenna characteristics.

4.2. Study of Antenna Bending Effects

One of the most important advantages of paper-based antennas is their flexibility, leading to the capability of making three-dimensional structures from them by bending and deforming according to the form of packages, but deformation can considerably affect the radiation patterns of the antennas. Effects of deformation of antennas on various flexible materials such as very thin Rogers RT/Duroid 5880 substrates, polylactic acid plastic or PET have intensively been studied [1, 6-10] with the main focus on wearable device applications at different frequency bands, and only the authors of [1] mentioned about curved wireless device application. In [3], the flexibility study of a PIFA was done with vertical bending around a cylinder of two different radii to verify the quality of fabrication. However, there was no complete study and analysis on flexibility of antennas on high-loss flexible paper material.

In this section, a study will be conducted about bending effects on antenna characteristics to predict its performance and prevent its undesirable behavior when it is needed to be placed in a package.

4.2.1. Basic theory for the study

The basic theory of this study consists of a simple dipole of the total length L comprising two misaligned parts shown in Figure 4.9 with the lengths of L_1 and $L - L_1$ where the second part is tilted under an angle of ε_θ from the first one. The main objective of this part is to analyze the modification of the radiation pattern of a bent antenna with a simple model. This will allow to a more comprehensive analyze of real antennas' behavior.

The electric field radiated by the first part of the dipole in the far-field region is given by

$$\begin{cases} E_{1\theta} = j\eta \frac{kI_0L_1}{4\pi r} \sin\theta \cdot e^{-jkr} \\ E_{1r} \approx 0 \end{cases} \quad (4.1)$$

where I_0 is the amplitude of current in the monopole, k is wave number, L_1 is the length of the first part of the dipole.

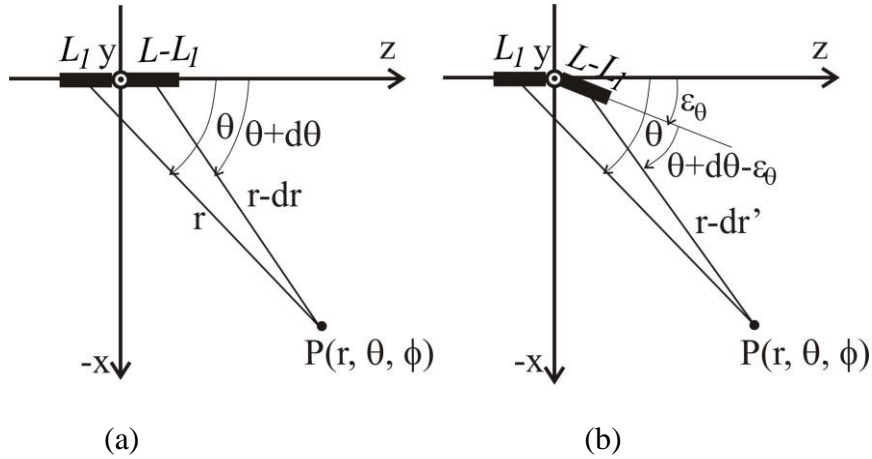


Figure 4.9. Basic theoretical study of a dipole: (a) The straight dipole; (b) The dipole consisting of two misaligned parts, the second one is tilted under an angle ε_θ .

As the dipole is very small, the current in the second part is nearly unchanged in value so that it can be considered as an independent dipole. Thus, the electric field radiated by the second part of the dipole in the far-field region is

$$\begin{cases} E_{2\theta} = j\eta \left[\frac{kI_0(L-L_1)}{4\pi(r-dr')} \sin(\theta+d\theta-\varepsilon_\theta) \cdot e^{-jk(r-dr')} \right] \\ E_{2r} \approx 0 \end{cases} \quad (4.2)$$

For the dipole consisting of two straight parts in Figure 4.9(a),

$$\begin{cases} E_{\theta} = E_{1\theta} + E_{2\theta} \\ = j\eta \left[\frac{kI_0 L_1}{4\pi r} \sin \theta \cdot e^{-jkr} + \frac{kI_0(L-L_1)}{4\pi(r-dr)} \sin(\theta+d\theta) \cdot e^{-jk(r-dr)} \right] \\ E_r \approx 0 \end{cases} \quad (4.3)$$

As $d\theta$ and dr are very small, $\sin(\theta+d\theta) \approx \sin \theta$ and

$$\frac{1}{(r-dr)} = \frac{1}{r} \cdot \frac{1}{1-\frac{dr}{r}} \approx \frac{1}{r} \left(1 + \frac{dr}{r} \right) \quad (4.4)$$

$$\begin{cases} E_{\theta} = j\eta \left[\frac{kI_0 L_1}{4\pi r} \sin \theta \cdot e^{-jkr} + \frac{kI_0(L-L_1)}{4\pi r} \sin \theta \cdot e^{-jkr} \cdot \left(1 + \frac{dr}{r} \right) \right] \\ = j\eta \frac{kI_0 L_1}{4\pi r} \sin \theta \cdot e^{-jkr} + j\eta \frac{kI_0(L-L_1)}{4\pi r} \sin \theta \cdot e^{-jkr} \cdot \frac{dr}{r} \\ E_r \approx 0 \end{cases} \quad (4.5)$$

where the second term of E_{θ} can be considered as very small.

Let us consider the case when the second part of the dipole is tilted under an angle ε_{θ} (Figure 4.9(b)).

The electric field is given by:

$$\begin{cases} E_{\theta} = E_{1\theta} + E_{2\theta} \\ = j\eta \left[\frac{kI_0 L_1}{4\pi r} \sin \theta \cdot e^{-jkr} + \frac{kI_0(L-L_1)}{4\pi(r-dr')} \sin(\theta+d\theta-\varepsilon_{\theta}) \cdot e^{-jk(r-dr')} \right] \\ E_r \approx 0 \end{cases} \quad (4.6)$$

Taking into account, that $d\theta$, dr and dr' are very small, the electric field radiated by two parts of the dipole in the far-field region is the superposition of two fields as follows

$$\begin{cases} E_{\theta} = E_{1\theta} + E_{2\theta} \\ \approx j\eta \frac{kI_0}{4\pi r} e^{-jkr} [L_1 \cdot \sin \theta + (L-L_1) \cdot \sin(\theta-\varepsilon_{\theta})] \\ E_r = E_{1r} + E_{2r} \approx 0 \end{cases} \quad (4.7)$$

where $E_{1\theta}, E_{2\theta}, E_{1r}, E_{2r}$ are the field components of two parts of the dipole, I_0 is the amplitude of current in the dipole, k is wave number, L_1 is the length of the first part of the dipole and L is the total length of both dipoles.

Thus, the radiation electric field depends on the coefficient in the parentheses as a function of θ and ε_θ . The normalized radiated power, i. e. radiation patterns, is given by

$$g(\theta, \varepsilon_\theta) = |L_1 \cdot \sin \theta + (L - L_1) \cdot \sin(\theta - \varepsilon_\theta)|^2 \quad (4.8)$$

The formula (4.8) allows us to predict approximately the maximum radiation direction of the dipole. As an example, Figure 4.10(a) shows this factor as a function of θ for $L_1 = L/2$, i. e. the dipole is bent at its middle point and three values of the tilting angle $\varepsilon_\theta = 0^\circ, 60^\circ, 90^\circ$. The maximum is achieved when $\sin\left(\theta - \frac{\varepsilon_\theta}{2}\right) = 1$, i. e. $\theta = \frac{\pi}{2} + \frac{\varepsilon_\theta}{2}$, the angle between the maximum radiation direction in each case and the direction $\theta = 90^\circ$ is $\varepsilon_\theta/2 = 0^\circ, 30^\circ$ and 45° , respectively. For a fixed ε_θ , changing the value of L_1/L one can also observe the rotation of the graph as illustrated in Figure 4.10(b).

In practice, we consider only the tilting angles $0^\circ \leq \varepsilon_\theta \leq 90^\circ$, according to bending of $90^\circ \leq 180^\circ - \varepsilon_\theta \leq 180^\circ$ studied in the next section.

This basic theoretical study of a dipole can also be applied for a microstrip-fed planar monopole when its ground plane is cleared under its radiation part to get omni-directional radiation patterns as a dipole.

In order to preliminary verify this basic theory, a planar dipole is designed at 2.45 GHz on E4D paper substrate with 0.21 mm thick, then its second half is bent under 120 degrees and 90 degrees (Figure 4.11). As a result, the resonant frequency is shifted to 2.8 GHz and 2.82 GHz for the dipoles bent under 120 degrees and 90 degrees, respectively, which is presented in Figure 4.12. With the equal lengths of two parts of the dipole, the realized gain radiation patterns at the straight dipole's resonant frequency 2.45 GHz in Figure 4.13(a) show the rotation of the beams by 30° (red line) and 45° (blue line) in two cases of a 120-degree and 90-degree bend in respect to that of the straight dipole (black line). Besides, the more the dipole is bent, the less its gain is (Figure 4.13(b)). The results confirm an excellent agreement with the above theoretical studies.

Now let us consider a simple planar monopole also designed at 2.45 GHz on 210- μm thick E4D paper substrate shown in Figure 4.14. Under bending with $L_1 = L/2$, the resonant frequency is shifted to 2.54 GHz and 2.62 GHz in case of a 120-degree and 90-degree bend, respectively (Figure 4.15). The radiation diagram is rotated by 30° and 45° in respect to that of the monopole without bending shown in Figure 4.16 as predicted for a dipole. This can be explained by the fact,

that the microstrip-fed planar monopole with the ground plane cleared under its radiation part has nearly the same omni-directional radiation diagram as a dipole so that the basic theory for dipoles can be applied.

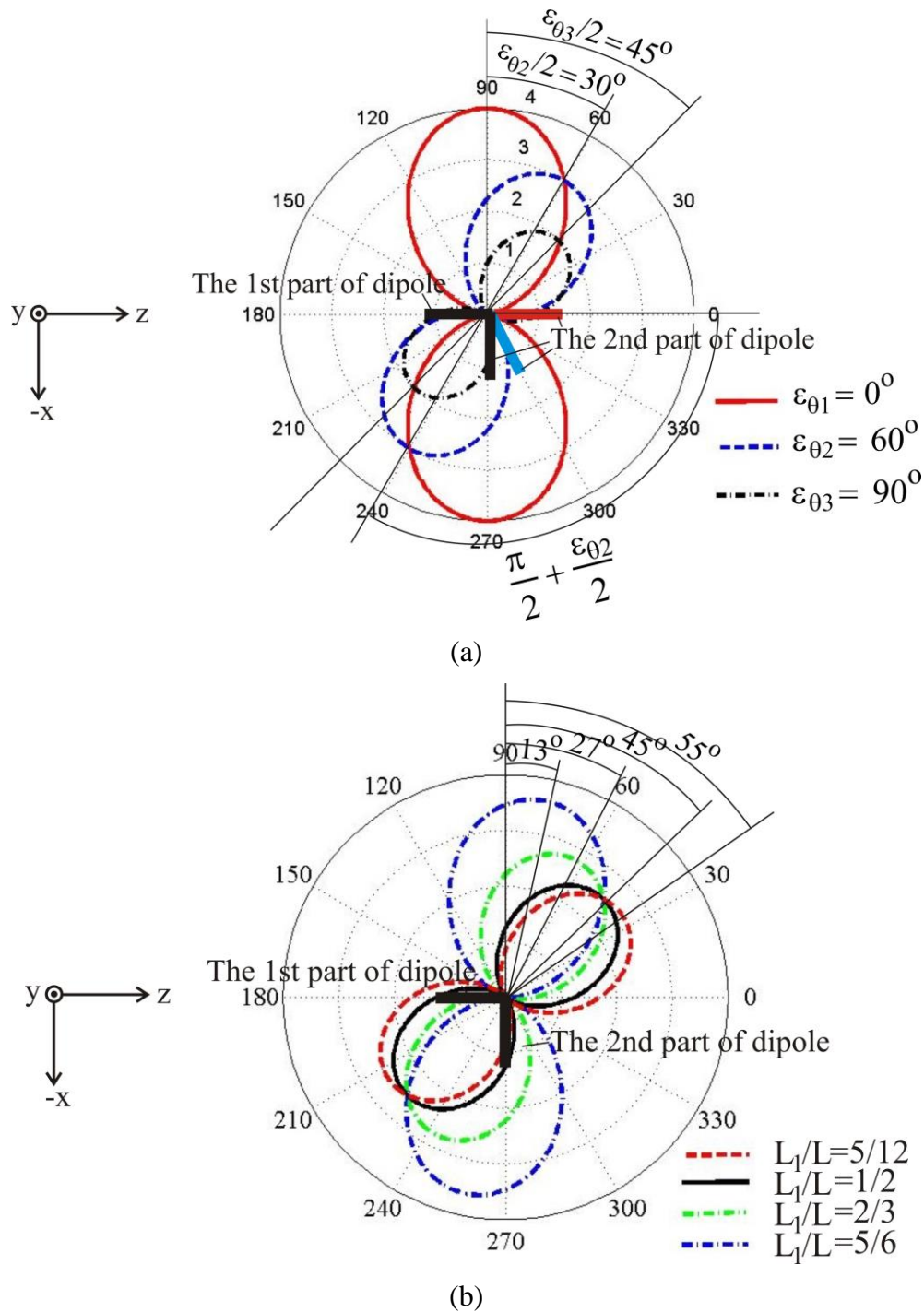


Figure 4.10. The normalized radiated power $g(\theta, \epsilon_\theta)$ of the studied dipole: (a) for $\epsilon_\theta = 0^\circ, 60^\circ, 90^\circ$ with the red, blue and black 2nd part of the dipole, respectively; (b) The case $\epsilon_\theta = 90^\circ$ for various ratios L_1/L .

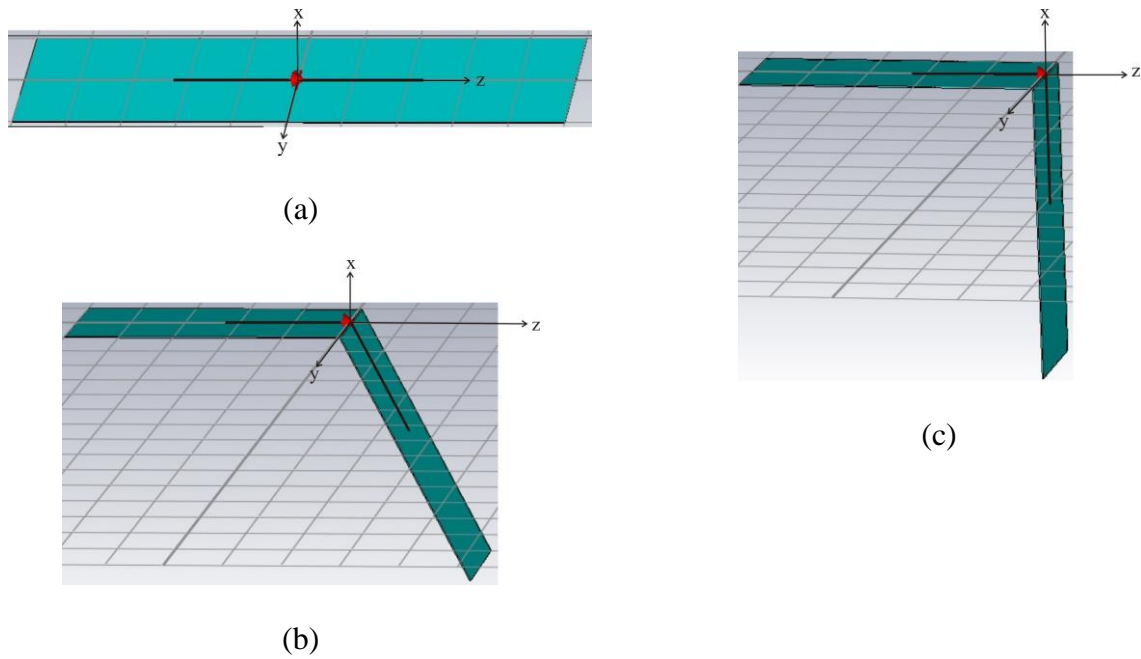


Figure 4.11. Planar dipole on 0.21 mm thick E4D paper substrate: (a) Straight; (b) Bent under 120 degrees; (c) Bent under 90 degrees.

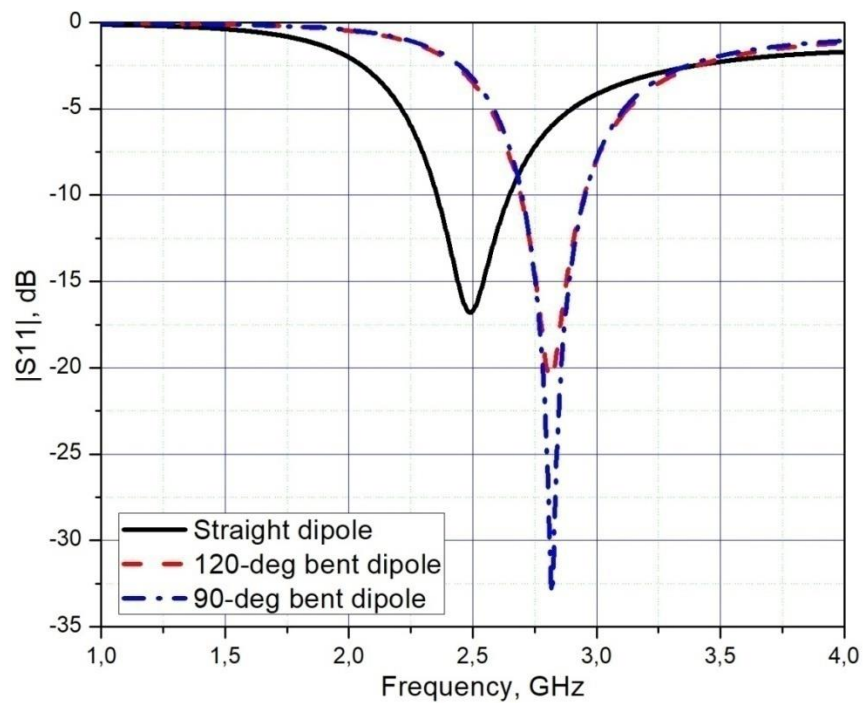


Figure 4.12. Return loss of a simple dipole on 0.21 mm thick E4D paper.

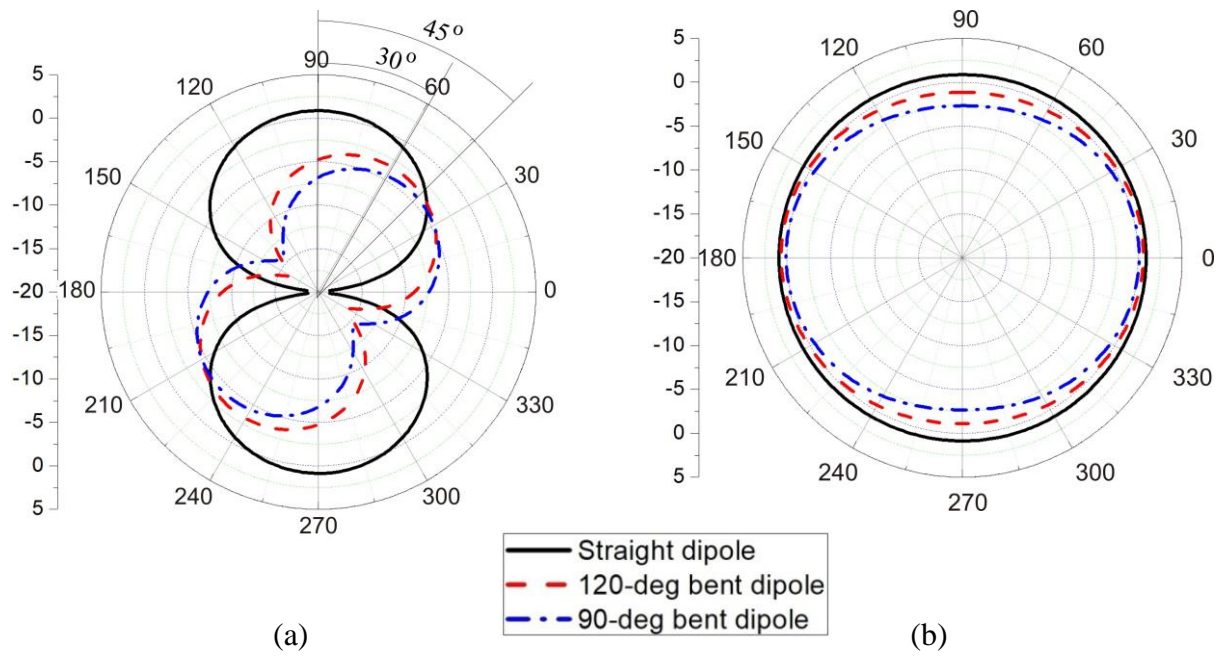


Figure 4.13. Realized gain radiation patterns at 2.45 GHz of the simple dipoles on 210- μm thick E4D paper: (a) In x-z plane ($\varphi = 0^\circ$); (b) In x-y plane ($\theta = 90^\circ$).

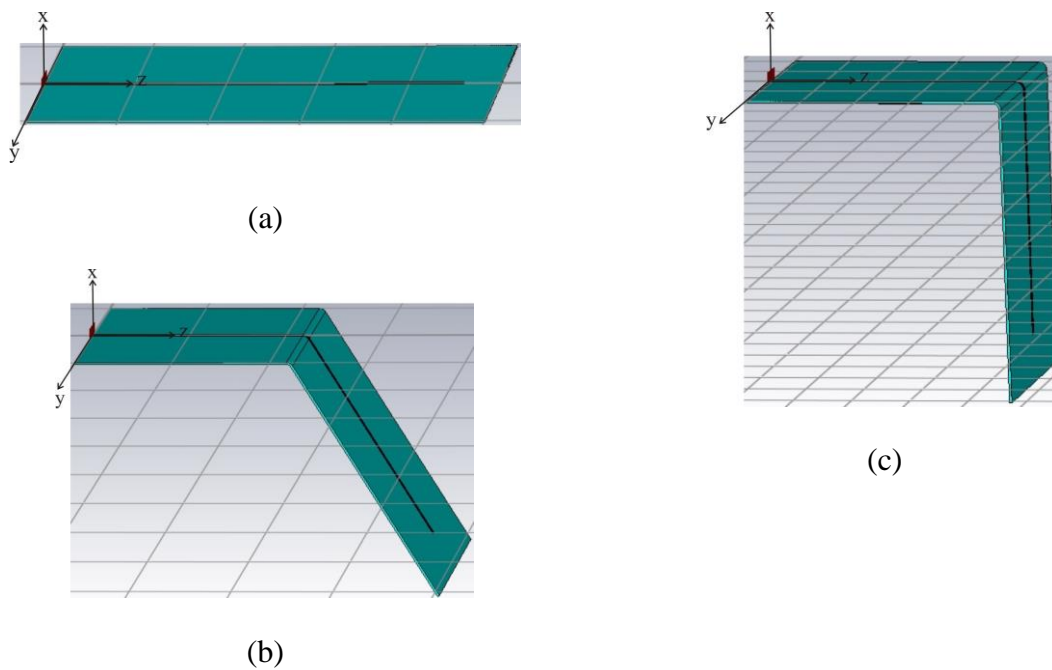


Figure 4.14. Planar monopole on 210- μm thick E4D paper substrate: (a) Straight; (b) Bent with $\varepsilon_\theta = 60^\circ$; (c) Bent with $\varepsilon_\theta = 90^\circ$.

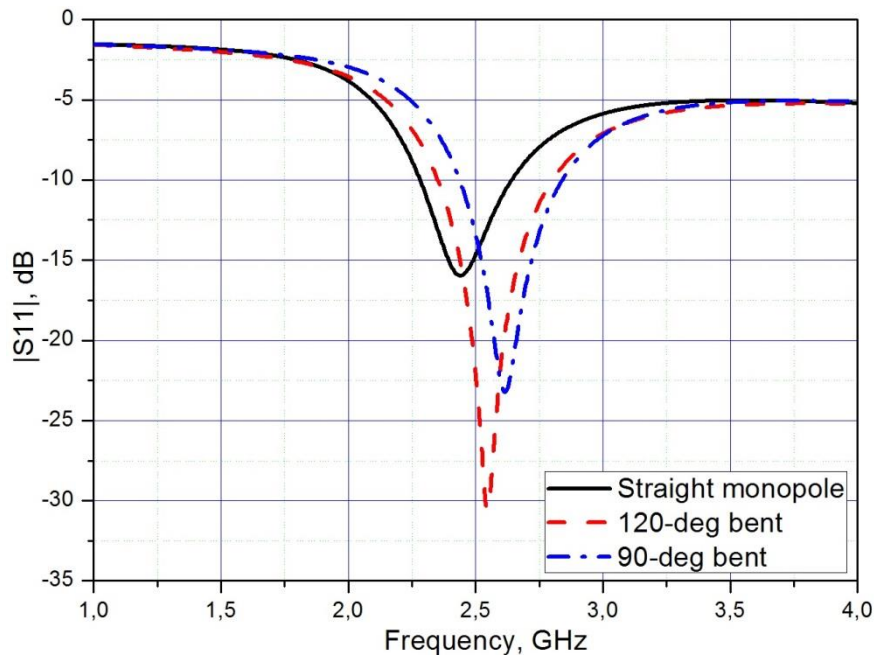


Figure 4.15. Return loss of a simple monopole on 210- μm thick E4D paper.

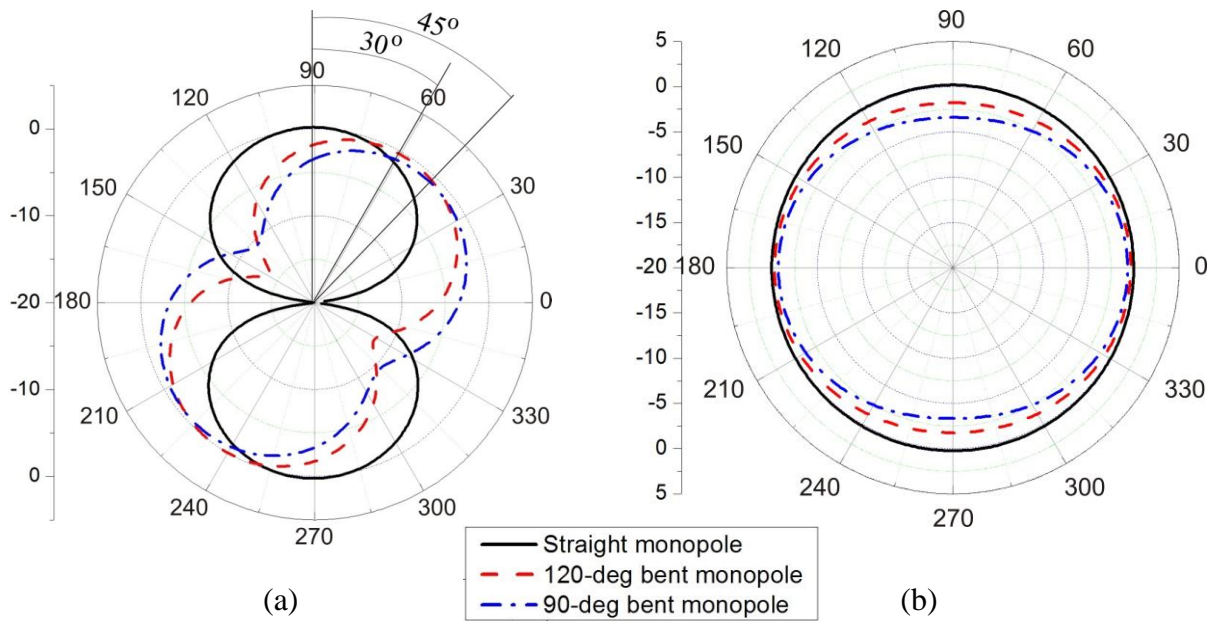


Figure 4.16. Realized gain radiation patterns at the resonant frequency of the simple monopoles on 210- μm thick E4D paper: (a) In x-z plane ($\varphi = 0^\circ$); (b) In x-y plane ($\theta = 90^\circ$).

4.2.2. Study of bending effects of a wide-band monopole antenna

The study of bending effects aims to predict the antenna performance in various deformations, especially when the antenna is located in a box with limited height. In this section, the antenna was experimentally bent in E-plane with two different angles: $\varepsilon_\theta = 60^\circ$, i. e. under 120-degree bending, and $\varepsilon_\theta = 90^\circ$, i. e. under 90-degree bending. In order to demonstrate the study, we use “Mushroom-shaped with two arms” antenna described in the section 3.4. Figure 4.17(a) illustrates the bending angle, the radius r_b and the location of bending h in the CST simulation structure and Figure 4.17(b) shows our bent fabricated prototype.

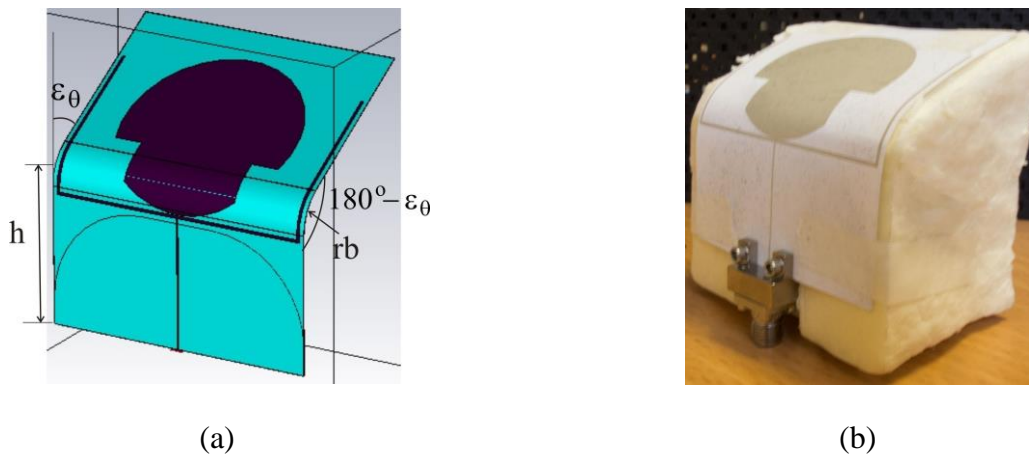


Figure 4.17. Study of bending effects of “Mushroom-shaped with two arms” antenna: (a) CST simulation structure with illustration of tilted angle ε_θ and the bending position h ; (b) Experimental realization.

In practice, the bending position h is chosen depending on the height of the package. Figure 4.18 shows the effect of h on the 90-degree bent antenna radiation patterns at 2.45 GHz for $h = 25, 30, 40$ and 50 mm, corresponding to the cases $L_1/L = \frac{5}{12}, \frac{1}{2}, \frac{2}{3}$ and $\frac{5}{6}$ illustrated Section II. It is shown in Figure 4.10, that the angles between the maximum radiation and the $\theta = 90^\circ$ directions are $55^\circ, 45^\circ, 27^\circ$ and 13° , respectively, as predicted and shown in Figure 4.10(b).

Besides, the simulation shows that the bending radius r_b does not much affect the antenna radiation patterns at all working frequencies. Figure 4.19 illustrates this effect at 2.45 GHz for 90-degree bending case.

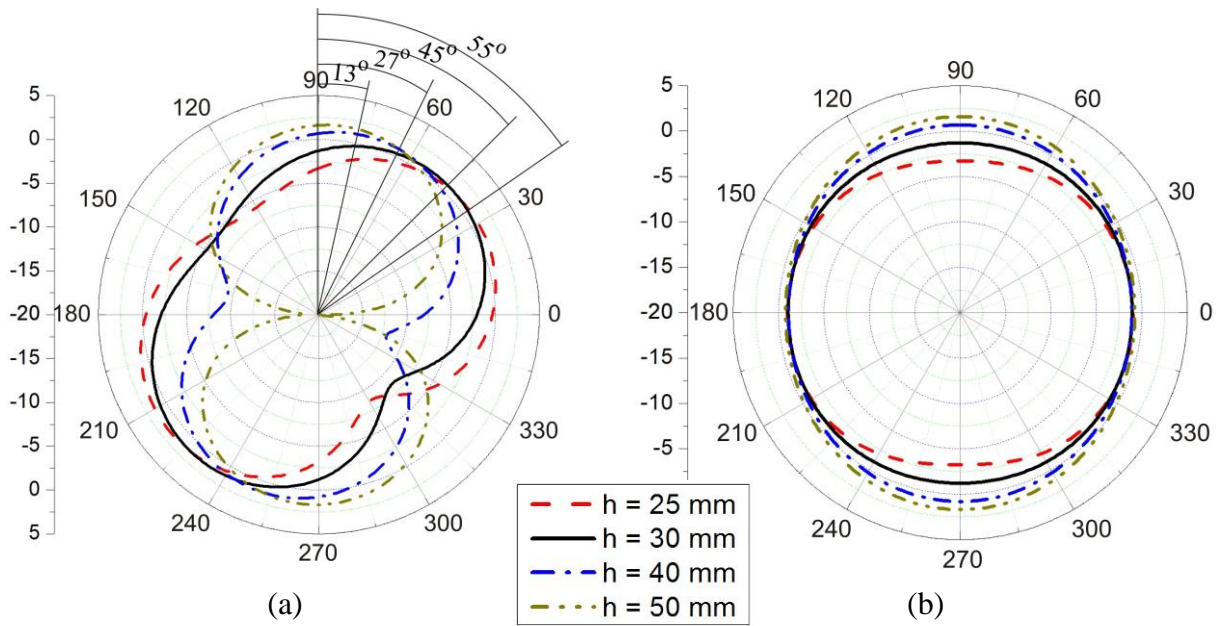


Figure 4.18. 2.45 GHz radiation patterns of 90-degree bent antenna at the various bending positions: (a) x-z plane (E-plane, $\varphi = 0^\circ$); (b) x-y plane (H-plane, $\theta = 90^\circ$).

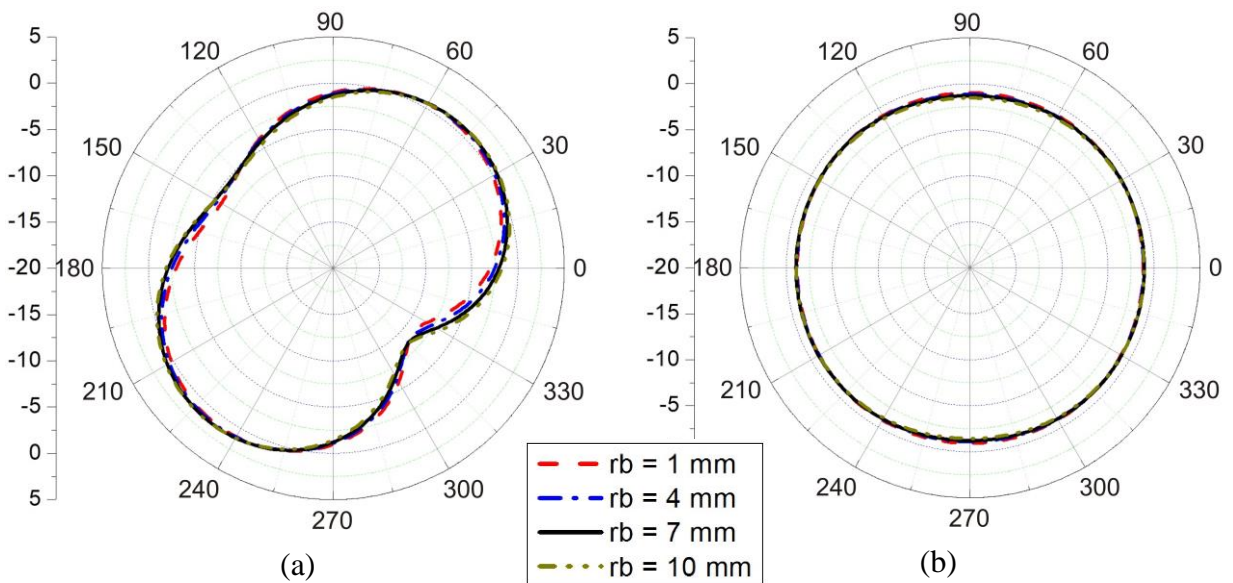


Figure 4.19. 2.45 GHz radiation patterns of 90-degree bent antenna at 30 mm for various bending radii: (a) x-z plane (E-plane, $\varphi = 0^\circ$); (b) x-y plane (H-plane, $\theta = 0^\circ$).

In our experimental study, the measurement was conducted for $h = 30$ mm, i. e. the case $L_1 = L/2$ in Section II, and the value $rb = 7$ mm as it could easily be realized and did not damage the antenna.

Both simulation and measurement studies show that the matching characteristics are not much affected by bending conditions (Figure 4.20), and despite a little resonant frequency shift, the antenna is still well matched in a very wide bandwidth, from 1.8 GHz to over 10 GHz.

The effect of bending on realized gain radiation patterns of the antenna by simulation for $h = 30$ mm is presented in Figure 4.21, where the antenna surface in y - z plane is bent toward $(-x)$ axis. The radiation patterns at 2.45 GHz when the antenna is under bending conditions rotate in the E -plane (y - z) as shown in Figure 4.21(a). The angles between the maximum radiation and x -direction in the case without bending, under 120-degree and 90-degree bending are 0° (black line), 30° (red line) and 45° (blue line), respectively as predicted in Figure 4.10(a) of Section II. Besides, radiation diagrams in the H -plane (x - y) of the antenna under bending become smaller at their upper and larger at their lower half (Figure 4.21(b) and (d)), especially for 90-degree bending, caused by more radiation surface bent toward $-x$ axis with more radiated field component that contributes to the lower half of the diagrams. At 5.5 GHz, when the antenna is bent, the maximum radiation directs to the opposite side of the antenna under 25° and 40° for 120-degree and 90-degree bending, respectively, with respect to the case without bending. (Figure 4.21(c)). This can be explained by the participation of the feed line in radiation and the stronger coupling between radiation elements as well as the ground plane at higher WLAN resonant frequency.

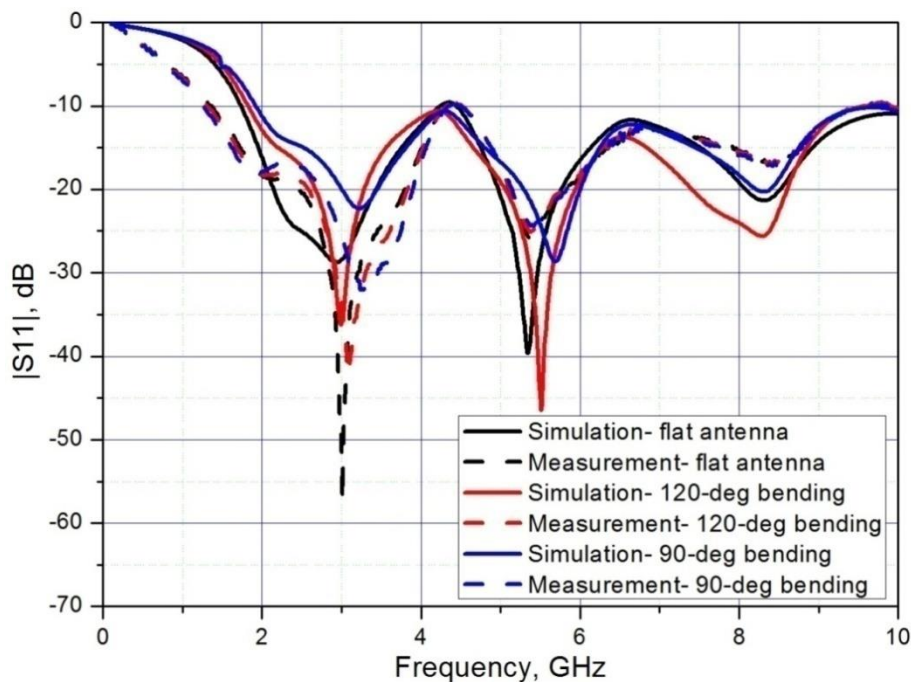


Figure 4.20. Reflection coefficient of a flat antenna and under bending.

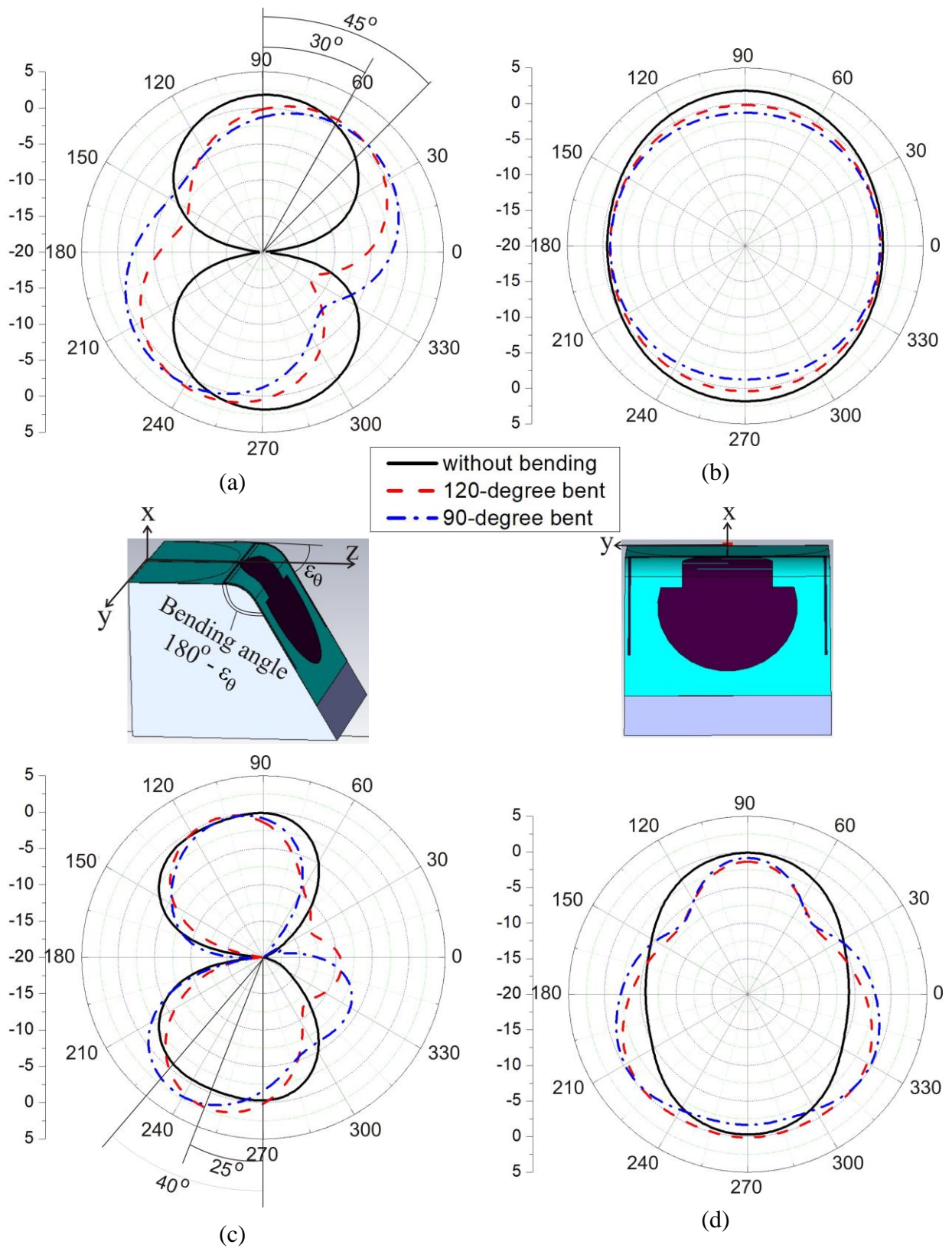


Figure 4.21. Radiation patterns of the antenna without bending and with bending: (a) x-z plane (E-plane), at 2.45 GHz; (b) x-y plane (H-plane), at 2.45 GHz; (c) x-z plane (E-plane), at 5.5 GHz; (d) x-y plane (H-plane), at 5.5 GHz.

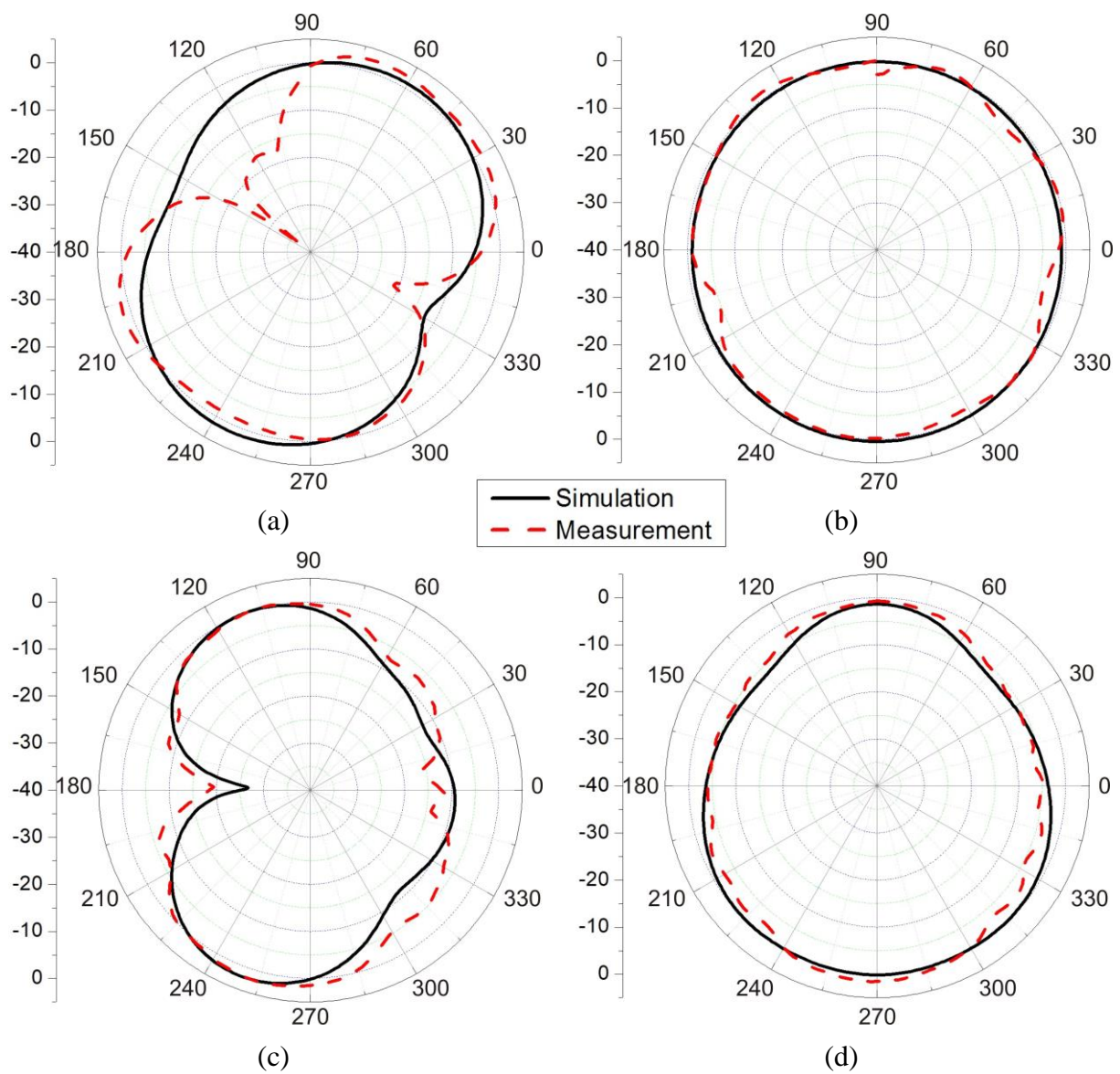


Figure 4.22. Radiation patterns of 120-degree bent antenna at the position 30 mm: (a) x-z plane (E-plane), at 2.45 GHz, (b) x-y plane (H-plane), at 2.45 GHz, (c) x-z plane (E-plane), at 5.5 GHz, (d) x-y plane (H-plane), at 5.5 GHz.

The measurement of radiation patterns was conducted in the anechoic chamber, where the antenna under test was located at the distance of 3 meters from the reference antenna, a horn with 10.0 dBi gain at 2.5 GHz and 11.3 dBi gain at 5.5 GHz, to satisfy the far-field condition (Appendix 2). Figure 4.22 and Figure 4.23 illustrate satisfactory agreement between simulation and measurement realized gain radiation patterns where the antenna is under bending. The mismatch between the measurement and simulation of about 2.5 dB and 2.7 dB at 2.45 GHz; 0.2 dB and 2 dB at 5.5 GHz at the maximum radiation direction in each case for 120-degree and 90-degree bending is

observed, that can be explained by the effect of the metallic motor and stretching/ twisting of the cable of the measurement system.

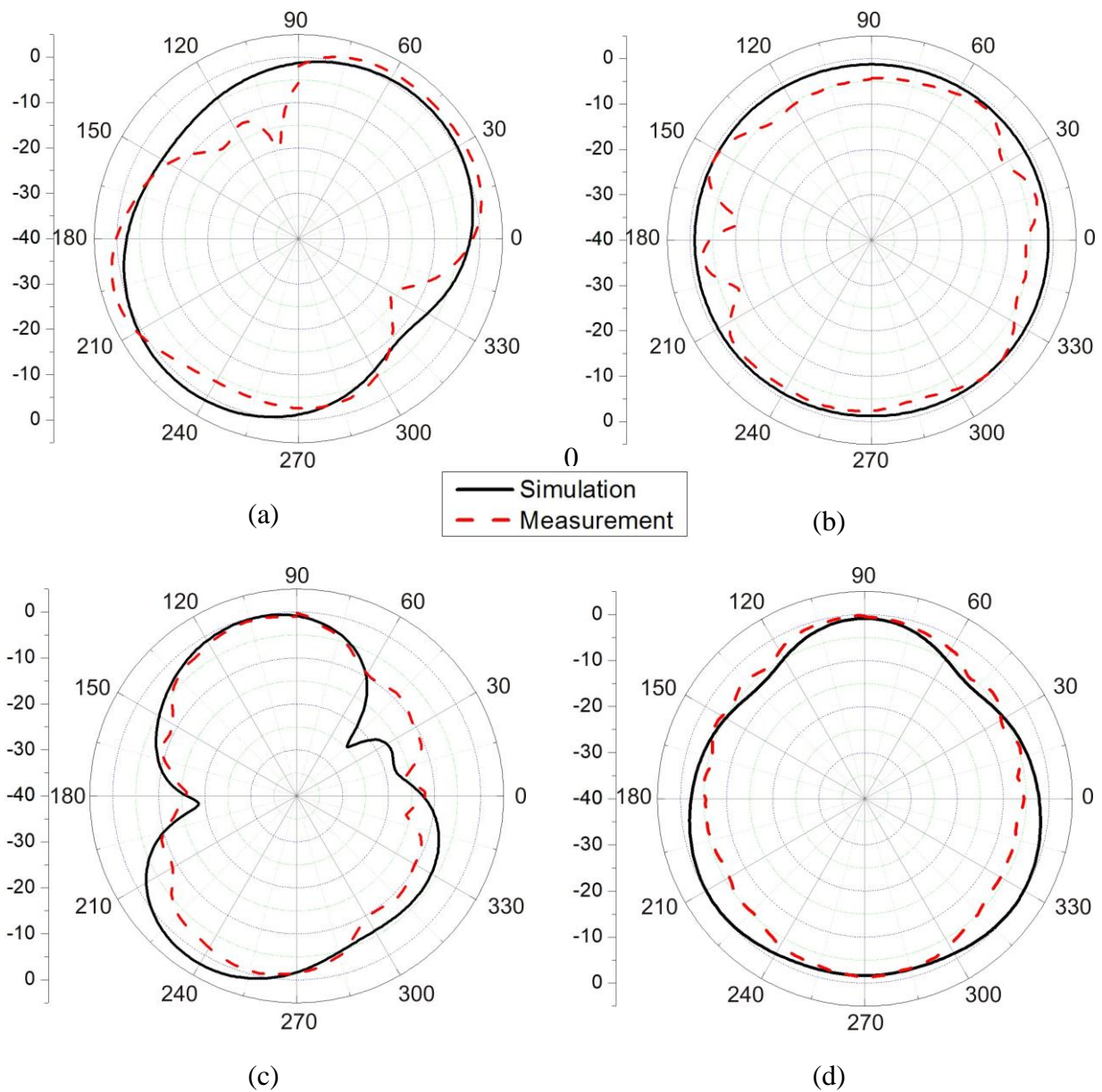


Figure 4.23. Radiation patterns of 90-degree bent antenna at the position 30 mm: (a) x-z plane (E-plane), at 2.45 GHz; (b) x-y plane (H-plane), at 2.45 GHz; (c) x-z plane (E-plane), at 5.5 GHz; (d) x-y plane (H-plane), at 5.5 GHz.

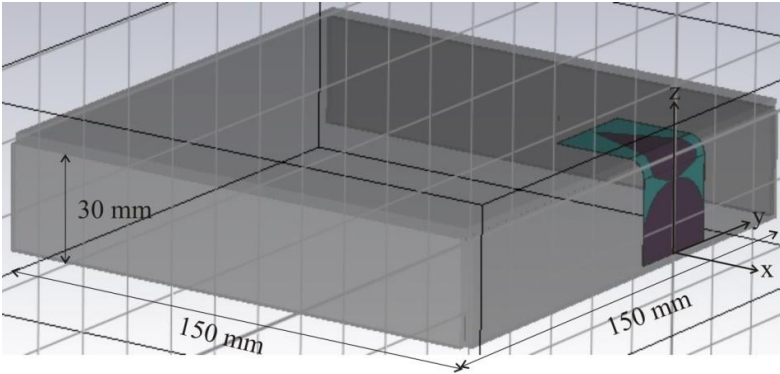
Due to the high loss property of the paper substrate ($\tan\delta = 0.092$), the total efficiency of the proposed monopole antenna is not high and is still reduced a little due to bending effects. At 2.45 GHz, the total efficiency of the antenna without bending is 74% and reduced to 68.9% and 64.2% with the 120-degree and 90-degree bend, respectively. At 5.5 GHz, these values are down to around 55% in all cases. The realized gain is strongly affected by bending, dropped from 2.03 dB

of the flat antenna to 1.58 dB and 1.07 dB (just a half as compared to the flat antenna) at 2.45 GHz in case of the 120-degree and 90-degree bend, respectively. Thus, bending causes a big reduction in realized gain of antennas, so that depending on antennas and requirements of a system, we should choose how much an antenna can be bent to prevent its undesirable behaviour.

4.3. System of antennas in a box with restricted dimensions

4.3.1. Wide-band antenna bent under 90 degrees placed in ABS box with restricted dimensions

When one of the box dimensions is very restricted compared to that of an antenna, the antenna needs to be deformed to be installed in this box.



(a)



(b)

Figure 4.24. A wide-band antenna bent under 90 degrees in a box: (a) CST Simulation structure; (b) Experimental realization.

Let us consider the case, when an ABS plastic box has the dimensions of 150 mm × 150 mm × 30 mm and the dimensions of the antenna “Sapin” on 210-μm thick E4D paper are 28 mm × 57 mm × 0.21 mm. The antenna is bent at the position depending on the height of the box, 30 mm in our case, and the position of the main card to connect the antenna, supposing at the bottom of the box (Figure 4.24).

Analyzing the return loss of the antenna shown in Figure 4.25, we can see that the 90-degree bend nearly does not change the resonant frequency at 2.45 GHz but shifts the higher WLAN frequency by about 200 MHz. The resonant frequency is shifted to 4.4 GHz if the bent antenna is attached to the internal wall of the ABS plastic box. However, in all cases the antenna is still well matched over a wide band of frequency from 2 GHz to over 8 GHz.

The simulation compared to measurement results of the bent antenna in the box realized gain radiation patterns are illustrated in Figure 4.26, where the errors are caused by the effect of the metallic motor and stretching/ twisting of the cable of the measurement system as well as the imperfection of printed antenna edges as mentioned in the previous section.

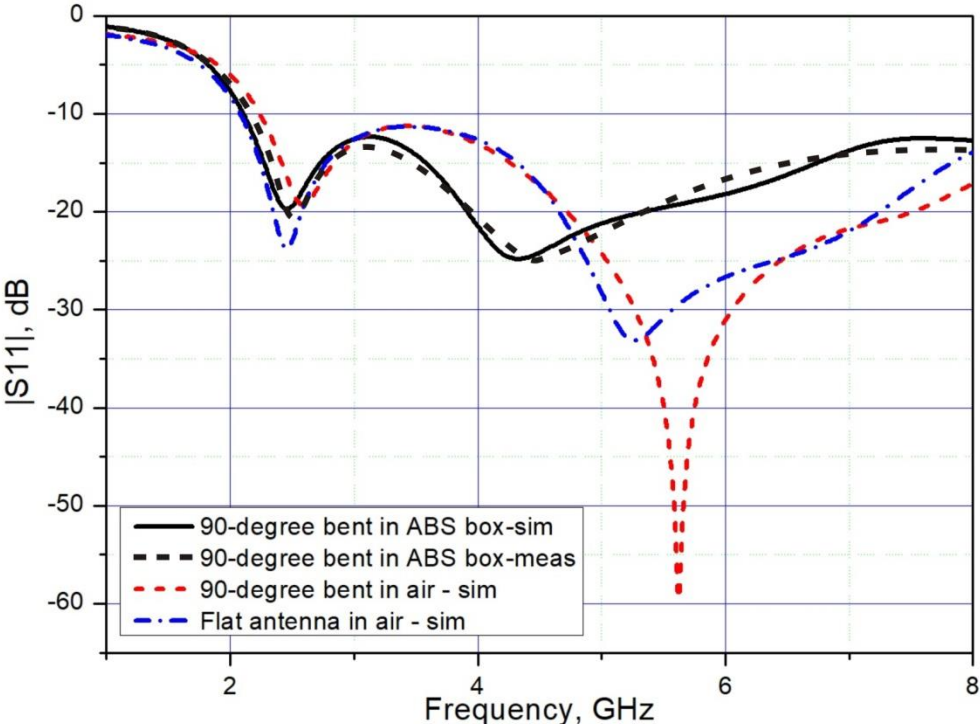
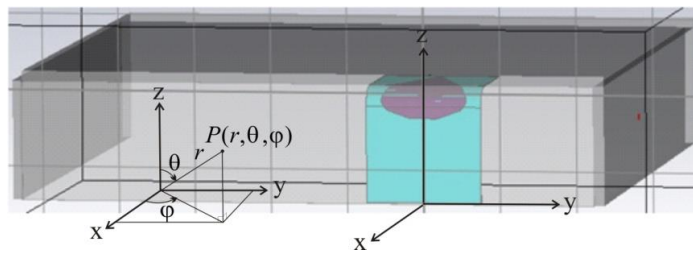


Figure 4.25. Reflection coefficient of the flat antenna and under bending in air and in ABS box.



(a)

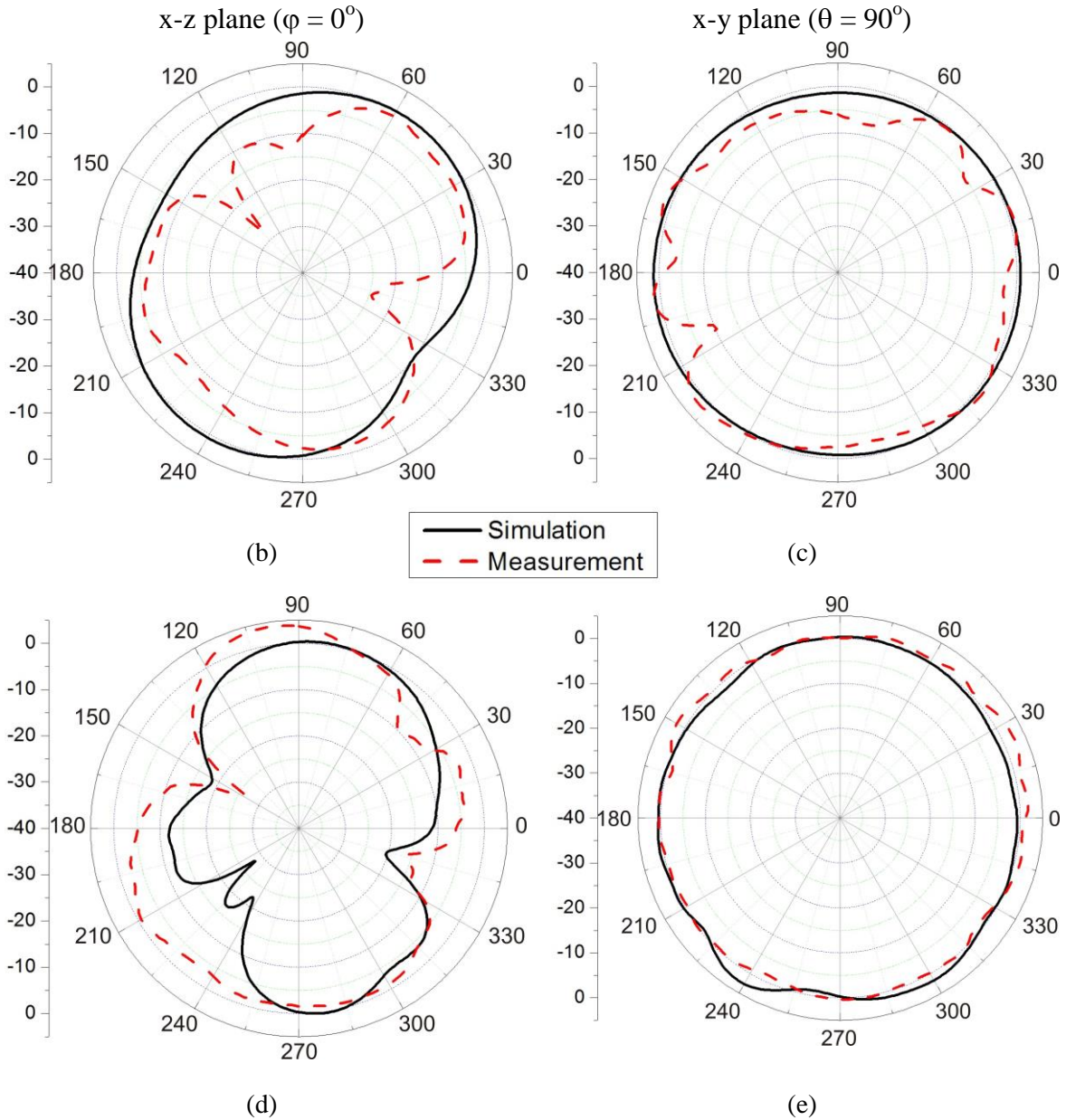
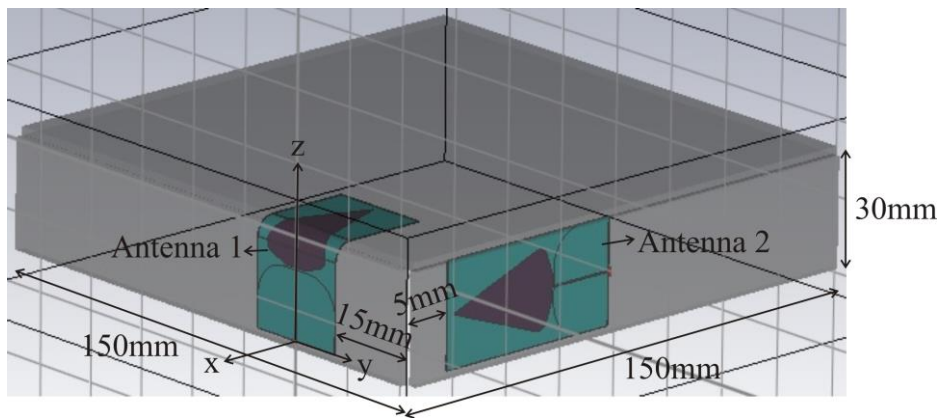


Figure 4.26. Simulated and measured realized gain radiation patterns of the bent antenna in a ABS plastic box: (a) Antenna in spherical coordinates; Realized gain radiation patterns of the antenna: (b) In x-z plane ($\varphi = 0^\circ$) at 2.45 GHz; (c) In x-y plane ($\theta = 90^\circ$) at 2.45 GHz; (d) In x-z plane ($\varphi = 0^\circ$) at 5.5 GHz; (e) In x-y plane ($\theta = 90^\circ$) at 5.5 GHz.

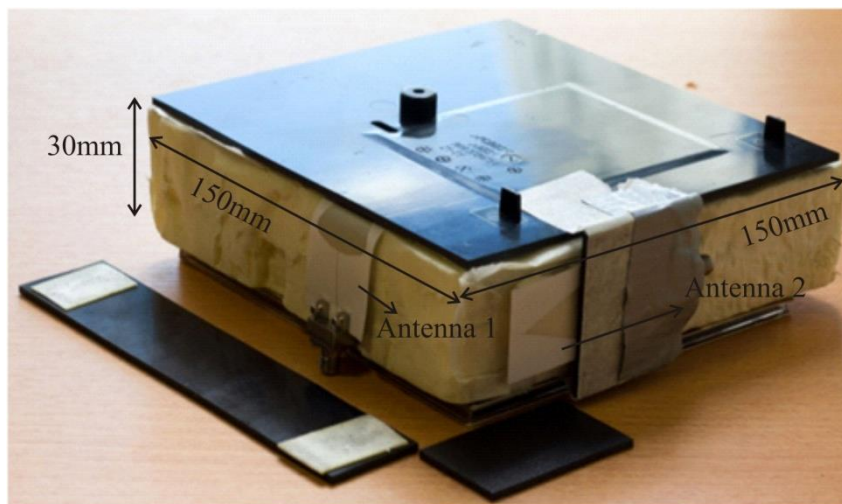
4.3.2. Two wideband antennas placed in an ABS box - one flat and another bent under 90 degrees

A. The box with the dimensions of 150 mm × 150 mm × 30 mm

This section provides the analysis of a system consisting of two antennas “Sapin” installed in an ABS box with the dimensions of 150 mm × 150 mm × 30 mm to create space diversity. Due to the limited height of the box, one of the antennas should be bent as shown in the previous section (Figure 4.27).



(a)



(b)

Figure 4.27. The system of two antennas in an ABS box with dimensions 150 mm × 150 mm × 30 mm : (a) CST simulation structure; (b) Experimental realization.

For the distance of 15 mm from the right edge of the first antenna to the edge of the box and the distance of 5 mm from the edge of the box to the upper edge of the second antenna, its S-parameters are depicted in Figure 4.29 where one can see that the behaviour of the reflection coefficients of two antennas in the system are like for single antennas without and with bending in ABS box. Moreover, there is good isolation between two antennas (Figure 4.29), of over 20 dB. The reason for the disagreement between simulation and measurement $|S_{21}|$, dB curves can be the capacitive coupling between two ground planes of the antennas that reaches the minimum at around 2.5 GHz, that is not taken into account in the simulation.

As for the system of two flat antennas shown in Section 4.1, the simulation and measurement of radiation patterns of two antennas in the system have been carried out in two planes, the x-z plane ($\varphi = 0^\circ$) and the x-y plane ($\theta = 90^\circ$) at two frequencies 2.45 GHz and 5.5 GHz. Figure 4.30 illustrates the antenna system in spherical coordinates and those planes. The realized gain radiation patterns of two antennas are illustrated in Figure 4.31 and Figure 4.32. It can be noted in the diagrams, that despite the bending effects of the first antenna, the space diversity of the system is still provided.

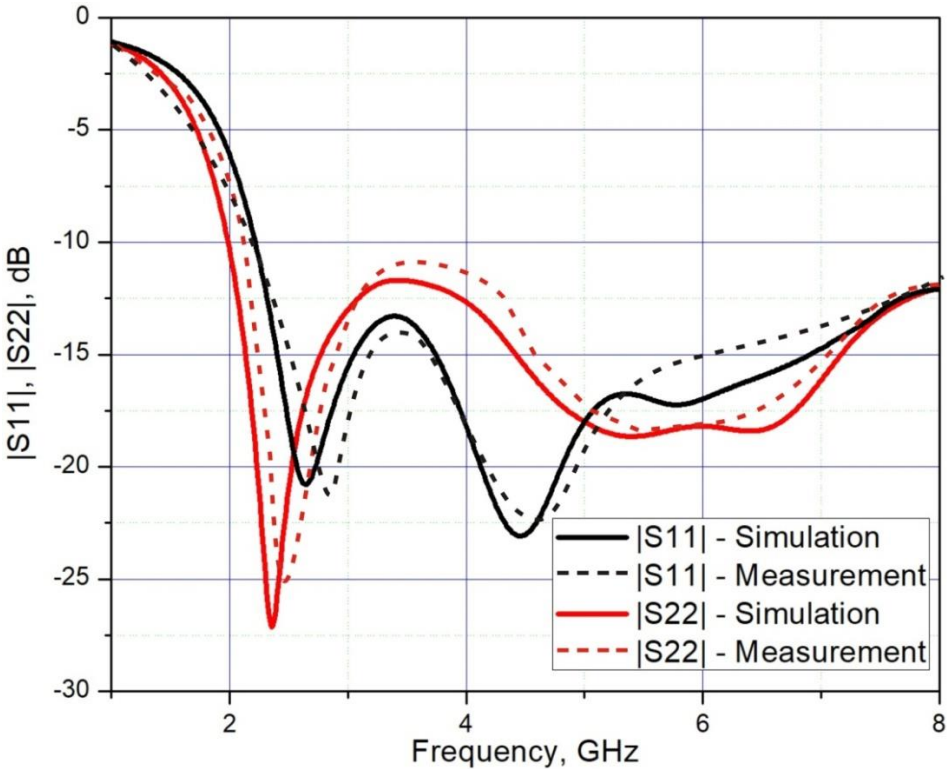


Figure 4.28. Return loss of the antenna system.

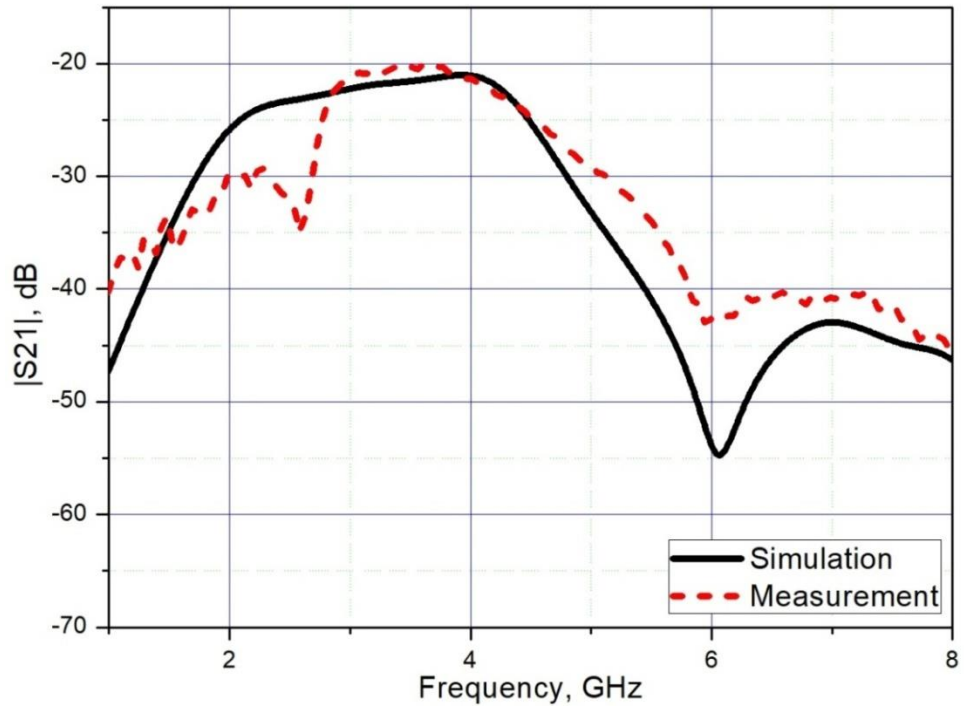
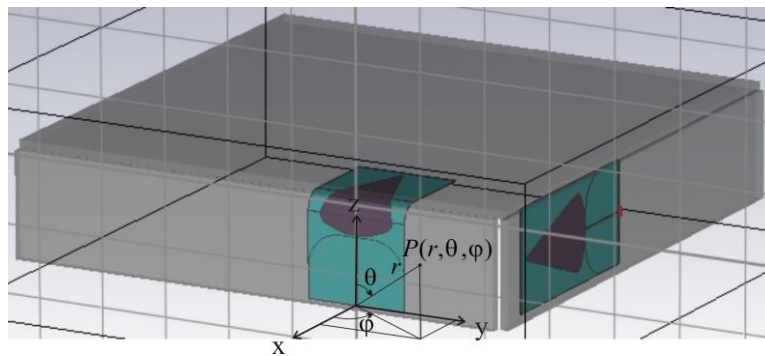
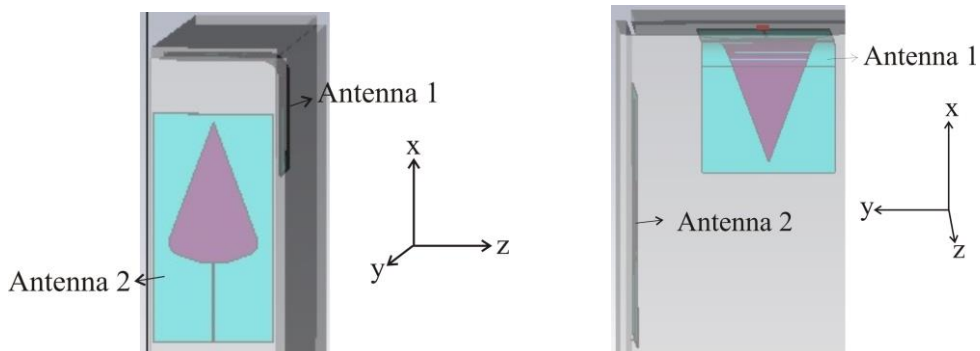


Figure 4.29. Isolation between the antennas in the system.



(a)



(b)

(c)

Figure 4.30. The antenna system in a 150 mm × 150 mm × 30 mm ABS plastic box: (a) Antenna system in spherical coordinates; (b) The x-z plane ($\varphi = 0^\circ$); (c) The x-y plane ($\theta = 90^\circ$).

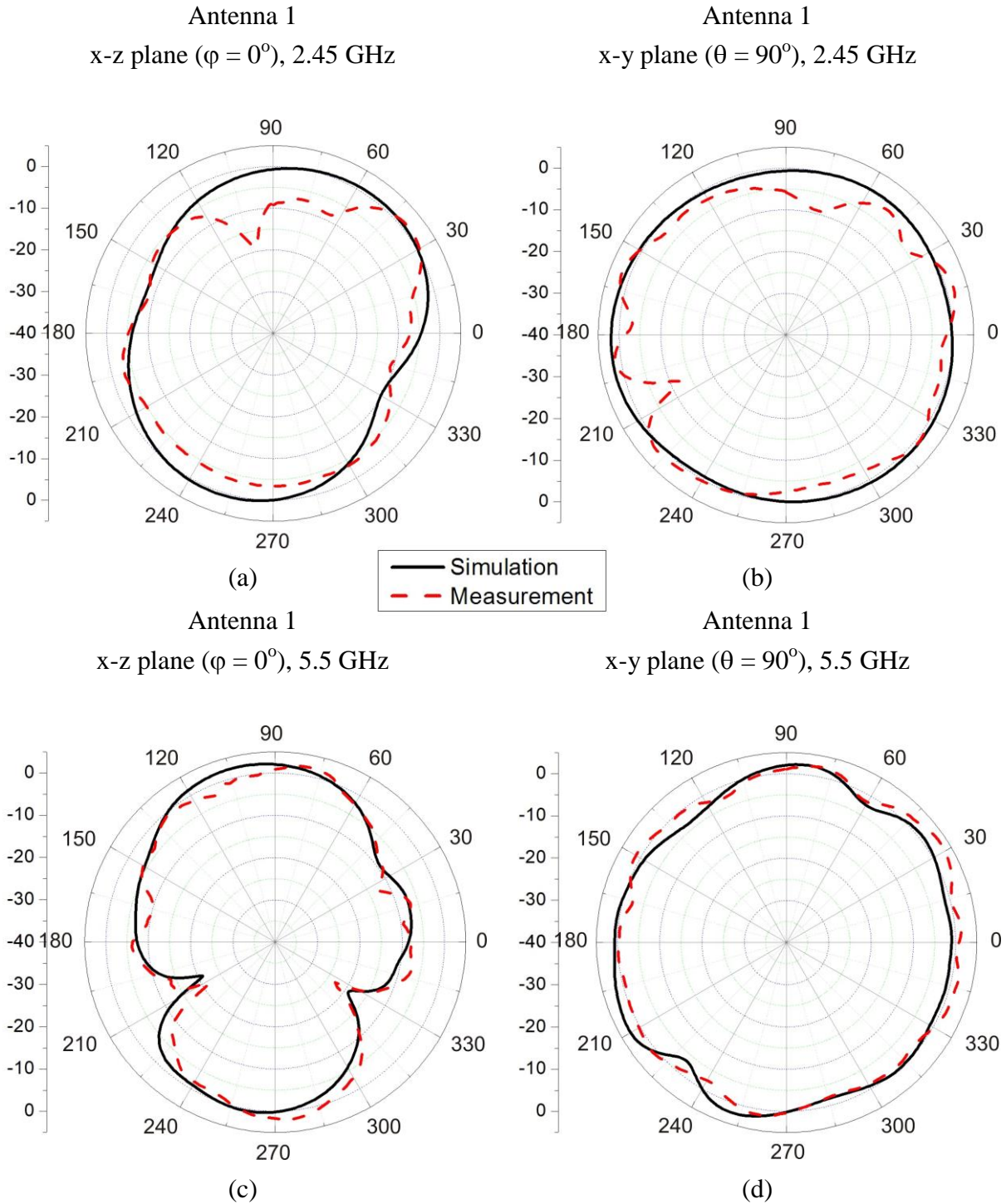


Figure 4.31. Simulated and measured realized gain radiation patterns of Antenna 1: (a) In x-z plane ($\varphi = 0^\circ$) at 2.45 GHz; (b) In x-y plane ($\theta = 90^\circ$) at 2.45 GHz; (c) In x-z plane ($\varphi = 0^\circ$) at 5.5 GHz; (d) In x-y plane ($\theta = 90^\circ$) at 5.5 GHz.

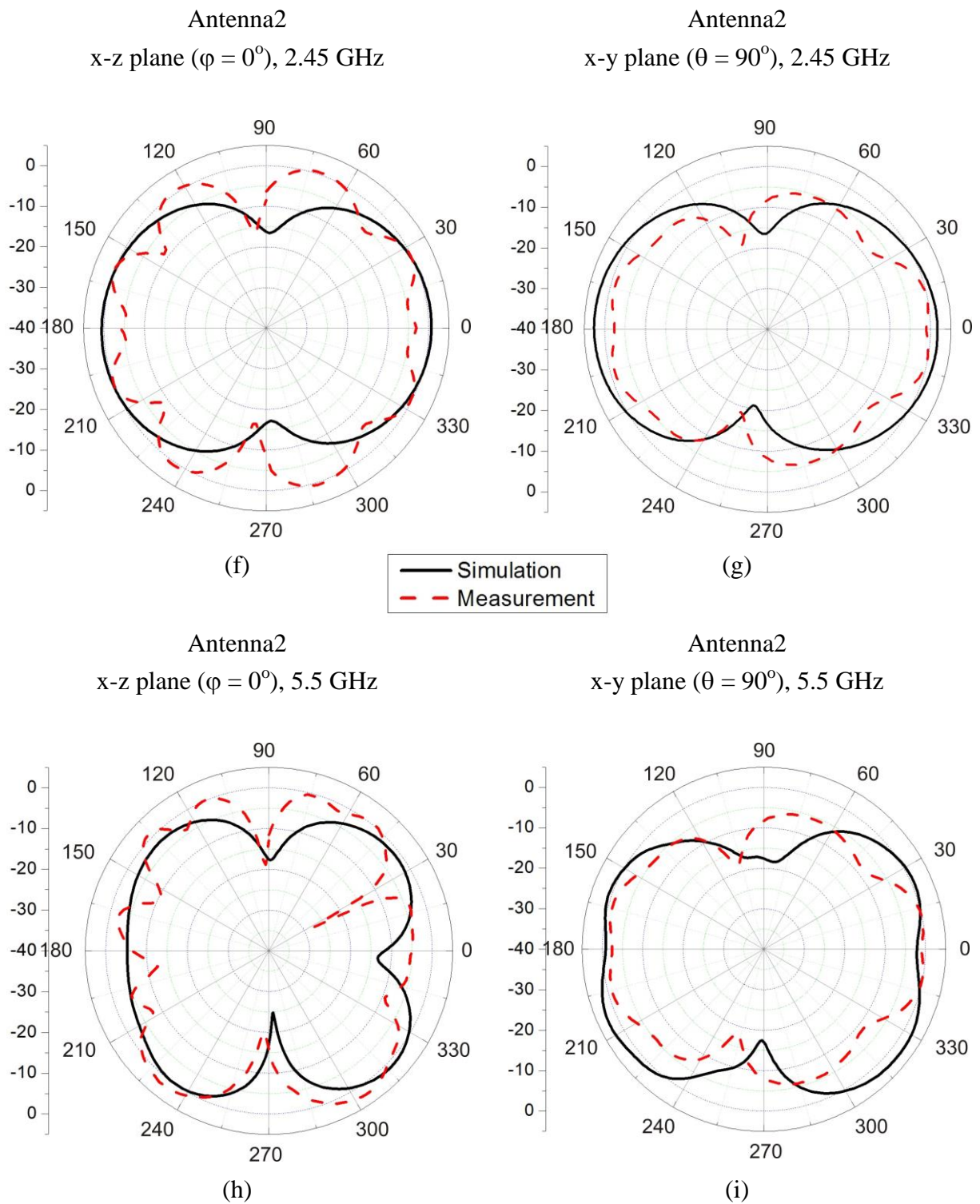


Figure 4.32. Simulated and measured realized gain radiation patterns of Antenna 2: (a) In x-z plane ($\varphi = 0^\circ$) at 2.45 GHz; (b) In x-y plane ($\theta = 90^\circ$) at 2.45 GHz; (c) In x-z plane ($\varphi = 0^\circ$) at 5.5 GHz; (d) In x-y plane ($\theta = 90^\circ$) at 5.5 GHz.

The big disagreement occurs sometimes between simulation and measurement is mainly due to the box in the experimental realization made of separate pieces of ABS plastic (Figure 4.29(b)) and the fragility of the contact between the antennas and the connectors that cause inaccuracy. Apart from this, the errors can be caused by the coupling effects between two antennas such as the influence of the ground plane of one antenna on another that is neglected in the simulation.

Although the antenna 1 is bent and the antennas are located in the box, their total efficiency of the antennas is acceptable. The simulated values of the antenna 2 are 80% at 2.45 GHz and 65% at 5.5 GHz while those of the antenna 1 are smaller due to bending, being 76% and 64% at these two frequencies, respectively.

B. The box with the dimensions of 310 mm × 207 mm × 45 mm

Now, let us consider a system of two same antennas placed in a real communications box with the dimensions of 310 mm × 207 mm × 45 mm shown in Figure 4.34 and its CST simulation structure is shown in Figure 4.34.

For the distance of 60 mm from the right edge of the first antenna to the edge of the box and the distance of 40 mm from the edge of the box to the upper edge of the second antenna, its S-parameters are depicted in Figure 4.35 and Figure 4.36 where one can see that the behavior of the reflection coefficients of two antennas in the system are like for single antennas without and with bending in ABS box. Moreover, there is good isolation between two antennas (Figure 4.36), over 20 dB. The reason for the disagreement between simulation and measurement $|S_{21}|$, dB curves can be the capacitive coupling between two ground planes of the antennas that reaches the minimum at around 2.5 GHz that is not taken into account in the simulation.

Figure 4.37 and Figure 4.38 show good fit between simulated and measured realized gain radiation patterns of the antennas in the system. A little difference between them occurs sometimes can be explained by the coupling effects between two antennas such as the influence of one antenna on another that is neglected in the simulation.

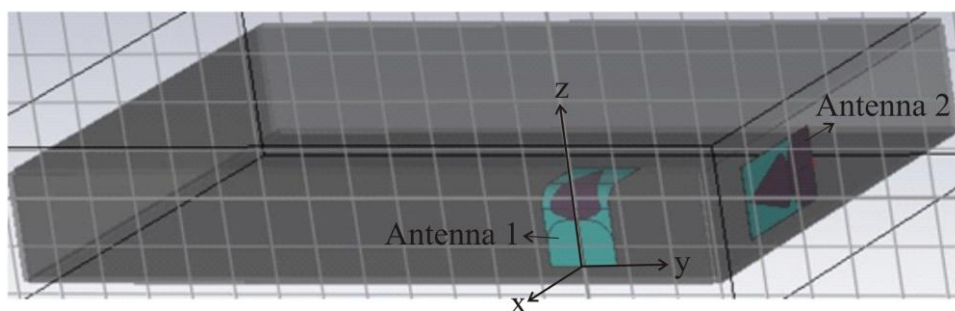
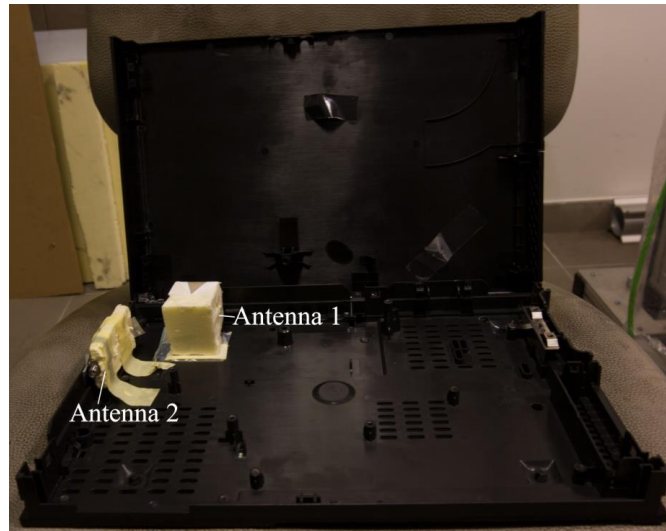


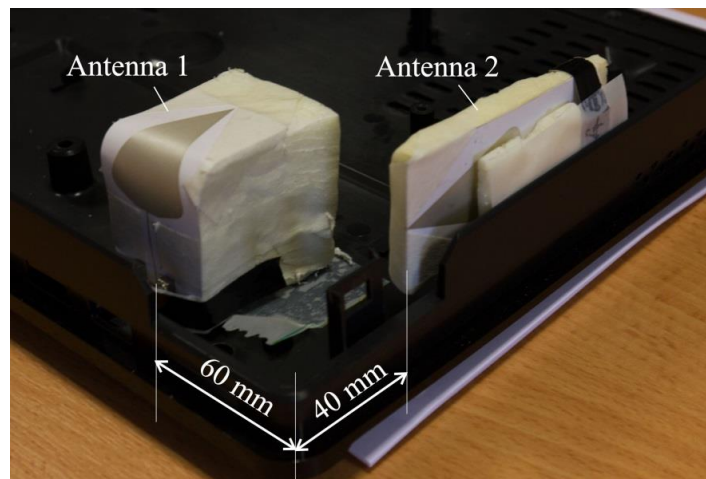
Figure 4.33. CST simulation structure of the system in a 310 mm × 207 mm × 45 mm ABS box.



(a)



(b)



(c)

Figure 4.34. System of two antennas in a real ABS box with the dimensions of $310 \text{ mm} \times 207 \text{ mm} \times 45 \text{ mm}$: (a) The ABS box in the experiment; (b) The open ABS box with 2 antennas; (c) The location of the antennas in the box.

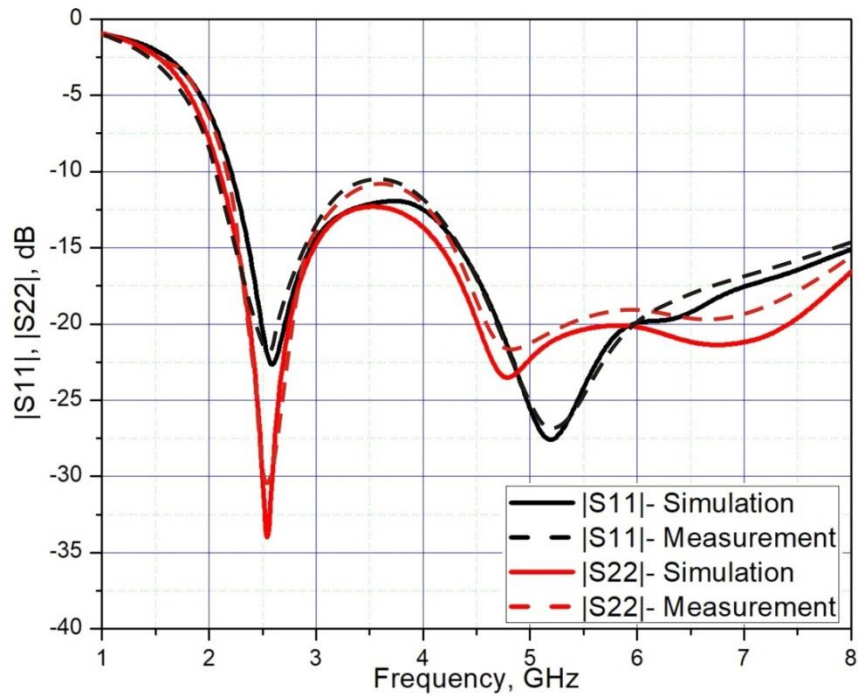


Figure 4.35. Return loss of the antenna system.

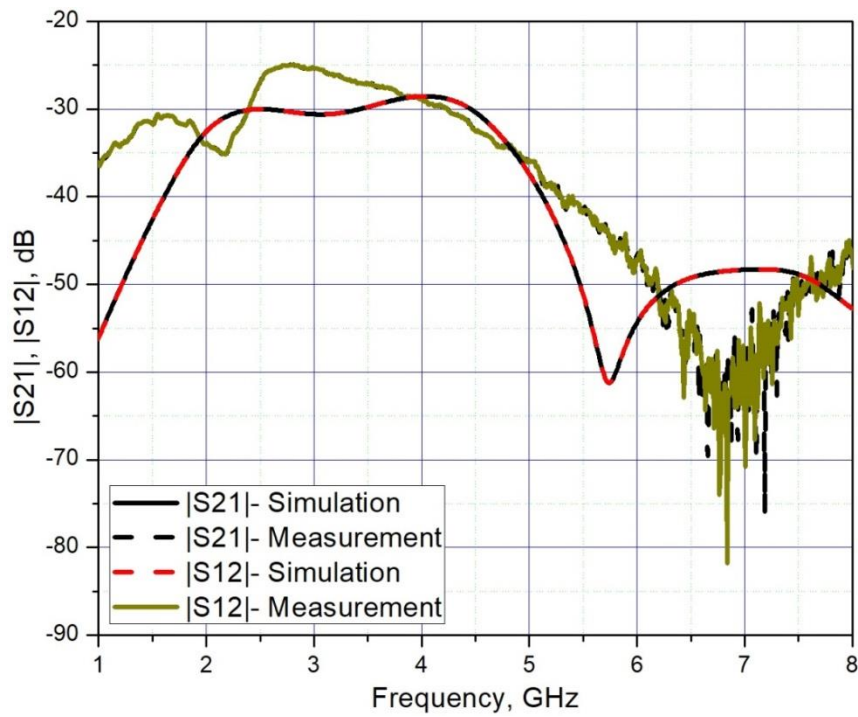


Figure 4.36. Isolation between the antennas.

The simulated total efficiency of the antenna 1 is 77% at 2.45 GHz and 65% at 5.5 GHz, the one of the antenna 2 is 80% at 2.45 GHz and 64% at 5.5 GHz. The Envelope Correlation Coefficient (ECC) calculated by the formula (1.3) is much less than 0.05 at both those frequencies.

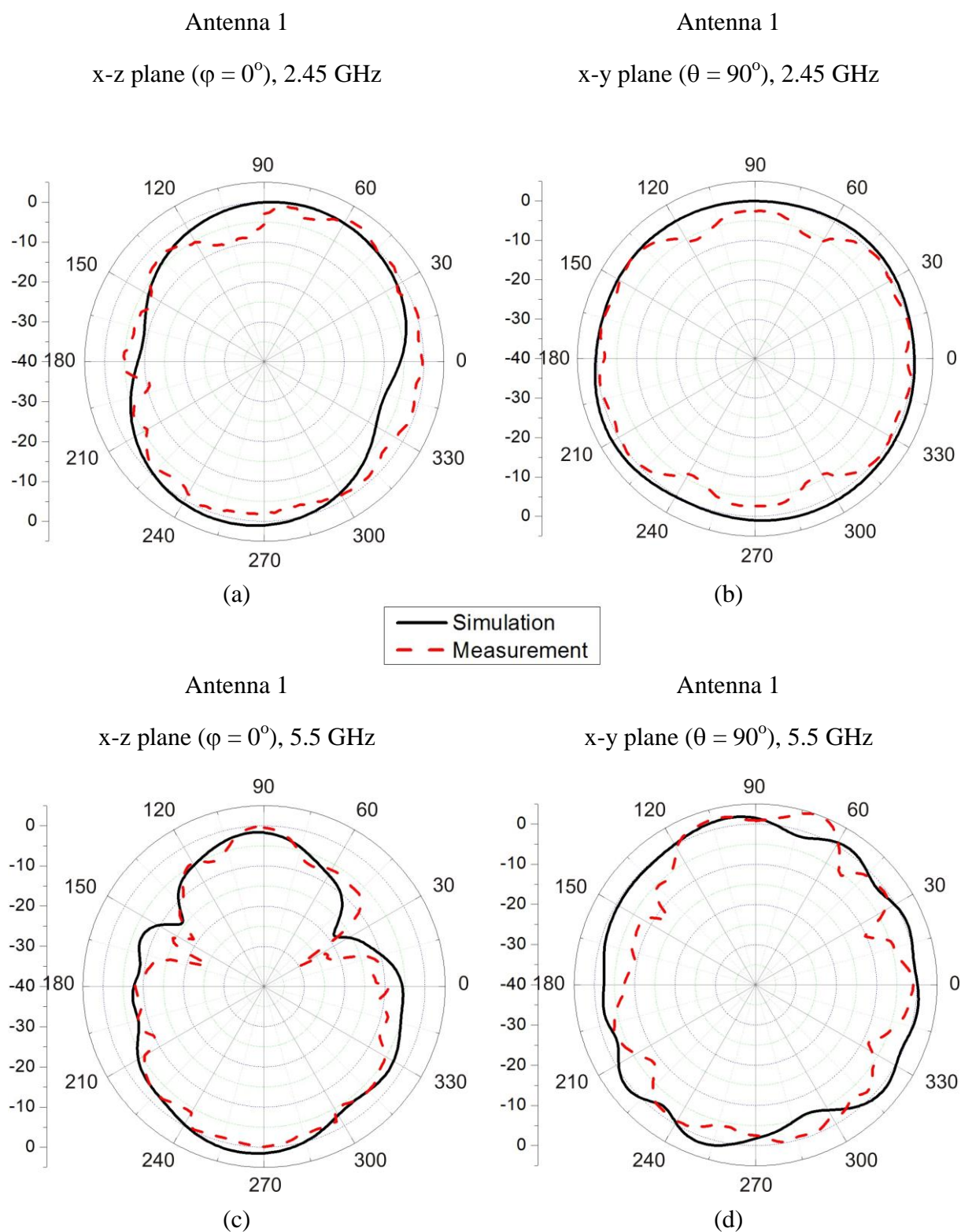


Figure 4.37. Simulated and measured realized gain radiation patterns of Antenna 1: (a) In x-z plane ($\varphi = 0^\circ$) at 2.45 GHz; (b) In x-y plane ($\theta = 90^\circ$) at 2.45 GHz; (c) In x-z plane ($\varphi = 0^\circ$) at 5.5 GHz; (d) In x-y plane ($\theta = 90^\circ$) at 5.5 GHz.

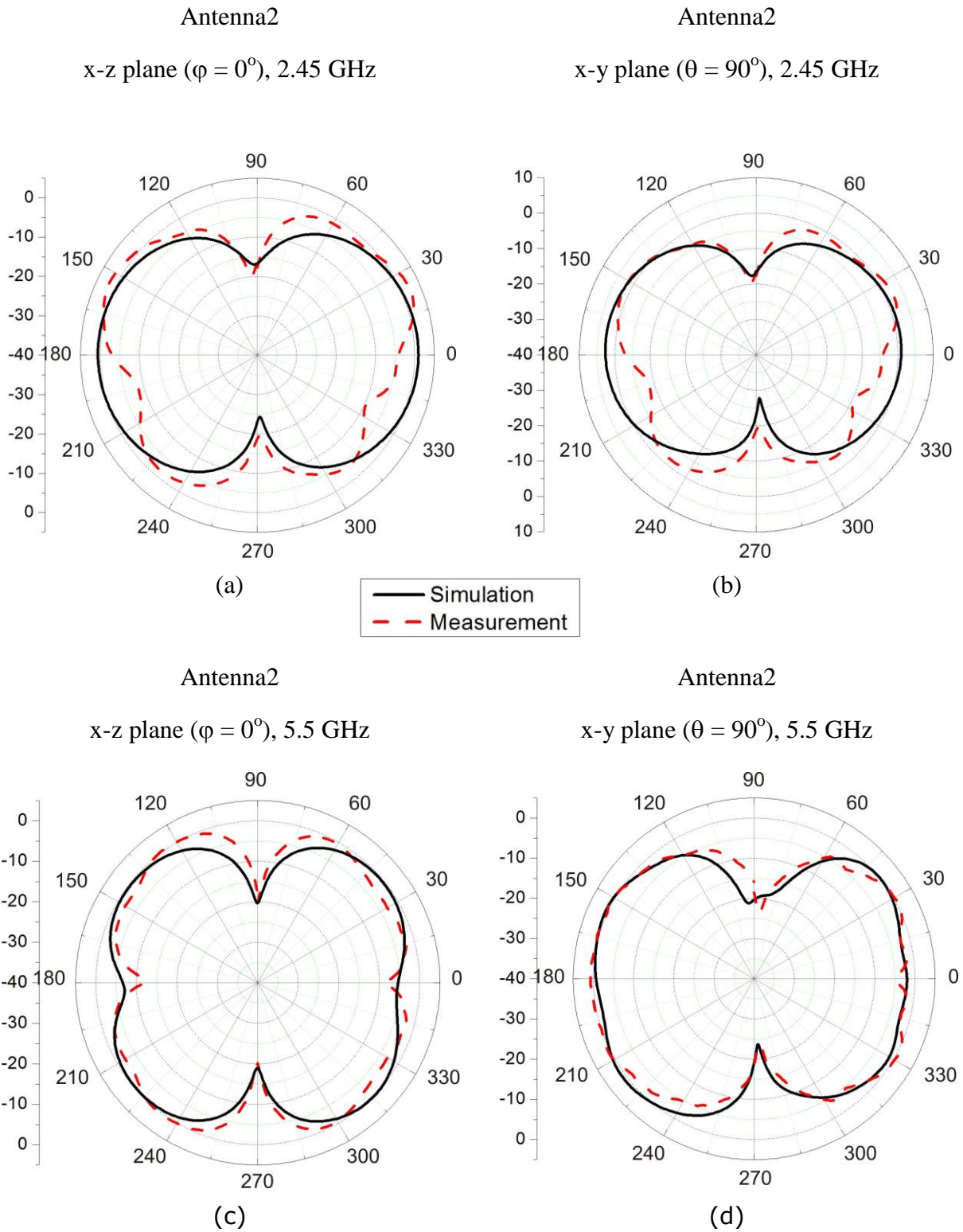


Figure 4.38. Simulated and measured realized gain radiation patterns of Antenna 1: (a) In x-z plane ($\varphi = 0^\circ$) at 2.45 GHz; (b) In x-y plane ($\theta = 90^\circ$) at 2.45 GHz; (c) In x-z plane ($\varphi = 0^\circ$) at 5.5 GHz; (d) In x-y plane ($\theta = 90^\circ$) at 5.5 GHz.

4.3.3. System of two 90-degree bent antennas placed in ABS box

The experiment is presented in this section with the same antennas in that box, but both of them are bent (Figure 4.39). Thus, the return loss of both antennas (black and red lines) is nearly the same. For the distance of 15 mm between two antennas the isolation (blue line in Figure 4.40) is acceptable, above 20 dB.

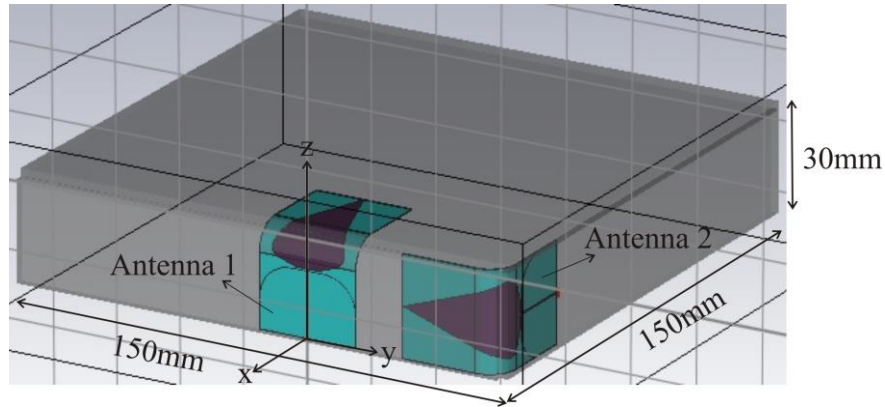


Figure 4.39. CST simulation structure of the system of two antennas in the box.

However, because of the fragility of the contacts for the paper-based antennas, the measurement has not been conducted.

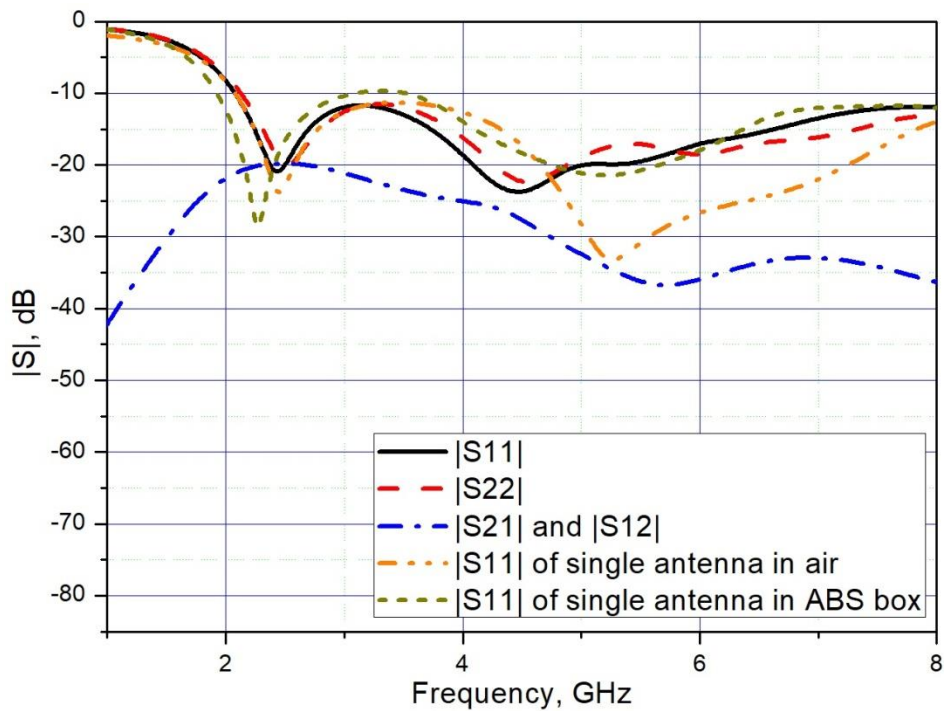
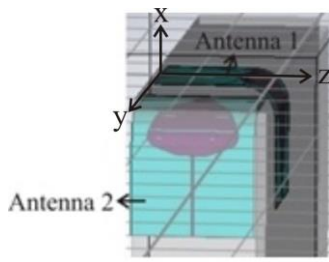
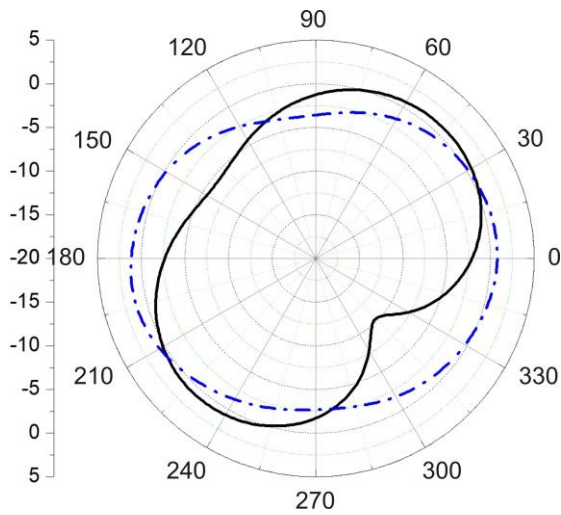
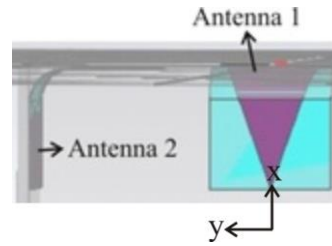


Figure 4.40. Simulated S- parameters of the system of two antennas, where both of them are bent under 90 degrees.

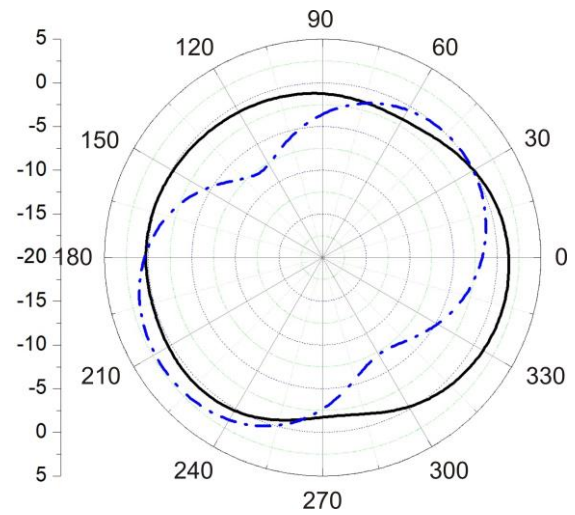
In x-z plane ($\varphi = 0^\circ$)



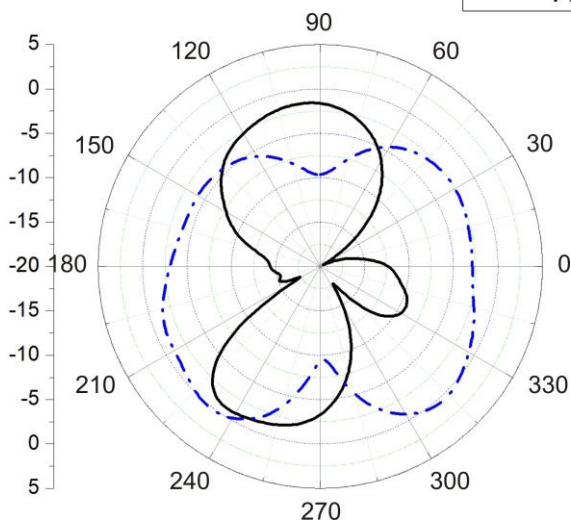
In x-y plane ($\theta = 90^\circ$)



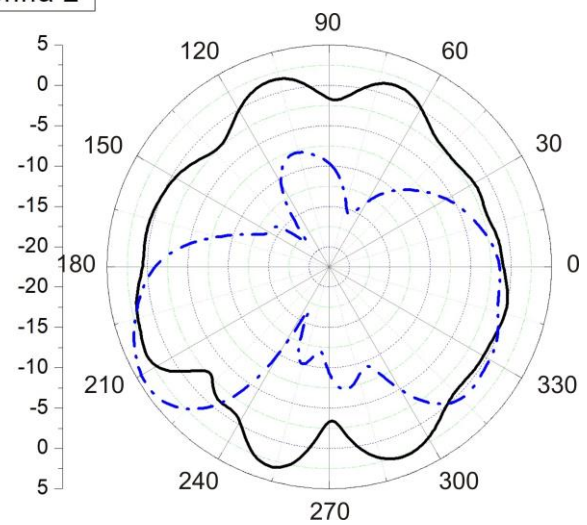
(a)



(b)



(c)



(d)

Figure 4.41. Simulated realized gain radiation patterns of the antennas in the system of two bent antennas in a 150 mm \times 150 mm \times 30 mm ABS plastic box: (a) In x-z plane ($\varphi = 0^\circ$) at 2.45 GHz; (b) In x-y plane ($\theta = 90^\circ$) at 2.45 GHz; (c) In x-z plane ($\varphi = 0^\circ$) at 5.5 GHz; (d) In x-y plane ($\theta = 90^\circ$) at 5.5 GHz.

Conclusions for Chapter 4

This chapter demonstrated an analysis of the practical cases of three-dimensional antenna systems when the antennas are located in a package (a rectangular ABS plastic box in our case). In this process, the wideband "Mushroom-shaped with two arms" antenna was chosen to study bending effects in the air as it has the largest size among the proposed antennas. However, this antenna is too big to be located in the ABS boxes provided by our industrial partner. Thus, another wideband antenna, the "Sapin" was chosen to study the systems of antennas orthogonally located in an ABS box.

1. First of all, it was noted, that the ABS material with $\epsilon_r = 2.7$, $\tan\delta = 0.005$ shifted a little the resonant frequencies of the antennas. For the "Sapin" antenna located at 3 mm from the ABS wall, this shift is about 50 MHz for the resonance of 2.45 GHz and 100 MHz for the resonance of 5.5 GHz. However, as the antennas are chosen to be wideband, that frequency shift does not affect too much the bandwidth of the antennas.
2. If the box has sufficient dimensions, two antennas can be located in it without deformation to create good space diversity with envelope correlation coefficient (ECC) much less than 0.05 if the distance from each antenna to the ABS wall is at least 2 mm and the distance between two antennas is about 16 mm.
3. When the space is very limited, at least one of the antennas must be bent. The study showed that bending does not much affect the matching property of the antenna. However, the radiation patterns "rotate" in the E-plane by an angle depending on bending angle and bending position of the antenna. For instance, if the antenna is bent in E-plane at the position of its middle under 90 degrees and 120 degrees, the radiation patterns "rotate" in the E-plane by 45 degrees and 30 degrees, respectively, compared to the radiation patterns without bending.
4. The study of MIMO systems of two wideband antennas placed orthogonally in two different ABS box provided by our industrial partner where one of the antennas is bent due to restricted height of the box showed, that:
 - For the distance of at least 2 mm up to 6 mm from each antenna to the ABS wall Resonant frequencies of each antenna were shifted by 50 – 150 MHz due to the ABS material ($\epsilon_r = 2.7$, $\tan\delta = 0.005$).
 - The matching property of the antenna is not much affected by bending.

- For the distance of about 16 mm between the antennas in the ABS box, the isolation of the system is over 20 dB and ECC is much less than 0.05 over all frequency band from 2 GHz to over 8 GHz

References for Chapter 4

- [1] H. F. Abutarboush, M. F. Farooqui, A. Shamim "Inkjet-Printed Wideband Antenna on Resin-Coated Paper Substrate for Curved Wireless Devices", *IEEE Antennas and Wireless Propagation Letters*, Vol. 15, pp. 20-23, 2016.
- [2] G. Shaker, S. S.-Naeini, N. Sangary, M. M. Tentzeris, "Inkjet Printing of Ultrawideband (UWB) Antennas on Paper-Based Substrates", *IEEE Antennas and Wireless Propagation Letters*, Vol. 10, pp. 111-113, 2011.
- [3] B. S. Cook, A. Shamim, "Inkjet Printing of Novel Wideband and High Gain Antennas on Low-Cost Paper Substrate", *IEEE Trans. On Antennas and Propagation*, Vol. 60, pp. 4148-4155, N. 9, 2012.
- [4] B. S. Cook, A. Shamim, "Utilizing Wideband AMC Structures for High-Gain Inkjet-Printed Antennas on Lossy Paper Substrate", *IEEE Antennas and Wireless Propagation Letters*, Vol. 12, pp. 76-79, 2013.
- [5] D.E.Anagnostou, A.A.Gheethan, A.K.Amert,K.W.White, "A Direct-Write Printed Antenna on Paper-Based Organic Substrate for Flexible Displays and WLAN Applications", *Journal of Display Technology*, Vol. 6, pp. 558-564, No.11, 2010.
- [6] S. Moscato, R. Moro, M. Pasian, M. Bozzi, L. Perregrini, "Innovative manufacturing approach for paper-based substrate integrated waveguide components and antennas", *IET Microwaves, Antennas & Propagation*, 2016, Vol. 10, Iss. 3, pp. 256–263.
- [7] A. R. Guraliuc, N. Chahat, C. Leduc, M. Zhadobov, R. Sauleau, "End-Fire Antenna for BAN at 60 GHz: Impact of Bending, On-Body Performances, and Study of an On to Off-Body Scenario", *Electronics*, pp. 221-233, No. 3, 2014.
- [8] S. Jun, B. Sanz-Izquierdo and M. Summerfield "UWB Antenna on 3D Printed Flexible Substrate and Foot Phantom", *Loughborough Antennas & Propagation Conference (LAPC)*, 2015.
- [9] M.-C. Tang, T. Shi, and Richard W. Ziolkowski «Flexible Efficient Quasi-Yagi Printed Uniplanar Antenna», *IEEE Trans. on Antennas and Propagation*, Vol. 63, pp. 5343-5350, No. 12, 2015.

- [10] D. Betancourt, K. Haase, A. Hübler, F. Ellinger “Bending and Folding Effect Study of Flexible Fully Printed and Late-Stage Codified Octagonal Chipless RFID Tags”, IEEE Trans. on Antennas and Propagation, Vol. 64, pp. 2815-2823, No. 7, 2016.

Conclusions and Perspectives

Conclusions

Recently, printed flexible electronics has developed intensively that put a milestone in electronics technology. In order to design flexible electronic circuits, it is critical to decide which substrate is suitable among numerous ones, where paper has been found as a solution for ultra-low cost flexible electronics substrate that enables direct write with good quality facilitates mass fabrication process.

This work focused on the antenna design on paper substrates in regards to the integrated electronic and the efficiency in a realistic environment. The main contributions of this work are conformable antennas design to adapt to various set-top boxes.

The main works done in this thesis are:

1. Overview of flexible substrates, from that paper substrate has been chosen according to the requirements for a substrate material that is flexible, low cost, with good RF properties, recycling ability, and especially ability to make 3D structures.
2. Overview of printing techniques for flexible substrates, screen printing technology has been chosen for its rapidity, low cost and adaptability to the future mass production.
3. Study of state-of-the-art of 3D and MIMO antennas as well as the techniques for reduction of mutual coupling between antennas in a MIMO antenna system.
4. Characterization of different flexible materials such as PET and different type of paper, from that the results for E4D paper would be used for the antenna design.
5. Design and test of single-band antennas on PET and paper substrate with CPW as well as microstrip feeding. A paper-based SIW cavity-back antenna has also been designed to show, that this kind of antenna is not suitable for our requirement because of its large dimensions and the fact that the bendability property of paper cannot be used.
6. Design and test of wide-band and multi-band antennas on paper.
7. Analysis of the practical cases of three-dimensional antenna systems when the antennas are located in a package (a rectangular ABS plastic box in our case provided by our industrial partner).

As a result, the main achievements of this thesis are:

1. Among different types of paper substrates, we chose E4D as it is compatible to our partner's fabrication process with screen printing technology and the future mass production. This paper was characterized by the method of perturbation on 50 samples with the results: $\epsilon_r = 3.184$, $\tan\delta = 0.092$ at 2.5 GHz with the dispersions of 0.25% for ϵ_r and 0.26% for $\tan\delta$.
2. An inverted-F antenna (IFA) was designed on 0.21-mm thick E4D paper with the resonant frequency of 2.3 GHz. The total efficiency of the antenna is about 70%, the radiation patterns of this antenna at the resonant are very similar to omni-directional that makes this kind of antennas attractive. Another IFA was designed on the same paper with two WLAN resonant frequencies of 2.45 GHz and 5.5 GHz, that showed one of the advantages of the modified IFA – the easiness of adding resonant frequencies. This type of antenna has stable electrical properties. However, it causes some technological difficulties because of the existence of via holes.
3. The Substrate-Integrated Waveguide (SIW) cavity-backed antenna was designed at 5.2 GHz on three layers of 0.387-mm thick E4D paper glued together and a slot radiation element. The difference from the other authors' previous works is the existence of an air cavity inside the antenna, which could easily be realized in the process of gluing the paper layers. The total efficiency of the antenna is about 65%, much higher than 25% in the case without air cavity, so that the realized gain reached 5.17 dB despite high paper dielectric losses. This kind of antennas presented in this work could be a good reference for those who need to design paper-based high gain antennas, but it does not meet our need for transforming into three-dimensional structure(s), its performance changes a lot under bending or deformation because the back cavity changes completely its form.
4. While most of existing paper-based wideband antennas use CPW-feeding method that causes fabrication difficulties, with double-side screen printing possibility, we proposed microstrip-fed wideband and multi-band antenna structures on paper substrate presented in the following table:

	Dimensions	Matching bandwidth	Total efficiency	Realized gain	Applications
"Sapin"	28 mm × 59 mm × 0.104 mm	2 GHz – over 10 GHz	78% at 2.45 GHz, 56.8% at 5.5 GHz	1.27 dBi at 2.45 GHz, 0.94 dB at 5.5 GHz	Wideband, multi-standard set-top boxes
"Sapin"	28 mm × 57 mm × 0.21 mm	2 GHz – over 10 GHz	80% at 2.45 GHz, 64% at 5.5 GHz	1.97 dBi at 2.45 GHz, 1.3 dB at 5.5 GHz	
"Modified Sapin"	24 mm × 50 mm × 0.104 mm	2.2 GHz – over 10 GHz	78% at 2.45 GHz, 68% at 5.5 GHz	1.1dBi at 2.45 GHz, 1.63 dB at 5.5 GHz	
"Robe"	28 mm × 49 mm × 0.104 mm	2.2 GHz – 3.2 GHz, 4.3 GHz – over 10 GHz	78% at 2.45 GHz, 60% at 5.5 GHz	1.21dBi at 2.45 GHz, 1.66 dB at 5.5 GHz	
"Mushroom-shaped with two arms"	50 mm × 65 mm × 0.104 mm	1.7 GHz – over 10 GHz	69% at 2.45 GHz, 51% at 5.5 GHz	1.67 dBi at 2.45 GHz, 1.1 dB at 5.5 GHz	
"Hello 1"	28 mm × 42 mm × 0.21 mm	2.3 GHz – 2.7 GHz; 4.2 GHz – 6.6 GHz	67% at 2.45 GHz, 65% at 5.5 GHz	0.62dBi at 2.45 GHz, 1.53 dB at 5.5 GHz	Dual-band WLAN
"Hello 2"	28 mm × 42 mm × 0.21 mm	2.3 GHz – 2.7 GHz; 4.3 GHz – over 10 GHz	69% at 2.45 GHz, 67% at 5.5 GHz	0.71dBi at 2.45 GHz, 1.51 dB at 5.5 GHz	
Multi-band antenna 1	24 mm × 30 mm × 0.21 mm	Resonant frequencies: 2.2 GHz; 2.45 GHz; 4 GHz; 5.5 GHz	22%; 40%; 75% ; 65%, respectively	-3.9dBi; -1.82 dBi; 1.38 dBi; 2.14 dBi, respectively	Multi-band, multi-standard set-top boxes
Multi-band antenna 2	24 mm × 30 mm × 0.21 mm	Resonant frequencies: 1.8 GHz; 2.45 GHz; 4 GHz; 5 GHz	17%; 58%; 73%; 60%, respectively	-5.55dBi; -0.365 dBi; 1.42 dBi; 1.96 dBi, respectively	

It can be seen, that the compact multiband antennas are suitable for using at higher frequencies over 4 GHz rather than at lower frequencies. The comparison of the performance of two antennas, “Sapin” and “Hello 2, with two paper-based wide-band ones proposed by other authors stated in the following table shows the excellent characteristics of our antennas.

	Dimensions	Frequencies	Efficiency	Gain
[58] G. Shaker et al, 2017	58mm × 58 mm	1,7GHz – 12.5GHz	Radiation efficiency 80%	-
[64] H. F. Abutarboush et al., 2012	35mm × 40 mm	1,71GHz - 3GHz ; 4,51GHz - 5,5GHz	45% – 58%	-2 – 1,1dBi at 1,71GHz - 3GHz; -1 – 2dBi at 4,51GHz - 5,5GHz
«Sapin» on 210 μm E4D paper	28mm × 57 mm	2,1GHz – over 10GHz	80% at 2,45GHz; 64% at 5,5GHz	1,87dBi at 2,45GHz; 1,24dBi at 5,5GHz
«Hello-2» on 210 μm E4D paper	28mm × 42 mm	2,2GHz – 3GHz; 4,5GHz – 6,8GHz	69% at 2,45GHz; 64% at 5,5GHz	0,71dBi at 2,45GHz; 1,51dBi at 5,5GHz

The main advantage of these proposed wideband and multiband antennas compared to the existing paper-based wideband antennas is the simplicity of the designs without too small details such as too narrow slots in CPW-feed lines. These antennas were designed and

fabricated based on double-side screen printing technology and can be developed to future mass production.

5. The study of the antennas in an ABS package showed that the ABS material with $\epsilon_r = 2.7$, $\tan\delta = 0.005$ shifted the resonant frequencies of the antennas. For the “Sapin” antenna located at 3 mm from the ABS wall, this shift is about 50 MHz for the resonance of 2.45 GHz and 100 MHz for the resonance of 5.5 GHz. However, as the antennas are chosen to be wideband, that frequency shift does not affect too much the bandwidth of the antennas.
6. If the box has sufficient dimensions, two antennas can be located in it without deformation to create good space diversity with envelope correlation coefficient (ECC) much less than 0.05 if the distance from each antenna to the ABS wall is at least 2 mm and the distance between two antennas is about 16 mm.
7. When the space is very limited, at least one of the antennas must be bent. The study showed that bending does not much affect the matching property of the antenna. However, the radiation patterns “rotate” in the E-plane by an angle depending on bending angle and bending position of the antenna. For instance, if the antenna is bent in E-plane at the position of its middle under 90 degrees and 120 degrees, the radiation patterns “rotate” in the E-plane by 45 degrees and 30 degrees, respectively, compared to the radiation patterns without bending.
8. The study of MIMO systems of two wideband antennas placed orthogonally in two different ABS box provided by our industrial partner where one of the antennas is bent due to restricted height of the box showed, that:
 - For the distance of at least 2 mm up to 6 mm from each antenna to the ABS wall Resonant frequencies of each antenna were shifted by 50 – 150 MHz due to the ABS material ($\epsilon_r = 2.7$, $\tan\delta = 0.005$).
 - The matching property of the antenna is not much affected by bending.
 - For the distance of about 16 mm between the antennas in the ABS box, the isolation of the system is over 20 dB and ECC is much less than 0.05 over all frequency band from 2 GHz to over 8 GHz.

Perspectives

In the continuation of this work, many perspectives can be considered.

1. For the antenna design, the miniaturization of the proposed antennas is necessary without losing their wideband performance for various applications.
2. In collaboration with other partners specialized in material studies, different types of paper can also be tested for antenna design, from that the best paper should be chosen to give the best antenna performance.
3. Besides, the further research can also be the optimization and design of three-dimensional antennas to place in a package with the best performance at frequency bands of interest if the form of the package to put the antenna in/on is known. On the other hand, if we are not sure about the package in advance, the analysis of deformation effects is always useful to predict the antenna performance and prevent its undesirable behavior.

5. Appendix 1 – Characterization of electromagnetic properties of substrate materials

In order to use a dielectric material as a substrate for designing a planar electronic circuit, its properties such as permittivity and loss tangent must be characterized. The authors of [1] have enumerated precisely the methods for characterization of dielectric properties that can be used to characterize solid as well as liquid materials.

According to their operating principles, the methods can be classified into two groups, methods using waveguides or transmission line (non - resonant) [1-3] and methods using cavities (resonant). One can choose a method based on the frequency band, the accuracy, the availability of the measuring equipment, the need for measurement "in situ", the type and shape and size of the sample, etc. Each method has its advantages and limitations. This sub-chapter provides a synthesis of measurement techniques used to characterize the complex permittivity of thin sheets of dielectrics such as different types of paper.

This appendix presents the methods of characterization of electromagnetic properties of substrate materials, including non-resonant methods using waveguides as well as planar transmission lines and resonant methods using cavities or dielectric resonators.

5.1. Non-resonance methods using waveguides or transmission lines

This section includes the description of non-resonant methods using waveguides, coaxial cables or planar transmission lines. These methods normally have a wide frequency band.

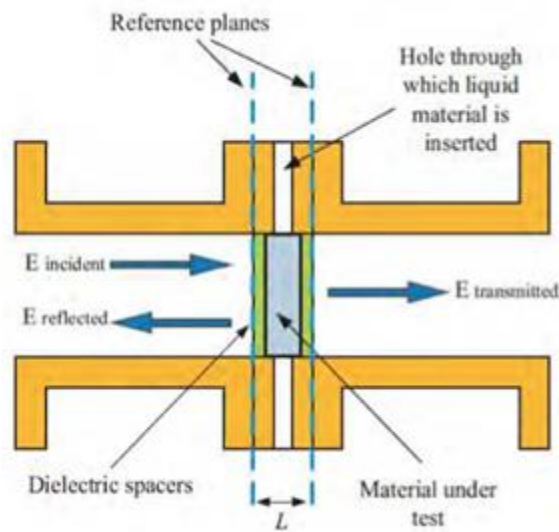
5.1.1. The techniques using waveguides

Figure 5.1 shows the experimental scheme for the measurement of a liquid material, where a section of a transmission line of certain length is filled with the sample to be measured. The variation of the propagation constant γ and the characteristic impedance Z_0 leads to partial reflections of the wave at the interfaces. The propagation constant $\beta + j\alpha = \gamma$ is related to the complex permittivity of a dielectric material as follows:

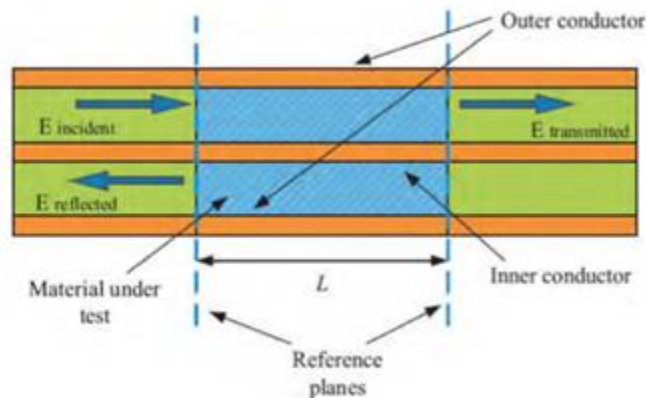
$$\gamma = j\sqrt{\frac{\omega^2 \mu_r \epsilon_r}{c^2} - \left(\frac{2\pi}{\lambda_c}\right)^2} \quad (5.1)$$

where ω is the angular frequency, μ_r is the permeability of the material which equals 1, c is the speed of light and λ_c is the cutoff wavelength of the transmission line [1],

$$\text{thus } \epsilon_r' = \left(\frac{c}{\omega}\right)^2 \left[\left(\frac{2\pi}{\lambda_c}\right)^2 - \alpha^2 + \beta^2 \right], \quad \epsilon_r'' = \frac{c^2 2\alpha\beta}{\omega^2} \quad (5.2)$$



(a)



(b)

Figure 5.1. (a) The sample in a waveguide, (b) The sample in a coaxial cable [1].

At frequencies below 2.4 GHz, coaxial lines are preferable to waveguides because of the large size of the waveguides and also the size of the sample needed.

To avoid higher TE and TM modes propagating in the line (without taking into account transitions and connectors), the 3.5 mm coaxial cables are used for the frequency band 0 – 34.5 GHz, 7 mm for 0 – 18.2 GHz and 14 mm for 0 – 8.6 GHz.

To use this technique for a solid sheet of dielectric material, B. K. Chung in [2] used this method to characterize a sheet of 0.5 mm Teflon located in a rectangular waveguide $a \times b$ as in Figure 5.2.

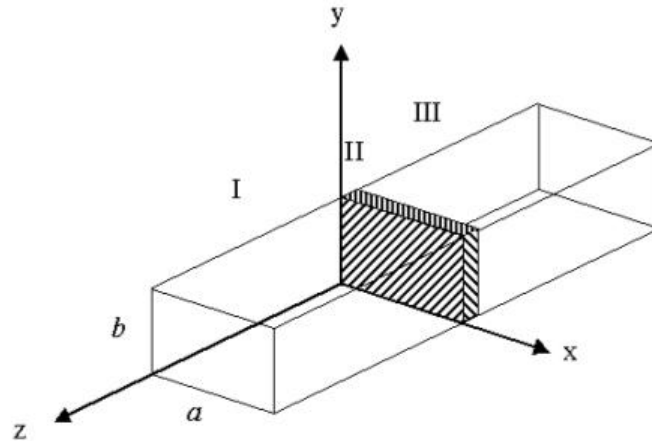


Figure 5.2. The method using a rectangular waveguide to characterize a thin sheet of a dielectric material.

The measurement of the transmission constant T , assuming that the thickness of the sample is small, allows obtaining the following expression:

$$T = \frac{1}{\left\{ 1 + \frac{(kd)^2}{8} \left(\frac{\lambda}{a} \right)^2 + j \frac{(kd)^2}{2(kd)} \left[1 - \frac{1}{2} \left(\frac{\lambda}{a} \right)^2 \right] \right\} - \varepsilon \left[\frac{(kd)^2}{2} - j \frac{(kd)^2}{2(kd)} \right]} \quad (5.3)$$

where d is the thickness of the material to be characterized, k is the phase constant

$$k = \frac{2\pi}{\lambda}.$$

The relative permittivity is

$$\varepsilon_r = \frac{\left\{ 1 + \frac{(kd)^2}{8} \left(\frac{\lambda}{a} \right)^2 + j \frac{(kd)^2}{2(kd)} \left[1 - \frac{1}{2} \left(\frac{\lambda}{a} \right)^2 \right] \right\} - \frac{1}{T}}{\left[\frac{(kd)^2}{2} - j \frac{(kd)^2}{2(kd)} \right]} \quad (5.4)$$

The error of ϵ' is less than 0.1%, and the error of ϵ'' is less than 0.2% for the plate thickness of the material less than 1% of $\lambda / |\epsilon|$. The limit of this method is the complexity of sample positioning and the presence of the air gap which can lead to significant errors. Hasar B. C., the author of two other publications [3, 4] also presented the use of this technique in the same structure of a rectangular waveguide but using the polynomial approximation to extract the permittivity of the sample. The method is tested for PTEE of thickness 2mm and 3mm at the frequency band 9.7 – 11.7 GHz. At 10 GHz, the error is 1.88% on ϵ_r' for PTEE of all two thicknesses 2mm and 3mm [3]. However, the error on ϵ_r'' is quite large, 55% for PTEE of thickness 2mm and 27.6% for PTEE of 3mm thickness. In another paper by the same author [4], this method was used for the liquid sample like ethyl alcohol and water and the error received is 0.299% – 24.298% on ϵ' and 0.543% – 18.587% on $\tan \delta$ for the thickness of the samples from 10 mm up to 4 mm.

In order to avoid inaccuracy of the position of the sample in the system, especially when characterizing thin materials, in [5], the authors used the method of reflection, a modification of the non-resonant waveguide technique, where the dielectric plate is placed directly on a metallic plate (Figure 5.3).

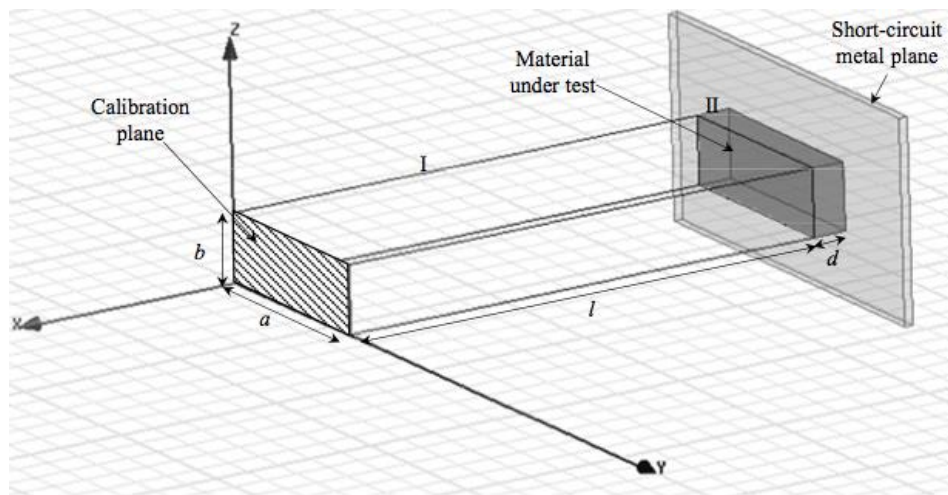


Figure 5.3. The reflection method to characterize thin materials.

The reflection coefficient at the reference plane is represented by the following expression:

$$S_{11} = R^2 \frac{\tanh(\gamma d) - (\gamma/\gamma_0)}{\tanh(\gamma d) + (\gamma/\gamma_0)} \quad (5.5)$$

where γ is propagation constant, $R = e^{-\gamma_0 d}$, $\gamma_0 = c/f$.

For the thin samples, γd is very small and we have the approximation:

$\tanh(\gamma d) \cong (\gamma d) - \frac{1}{3}(\gamma d)^3 + \frac{2}{15}(\gamma d)^5 - \frac{17}{315}(\gamma d)^7$ in order to put into the formula (5.7), we obtain an equation where $\gamma = \alpha + j\beta$ is unknown.

Then α contains information about permittivity, and β contains the information about the dielectric loss.

The method has been tested for Teflon, wood and distilled water of different thickness (5 mm, 2 mm and 1 mm). It has been found that the order of approximation and the thickness of the samples affect the accuracy of results, and recommended to use the 7th order and thinner thickness. The algorithm of this method is simple, however inaccuracy due to air gap between the material and the metallic plate is not completely avoided.

5.1.2. The techniques using planar transmission lines

The paper [6] is a good example for the representation of these techniques. In the first method proposed by the authors, the material to be characterized serves as a substrate. Two 50 ohm microstrip lines of different lengths were etched and the difference in electrical length Δl_e between the two lines is measured (Figure 5.4).

The effective permittivity was then extracted from the formula

$$\Delta l_e = \sqrt{\epsilon_{eff}} \cdot \Delta l_p$$

and the precision on the dielectric constant is evaluated by the formula:

$$\frac{\delta \epsilon_r}{\epsilon_r} \approx \frac{\delta \epsilon_{eff}}{\epsilon_{eff}} = 2 \left(\frac{\delta \Delta l_e}{\Delta l_e} + \frac{\delta \Delta l_p}{\Delta l_p} \right),$$

where Δl_p and Δl_e are the differences of physical and electrical lengths of two lines.

The result is more accurate when the phase difference of $\Delta \phi$ is measured across the two lines at a set of frequencies, then extracted at different frequencies. The disadvantage of this method has been analyzed and for example the inaccuracy of the position of the connector, but the determination of loss tangent has not been mentioned in [6]. In [7], an expression for the loss tangent of the substrate has been proposed:

$$\tan \delta = \frac{\alpha_d \lambda_0 \sqrt{\epsilon_{eff}} (\epsilon_r - 1)}{\pi \epsilon_r (\epsilon_{eff} - 1)} \quad (5.6)$$

where λ_0 is the free-space wavelength, ϵ_e is the effective permittivity of the line and ϵ_r is the relative permittivity of the material to be characterized. The use of two microstrip lines of different lengths (two-line method), the attenuation constant α_d has been measured in relation to the frequency, from which the average value of $\tan\delta = 0.077$ is obtained over a frequency band from 1.2 GHz to 0.2 GHz.

However, this assumes that the conduction loss constant due to the conducting material of the line is negligible compared to the dielectric loss constant, and the radiation losses are not taken into account. To avoid errors, the authors proposed the combination of simulation of losses on the conductor and radiation that is subtracted from the measured total losses. This point must be verified with standard substrates for which the tangent of losses is precisely known.

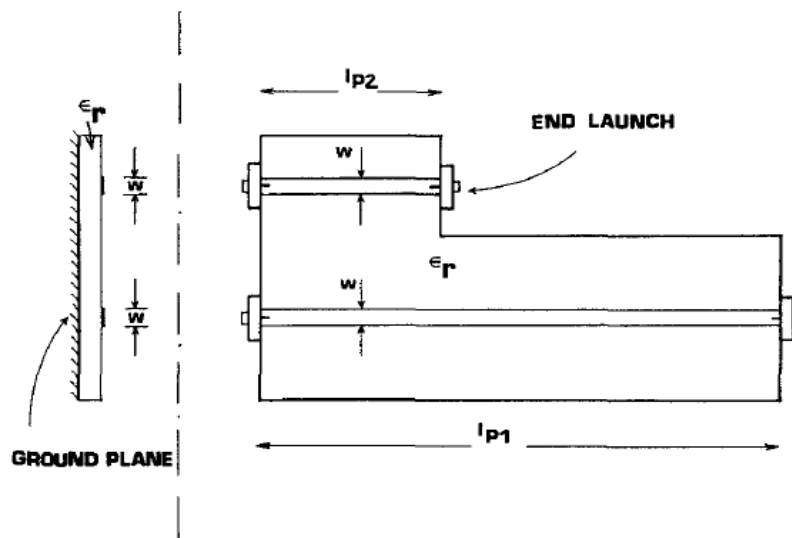


Figure 5.4. The method of two transmission lines.

H. Riedell et al. in the paper [8] also used a transmission line engraved on the substrate to be tested, but he then proposed a procedure for calculating the complex permittivity by transforming the measured S parameters of the transmission line, in order to obtain the constant of propagation of the transmission line.

$$\gamma = \frac{1}{L} \left(\ln \sqrt{A + A^2 - 1} \right), \quad A = \frac{(1 + S_{11})(1 + S_{22}) + S_{12}^2}{2S_{21}}, \quad (5.7)$$

Then ϵ and $\tan\delta$ are calculated as function of γ :

$$\epsilon = \epsilon_0 \epsilon_r = \epsilon_0 \left(\epsilon_r' - j \epsilon_r'' \right) = - \frac{\gamma^2}{\omega^2 \mu_0}, \quad \tan \delta = \frac{\epsilon_r''}{\epsilon_r'}, \quad (5.8)$$

The authors tested for FR4 materials at the frequency band 200 MHz – 2 GHz and obtained the error of about 10% on ϵ_r and 25% on $\tan \delta$ at 800 MHz compared to a resonance method. The method worked well with a FR4 type epoxy glass substrate and the accuracy obtained is affected by the numerical accuracy of the measured data. In order to improve accuracy, the authors of [9] proposed the transmission line circuit model, including the connectors and taking into account its asymmetry and the effect of roughness on the conductor's surface. to obtain a procedure of extraction of ϵ and $\tan\delta$ and shown that the deflection of the loss tangent is decreased from 36% to 5% by testing 9 FR4 samples at the 10.9 GHz – 11.1 GHz band.

The two-line method can be used for powdered materials such as silicon carbide SiC [10], in which the material to be tested is placed in a mechanical support which is put directly on the two microstrip lines with different lengths (Figure 5.5), then the parameters S are measured and the propagation constant γ is extracted [10],

$$2 \cosh(\gamma \Delta L) = \frac{S_{12L1}^2 + S_{12L2}^2 + S_{11L1}S_{22L2} + S_{11L2}S_{22L1} - S_{11L1}S_{22L1} - S_{11L2}S_{22L2}}{S_{12L1}S_{12L2}} \quad (5.9)$$

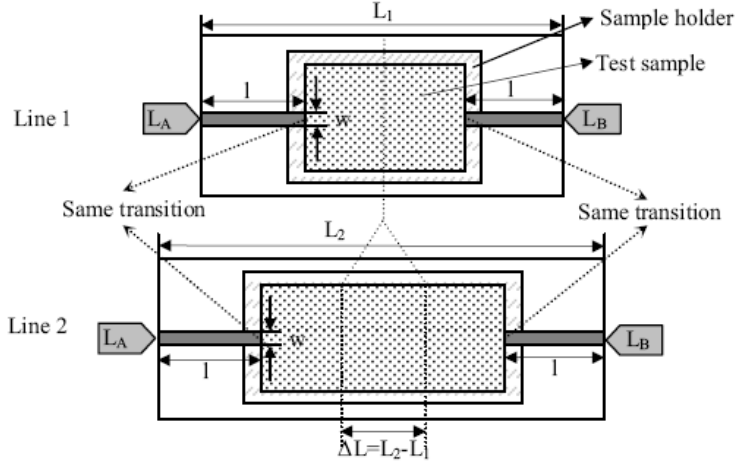


Figure 5.5. Measurement of powder samples using the transmission line method.

In some methods using transmission lines, the material to be characterized can serve as a superstrate while the transmission line is made of a well-known traditional dielectric material [6, 11, 12]. An important advantage of this method is to avoid fabrication difficulties of particular materials when used as substrates. However, the existence of an air gap between the transmission line and the superstrate can cause huge inaccuracies because these spaces are not controllable.

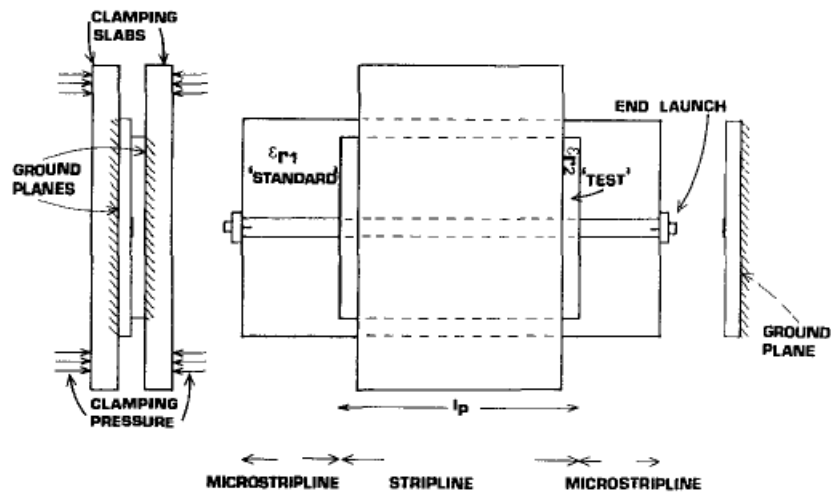


Figure 5.6. The transmission line method where the sample is a superstrate [6].

Generally, the methods using transmission lines are simple, give results in a wide frequency band. However, they are less effective for characterization of low-loss materials.

5.2. Resonance methods using resonators

These methods use cavities, such as different dielectric resonators or Fabry-Perot in a single or multi-mode operation.

5.2.1. Waveguide resonance cavity

The cavity resonator is realized using a short-circuit waveguide at both ends and a coupling device to excite it. The sample must be loaded inside the resonator before the measurements. In order to determine the dielectric properties, the resonance frequency and 3 dB bandwidth of the resonator are measured with and without the sample.

A widespread type of resonator is based on a waveguide using the perturbation method, dielectric samples usually take the form of a rod. The introduction of the sample into the resonator causes a disturbance that shifts the resonant frequency and reduces the void quality factor of the resonator (Figure 5.7). We will return in more detail on this method in the next section of this appendix.

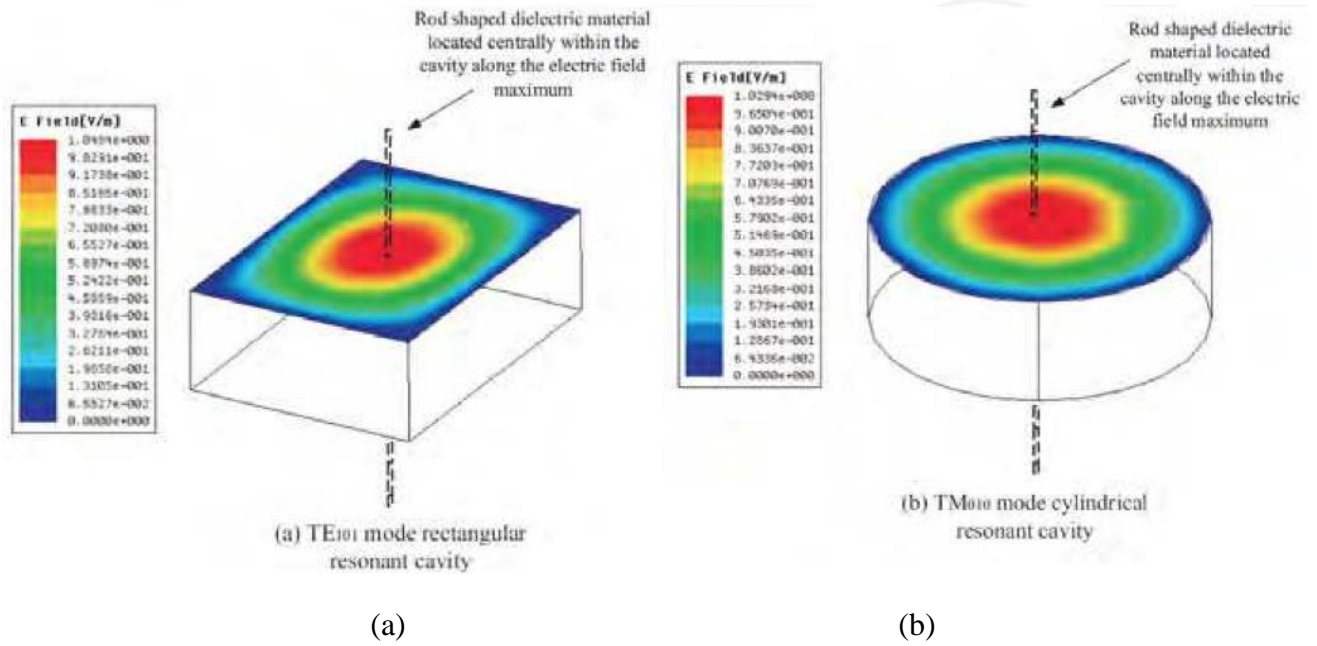


Figure 5.7. A resonance cavity to characterized complex permittivity of a material [1]: (a) TE_{101} mode in rectangular resonant cavity; (b) TM_{010} mode in cylindrical resonant cavity.

There are several publications on another resonant method using the split cylindrical cavity (Figure 5.8(a)) to characterize the permittivity of dielectric substrates [5, 13-15]. The paper [13] presents a detailed analysis, where the resonance conditions are found analytically by analyzing fields in the upper, lower and sample regions and boundary conditions. In [15], the authors developed a new theoretical model, based on the mode adaptation method. By measuring the resonance frequencies and quality factor for the TE_{1np} mode and higher TE_{0np} modes the authors have determined the dielectric properties over a very wide frequency band, from 10 up to 50 GHz.

The paper [5] presents this method in detail, where two circular cylindrical cavities of radius $a = 6.58$ mm and 7.06 mm length L are used and separated by a space to introduce the material to be characterized as Kodak photo paper (Figure 5.8(a)). Without a substrate, a TE_{011} resonance mode was excited at the frequency:

$$f_{011} = \frac{3 \times 10^8}{2\pi} \sqrt{\left(\frac{3.8317}{a}\right)^2 + \left(\frac{\pi}{L}\right)^2} = 34.54 \text{GHz} \quad (5.10)$$

This value is shifted by 33.78 GHz when a hydrophobic paper with a thickness of 263 μm is put into the slot (Figure 5.8(b)). From this information, the authors got $\epsilon_r = 1.6$.

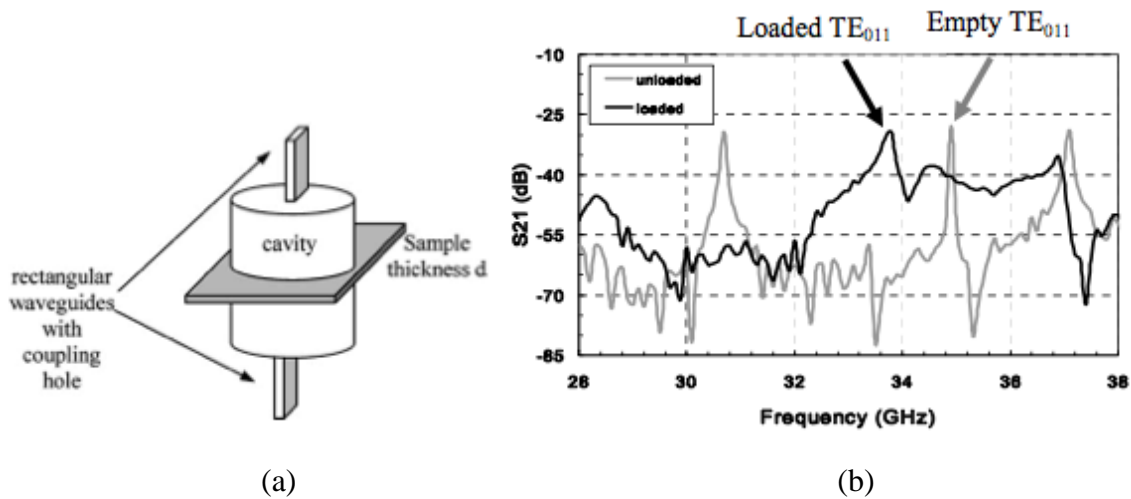


Figure 5.8. (a) Split-cylinder cavity; (b) Shifting S_{21} between an empty and a loaded cavity [5].

In [13-15], the method was tested for different material purposes and gives the average error of 3.9% on the dielectric constant of and 25% on the loss tangent.

There are several versions of this resonator process. In [16], Jerzy Krupka and his group proposed two measurement configurations using a cylindrical resonator at different temperatures, where the difference between two configurations is that the sample is located inside a ceramic ring resonator in the second configuration (Figure 5.9). Thus, in the second scheme of the experiment, the contribution to the Q-factor due to losses in the sample has greatly increased compared to the first measurement configuration. This makes it possible to measure the loss tangent more precisely than can be measured in the first configuration. Therefore, the second configuration makes it possible to measure very low Q-factor samples.

The sample may also be located at the open end of a resonator (Figure 5.10). This method is suitable to characterize samples with high losses and does not require sample preparation. When the material is placed at the open end of the resonator, the frequency is shifted. The length L_1 (Figure 5.10) can be changed to find the frequency initially present without the sample. The variation of the length L_1 is proportional to the permittivity of the material. The variation of the quality factor after adjustment gives information on the losses of the material.

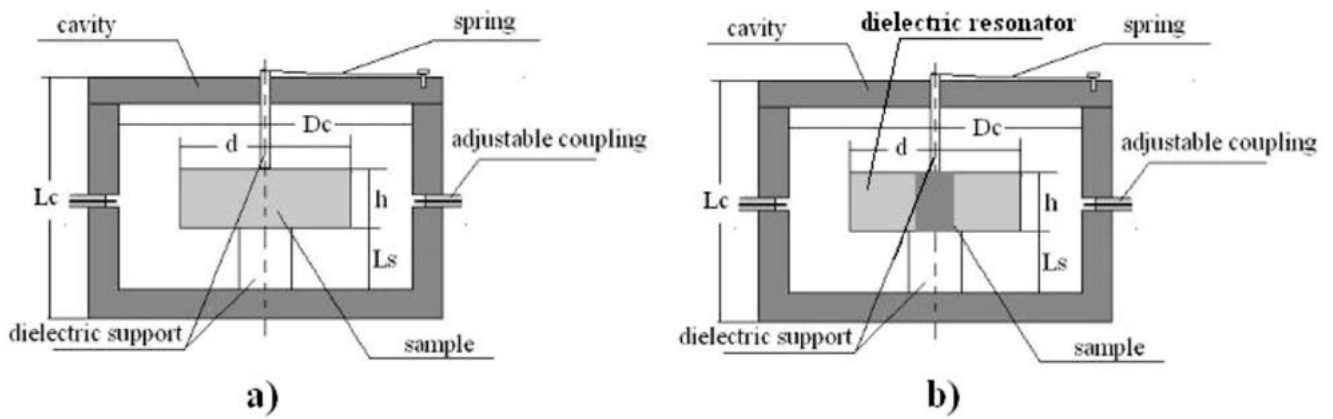


Figure 5.9. (a) The sample is loaded in a cylindrical cavity; (b) The sample is loaded in a dielectric resonator then put in a cylindrical cavity [16].

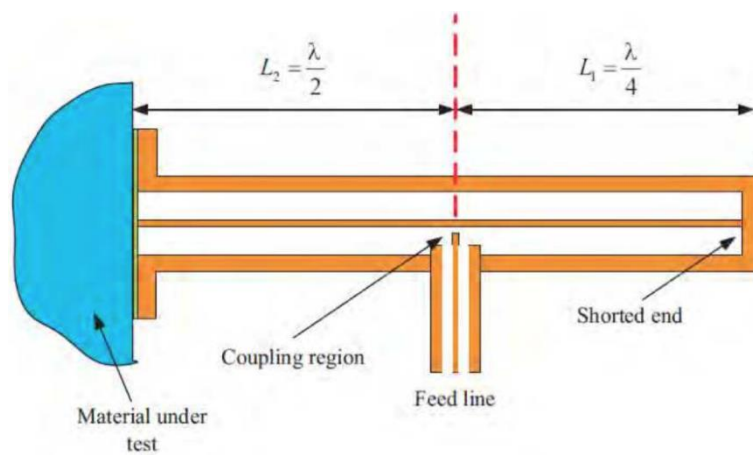


Figure 5.10. Open cavity at one side [1].

5.2.2. Planar transmission line resonators

Figure 5.11 shows a structure for measuring resonance disturbance on liquid samples, where the sample is located in a small cavity pierced within the substrate. The electric fields are concentrated at the end of the resonator, so the sample should be inserted near the end. The electric fields interact with the material which causes a capacitive disturbance. This method has many advantages such as simplicity of implementation, only a small amount of the sample is needed for characterization. However, the low Q factor can lead to an inaccurate determination of the tangent of the sample losses.

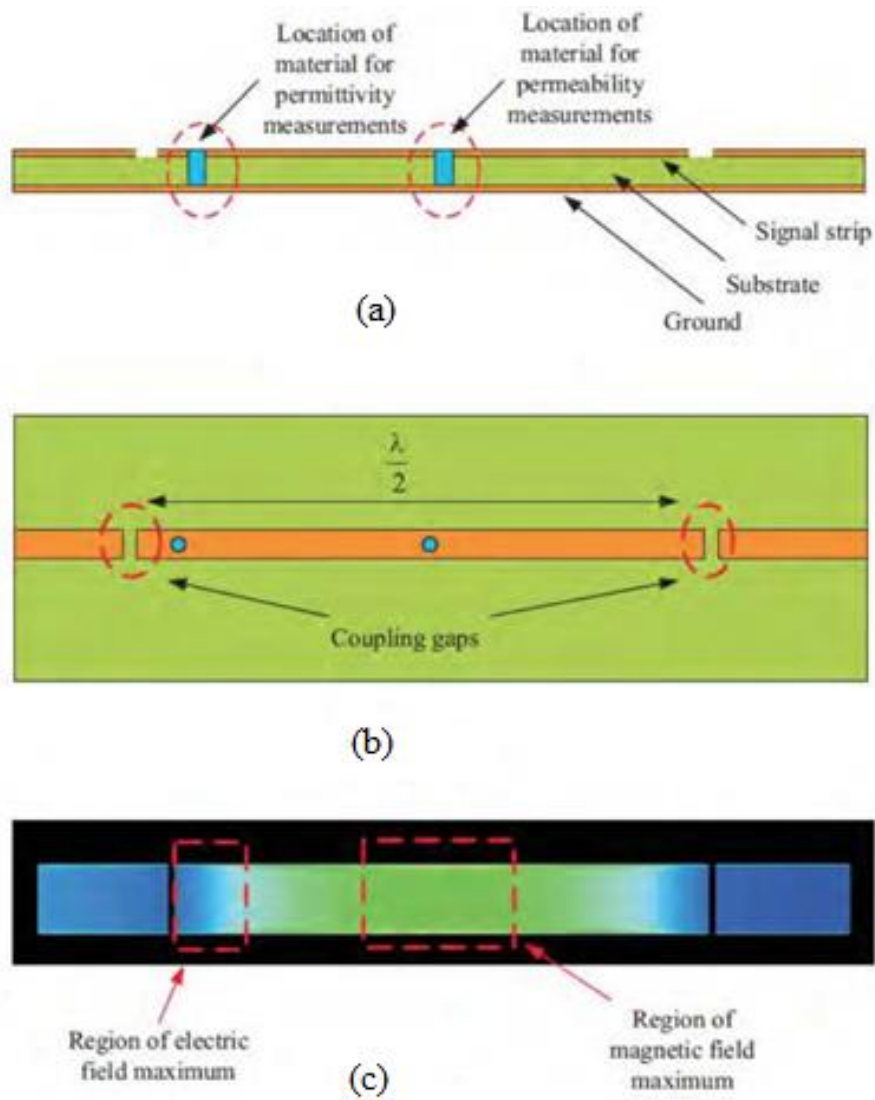


Figure 5.11. Planar transmission lines to characterize liquid materials [1]: (a) Longitudinal view; (b) Top view; (c) Current distribution.

5.2.3. Microstrip resonator

The ring resonator is a basic resonant structure that offers high Q factors when not charged due to reduced radiation losses. For rings made on substrates which have a thickness much greater than that of the conducting ribbon, at resonance,

$$l = \frac{n\lambda_g}{2} = \frac{n \cdot c}{2f\sqrt{\epsilon_{\text{eff}}}} \quad \text{for the } n\text{-th resonance frequency} \quad (5.11)$$

In [17, 18], the authors use this method to characterize the dielectric properties of paper. In this procedure, a commercial paper with a hydrophobic coating was chosen with a thickness of $260 \pm 3 \mu\text{m}$ two faces of which are covered by copper sheets of $18 \mu\text{m}$. A ring resonator is formed using the photolithography method, and the paper substrate is then dried at 100°C for 30 minutes. Figure 5.12 shows the ring resonator designed and manufactured with $r_m = 40\text{mm}$, $w = 7.46\text{mm}$.

To determine the permittivity ϵ , S21 of the resonator was measured over the 0.5 GHz to 2.5 GHz frequency band using an Agilent 8530A Network Analyzer (VNA), the simulated and measured S21 parameters are presented in Figure 5.13.

ϵ can be determined by the formula:

$$f_0 = \frac{nc}{2\pi r_m \sqrt{\epsilon_{\text{eff}}}} \quad \text{or} \quad \epsilon_{\text{eff}} = \left(\frac{nc}{2\pi r_m f_0} \right)^2 \quad (5.12)$$

where f_0 is resonance frequency of the ring with radius r_m .

The relative permittivity can be calculated by the following relation:

$$\epsilon_r = \frac{2\epsilon_{\text{eff}} + M - 1}{M + 1} \quad (5.13)$$

where M is a function of paper thickness and bandwidth due to fringing effect:

$$M = \sqrt{1 + \frac{12h}{w_{\text{eff}}}} \quad (5.14)$$

$$w_{\text{eff}} \text{ is the effective width of the strip } w_{\text{eff}} = w + \frac{1.25t}{\pi} \left(1 + \ln \left(\frac{2h}{t} \right) \right) \quad (5.15)$$

The loss tangent of paper is a function of the dielectric attenuation at the resonant frequency and can be calculated by the relation (A1.18):

$$\tan \delta = \frac{\alpha_d \lambda_0 \sqrt{\epsilon_{\text{eff}}} (\epsilon_r - 1)}{8.686 \pi \epsilon_r (\epsilon_{\text{eff}} - 1)} \quad (5.16)$$

where α_d is obtained by subtracting conductor and radiation attenuation α_{total} [17]. As a result, the loss tangent obtained is 0.082, 0.066 and 0.073 at 711.5 MHz, 1408 MHz and 2173 MHz, respectively. 260- μm thick hydrophobic paper is tested by this method at the band 0.5 GHz – 2.5 GHz, with the error of 5.9-13% on the dielectric constant and 10% of measured quality factor uncertainty (the source of main error). This method offers a high precision for determining the permittivity of the substrates at resonant frequencies, however it is not very

good for determining the tangent of losses because it is difficult to evaluate radiation losses to obtain precisely α_d .

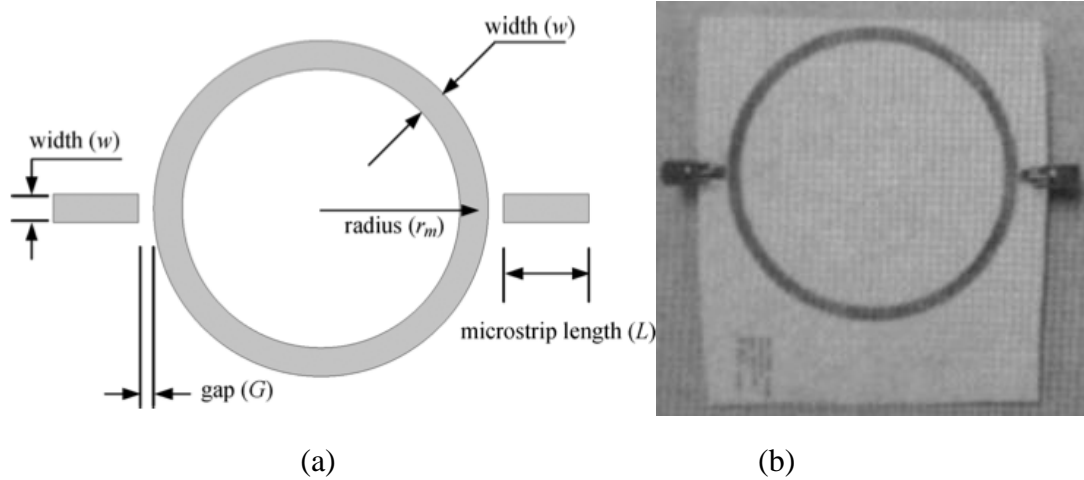


Figure 5.12. Microstrip ring resonator (a) Configuration diagram; (b) Fabricated prototype [17, 18].

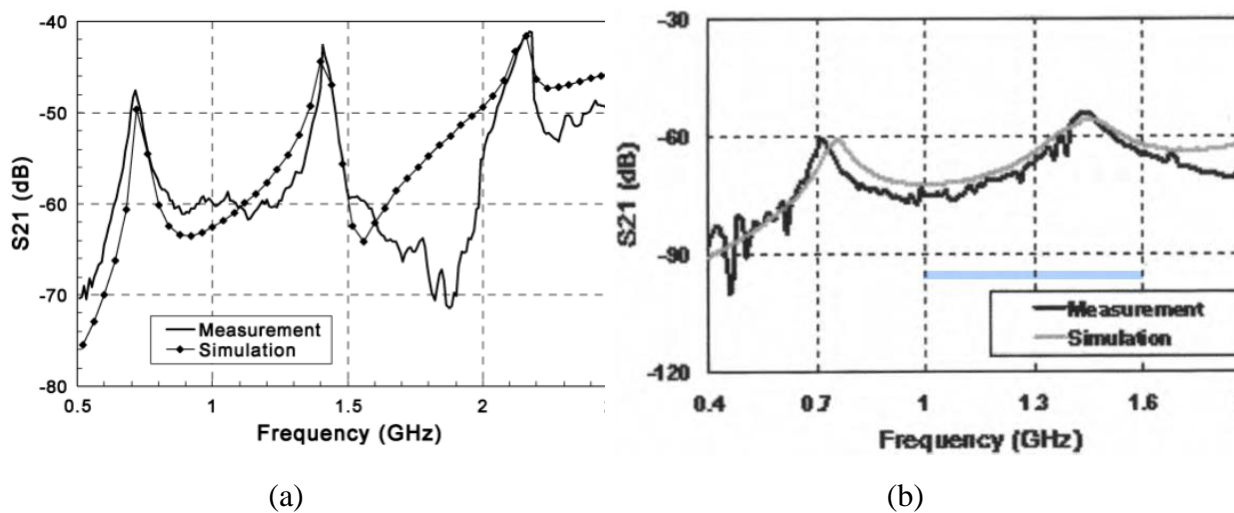


Figure 5.13. Simulated and measured $|S_{21}|$ by the ring resonator in (a) [17], (b) [18].

In order to validate the permittivity determined by the process presented above and to estimate the tangent of losses, Anagnostou D. E et al. [19, 20] used a 50 ohm microstrip line with $L = 69.5$ mm and $w = 3.7$ mm on a photo paper substrate (HP Advanced Glossy Photo Paper) of 700- μm thickness. In order to have this thickness and to study the sensitivity of the results according to the thickness of the paper, four sheets of 263- μm thick photo paper were pressed using the PHI laminator Q-247C4. The same relation (A1.18) is used to determine $\tan\delta$.

Moreover, other microstrip resonators can also be used as a coupled ring [21], where the authors have created three closed ring resonators and three other open ring resonators (Split

Ring Resonators).): 1CRR / 1SRR with a closed / open ring of one wavelength λ , 2CRR/2SRR with two closed/open rings of lengths λ and $\lambda/2$, 3CRR/3SRR with three closed/open rings of lengths $\lambda, \lambda/2$ and $\lambda/4$. Two materials Spirulina Platensis-Gietler and Ferrite have been characterized, it has been found that CRRs can be used for both materials, however SRRs are only effective for Ferrite. The typical order of magnitude of the uncertainties is 0.5% - 2.5% on the dielectric constant using CRRs, 3.2% - 3.7% on the dielectric constant using SRRs to characterize Spirulina Platensis-Gietler. However, the accuracy of Ferrite characterization is much better, from 0.06% - 0.3% on the dielectric constant using CRRs, 0.22% - 0.4% on the dielectric constant using SRRs.

Other versions of this method are the use of T-shaped resonators [22] or planar antennas that can also be designed on traditional substrates so the sample serves as the top layer. An example of using antennas is shown in Figure 5.14 [23] where a slot antenna is used, or in Figure 5.15 [24] where the sample can be placed on the surface of a microstrip antenna.

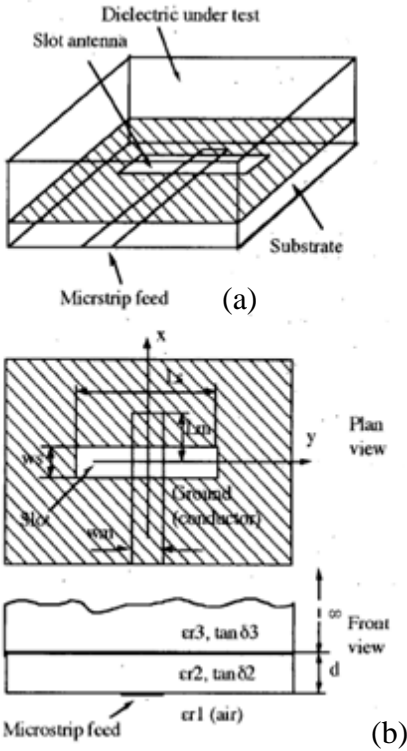


Figure 5.14. The method using a slot antenna [23]: (a) 3D view; (b) Section views.



Figure 5.15. The method using a microstrip antenna [24].

5.3. Recommendations for choosing methods

The methods for characterization of the dielectric properties of materials are summarized in **Erreur ! Référence non valide pour un signet.** and the recommendations for choosing a method for characterizing a material are given in Table 5.2.

Table 5.1. Comparison of methods.

Method	Authors	Thickness and accuracy	Advantages	Disadvantages
Non-resonant				
Method using a rectangular waveguide	B. K. Chung, 2007[2]	The error of ϵ' is less than 0.1%, and the error of ϵ'' is less than 0.2% for the sample thickness less than 1% of $\lambda/ \epsilon $.	Simple algorithm for determining the complex permittivity.	Complicated to place samples, the presence of air gap can lead to errors.
Method using a rectangular waveguide, determination of ϵ by polynomial approximation	U. C. Hasar, 2008 & 2009[3, 4]	At 10 GHz, the error is 1,88% for ϵ_r' for PTEE of both thicknesses of 2mm and 3mm, the error for ϵ_r'' is big, 55% for PTEE of 2mm thickness and 27,6%	Simple algorithm for determining the complex permittivity.	Complicated to place samples, the presence of air gap can lead to errors.

		for PTEE of 3mm thickness.		
Reflection method using a waveguide where the sample is placed directly on a metal plate.	Nawfal Jebbor, 2012 [5]	The tested materials: Teflon, wood and distilled water. The 7th order approximation is recommended to use for thinner samples.	Easier to place the sample in the waveguide compared to the previous methods The method is good for low loss materials and thinner samples.	The presence of air gap can lead to errors, big error for thick materials.
Planar transmission line method, the sample is the substrate	H. Riedell, Mike Kay et al., 1989 [8]	Tested for FR4 materials in the 200 MHz - 2 GHz frequency band. The error is about 10% for ϵ_r and 25% for $\tan \delta$ at 800 MHz compared to a resonant method.	Simple algorithm for determining the complex permittivity.	Not effective for low loss materials, accuracy depends on the numerical accuracy of measured data.
Method of a microstrip line, the sample is the substrate	A. Koul, Praveen, 2014 [9]	The tolerance of the loss tangent is decreased from 36% to 5% by testing 9 FR4 samples at the band	The model of the transmission line is more precise, including connectors and taking into account its asymmetry as well as the effect	Complexity when applying for thin materials.

		10.9 GHz – 11.1 GHz.	of roughness on the conductor's surface	
Microstrip lines with different lengths (Two-line method)	N. K. Das, S. M. Voda, D. Pozar, 1987 [6]	Tested for Rogers materials with accuracy of dielectric constant as follows: - Rogers RT5880 1.57mm thickness: 0.5%, - Rogers RT5880 of 0.787mm thickness: 0.45%, - Rogers RT6010 1.27mm thickness: 5.8%.	Simple realization	Accuracy depends on etching quality, connectors, and line length measurement results. It is not possible to measure loss tangent with high accuracy because of radiation losses, sonot effective for low loss materials.
Two-line method for determining loss tangent	M. Tentzeris & his group, 2007 [7]	Sample: hydrophobe paper d=1,2mm is characterized in the frequency band of 0,2 GHz – 1,2 GHz.	Simple loss tangent extraction algorithm (combination of simulation of conductor and radiation losses subtracted from measured total losses)	The accuracy depends on the quality of inkjet printing.

Two-line method to characterize a powder material	Q. Lu, L. Dubois et al., 2010 [10]	15 mm thickness Plexiglass and 5mm SiC powder are tested at the frequency band of 0 – 6 GHz.	The method can be applied for several liquid as well as solid materials.	It is necessary to choose the materials of the mechanical support with low losses.
Microstrip line method, the sample is the superstrate	N. K. Das, S. M. Voda, D. Pozar, 1987 [6] K. C. James Raju, K. Sudheendra, 2008[12]	Tested for materials with accuracy on dielectric constant as follows: - OAK with a thickness of 1.524mm: 0.39%, - OAK with a thickness of 0,762 mm: 0,78%, - Rogers RT5880 with a thickness of 1.57 mm: 0%, - Rogers RT5880 with a thickness of 0,787 mm: 0,45%, Rogers RT6010 Thickness 1.27 mm: 0.49%,	Simple realization	The presence of air gap between the sample and the line can lead to errors; The accuracy is not good for loss tangent due to radiation losses.

Method of a microstrip line with the coplanar feeding, the sample- a liquid crystal the LC (liquid crystal) serves as the superstrate.	PrafullaDeo et al., 2015 [11]	The substrate is Rogers 4350B which is removed in the area under the material to be characterized. The sample is a liquid Crystal, the precision on the dielectric constant is 2.5% at the band 15 GHz - 65 GHz.	Broadband, can be used for low-loss materials	For solid samples, the presence of air gap between the sample and the line can cause errors.
Resonant				
“Split-cylinder” cavity	M. Tentzeris& his group, 2007[7] M. D. Janezic and his group, 1998, 1999, 2004 [13-15]	Different thin materials (0.1 mm - 5 mm) are tested with the 0.013% - 0.784% error on the dielectric constant and 0.172% - 9.1% on the loss tangent.	Can be used for low loss materials	Not used to characterize thick samples.

Modified method using waveguide resonators	Jerzy Krupka and his group, 2006 [16]	The 6 mm silicon sample is measured with the accuracy of 0.1% on the dielectric constant and 0.5% on the loss tangent.	Can be used for low loss materials.	Not wideband.
Microstrip ring resonator	M. Tentzeris&s on groupe, 2007, 2009 [17, 18] Anagnostou D. E. and his group, 2010	260 μm hydrophobic paper is tested at the 0.5 GHz - 2.5 GHz band, with the 5.9-13% error on the dielectric constant and 10% measured quality factor uncertainty (the main source of error) HP Advanced Glossy Photo Paper 700-μm thick (4 layers of 263-μm photo paper was pressed using laminator Q-247C4).	Can be used for thin materials	Not good for determining the loss tangent; The accuracy depends on inkjet print quality or other etching technologies.

	[19, 20]			
Coupled ring resonator	M. Kapoor, K. S. Daya, 2012 [21]	Spirulina Platensis-Gietler (0.5% accuracy on dielectric constant using 1CRR, 2.5% for 2CRR, 0.6% for 3CRR, 3.4% for 1SRR, 3.2% for 2SRR, 3.7 % for 3SRR) and Ferrite of 1mm thickness (accuracy of 0.3% for 1CRR, 0.06% for 2CRR, 0.2% for 3CRR, 0.28% for 1SRR, 0.4% for 2SRR, 0.22% for 3SRR).	Possibility of having high accuracy	Accuracy depends on the quality of inkjet printing or other etching technologies, and the materials to be characterized
T-shaped resonator with an open $\lambda / 4$ stub, the sample serves as the substrate	Y.-H. Chou, 2008 [22]	FR4 0,76 mm	Simple realization	Accuracy depends on the quality of inkjet printing or other etching technologies, and the materials to be characterized

Slot antennas, the sample serves as the superstrate	H. G. Akhavan, D. Mirshekar-Syahkal, 1999 [23]	12mm thickness Perspex sheet	The sample serves as the superstrate so the resonator can be used for different samples	The thickness of the sample must be big For solid samples, the presence of air gap between the sample and the line can cause errors
Microstrip antenna, sample serves as the superstrate	Nabila Aouabdia et al. [24]	Organic materials (liver, fat, potato, salmon)		
Cylindrical resonator with perturbation technique	H. Kawabata, T. Kobayashi et al., 2006 [25]	d=2.49 ±0.01mm polyethylene	The resonator can be used for different samples, High accuracy There is no need to prepare the sample before measuring	Not wideband

Table 5.2. Recommendations of methods for characterization of different materials.

Method of characterization	Thin substrate	Thick substrate	Low loss (<0.05)	High loss	Low ϵ	High ϵ
Transmission method using a waveguide						
Reflection method using a waveguide						
Planar transmission line method, the sample is the substrate						
Two-line method						
Planar line method, the sample is the superstrate						
Split-cylindercavity						
Perturbation method using a waveguide resonator						
Planar resonator (ring / coupled rings / T-shaped), the sample is the substrate						
Planar resonator / Antenna, the sample is the superstrate						

Conclusions for Appendix 1

Based on the summary and analysis above, and based on the properties of the substrates used to design antennas in this thesis, we chose the cavity perturbation method to characterize our E4D paper.

References for Appendix 1

- [1] K. Saeed et al. "Planar Microwave Sensors for Complex Permittivity Characterization of Materials and Their Applications", www.intechopen.com
- [2] B.-K. Chung, "Dielectric Constant Measurement for Thin Material at Microwave Frequencies", *Progress in Electromagnetics Research*, 2007, pp. 239-252.
- [3] U. C. Hasar, "An Accurate Complex Permittivity Method For Thin Dielectric Materials", *PIER* 91, 123-138, 2009.
- [4] U. C. Hasar, "A Fast and Accurate Amplitude-Only Transmission-Reflection Method for Complex Permittivity Determination of Lossy Materials", *IEEE Trans. On Microwave Theory and Techniques*, Vol. 56, No. 9, September 2008, pp. 2129-2135.
- [5] N. Jebbor, "A Microwave Method for Complex Permittivity Extraction of Thin Materials", *J. of Microwave, Optoelectronics and Electromagnetic Applications*, Vol. 11, No. 2, December 2012, pp. 285-295.
- [6] N. K. Das, S. M. Voda, D. Pozar "Two Methods for the Measurement of Substrate Dielectric Constant", 1987, *Trans. On Microwave Theory and Techniques*, vol. 35, N7, pp. 636-642.
- [7] A. Rida, L. Yang, M.M. Tentzeris, "Design and Characterization of Novel Paper-based Inkjet-Printed UHF Antennas for RFID and Sensing Applications", *IEEE Antennas and Propagation Society International Symposium*, 2007, pp. 2749-2752.
- [8] H. Riedell, M. Kay et al. "Dielectric Characterization of Printed Circuit Substrates", *IEEE Proceedings* – 1989, pp. 102-106.
- [9] A. Koul, P. K. R. Anmulla et al. "Improved Technique for Extracting Parameters of Low-Loss Dielectrics on Printed Circuit Boards", *IEEE Transactions on Electromagnetic Compatibility*, 2014, Vol. 56, N6, pp. 191-196.
- [10] Q. Lu, L. Dubois et al. "New Method for Dielectric Properties Characterization of Powder Materials : Application to Silicon Carbide", *Proc. Of the 40th European Microwave Conference*, 2010, pp. 1595-1598, 28-30 Sep 2010, Paris, France.
- [11] P. Deo et al., "Microstrip Device for Broadband (15-65 GHz) Measurement of Dielectric Properties of Nematic Crystals", *Trans T-MTT*, 2015, vol. 63, N4, pp. 1388-1398.

- [12] K. C. J. Raju, K. Sudheendran "Tunable Materials and Their Microwave Characterization", Proc. of Int. Conference on Microwave, 2008
- [13] M. D. Janezic, J. B. Jarvis "Full-Wave Analysis of a Split-Cylinder Resonator for Nondestructive Permittivity Measurements", IEEE T-MTT, 1999, vol. 47, N10, pp. 2014-2020.
- [14] J. B. Jarvis, M. D. Janezic et al. "Dielectric Characterization of Low-Loss Materials. A Comparison of Techniques", IEEE Trans on Dielectrics and Electrical Insulations, 1998, Vol. 5, No. 4, pp. 571-577.
- [15] M. D. Janezic, E. F. Kuester, J. B. Jarvis "Broadband Complex Permittivity Measurement of Dielectric Substrates using a Split-Cylinder Resonator", IEEE MTT-S Digest, 2004, pp. 1817-1820.
- [16] J. Krupka et al. "Measurement of Permittivity, Dielectric Loss Tangent and Resistivity of Float-Zone Silicon at Microwave Frequencies", IEEE T-MTT, 2006, vol. 54, N11, pp. 3995-4001
- [17] L. Yang., A. Rida, R. Vyas, M. Tentzeris, "RFID Tag and RF Structures on a Paper Substrate Using Inkjet-Printing Technology", IEEE Trans. On Microwave Theory and Techniques, Vol. 55, No. 12, December 2007, pp. 2894-2901.
- [18] A. Rida, R. Vyas, M. Tentzeris, M. "Conductive Inkjet-Printed Antennas on Flexible Low-Cost Paper-Based Substrates for RFID and WSN Applications", IEEE Antennas and Propagation Magazine, Vol. 51, No. 3, June 2009, pp. 13-23.
- [19] D. E. Anagnostou, A.A. Gheethan et al., "A Direct-Write Printed Antenna on Paper-Based Organic Substrate for Flexible Displays and WLAN Applications", Journal of Display Technology, Vol. 6, pp. 558-564, No.11, 2010.
- [20] H. Khaleel, "Innovation in Wearable and Flexible Antennas", WIT Transactions on State-of-the-art in Science and Engineering, 2014.
- [21] M. Kapoor, K. S. Daya "Coupled ring resonator for microwave characterization of dielectric materials", International Journal of Microwave and Wireless Technologies, N 04/2012, pp. 241-246.

- [22] Y.-H. Chou, "Measurement of RF PCB Dielectric Properties and Losses", Progress in Electromagnetics Research Letter, Vol. 4, 2008, pp. 139-148.
- [23] H. G. Akhavan, D. Mirshekar-Syahkal "Slot Antennas for Measurement of Properties of Dielectrics at Microwave Frequencies", IEE National Conference on Antennas and Propagation, 30 Mar – 1 Apr, 1999, pp. 8-11.
- [24] N.Aouabdia et al. "Rectangular Patch Resonator Sensors For Characterization of Biological Materials", SSD'14.
- [25] H. Kawabata, T. Kobayashi et al. "Measurement Accuracy of a TM_{0m0} Mode Cavity Method to Measure Complex Permittivity of Rod Samples", Proc. of Asia-Pacific Microwave Conference, 2006.
- [26] V. H. Nguyen; M. H. Hoang, H. P. Phan, T. Q. V. Hoang, T. P.Vuong, "Measurement of complex permittivity by rectangular waveguide method with simple specimen preparation", 2014 International Conference on Advanced Technologies for Communications, pp.397-400, October 15-17, 2014, Hanoi, Vietnam.

6. Appendix 2 – Antenna fabrication and measurement

Many of paper-based antennas in the previous studies were fabricated by inkjet-printing technology with rather thin single metallic layer and time-consuming multiple inkjet-printing process. Our designed antennas have been realized at Technical Center of Paper (CTP), Grenoble, France by using double-side Screen Printing Technology with silver ink that is faster, with more reasonable cost than inkjet-printing, thus more suitable for industrial applications. This technology of printing gives good thickness of the metal (5.2 to 8 μm) with a rather good conductivity of $1.7 \times 10^6 \text{ S/m}$ without repetitive printing multiple layers.

In the first printing run, the antennas have been realized on 104- μm thickness E4D paper (E4D 100) with $\epsilon_r = 3.184$ and $\tan \delta = 0.092$, in six prototypes. This run was related to the antennas “Sapin” (3.1.1), “Modified Sapin” (3.1.2), “Robe” (3.1.3) and “Mushroom-Shaped with Two Arms” (3.1.4). The next runs is performed on the same E4D paper but with 210- μm thickness, related to the antennas “Sapin 2”, “Hello-Shaped”, IFAs (2.3) and multi-band antennas.

In order to characterize antennas, 2.92-mm Jack End Launch Connector is used.

The reflection coefficient of the antennas was characterized by using a Vector Network Analyzer (VNA) Agilent 8720ES. In the measurement, the prototypes were placed in the anechoic chamber to avoid any oscillation caused by the ambience around them (Figure 6.1).

The measurement of radiation patterns of antennas was performed in IMEP-LAHC anechoic chamber. The transmit antenna is a horn with 10.0 dBi gain at 2.5 GHz and 11.3 dBi gain at 5.5 GHz. The antenna under test is located at the distance of 3 meters from it that is much bigger than the dimensions of the horn providing the far-field condition. The experimental setup for measuring radiation patterns of the antennas is shown in Figure 6.2, where the measurement was carried out in the x-z plane ($\varphi = 0^\circ$) and the x-y plane ($\theta = 90^\circ$).

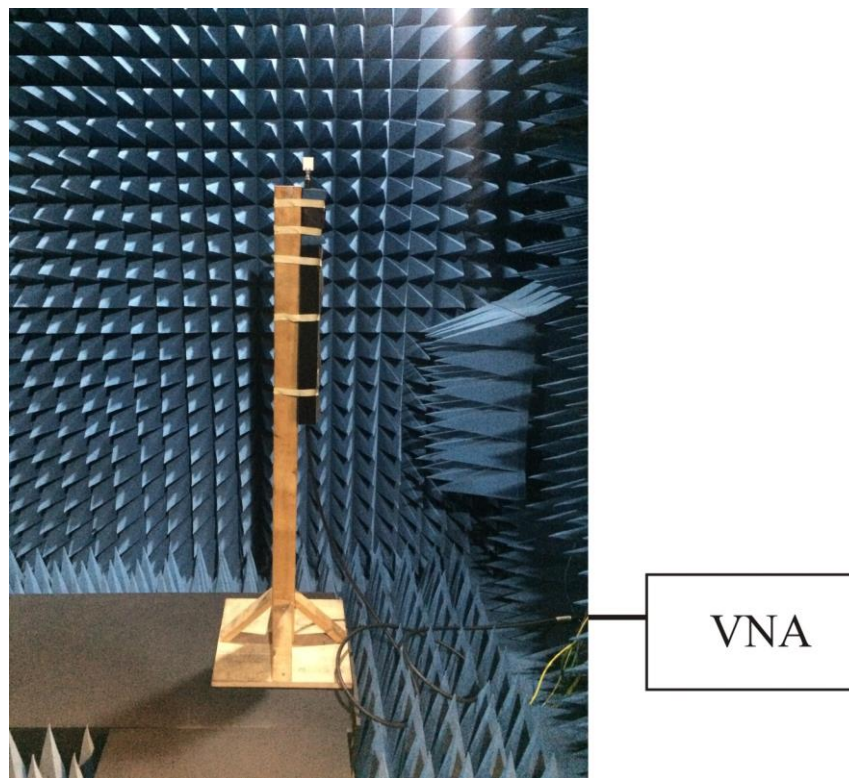


Figure 6.1. Measurement of reflection coefficient of the antenna.

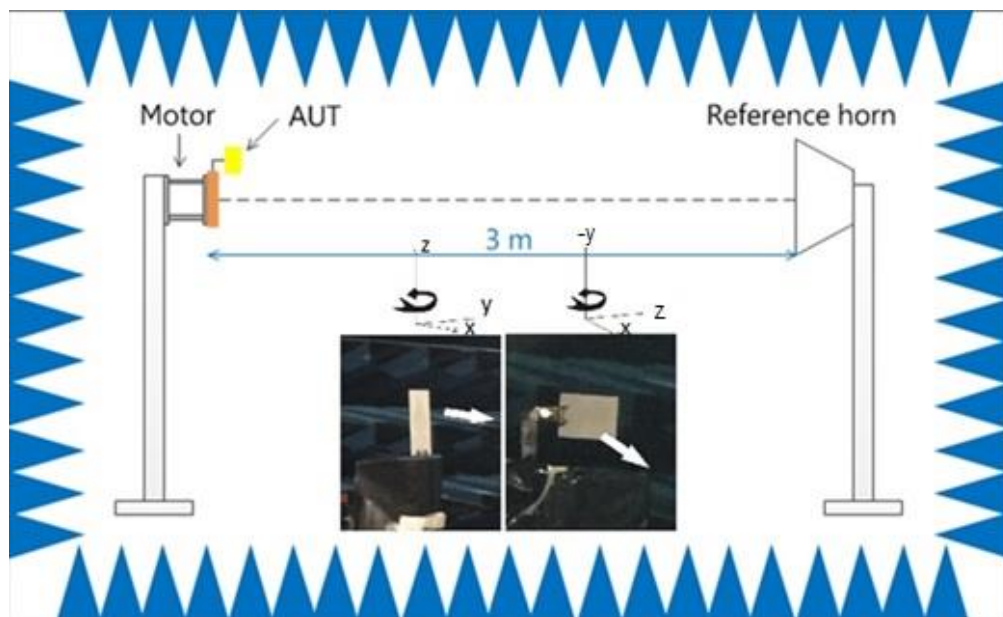


Figure 6.2. Experimental setup for measurement of radiation patterns of the antenna, where the transmit antenna is at x-direction: (a) x-y plane ($\theta = 90^\circ$) measurement; (b) x-z plane ($\phi = 0^\circ$) measurement.

Abstract

Design of 2D and 3D Antennas on Flexible Substrates

The thesis was carried out within the ANR project « Stick'It » that aimed at developing new, low-cost and innovative technologies devoted to the design of 2D, 2.5D and 3D radiofrequency (RF) components including antennas printed on conformable materials. The targeted applications are primarily home-networking devices such as set-top boxes where their forms and dimensions are widely varied. Therefore, it is necessary to design antennas on flexible substrates.

According to our needs for a substrate material that is flexible, low cost, with good RF properties, recycling ability, and especially ability to make 3D structures, after considering various dielectric materials for flexible electronics, paper substrate appeared to be the most suitable for our purpose.

The work of this thesis conducted in three phases.

In the first phase, the method of perturbation using a cylindrical cavity was chosen for characterization of paper. The first results of this process were verified by realization and testing of simple antennas such as CPW-fed monopoles on paper and PET. Then, the measurement of E4D paper substrate was performed with 50 samples cut from various E4D paper sheets of three different thicknesses, 104 μm , 210 μm and 387 μm . The results were analyzed statistically and gave $\epsilon_r = 3.184$, $\tan\delta = 0.092$. The dispersions of the results measured at 2.5 GHz are 0.25% for ϵ_r and 0.26% for $\tan\delta$. These results were used for the next phase.

In the second phase, different antennas were designed on 0.104-mm and 0.21-mm thick E4D paper including IFAs, SIW cavity-back antenna and microstrip-fed wideband monopole antennas. The prototypes were realized using screen printing technique and tested for matching property and radiation patterns.

In the third phase the proposed antennas were studied in realistic package conditions, where a set-top box was made of ABS plastic with different dimensions. The first case was with two MIMO antennas orthogonally located in different ABS boxes with sufficient space, so that both of them can remain flat. The second case was a box with a restricted height, so that at least one of the antennas needs to be bent.

Thus, a study of bending effect was carried out, first of all, with a simple straight dipole and a straight monopole on E4D paper, then with a wideband antenna proposed in the second phase. The study showed that bending does not much affect the matching of the antenna over a wide frequency band. However, its radiation patterns rotate in the E-plane with a rotation angle depending on the bending location and bending angle.

Then, the MIMO system of two antennas placed orthogonally in an ABS box with restricted height so that one antenna needed to be bent and another remained flat. In all cases of MIMO antenna system, we obtained good isolation (>20 dB) and Envelope Correlation Coefficient (ECC) less than 0.05.

Keywords: paper-based antenna; printed antennas, flexible electronics; deformation effect of antenna; bending effect of antenna; 3D antenna

Résumé

Conception d'antennes 2D et 3D sur des matériaux flexibles

Le travail de thèse a été réalisé dans le cadre du projet ANR «Stick'It» visant à développer de nouvelles technologies peu coûteuses et innovantes dédiées à la conception de composants radiofréquences (RF) 2D, 2,5D et 3D, notamment des antennes imprimées sur des matériaux conformes. Les applications ciblées sont principalement des appareils de réseau domestique, tels que les décodeurs, dont les formes et les dimensions sont très variées. Par conséquent, il est nécessaire de concevoir des antennes sur des substrats souples.

Selon nos besoins pour un matériau de substrat flexible, peu coûteux, avec de bonnes propriétés RF, la capacité de recyclage et en particulier la capacité à fabriquer des structures 3D, après avoir étudié différents matériaux diélectriques pour l'électronique flexible, le papier s'est trouvé le plus adapté.

Les travaux de cette thèse se sont déroulés en trois phases.

Dans la première phase, la méthode de perturbation utilisant une cavité cylindrique a été choisie pour la caractérisation du papier. Les premiers résultats de ce processus ont été vérifiés en réalisant et en testant des antennes simples telles que des monopoles alimentés par CPW sur du papier et du PET. Ensuite, la mesure du papier E4D a été effectuée avec 50 échantillons découpés dans différentes feuilles de papier E4D de trois épaisseurs différentes, 104 μm , 210 μm et 387 μm . Les résultats ont été analysés statistiquement et ont donné $\epsilon_r = 3.184$, $\tan\delta = 0.092$. Les dispersions des résultats mesurés à 2,5 GHz sont 0.25% pour ϵ_r et 0.26% pour $\tan\delta$. Ces résultats ont été utilisés pour la phase suivante.

Au cours de la deuxième phase, les antennes différentes ont été conçues sur le papier E4D d'épaisseur 0,104mm et 0,21 mm, notamment des IFA, des antennes SIW et des antennes monopoles alimentées par une ligne microruban. Les prototypes ont été réalisés à l'aide d'une technique de sérigraphie et testés pour déterminer les propriétés de l'adaptation et les diagrammes de rayonnement.

Dans la troisième phase, les antennes proposées ont été étudiées dans des conditions d'emballage réalistes, où un boîtier décodeur était en plastique ABS avec différentes dimensions. Le premier cas concernait deux antennes MIMO placées orthogonalement dans des boîtiers ABS différents,

avec un espace suffisant pour que les deux puissent rester plats. Le second cas était une boîte à hauteur limitée, de sorte qu'au moins une des antennes doit être pliée.

Ainsi, une étude de l'effet de flexion a été réalisée, tout d'abord avec un simple dipôle droit et un monopole droit sur le papier E4D, puis avec une antenne à large bande proposée dans la seconde phase. L'étude a montré que la flexion n'affecte pas beaucoup l'adaptation de l'antenne sur une large bande de fréquences. Cependant, ses diagrammes de rayonnement tournent dans le plan E avec un angle de rotation dépendant de la position de pliage et de l'angle de flexion.

Ensuite, le système MIMO de deux antennes placé orthogonalement dans un boîtier ABS de hauteur limitée, de sorte qu'une antenne doit être pliée et une autre reste plate. Dans tous les cas de système d'antenne MIMO, nous avons obtenu une bonne isolation (> 20 dB) et un coefficient de corrélation (ECC) inférieur à 0,05.

Mots clés: antennes sur papier; antennes imprimées; circuits électroniques flexibles; effet de déformation de l'antenne; effet de flexion de l'antenne

Liste des publications

1. H. P. Phan, T.-P. Vuong, P. Benech, P. Xavier, J.-M. Duchamp, “Caractérisation de propriétés diélectriques des matériaux souples”, GDR Ondes, Lyon, 19-21 Oct. 2015.
2. H. P. Phan, T. P. Vuong, P. Benech, P. Xavier, P. Borel and A. Delattre, "Printed Flexible Wideband Microstrip Antenna for Wireless Applications", 2016 International Conference on Advanced Technologies for Communications (ATC'16), October 12-14, 2016, Hanoi, Vietnam
3. H. P. Phan, T. P. Vuong, P. Benech, P. Xavier, P. Borel and A. Delattre, “Low cost Wideband Antenna on Paper Substrate”, EuCAP 2017, pp. 2177-2180, March 19-24, 2017, Paris, France.
4. H. P. Phan, T. P. Vuong, P. Benech, P. Xavier, P. Borel and A. Delattre, “Antenne à large bande sur papier”, JNM 2017, 16-19 mai 2017, Saint-Malo, France.
5. H. P. Phan, T. P. Vuong, P. Benech, P. Xavier, P. Borel and A. Delattre, “Novel Ultra-Wideband “Robe” Antenna on High-Loss Paper Substrate”, AP-S 2017, pp.319-320, July 9-14, 2017, San Diego, USA.
6. H. P. Phan, T. P. Vuong, P. Benech, P. Xavier, P. Borel, “”Hello-Shaped” Wideband Monopole Antennas on Paper Substrate”, International Conference on Advanced Technologies for Communications (ATC'17), October 18-20, 2017, QuyNhon, Vietnam.
7. H. P. Phan, T. P. Vuong, P. Benech, P. Xavier, P. Borel and A. Delattre, “Study of Bending Effects of A Wideband Paper-Based Printed Microstrip-Fed Antenna”, IET Microwaves, Antennas & Propagation (to be submitted).